

**Evaluation of Multi-Vehicle Architectures for the  
Exploration of Planetary Bodies in the Solar System**

by

**Farah Alibay**

B.A., University of Cambridge (2009)  
M.Eng., University of Cambridge (2010)  
M.A., University of Cambridge (2013)

Submitted to the Department of Aeronautics and Astronautics  
in Partial Fulfillment of the Requirements for the Degree of

**Doctor of Philosophy**

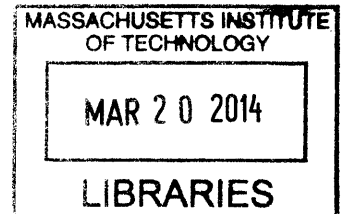
at the

**Massachusetts Institute of Technology**

February 2014

© 2014 Farah Alibay  
All rights reserved

ARCHIVES



The author hereby grants to MIT permission to reproduce and to distribute publicly paper and electronic copies of this thesis document in whole or in part in any medium now known or hereafter created

Signature of Author.....  
Department of Aeronautics and Astronautics  
January 15, 2014

Certified by .....  
Jeffrey A. Hoffman  
Professor of the Practice of Aeronautics and Astronautics  
Thesis Supervisor

Certified by .....  
David W. Miller  
Professor of Aeronautics and Astronautics

Certified by .....  
Olivier de Weck  
Professor of Aeronautics and Astronautics and Engineering Systems

Certified by .....  
Julie Shah  
Assistant Professor of Aeronautics and Astronautics

Certified by .....  
Paulo C. Lozano  
Associate Professor of Aeronautics and Astronautics  
Chair, Graduate Program Committee



# **EVALUATION OF MULTI-VEHICLE ARCHITECTURES FOR THE EXPLORATION OF PLANETARY BODIES IN THE SOLAR SYSTEM**

by

Farah Alibay

Submitted to the Department of Aeronautics and Astronautics  
on January 15, 2014 in Partial Fulfillment of the  
Requirements for the Degree of Doctor of Philosophy in  
Aeronautics and Astronautics

## **ABSTRACT**

Planetary exploration missions are becoming increasingly complex and expensive due to ever more ambitious scientific and technical goals. On the other hand, budgets in planetary science have suffered from dramatic cuts over the past decade and projections estimate a flat budget of approximately \$1.2B/year for the upcoming years. This has led to a desire for a reduction in the risk and complexity, as well as an increase in the robustness and reliability, of planetary exploration vehicles. One of the methods proposed to deal with this issue is the use of distributed, multi-vehicle architectures as a replacement for the traditional large, monolithic systems used in flagship missions. However, mission concept formulation engineers do not possess the tools to include multi-vehicle architectures in their early trade space exploration process. This is mostly due to the fact that these types of architectures cannot be readily evaluated against monolithic systems through the use of traditional mass-based metrics. Furthermore, in multi-vehicle system, architectural decisions about one vehicle, such as instrument or capability selection, quickly propagate through the entire system and impose requirements on the other vehicles. This can be difficult to model without going through detailed point designs.

The objective of this thesis is to explore the potential benefits of both spatially and temporally distributed multi-vehicle systems, where the vehicles are heterogeneous, as compared to monolithic systems. Specifically, a set of metrics mapping the effects of using multi-vehicle systems on science benefit, complexity, mass, cost, coverage, productivity and risk are developed. Furthermore, a software tool to simulate the performance of teams of planetary surface vehicles in their operational environment has been built and its use demonstrated. Finally, the framework put forward in this thesis is used to perform several case studies, including a case study on the exploration of the Jovian moon Europa and another on the ascent and return components of a Mars Sample Return mission. From these, distributed systems are shown to provide increased science return and robustness as well as lower development and manufacturing costs as compared to their monolithic equivalents.

**Thesis Committee Chair:** Jeffrey A. Hoffman, Ph.D.  
Title: Professor of the Practice of Aeronautics and Astronautics  
Department of Aeronautics and Astronautics

**Thesis Committee Member:** David W. Miller, Sc.D.  
Title: Jerome C. Hunsaker Professor of Aeronautics and Astronautics  
Department of Aeronautics and Astronautics

**Thesis Committee Member:** Olivier de Weck, Ph.D.  
Title: Professor of Aeronautics and Astronautics and Engineering Systems  
Department of Aeronautics and Astronautics

**Thesis Committee Member:** Julie Shah, Ph.D.  
Title: Assistant Professor of Aeronautics and Astronautics  
Department of Aeronautics and Astronautics

**Thesis Reader:** Jessica E. Duda, Ph.D.  
Title: Senior Research Scientist  
Aurora Flight Sciences

# ACKNOWLEDGEMENTS

This thesis is dedicated to my parents, Nazir Alibay and Nadine Soundarjee, without whose love and sacrifices I would not be where I am today. I would also like to thank the countless mentors, friends and colleagues who have helped me on my path to getting my PhD; enjoy finding your name below!

C G L G H A S N K Z G U N A J M S S L P J A W G Z G F O G Z  
D E H R T C P A S I O X X Q H G Y H T A K H A I N C R R V F  
C O Y V E K P T Y O R D N A S S E L A U M N V S A J E I E Y  
H K C Z B Z N B O H C C I W N I A C D D J O N K D N I Z R G  
A N R M A A W W C D T G F V N Y P T K N I R R K A I V A M S  
R Q T Y M A H Q U A K A N O B V F O A T U T E G N U I N V M  
L T M E T J Q F H V Z G S B V N R Q Q N A S H H A O L H F I  
E A H V M Z M J F E W D Y V O T I B I O R A R W T N O J X F  
S B H Z H U B H X E I C G N I B C M L A A O G V L U M P Z A  
K H X Y E Q H M N G J A N I G Y B M A A M R T I M L L H H R  
Z I U K E I T H L I T Q V T P D I Y E J M E A Q Z O Z P E Q  
L H F I M X N I D O H T I I A H W N V S N A T T A M O X H T  
A H K P I I W G B S I T K N S I A K F V G E N Q K H K J N G  
Y D G A K Y A T N O Z R R V C H E L S E A B B I H N W E P K  
R E I D E H B H W B D R F I T G N S N U W S C G A Z S M F U  
C T C C I M P G P A F R G A Y T G U D E L C R T E I R A M I  
W O N L L Y N Z L W I L N S N K C H R I S S W Y L B K C H X  
D S D I U D E C D N G V P D T C Y D A A R O N G X A X Z U B  
L W S Y J M R O Q Q B S M O C A N Y L I R A M B R K I A Z D  
H O V N N F I A U Z U T E O P A A O X J P A J E E R S Z X S  
F R J A K I K E H D B L N E T D G E J T S C N V D K I M M Z  
N I K E I D V O H C R K J E O J L X K T M D L T U B W D E E  
F G B O R R U E K B I B U I Y N O M A D R E R H C A Z B L K  
W C X H C N K A K T T R H B L G J E S S I C A E J F H N J T  
W S Y Q D D S E M A T Q R A E T Y R Q K Y A Q R Y A E J L Y  
R R F A B A Y W R F A E P W I E X G E O L I U E L Y A E M W  
H N N A D I N E M P N E J O N R R O B E R T E S A S I I V G  
L A L M T R U W H T Y O P D A V A V X L C V L A O N U A F M  
R B K A V V I L Z F A P Y Y D X Q M C Y J S H N N F T F Q F  
X P I L L I H P Y N O S P N R C Y W J O S H M A G M O G N Z

Additionally, this work for this thesis was partially funded by the following sources:

- NASA Phase II STTR Contract NNX10CB56C (2011-2012)
- Jet Propulsion Laboratory (JPL) Graduate Research Fellowship, funded by the JPL Innovation Foundry (2012) and the JPL Mars Program Formulation Office (2013)
- MIT AeroAstro Department Dupont Fellowship (2013)
- MIT Ida Green Fellowship (2010-2011)
- Zonta International Amelia Earhart Fellowship (2012-2014)



# TABLE OF CONTENTS

<b>Chapter 1: Introduction and Problem Formulation .....</b>	<b>17</b>
1.1 Background and Motivation.....	17
1.1.1 Motivation.....	17
1.1.2 Background .....	18
1.2 Problem Formulation and Objectives.....	25
1.2.1 Problem Formulation .....	25
1.2.2 Thesis Objectives .....	27
1.2.3 Hypotheses.....	27
1.2.4 Overview of Framework .....	28
1.2.5 Case Studies .....	28
1.3 Literature Review.....	29
1.3.1 Multi-Asset Systems Theory.....	29
1.3.2 Conceptual Design Tools .....	36
1.4 Overview of Thesis .....	40
<b>Chapter 2: Framework and Metrics.....</b>	<b>43</b>
2.1 Overview of Framework .....	43
2.2 Functional Decomposition and Trade Space Generation.....	44
2.2.1 Functional Decomposition .....	44
2.2.2 Trade Space Generation.....	45
2.3 Trade Space Evaluation .....	46
2.3.1 Mass.....	46
2.3.2 Science Benefit .....	47
2.3.3 Complexity.....	49
2.3.4 Cost .....	54
2.3.5 Productivity.....	54
2.3.6 Coverage .....	59
2.3.7 Uncertainty and Risk.....	60
2.3.8 Summary .....	65
2.4 Trade Space Visualization .....	65
<b>Chapter 3: Spatially Distributed Systems for Martian Surface Exploration .....</b>	<b>67</b>
3.1 Introduction.....	67
3.2 Mass Metric .....	68
3.3 “Multi-MER” System Case Study .....	70
3.3.1 Overview of MER Goals and Designs .....	70
3.3.2 Most Significant Trades .....	71
3.3.3 Effects of Sharing Supplying Supporting (SS) Functions.....	79
3.3.4 Hibernation .....	79
3.3.5 Energy Generating .....	80
3.3.6 Communication.....	81

3.3.7	Long-Range Traversing .....	82
3.3.8	Effects of the Different Types of Spatial Distribution .....	83
3.4	The Addition of Micro-Rovers to a System .....	90
3.5	Mars Science Laboratory (MSL) Case Study .....	95
3.6	Conclusion .....	99
<b>Chapter 4:</b>	<b>SEXTANT as a Multi-Vehicle System Simulation Tool.....</b>	<b>101</b>
4.1	Introduction.....	101
4.2	SEXTANT Features for Single Vehicles .....	102
4.2.1	Overview of Existing Features.....	102
4.2.2	New Single Vehicle Features .....	105
4.2.3	Single-Vehicle Case Study.....	107
4.3	SEXTANT Features for Multi-Vehicle Systems .....	110
4.3.1	Collision Avoidance.....	110
4.3.2	Traveling Salesman Problem .....	113
4.4	Lunar South Pole Case Study.....	116
4.4.1	Science Definition.....	116
4.4.2	Trade Space Generation and Architecture Selection.....	118
4.4.3	Mission Path-Planning using SEXTANT .....	121
4.5	Conclusion .....	124
<b>Chapter 5:</b>	<b>Temporal Distribution for the Exploration of Europa.....</b>	<b>125</b>
5.1	Introduction.....	125
5.2	Science at Europa.....	126
5.2.1	The Importance of Europa .....	126
5.2.2	Mission Goals and Payload Identification .....	126
5.2.3	Review of Proposed Designs .....	129
5.3	Architecture Generation and Evaluation Metrics.....	133
5.3.1	Architecture Generation .....	133
5.3.2	Evaluation Metrics .....	134
5.4	Trade Space Exploration.....	139
5.4.1	Evaluation of the EHM Design.....	140
5.4.2	Focused Missions.....	141
5.4.3	General Missions.....	143
5.5	Effects of Uncertainty and Risk.....	145
5.5.1	Effects of Instrument Choice on Uncertainty.....	145
5.5.2	Effects of Platform Choice on Uncertainty .....	146
5.5.3	Effects of Temporal Distribution on Uncertainty .....	147
5.5.4	General Effects on Trade Space.....	148
5.6	Conclusion .....	150



<b>Chapter 6: Spatially and Temporally Distributed Systems for Mars Sample Return.....</b>	<b>151</b>
6.1 Introduction.....	151
6.2 History of Mars Sample Return .....	152
6.2.1 Why Sample Return? .....	152
6.2.2 Overview of Past and Current Designs .....	153
6.2.3 2011 MSR Baseline .....	154
6.2.4 Mars 2020 Rover.....	155
6.2.5 Current Trades for Retrieval, Ascent and Return.....	155
6.3 Architecture Generation and Evaluation Metrics.....	158
6.3.1 Architecture Generation.....	158
6.3.2 Evaluation Metrics .....	159
6.4 Trade Space Exploration.....	168
6.4.1 Trade #1: Rover Range .....	170
6.4.2 Trade #2: MAV Capability .....	171
6.4.3 Trade #3: MAV Mobility .....	172
6.4.4 Trade #4: Direct Return .....	173
6.4.5 Trade #5: Orbiter Propulsion .....	175
6.4.6 Trade #6: MAV Target Orbit .....	178
6.4.7 Trade #7: Sequencing.....	179
6.4.8 Trade #8: Orbiter Destination .....	181
6.5 Conclusions.....	182
<b>Chapter 7: Conclusions and Recommendations .....</b>	<b>183</b>
7.1 Thesis Summary.....	183
7.2 Contributions.....	187
7.3 Recommendations for Future Work.....	189
7.3.1 Spatially Distributed Systems .....	189
7.3.2 Temporally Distributed Systems.....	189
7.3.3 Framework and Metrics .....	190
7.3.4 SEXTANT .....	190
7.3.5 Case Study Specific Further Work.....	190
<b>Bibliography.....</b>	<b>193</b>
<b>Appendix A: Rover Mass Modeling.....</b>	<b>211</b>
A.1 Assumptions.....	211
A.2 Subsystems .....	213
A.2.1 Chassis Module.....	213
A.2.4 Steering Module.....	217
A.2.5 Vehicle-Terrain Interaction Module .....	218
A.2.6 Drive System Module .....	221
A.2.7 Power System Module .....	223
A.2.8 Suspension Module.....	224
A.2.9 Payload Module .....	224
A.2.10 Communications .....	224

A.2.11 Navigation Subsystem .....	225
A.3 Benchmarking .....	225
A.4 Works Cited .....	227
<b>Appendix B: Low-Thrust Trajectories for Mars Sample Return .....</b>	<b>229</b>
B.1 Summary of Low-Thrust Trajectories and SEP Orbiter Sizing.....	229
B.2 2020 Trajectories.....	230
B.3 2022 Trajectories.....	231
B.4 2024 Trajectories.....	234
B.4.1 Earth Return .....	234
B.4.2 Lunar Return .....	235
B.5 2026 Trajectories.....	237
B.5.1 Earth Return .....	237
B.5.2 Lunar Return .....	238
B.6 2028 Trajectories.....	240
B.6.1 Earth Return .....	240
B.6.2 Lunar Return .....	241
<b>Appendix C: Software and Supporting Documents .....</b>	<b>243</b>

## FIGURES

Figure 1: Changes in Mars surface traversing systems .....	21
Figure 2: Overview of framework .....	28
Figure 3: MILSATCOM systems and owners.....	30
Figure 4: DSS research program overview slide .....	32
Figure 5: Overview of framework .....	43
Figure 6: Overview of the problem decomposition process.....	44
Figure 7: OPD showing the difference between value delivery and supporting functions .....	45
Figure 8: OPD showing the difference between ES and SS functions .....	46
Figure 9: Three types of complexity .....	50
Figure 10: Example of interactions between a 3-rover system.....	54
Figure 11: Example of a Markov Model and the Corresponding $A$ Matrix.....	56
Figure 12: State transition curves for the 1- (left) 2-rover (right) architectures. ....	58
Figure 13: Value functions for the number of sites visited and their area.....	60
Figure 14: Example trade space with error bars showing uncertainty range.....	61
Figure 15: Example of non-dominated, weakly dominated and strongly dominated architectures.....	63
Figure 16: Plot illustrating the concept of $\epsilon$ -dominance.....	64
Figure 17: Example of a display of the trade space.....	66
Figure 18: Mass vs. vehicle-level complexity trade .....	72
Figure 19: Science benefit vs. total mass .....	73
Figure 20: Science benefit vs. average vehicle-level complexity.....	73
Figure 21: Vehicle- vs. system-level complexity .....	74
Figure 22: State transition curves of the monolithic system with baseline reliability .....	75
Figure 23: State transition curves of a 2-vehicle architecture with baseline reliability.....	76
Figure 24: State transition curves of a 3-vehicle architecture with baseline reliability.....	77
Figure 25: State transition curves of a 3-vehicle architecture with reduced reliability .....	78
Figure 26: Sensitivity analysis of productivity for multi-rover systems .....	78
Figure 27: System mass against nighttime power requirement.....	80
Figure 28: System mass against power supply requirement.....	81
Figure 29: Effects of carrying/towing a vehicle on system mass .....	83
Figure 30: DRACO micro-rover .....	93
Figure 31: Micro-rover concept of operations.....	94
Figure 32: Adding 2 micro-rover systems could increase the coverage at each site of interest.....	94
Figure 33: Details and evaluation of twelve representative architectures .....	97
Figure 34: 60 km <sup>2</sup> map of the South Pole of the Moon, with 10m per pixel resolution.....	103
Figure 35: Shadowing on the vehicle throughout the mission duration. ....	105
Figure 36: Rover energy levels before waiting times are added (top) and after (bottom).....	106
Figure 37: Communication link availability.....	107
Figure 38: Chosen example traverse (left) and corresponding elevation during the traverse (right) .	108
Figure 39: Energy level (left) and Earth visibility (right) of the rover during the traverse. ....	108
Figure 40: Evaluating the opportunity for multiple rovers to share communication systems .....	109
Figure 41: Start & end waypoints for three rovers and collision-free paths.....	111
Figure 42: Distance between all pairs of rovers over the course of the traverse. ....	111
Figure 43: Collision-free traverse for six rovers .....	112
Figure 44: Distance between all pairs of rovers – always remain greater than 2m .....	112
Figure 45: System mass against nighttime power requirement .....	120
Figure 46: Points to be visited during the traverse .....	121
Figure 47: Path for single-vehicle architecture.....	122
Figure 48: Paths for the two-vehicle architecture.....	123

Figure 49: Paths for the three-vehicle architecture.....	123
Figure 50: In-orbit trajectory for the Clipper flyby mission.....	127
Figure 51: Science benefit vs. complexity for the EHM concepts .....	137
Figure 52: Science benefit vs. complexity for the trade space explored .....	138
Figure 53: Science benefit vs. cost (normalized) for the trade space explored .....	139
Figure 54: Existing designs' sensitivity to objective weightings .....	140
Figure 55: Trade space evaluation for focused missions.....	142
Figure 56: Trade space evaluation for evenly weighted goals .....	143
Figure 57: Addition of a laser altimeter on the carrying orbiter.....	144
Figure 58: Effect of instrument choice on uncertainty .....	146
Figure 59: Effect of platform choice on uncertainty .....	147
Figure 60: Effect of temporal distribution on uncertainty .....	148
Figure 61: $\epsilon$ -Pareto front.....	149
Figure 62: Basic trade tree of technology options explored .....	159
Figure 63: Event sequence for returning a sample back to Earth.....	161
Figure 64: Example probability tree.....	164
Figure 65: Overview of interdependencies between vehicles .....	165
Figure 66: Example of a SEP trajectory with a 2022 departure and an 11-month stay at Mars.....	166
Figure 67: Correlation between cost and complexity.....	168
Figure 68: Architectures with a lander, fetch rover, a MAV and chemical orbiter;.....	169
Figure 69: Effect of changing landing ellipses.....	170
Figure 70: Single- vs. dual-string MAV.....	171
Figure 71: Comparison of the lander & fetch option to the roving MAV .....	172
Figure 72: Configuration of the low-cost, direct return option .....	173
Figure 73: Trade space with low cost direct return options .....	174
Figure 74: Full trade space for 2024 orbiter launch .....	175
Figure 75: Full trade space for a 2022 orbiter launch.....	176
Figure 76: Full trade space for a 2026 orbiter launch.....	177
Figure 77: Trade space of different MAV orbit destinations .....	178
Figure 78: Full trade space, 2024 launch, orbiter first option .....	179
Figure 79: Full trade space, 2024 launch, lander first option.....	180
Figure 80: Architectures returning the sample to the Moon.....	181
Figure 81: Full Trade Space for the Europa Case Study. ....	186
Figure 82: Full Trade Space for the MSR Case Study. ....	187
Figure 83: $N^2$ diagram showing subsystem interactions.....	211
Figure 84. Load modeling of chassis side rail .....	214
Figure 85. Schematics of wheel sinkage in soft terrain.....	215

# TABLES

Table 1: Overview of past exploration missions to the outer solar system .....	19
Table 2: Overview of the NASA mission opportunity programs .....	19
Table 3: Vehicles sent to the surface of Mars by NASA.....	20
Table 4: System envelope for distributed multi-vehicle planetary surface systems.....	26
Table 5: Hypothesized effects of distribution on system properties.....	27
Table 6: Overview of the thesis case studies.....	28
Table 7: Definitions of Systems of Systems.....	31
Table 8: GT-FAST metrics.....	34
Table 9: Phase I VCDM tools .....	37
Table 10: Parametric models of planetary surface vehicles available in the public literature.....	38
Table 11: Value weightings scale.....	48
Table 12: <i>CW</i> allocation scheme for instruments and key technologies .....	53
Table 13: Types of interactions between vehicles.....	54
Table 14: Inputs and outputs to the rover modeling tool.....	68
Table 15: Connection between each subsystem .....	69
Table 16: Overview of the assumptions used for the design of each sub-system .....	69
Table 17: Functional decomposition of the MER design .....	71
Table 18: VD and SS functions possessed by the vehicles in the architectures circled in Figure 18...	72
Table 19: Different types of spatial distribution.....	84
Table 20: Effects of different types of spatial distribution on science benefit and productivity .....	85
Table 21: Effects of different types of spatial distribution on system mass and mission coverage .....	86
Table 22: Effects of different types of spatial distribution on vehicle- and system-level complexity .....	87
Table 23: Overview of the micro-rover literature .....	91
Table 24: Functional decomposition for the MSL case study .....	96
Table 25: Instruments onboard MSL used in the case study .....	96
Table 26: Functional decomposition .....	119
Table 27: Functions considered in the case study .....	119
Table 28: Architectures of interest .....	119
Table 29: Architecture properties.....	120
Table 30: Route for each of the down-selected architectures.....	122
Table 31: Europa science traceability matrix .....	128
Table 32: EHM instrument suite .....	132
Table 33: Instruments considered for the trade space exploration of possible Europa missions .....	133
Table 34: Value weightings scale.....	135
Table 35: Weighting scheme for the complexity metric .....	135
Table 36: $\Delta V$ and ISP values for wet mass estimation.....	136
Table 37: Value ranges for select architectures, normalized by the JEO ranges.....	149
Table 38: Baseline architecture .....	154
Table 39: Summary of main trades explored.....	156
Table 40: Functional decomposition of the Fetch, Ascent and Return part of a MSR campaign .....	157
Table 41: Conditional probability of success of the most important events.....	162
Table 42: Historical lifetime of platforms .....	163
Table 43: Overview of mass models .....	165
Table 44: $\Delta V$ requirements for return orbiters with chemical propulsion;.....	166
Table 45: Complexity weightings ( <i>CW</i> ) applicable to all technologies.....	167
Table 46: Types of spatially distributed systems.....	184
Table 47. List of all variables used in the master script .....	212
Table 48. Inputs and outputs of chassis module.....	213

Table 49. Inputs and outputs of wheel dimensioning module.....	215
Table 50. Inputs and outputs of steering module.....	217
Table 51. Inputs and outputs of vehicle-terrain interaction module.....	218
Table 52. Inputs and outputs of drive system module.....	221
Table 53. Inputs and outputs of power system module .....	223
Table 54: Benchmarking with MER.....	225
Table 55: Benchmarking with MSL .....	226







# Chapter 1

## INTRODUCTION AND PROBLEM FORMULATION

### 1.1 Background and Motivation

#### 1.1.1 Motivation

Missions to other planetary bodies in the solar system, and in particular to bodies in the outer solar system, have traditionally been flagship missions with a wide range of science objectives. This has led to large, complex systems with high costs and long development timelines. Historically, missions to Mars have been the exception to that rule. Being the second closest planet to Earth and much more environmentally benign as compared to Venus, Mars is the subject of a campaign of missions. [1] The aim of this campaign is to have a sequence of missions over several decades, all building on each other, both in terms of answering science questions and achieving technology developments. However, if the most recent missions to Mars are considered, in particular Curiosity, the Mars Science Laboratory (MSL), [2] and the proposed Mars Sample Return Mission (MSR), [3] it can be seen that these systems are also becoming highly complex and increasingly massive. This has led to significant delays and cost overruns in the Mars Program. In turn, this reflects the fact that the cost of a system is closely correlated with its complexity, [4] and that we are currently reaching the limits in terms of the levels of complexity that can be successfully dealt with in robotic systems for planetary exploration.

On the other hand, NASA's budgets for planetary science were recently cut by approximately 20%, [5] while the science goals set out by the Planetary Science Decadal Survey for the period of 2013-2022 [6] were more ambitious than ever before. Additionally, the high visibility of NASA missions and the detrimental effects of the Mars mission failures of the 1990s on public opinion have led to an increased desire for robust and reliable missions. Consequently, there is a clear need for a change in paradigm in the way planetary exploration is currently approached, and a move away from the traditional large monolithic system approach.

One proposed attempt to address these conflicting desires is a *multi-vehicle* approach to planetary exploration, where the vehicles may be *heterogeneous* (i.e. of different *type*) and are *distributed* in *space* and/or *time*. This thesis argues that multi-vehicle systems can lead to higher science return for a given investment, reduce system complexity, and increase robustness and productivity due to their inherent redundancies. The rest of this section explores more deeply the history of planetary exploration, the broader background on multi-vehicle systems and the concept of systems architecture.

## 1.1.2 Background

### 1.1.2.1 History of Planetary Exploration

This thesis particularly focuses on the exploration of Mars and the planetary bodies in the outer solar system (Jupiter and beyond). A historical overview of missions to these bodies is therefore presented, to highlight the need for a change in paradigm for planetary exploration.

#### 1.1.2.1.1 Missions to Planetary Bodies in the Outer Solar System

The exploration of the outer solar system began in the early 1970s with the Pioneer 10 and 11 spacecraft that provided the first set of data on magnetic fields, energetic particle radiation and dust populations in the outer solar system. Contact with Pioneer 10 and 11 has long been lost. These missions were closely followed by Voyager 1 and 2 in 1977, which are still active today. Despite these early successes, a shift in agency priorities, a reduction in NASA's budgets and the *Challenger* accident led to a 15 year gap until another mission, Galileo, was sent to Jupiter in 1989. Due to complications that are thought to have been related to launch delays, Galileo suffered from a failure of its high gain antenna, but was still successful in achieving most of its main mission objectives. It was deliberately crashed into Jupiter in 2003. By the time Galileo was designed, the approach to the exploration of the outer solar system had changed significantly. As can be seen, approximately only one mission per decade was being sent to the outer solar system. Consequently, missions being suggested were large flagship missions achieving a large range of science goals and thus satisfying the needs of all different science groups, but at high price tags. Under this paradigm, Galileo was followed by Cassini, another flagship mission that

was launched in 1997. This was again a high-cost, high-complexity mission, but this mission was also extremely successful and is still operating around Saturn today. It is to be noted that both Galileo and Cassini each carried a small probe that crashed/landed on Jupiter and Titan respectively.

At the turn of the century, NASA introduced two new mission categories: New Frontiers and Discovery missions. These are lower cost, more focused missions, aimed to answer a specific science question and/or demonstrate a particular technology. Under the New Frontiers program, two more missions were sent to the outer solar system: Juno and New Horizons. An overview of the cost of the most recent missions is provided in Table 1 and details of the different NASA programs for exploration missions are given in Table 2.

**Table 1: Overview of past exploration missions to the outer solar system [7]**

Name	Approx. Total Cost (in \$B FY2012)	Launch Year
Voyager 1	1	1977
Voyager 2	1	1977
Galileo	3	1989
Cassini	4.5	1997
New Horizons	0.8	2006
Juno	1.1	2011

**Table 2: Overview of the NASA mission opportunity programs, all costs exclude launch vehicle costs [8]**

Program	Max. Mission Cost (\$B)
Flagship	2-3
New Frontiers	0.7-1
Discovery	0.425

The original intention was for there to be a mix of Flagship and New Frontiers missions to the outer solar system. However, since the release of the Planetary Science Decadal Survey in early 2011, [6] a debate has emerged leading to the following questions being posed by the scientific community: “Are flagship missions sustainable under the current economic climate?”, “How does the science return from smaller New Frontiers missions compare to that of Flagship missions?”.

One of the main drivers for this debate is the proposed mission to Europa, one of the Galilean moons. The Decadal Survey identified a mission to Europa as the second most important target in the solar system, following a Mars Sample Return mission. However, it also stated that the proposed Flagship mission to Europa, the Jupiter Europa Orbiter (JEO), was too large, complex, expensive and risky. The Outer Planets Assessment Group (OPAG) and the Jet Propulsion Laboratory (JPL) were therefore tasked to identify whether a *sequence* or *set of multiple smaller missions* could replace JEO; or if a smaller, less risky mission could achieve comparable goals. This led to the development of the Europa Habitability Mission (EHM), which consists of a flyby and an orbiter spacecraft [9] that would probably have been

launched at separate times. In this case and any other *temporally distributed* multi-vehicle missions, the main challenge faced by engineers and scientists is that they lack a framework to rapidly generate multi-vehicle architectures in the early phases of mission design and to evaluate them against each other and against their single vehicle equivalent. When trying to evaluate these types of missions, they must currently go through detailed in-depth studies of a few options and are unable to evaluate a large trade space of multi-vehicle options. Although there is a desire to move away from the Flagship mission paradigm, there are still difficulties in identifying what opportunities a multi-vehicle approach, with different *types* of vehicles, would have for missions to the outer solar system.

#### 1.1.2.1.2 Mars Surface Exploration Program

This section concentrates on the history of the exploration of the *surface* of Mars, since it has evolved significantly over time and is also fraught with failures and changes in strategic approaches. Furthermore, surface exploration missions to Mars are arguably some of the most complex robotic missions ever flown by NASA. Finally, the effects of the changes in the approach to the exploration of Mars on the plans for a sample return mission are discussed. An overview of the different spacecraft flown to the surface of Mars is provided in Table 3

**Table 3: Vehicles sent to the surface of Mars by NASA**

<b>Mission</b>	<b>Year</b>	<b>Outcome</b>
Viking 1	1976	Successful
Viking 2	1976	Successful
Pathfinder	1996	Successful
Mars Polar Lander	1999	Lost on arrival
Spirit	2003	Successful
Opportunity	2003	Successful
Phoenix	2008	Successful
Curiosity	2012	Successful

NASA's Viking Project was the first to ever successfully land a spacecraft safely on the surface of Mars. It involved two identical spacecraft, Viking 1 and 2, weighing nearly 600kg each. The landers flew separately to Mars with their own orbiters and landed in 1976. Both missions were highly successful and remained operational until the early 1980s. Analogously to the exploration of the outer solar system, there was then a 15 year gap until any other spacecraft was successfully landed on Mars. In 1996, the Mars Pathfinder lander was launched for Mars. This mission carried a small 10kg rover, Sojourner. However, this rover was a later addition to the mission, meant to be a technology demonstration. This program was also highly successful and led to a renewed interest in Mars. At that time, NASA was following the "faster-better-cheaper" program that encouraged smaller, cheaper but higher risk missions with shorter timelines, while accepting higher probabilities of failure. Pathfinder was successful under this program,

but its successor, the Mars Polar Lander, was not. The latter was also a multi-vehicle mission, consisting of a large lander and two small probes (Deep Space 2) designed to impact the Martian surface to test new technologies. This mission was lost at arrival, in 1999. Following this failure and that of the Mars Climate orbiter, also in 1999, NASA moved away from the “faster-better-cheaper” paradigm. The next mission to land on Mars, in 2003, consisted of a pair of rovers, Spirit and Opportunity, under the Mars Exploration Rovers (MER) program. Each of these rovers weighed 185kg, and the mission was highly successful. It is to be noted that although there were two vehicles in this system, they were not working together nor collaborating in any way. In 2008, the Phoenix lander arrived on Mars. This mission reused the technology developed for the Mars Polar Lander and the cancelled Mars Surveyor mission. This mission was highly successful and also demonstrated that there are possible cost savings by reusing certain technologies between different spacecraft. In fact, the next planned Mars lander, InSight, will also reuse some of the Phoenix technology. Finally, in the summer of 2012, the Mars Science Laboratory (MSL) was landed on Mars. Two years late and significantly over budget, this \$2.5B rover weighing just over 930kg is a highly integrated and complex system, mainly due to the ambitious science goals it was built to accomplish.

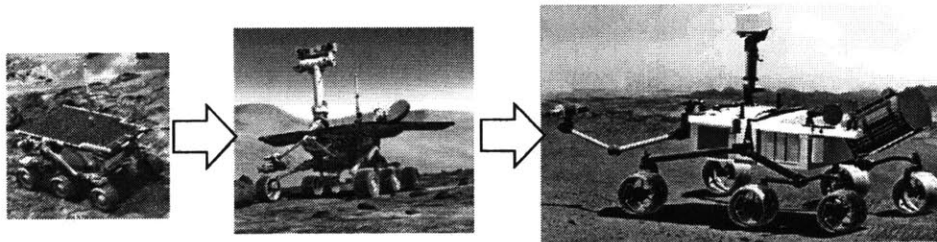


**Figure 1: Changes in Mars surface traversing systems:  
Sojourner (10 kg), Spirit/Opportunity (185 kg) and Curiosity (930 kg)**

From the history of Mars missions, it can be observed that, although a programmatic and sequential approach was taken for the exploration of Mars, traversing planetary surface assets are becoming increasingly large and complex, with costs reaching that of Flagship missions. In fact, MSL nearly reached the limits in terms of what mass can be landed on Mars using the current sky-crane technology and in terms of the levels of system complexity which engineering teams can deal with. The next step identified by the Decadal Survey for the exploration of Mars is a Sample Return Mission. Due to budget constraints, the decision was made to *temporally distribute* the different aspects of the mission, leading to a 3-phase mission: a caching rover, an ascent vehicle and a return mission. Some of the considered scenarios also propose a 2-phase mission, where the caching rover and the ascent vehicle are combined. This decision is still in flux since there is a lack of information on how *separating or combining* these missions affects the science benefit and mission risk. One point of interest is that the caching rover part of the mission was originally meant to be a two-rover mission, with the rovers landing at the same site and

collaborating to achieve the mission goal. This is an example of a *spatially distributed* system with completely different vehicles collaborating to achieve higher science return than they would have done separately. [10] The Max-C and ExoMars vehicles were meant to be developed by NASA and ESA respectively. Their design, however, was done separately and opportunities for collaboration were only established after the fact. There is therefore a gap in terms of being able to identify and evaluate, in the early phases of the design process, multi-vehicle systems that are able to provide more value than their equivalent monolithic system. Max-C has now been cancelled while ESA is proceeding forward with the ExoMars rover. This rover, weighing approximately 350kg, will be ESA's first asset on the surface of the red planet. NASA, on the other hand, has recently announced that it will send a rover to Mars in 2020 to perform the first step of a Mars Sample Return mission: sample caching. [11].

### **1.1.2.2 Multi-Agent Systems**

As was demonstrated in the last section, the approach taken by NASA for planetary exploration has mostly involved single, large, highly complex vehicles with high functionality, performing exploration on their own. However, high functionality systems are not the only types of systems that can be observed. Both in nature and from an engineering perspective, multi-agent systems are commonly used. This section presents examples and advantages of multi-agent systems from biology, non-space related fields and aerospace.

#### **1.1.2.2.1 Multi-Agent "Systems" in Biology**

In nature, high functionality systems are analogous to predators: these are highly skilled and evolved "agents" that have low populations and long life expectancies. While predators perform well in the food chain, they are not the only type of species that have survived evolution. On the other end of the scale, swarms of low functionality animals and insects also exist. For example, in ant colonies, each ant has limited functionality but, by working together as a system, they can achieve more than they would individually. In the field of controls, this swarm behavior has been mimicked to take advantage of the enhanced capabilities it brings. [12], [13], [14] Between these two extremes, there also exist examples of many animals that are mostly independent but benefit from collaboration (flock of birds flying together are an example of positive emergent behavior from a multi-agent system, beavers building dams together is another example). The key point is that single, high functionality systems are not the only systems that have evolved in nature. Therefore, by analogy, it can also be assumed that lone, high complexity systems are also not always the only solution to address a set of goals.

#### *1.1.2.2.2 Multi-Agent Systems in Non-Space Related Fields*

In non-space related fields of engineering, multi-agent systems are used in a range of applications. For example, teams of autonomous underwater vehicles have been developed to cooperatively map and explore deep oceans. [15] Multi-rover teams on Earth have also demonstrated some of the advantages of collaborative systems of vehicles, including better navigation and localization, as well as improved ability to perform tasks. [16] Additionally, teams of Unmanned Air Vehicles (UAVs) and quadrotors have been used to perform surveillance tasks [17] or even work together to build simple structures. [18] Finally, teams of *heterogeneous* rovers are often used in demining activities. [19] In this case, small scout rovers with low functionality and low cost are sent out to first detect the mine. Because they are simple and inexpensive, they are more disposable than the larger systems, which is advantageous if they accidentally detonate a mine. Once they locate a mine, a larger rover is then sent to deactivate and retrieve it. This is a clear example of how multi-vehicle systems can be more robust and perform better than their monolithic equivalent when operating in treacherous environments.

#### *1.1.2.2.3 Multi-Agent Systems in Aerospace*

Multi-vehicle systems are slowly emerging in the aerospace field, mostly for Earth observing systems. Constellations, both for communication and navigation (e.g. GPS), are systems where the large number of vehicles is used to enable maximum coverage and triangulation, respectively. Other multi-vehicle systems have been put forward in the literature, or are currently being designed and have yet to be flown. For example, spacecraft fractionation is being investigated under the DARPA F6 program, [20] whose goal is to replace traditional, highly-integrated, monolithic satellites with wirelessly-networked clusters of heterogeneous modules incorporating the various payload and infrastructure functions. Finally, swarms, constellations and clusters of small satellites have also been put forward to increase system robustness using small, cheap and low functionality systems [21], [22].

All these examples of multi-agent systems suggest that there may be opportunities arising from using multi-vehicle systems for the exploration of the solar system. One such example is a theoretical study called “Snow White and the 700 dwarves,” which was undertaken at JPL [23]. In this study, Wilcox proposed a system where several hundred small rovers would be brought along with a mothership vehicle to excavate the surface of the Moon or Mars. The excavation of open trenches is of particular interest to the human exploration community due to its applicability to topics such as the emplacement of habitats under radiation shielding, the digging utility trenches or the extraction and processing of near-surface volatiles. Wilcox leveraged redundancy to perform excavation at low cost and low risk. In another example, Lamamy [24] investigated the advantages of carrying a small explorer rover on board a larger vehicle. He found that there were few advantages to this approach and that it led to increased complexity

and mass. The main reason for this is because the explorer was a later addition to the design and off-loaded few of the main vehicle's tasks, rather than truly acting as a coordinated system.

The works overviewed in this section have several limitations. First, many of these systems involve homogenous vehicles. However, in the case of planetary exploration, making use of a range of different vehicles could have beneficial properties, such as increased accessibility, range and resolution. Finally, most of these examples have involved single point designs of multi-agent systems: if multi-vehicle systems are to be traded alongside monolithic options in the early phases of the design process, a formal framework and tools must be developed to enable this trade space exploration.

### *1.1.2.3 Systems Architecture*

Systems architecture is a field that takes a holistic approach to high-level systems design. It was first introduced by Retchin [25], [26] in the 1980s and takes its origins from similarities that were observed between the architecture of buildings and the design of large complex systems in other fields. Systems architecture differs from traditional design in three ways. First, it prioritizes stakeholder value delivery, rather than solely optimizing profit or performance, for example. Second, it takes into account both technical and non-technical factors and third, it includes all the phases of the lifecycle process. Systems architecture lays the foundation for the design of a system. During the architecture process, the first decisions about the system are made, which commits the largest part of the lifecycle cost of the system. [27] These decisions therefore have a large impact on subsequent design decisions, as well as complexity, value returned, risk, etc. Ultimately, good systems architecture is essential for the success of a complex system. The popularity of systems architecture in academia has grown significantly over the past few years. Crawley et al. [28] identify three key themes in systems architecture: complexity, ambiguity and creativity. Other topics include flexibility [29], [30], [31], which is how robust a system is to change in internal or external properties; commonality [32], which identifies the gains can be made from designing portfolios of modular systems; and value delivered to the stakeholders, which is particularly addressed in the field of value centric design [33].

Systems Architecture Tradespace Exploration (SATE), or systems architecting, involves the combination of a system modeling tool and a search tool to explore the trade space of possible architectures. This enables the exploration of the whole trade space of possible solutions to a design problem and to identify families of architectures that perform well. Typically, the process involves a functional decomposition of the system goal, an enumeration of the possible solutions, and an evaluation of the trade space. Finally, the trade space is downsized to a few interesting architectures that can then be evaluated in further detail. Details of specific trade space exploration tools and methodologies used for the evaluation of planetary exploration missions are discussed in Section 1.3.2.



## 1.2 Problem Formulation and Objectives

### 1.2.1 Problem Formulation

Thus far, it has been demonstrated that planetary exploration systems are typically large, complex, single vehicle systems with high functionality and high potential science value return. Although some missions have had a smaller spacecraft fly along (e.g.: Sojourner, Huygens), generally only single vehicle systems are considered in the early phases of the design process. However, these missions suffer from significant programmatic and operational risks and high annual costs that cannot be afforded under the current economic climate. Additionally, single vehicle systems can have limited productivity and redundancy, since tasks cannot be parallelized. Furthermore, as science requirements become increasingly demanding, as is the case for the robotic surface exploration of Mars and the Moon for example, these systems become increasingly complex, leading to cost overruns and project delays.

On the other hand, missions with small spacecraft tend to have shorter project timelines and lower annual budgets. Moreover, it has been shown that multi-agent systems are common in biology and engineering, and have a growing popularity in communication and Earth observing systems. In communications satellites, however, the systems often involve homogeneous spacecraft.

This thesis therefore proposes to investigate the potential advantages and limitations of using multi-vehicle architectures to accomplish science goals for the exploration of planetary bodies in the solar system, where the vehicles are *heterogeneous* (i.e. of different *type*) and are *spatially* and/or *temporally distributed*. Here, *task distribution* is defined as the spreading of the functions that one vehicle would accomplish during a mission across several vehicles. *Temporal distribution* is the separation of a large vehicle into a sequence of vehicles that are launched and operated separately to achieve the original mission goal. Finally, *spatial distribution* is the spreading of vehicles across an area, either on a surface, on orbit, or a combination of both.

For spatially distributed systems, the system size and boundary must also be defined. Orbital assets can be described as clusters and constellations [34]. A cluster consists of a locally grouped set of satellites that are in close proximity. Constellations are systems that feature a large number of satellites each with their own unique set of orbital parameters. In the case of planetary surface vehicles, there are two defining properties: independence and coordination.

Independent systems do not need each other to survive, whereas dependent systems share certain resources, such as power or traversing abilities for example. Coordinated systems work together to achieve the mission goals and operate in the same planetary region, whereas systems that are not coordinated achieve the mission goals separately and operate in different regions. An example of

independent but coordinated planetary surface systems is the MAX-C and ExoMars mission that was proposed in 2011 [10]. An example of independent and non-coordinated system is the pair of Mars Exploration Rovers (MERs). The system boundaries for these types of systems are given in Table 4. This thesis will evaluate and compare the advantages and limitations of all these types of distributed systems.

**Table 4: System envelope for distributed multi-vehicle planetary surface systems**

	<b>Coordinated</b>	<b>Non-Coordinated</b>
<b>Dependent</b>	Vehicles are always in visible (i.e. line of sight) contact. The system consists of the vehicles only.	N/A
<b>Independent</b>	Vehicles do not have to be visible to each other at all times, but are always in the same region. The system consists of the vehicles and at least one orbiter.	Vehicles do not have to be visible to each other, and are not in the same region. The system consists of the vehicles and at least one orbiter.

The main issue with distributed architectures is that they cannot be compared on a one-to-one basis with monolithic systems using mass-based metrics [34]. Traditionally, systems are compared to each other based on their launch mass, and parametric cost models typically only model correlations between vehicle mass and development cost, often ignoring other potential cost drivers. Distributed systems are likely to often be heavier than their equivalent monolithic system due to the inherent mass cost associated with additional platforms but, as is hypothesized in Section 1.2.3, it is expected that distributed systems present advantages in terms of science benefit, complexity, productivity, risk and coverage. The overarching thesis problem statement is therefore as follows:

*How can architectures with multi-vehicle types be evaluated against monolithic architectures on a one-to-one basis, in the trade space exploration phase, without going through detailed point designs?*

This also leads to a range of more specific research questions:

- 1) On planetary surfaces, how can teams of *spatially distributed* heterogeneous rovers achieve a set of science goals and how does their performance compare to that of a monolithic vehicle?
- 2) How can the performance of these multi-vehicle system concepts be simulated in their operational environment? How do they perform in challenging environments, as compared to their monolithic equivalent?
- 3) Can large flagship missions be replaced by *temporally distributed* systems consisting of different types of vehicles? What are the effects on cost, risk and value?
- 4) How can multi-vehicle-type systems that are both *spatially* and *temporally distributed* be considered in the early phases of mission design? How do such missions perform as compared to the single vehicle alternative?

In order to achieve this, a framework is developed to allow for the generation and evaluation of multi-vehicle architectures for such missions. This framework can be applied to: (1) planetary surface assets, where teams of vehicles are used to explore a planet; (2) to flyby/orbiter assets, where flagship missions are replaced by smaller missions; and (3) to a combination of the two, where a range of different vehicles are used to achieve a given science objective, such as a sample return mission.

### 1.2.2 Thesis Objectives

The overarching objective of this thesis is to explore the effects of utilizing multi-vehicle architectures to achieve a given set of goals for planetary exploration by developing a framework to allow for the direct comparison of systems containing multiple heterogeneous vehicles. The specific sub-goals are to:

1. Enable the exploration of multi-vehicle trade spaces where the vehicles are: of different *types*, *spatially distributed* and/or *temporally distributed*.
2. Evaluate the effects of distribution and coordination on mission properties through multiple case studies
3. Develop a software-based framework to simulate early (pre-phase A) distributed mission concepts for planetary surface exploration

### 1.2.3 Hypotheses

This research is based on the hypothesis that the advantages and limitations of multi-vehicle systems cannot be illustrated using traditional (mass-based) metrics. An overview of the possible effects of distribution on system properties is presented in Table 5.

**Table 5: Hypothesized effects of distribution on system properties**

<b>Advantages</b>	<b>Uncertain</b>	<b>Limitations</b>
Lower vehicle complexity	Science benefit	Higher system complexity
Greater productivity through parallelization of tasks	Total cost	Increased total mass
Lower mission risk	Performance in environment	
Greater coverage/number of sites visited	Timeline	

Specifically, potential advantages involved with *spatial distribution* are redundancy, parallelization of tasks (increased productivity), greater coverage (greater amount of science), reduced risk in cost and productivity, and improved performance in challenging environments. Expected disadvantages for this type of distribution are increased total system mass and system-level complexity. As for *temporal distribution*, the hypothesized advantages are that one mission can inform another (reduced risk, greater

science return), the opportunity for pre-deployment of functionality (shorter time until *some* goals are achieved) and reduced vehicle complexity. On the other hand, there is a potential for increased launch vehicle cost and increased operational timeline (longer time until *all* goals are achieved). These hypotheses will be explored throughout all the case studies in this thesis.

### 1.2.4 Overview of Framework

A 5-step framework has been developed to evaluate the advantages and limitations of multi-vehicle systems. It is described in detail in Chapter 2, but an overview is provided in Figure 2.

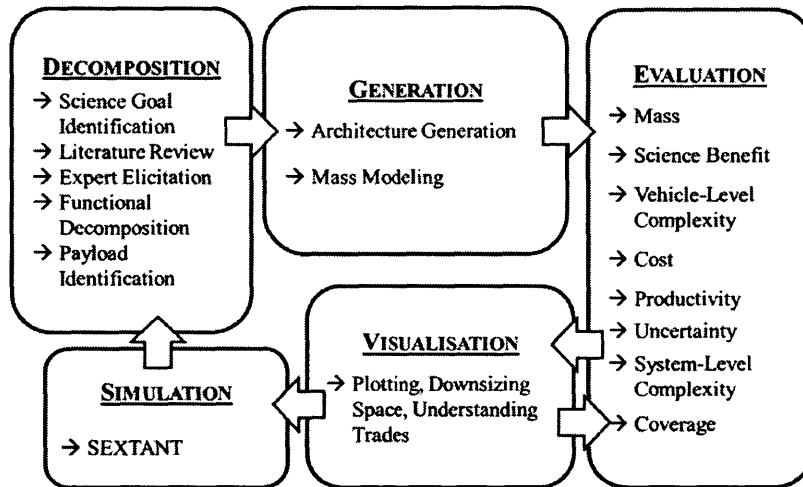


Figure 2: Overview of framework

### 1.2.5 Case Studies

The hypotheses presented are tested through several case studies, an overview of which is presented in Table 6.

Table 6: Overview of the thesis case studies

Case Study	Section	Type of Distribution
Mars Surface Exploration	Chapter 3, Section 3.3	Spatial
Addition of Micro-rovers	Chapter 3, Section 3.4	Spatial
MSL Redesign	Chapter 3, Section 3.5	Spatial
Lunar South Pole Exploration	Chapter 4	Spatial, with SEXTANT
Europa Exploration	Chapter 5	Temporal
Mars Sample Return (ascent and return)	Chapter 6	Spatial and Temporal

The starred studies in Table 6 represent the five main case studies of the thesis. The first case study involves a higher level investigation of the effects of different aspects of spatial distribution and fractionation on a system. Vehicles having the size of the Mars Exploration Rovers (MERs) are used to

systematically investigate to explore the design space of spatially distributed vehicles, thus helping to achieve the second thesis objective. The second case study involves investigating how the Mars Science Laboratory (MSL), which landed on Mars in August 2012, might have been designed as a multi-vehicle system. The case study demonstrates the use of the framework and investigates the possible advantages of spatially distributed architectures with dependent and coordinated vehicles to achieve the goals of MSL [2]. The third short case study addresses the third thesis objective by demonstrating how the performance of coordinated spatially distributed vehicles can be evaluated using a path-planning tool called SEXTANT. The fourth case study explores the effects of temporal distribution on mission architectures, using the current goals for the exploration of the Jovian moon Europa as the motivation [9]. Finally, the fifth case study investigates the effects of using both spatial and temporal distribution when trying to achieve highly complex mission objectives. The ascent and return portions of NASA's Mars sample return (MSR) campaign are used as the basis for this case study [6].

## **1.3 Literature Review**

Having defined the research objectives, this section describes the context of the thesis within the body of literature. The latter is split into two major areas, reflecting the underlying theory and the application of the thesis, respectively. The first section deals with existing literature and theory for multi-vehicle systems in systems architecture and engineering. The second details a range of tools and methodologies that have been developed and used for the modeling of planetary exploration missions. Each subsection concludes with the identification of a literature gap to be filled by this thesis.

### **1.3.1 Multi-Asset Systems Theory**

In Systems Engineering, there are two main fields that deal with systems containing multiple assets, or vehicles. The first is Systems of Systems and the second is the field of distributed systems. These fields sit at opposite ends of the spectrum in terms of how heterogeneous the vehicles within each system are, and how the systems are designed and managed. An overview of both fields is given in this section, with a particular emphasis on the trade space exploration methodologies that have been developed to evaluate them.

#### **1.3.1.1 *Systems of Systems***

The field of Systems of Systems (SoS) is wide and varied, with views coming from the technical design, enterprise engineering and management standpoints. With no single authority on the matter, and

since it is a field that is still in its developing stages, [37-38] there are also several different definitions of what a SoS is. This section offers a succinct overview of the field and of the efforts to develop a unified SoS theory.

SoS theory takes its origins from the Department of Defense (DoD) [36-37], where it is used to manage different assets to address broad “user capability needs.” An example of a SoS, the Military Satellite Communications Systems Directorate (MILSATCOM), is shown in Figure 3. MILSATCOM develops, acquires and sustains space-enabled, global communications capabilities to support national objectives. [39]

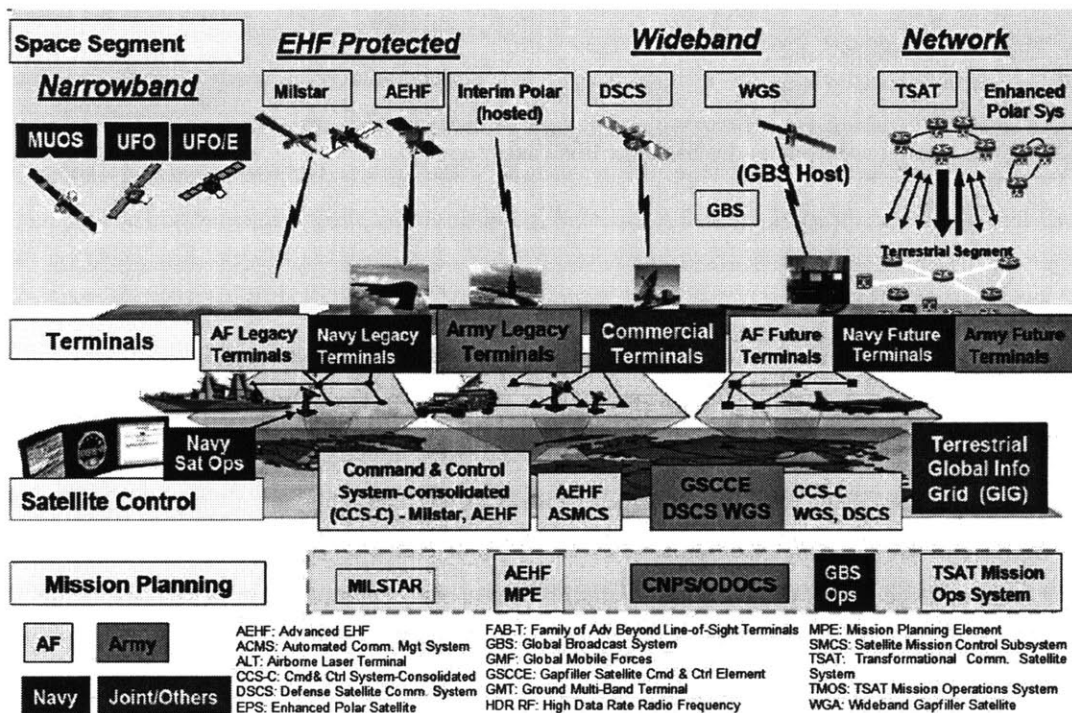


Figure 3: MILSATCOM systems and owners [40]

More recently, there has been an increased interest in using SoS to achieve synergy between independent systems in order to achieve greater overall system performance in fields including defense, security, aerospace, space, manufacturing, service, environmental systems and disaster management. [41], [42], [43] SoS is believed to more effectively implement and analyze large, complex, independent and heterogeneous systems working (or made to work) cooperatively. [44] Multiple definitions for SoS are available in the literature. Three of the most holistic and widely accepted ones are presented in Table 7. The key concept is that the individual systems within SoS are independent and are operated separately. Each of the systems often fall under different jurisdictions and are brought together to provide greater value than they would separately.

**Table 7: Definitions of Systems of Systems**

<b>Author</b>	<b>Definition</b>
INCOSE [45]	SoS applies to a system-of-interest whose system elements are themselves systems; typically these entail large scale inter-disciplinary problems with multiple, heterogeneous, distributed systems
SoSE Guide [38]	A set or arrangement of systems that results when <i>independent</i> and useful systems are integrated into a large system that delivers unique capabilities
Maier [46]	A system-of-system is an assemblage of components which individually may be regarded as systems and which possess two additional properties: operational independence of components, and managerial independence of the components

There are also several descriptive characterizations of SoS presented in the literature, explaining how SoS differ from traditional systems. Sage and Cuppan [47] have a similar view to Maier's and propose that SoS have the following five characteristics: (1) operational independence, (2) managerial independence, (3) geographical distribution, (4) emergent behavior, and (5) evolutionary development. Boardman and Sauser [48] have a similar list to define SoS, with the following properties: autonomy, belonging, connectivity, diversity and emergence. DeLaurentis proposes "networks" and "trans-domain" as two additional properties [49], where "networks" defined the connections between independent component systems within a SoS and "trans-domain" suggests that SoS incorporates a range of domains beyond just engineering. Finally, Sage and Biemer [50] also added two characteristics to the list of properties that differentiate SoS to monolithic systems: adaptation and self-organization, which are similar to the concept of evolutionary development, suggesting that the system changes over time to adapt to changes in functional needs.

Systems of Systems Engineering (SoSE) is a new field developed to deal with the added complexity that exists in SoS. It made its first appearance in 1991, when Eisner [51] presented the differences between traditional systems engineering and SoSE, and discussed three key aspects of SoSE: Integration Engineering, Integration Management and Transition Engineering. The Defense Acquisition Guidebook [52] then defined SoS as dealing with "planning, analyzing, organizing, and integrating the capabilities of a mix of existing and new systems into an SoS capability greater than the sum of the capabilities of the constituent parts." Finally, Keating et al. [53] point out that SoSE primarily deals with methods that have a multidisciplinary focus and an iterative approach, with a decreased focus on optimization, as compared to traditional systems engineering.

Most of the methodologies presented in the literature have been qualitative and descriptive of existing SoS. Examples of the development and implementation of existing systems of systems include the Space-Based Infrared System program [54] and GEOSS [55], [56]. However, more recently, Chattopadhyay [57], [58], [59], [60], [61] put forward a quantitative engineering methodology to evaluate systems of systems, based on Multi-Attribute Utility Theory (MAUT), which she illustrates with a case study

bringing together existing observation systems and a new spacecraft, to meet a range of diverging stakeholder needs. In parallel, Shah [62], [63] concentrated on reconciling stakeholder needs and translating them into systems-of-systems requirements. In her approach, Chattopadhyay used a range of metrics to evaluate the potential architectures. These include utility (or how well the system meets the different stakeholders' requirements), benefit-cost perception, likelihood of perception, attributed combination complexity and cost. There are several limitations with this methodology which make it inapplicable to the problem at hand. First, the methodology concentrates on enticing stakeholders to collaborate with their existing systems, and on filling gaps in performance with additional spacecraft, rather than being a "ground-up" methodology. The trade space of spacecraft explored for each problem is highly constrained by the design of the existing systems (the entire possible trade space is not generated) and the model does not offer enough granularity and fidelity. Additionally, the complexity metric is loosely defined with "low," "medium," and "high," complexity labels depending on whether the data from different systems is shared, time-averaged or fused. The complexity metric does not accurately demonstrate the increase in system complexity (and thus cost) when spacecraft are built to collaborate closely and where more than just data is shared between systems.

### 1.3.1.2 Distributed Systems

The concept of distributed systems emerged from the field of computer science, where distributed systems consist of multiple autonomous computers communicating through a network, to achieve a common goal. In distributed computing, the goal or problem is divided into multiple tasks, each one of which is addressed by one or more computers, thus moving away from the concept of using large, expensive mainframes to solve these types of problems [64], [65], [66].

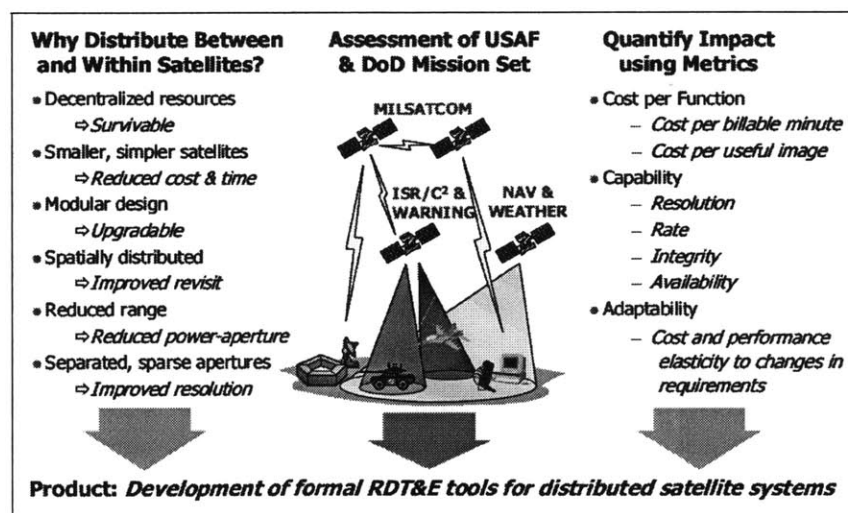


Figure 4: DSS research program overview slide [34]



Inspired by this approach, the Distributed Satellite Systems (DSS) program, a joint program between the MIT Space Systems Laboratory (SSL) and the Air Force Research Laboratory (AFRL), was created to investigate the opportunities arising from replacing single, large, expensive satellite programs by a network of smaller satellites that collaboratively execute the same mission more cost-effectively. Shaw [34] describes a distributed satellite system as a “system of multiple satellites designed to work together in a coordinated fashion to perform a mission.” Notably, these satellites are often *homogeneous*. The MIT-AFRL DSS research program aimed at quantitatively demonstrating that this methodology could be feasible for a satellite system. An overview of the program is presented in Figure 4.

In order to achieve this, a systems engineering methodology, called the Generalized Information Network Analysis (GINA), was developed [67] to create a model of the space system to be architected. GINA uses an information network analogy, where it assumes that the purpose of all Earth-orbiting spacecraft is to “push” or “pull” information. GINA uses four metrics to evaluate the trade space: cost, capability (in terms of isolation, rate, integrity and availability), performance (which is the probability of satisfying requirements for the capability parameters) and adaptability (the sensitivity to changes). GINA differs from the approach needed to deal with the problem at hand, since it assumes that there is only one mission goal (to transfer information). Additionally, the network analogy does not readily translate over to science-driven missions. The method also does not account for the increase in system-level complexity when multi-vehicle systems are used, and the metrics put forward are specific to systems whose purposes are solely to relay information from one agent to another. It does not allow for the evaluation of different science returns when a variety of payloads are used on the spacecraft.

The Multiobjective, Multidisciplinary Design Optimization Systems Architecting (MMDOSA) methodology was then developed to demonstrate that DSS design problems can be formulated mathematically as optimization problems and solved to balance the system objectives and constraints during the conceptual design phase. [68] This methodology was applied to the military, civil and commercial domain through case studies on TechSat 21 [69], [70], Terrestrial Planet Finder (TPF) [71], [72], [73] and broadband communication.

Fractionated spacecraft systems are a type of distributed systems, where distributed spacecraft interact with each other through more than just communication. The first research directly assessing fractionated spacecraft was published in 1984 [74], where Molette argued that although fractionation increases the mass of the system, the benefits in terms of adaptability, growth potential, flexibility, orbit maintenance and availability far outweigh this increase in mass. From 2004 to 2008, Brown et al. [33], [75], [76], [77], [78] published several papers on the effects of fractionation on Department of Defense (DoD) spacecraft.

Overall, the papers showed some trends in potential reduced lifecycle costs and other benefits similar to those identified by Molette, but again at the cost of increased mass.

In parallel, work was conducted in academia, using Multi-Attribute Tradespace Exploration (MATE) to evaluate fractionated systems [79], [80]. Mathieu [81], [82] assessed the cost and benefits of several fractionated spacecraft relative to a comparable monolithic spacecraft. The major conclusions of her research are that fractionated spacecraft can, in certain situations, provide more benefit than monolithic spacecraft. O'Neill [83], [84], [85], [86] developed a quantitative methodology to assess the impacts of various fractionated spacecraft architecture strategies on the lifecycle cost, mass, propellant usage, and mission lifetime of pointing-intensive, remote sensing spacecraft. Overall, he found that fractionated spacecraft were sometimes less costly than the monolithic equivalent and, in some cases, could even lead to fuel savings. However, his approach was limited because he assumed that the payload had to be contained within one vehicle, and that the value provided by the spacecraft was constant (what varied was the lifecycle cost). Lafleur and Saleh [87], [88] also developed a tool (GT-FAST) to enumerate fractionated spacecraft systems and evaluate the cost and benefits of such systems. The trade space generation component of GT-FAST uses traditional enumeration techniques which could directly be used for the work at hand. However, they put forward twelve metrics, as shown in

Table 8, for the trade space evaluation of fractionated spacecraft. In this table, metrics with fine resolution have some quantitative analysis associated with them whereas coarse metrics are qualitative. It can be seen that the metrics with higher resolution focus on programmatic aspects, and that performance and value return is secondary (in their problem formulation, return is more or less constant). Furthermore, while the spacecraft can be launched separately, they are expected to operate all together at the same time. The methodology therefore allows for the evaluation of a different problem than that put forward in this document. Specifically, it does not account for large-scale *spatial* or *temporal* distribution and thus is not directly transferable to the problem at hand.

**Table 8: GT-FAST metrics [88]**

<b>Metric</b>	<b>Resolution</b>
Ground signature minimization	Coarse
Payload performance	Coarse
Program cost	Fine
Programmatic risk	Coarse
Incremental launches	Fine
Time to operational capability	Fine
Manufacturability	Fine
Upgradeability	Fine
Relevance to customer	Fine
Robustness to failure	Coarse
Robustness to threats	Fine
TRL	Fine

This work led to the System F6 (Future, Fast, Flexible, Fractionated, Free-Flying) Program, led by the Defense Advanced Research Projects Agency (DARPA) [20], with a long-term objective of demonstrating that a monolithic spacecraft can effectively be replaced by a set of smaller spacecraft modules, that is, a fractionated spacecraft. Large-scale implementation of the work resulting from the DARPA F6 Program could lead to a significant shift in the design, development, deployment, and subsequent operation of spacecraft for commercial and military space missions. The first phase of this program ended in 2009, with the development of four architecture tools (described in the next section), and the program itself is still ongoing.

### 1.3.1.3 Gap Analysis I

In this section, it has been shown that SoS theory is able to deal with collaborating heterogeneous systems. However, these systems are typically built by different agencies and thus are under different management and are usually *retroactively* made to collaborate with each other. Often, work in SoS deals with emerging properties at the interfaces, or relates more closely to the field of logistics and strategic planning than that of systems architecture per se. Furthermore, mission goals for SoS are more loosely defined and evolve over the lifetime of the system. The primary goal of SoS is not maximizing return for a given cost, but rather it is to offer a compromise when dealing with diverging stakeholder needs. SoS theory is therefore too broad and does not provide enough granularity to compare specific architectures for well-defined goals. However, the holistic approach presented in the SoS literature is a valuable way to address *heterogeneous* systems and is a good starting point for the framework presented in this document.

On the other hand, distributed systems deal with very specific mission goals, and offer a way to reduce cost and improve performance, reliability, survivability and upgradability. In particular, fractionated spacecraft share functionality in order to increase system robustness. However, distributed systems only consist of one vehicle type, and are typically homogeneous. They are also only *spatially distributed*, and the current models for distributed systems do not deal with *temporal distribution*. The latter is a limitation that was indicated by Jilla as a suggestion for future work. [68]

Although there are some examples of systems that somewhat span the range between SoS and distributed systems by putting forward teams of vehicles for exploration [12], [13], [89], they are all qualitative single point designs. There is no complete formal and quantitative framework to deal with the problem described earlier in this document. Consequently, the first gap in the literature is that, in systems theory, there is no framework to evaluate trade spaces of multi-vehicle architectures for science-driven missions, where the vehicles are heterogeneous, of different types, and potentially launched sequentially to address a given set of mission goals.

## 1.3.2 Conceptual Design Tools

This section presents three types of tools that are used in the early conceptual design phase: trade space exploration tools, vehicle modeling tools and path-planning and validations tools.

### 1.3.2.1 Trade Space Exploration Tools and Methodologies

The field of design methodologies for exploring the trade space of feasible architectures aims to enable exhaustive, consistent, rigorous, and value-centric exploration of architecture trade spaces. Several new methodologies have been developed over the past decade. The methodologies described in this section include MATE-CON, GINA, MMDOSA, VCDM, AGD and OPN, and provide a broad overview of the types of methodologies that are available in the literature.

The Multi-Attribute Tradespace Exploration (MATE) methodology was developed by Ross [90] to formally solicit and capture the stakeholder preferences and explore the utility-cost trade space. It was further developed into MATE with Concurrent Design (MATE-CON) [79], [91], which uses an Integrated Concurrent Engineering (ICE) environment to enable convergence on a solution that satisfies user needs. The Generalized Information Network Analysis (GINA) methodology uses a network analysis theory analogy to evaluate satellites systems. [34] MATE and GINA were then combined by Jilla [68], [92], [93] to form the Multiobjective, Multidisciplinary Design Optimization Systems Architecting (MMDOSA) methodology. MMDOSA uses principles of Multidisciplinary Design Optimization (MDO) to evaluate distributed satellite systems using a metaheuristic optimization algorithm.

A different type of trade space exploration method is the Architectural Decision Graph (ADG), which is a decision-based method where architectures are formed through a sequence of decisions. [94] This methodology includes decision nodes, for each of which there are option nodes. Thus the generation of a trade space of options occurs through the enumeration of the decisions needed to be made to attain the final design. Another example of a more formal decision-based architecting methodology is the Object-Process Network (OPN) modeling meta-language, developed by Koo and Crawley [95], [96].

A set of Value-Centric Design Methodology (VCDM) tools were developed as part of the Phase I of above-mentioned DARPA-F6 program, a version of each of which was made publically available through the DARPA Tactical Technology Office System F6 website. [20] Four tools were developed independently by different industry-led teams to quantitatively assess the risk-adjusted, net value of fractionated spacecraft, relative to comparable monolithic spacecraft. The four tools, and their respective industry leaders, are listed in Table 9 and additional detail can be found in [97].

**Table 9: Phase I VCDM tools [97]**

<b>Team</b>	<b>Tool Name</b>
Lockheed Martin Company (LM)	System Value Modeling (SVM) Tool
Northrop Grumman Corporation (NG)	SVM Tool (Space Architecture Design Tool with System Value Modeling Tool)
Orbital Sciences Corporation (OSC)	Pleiades Innovative VCDM Optimization Tool (PIVOT), uses GT-FAST [87], [88]
Boeing Company (BC)	Risk Adjusted, Flexible, Time Integrated, Free-Flying, Multi-Attribute Tradespace Exploration (RAFTIMATE)

In addition to these tools, since systems architecting problems often have conflicting objectives, a set of methodologies exist to help balance the tradeoffs between these objectives. Multi-objective optimization can be used to establish non-dominance. A feasible solution is non-dominated if and only if there exists no other feasible solution that is better than or equal to the former in all metrics simultaneously and is strictly better than the former in at least one metric. [98] Other multiple-criteria decision making algorithms include the Analytic Hierarchy Process (AHP), where a hierarchical method is used to make decisions based on pairwise comparisons [99] and Multi-Attribute Utility Theory (MAUT), which is an extension of utility theory. [100] Many of the concepts of multi-criteria decision making are used in this thesis, although the metrics used in the decision making process are specific to multi-vehicle architectures. Finally, in addition to all these methodologies, a list of industry-specific systems engineering tools is offered in [68].

### **1.3.2.2 Planetary Exploration Vehicle Modeling Tools**

In order to ensure that a concept is feasible and to evaluate mission properties in an architecture trade space, an engineering modeling tool with *reasonable* accuracy is required ( $\pm 30\%$  uncertainty). Pre-phase A is the first step of the design process, where trade space exploration is performed. When designing vehicles in this phase, there are two main types of spacecraft models: parametric models and physical models. Parametric models use historical data to establish the properties and estimated mass of a system. They typically have low fidelity (20-30% error), but still allow for different technologies and payload packages to be traded. Parametric models provide a reasonable estimate for mass of spacecraft designed for deep space conditions. [101] Parametric models for deep space spacecraft tend to rely on historical data from other, more in depth, studies due to the fact that only very few spacecraft have been built for deep space. This adds an element of uncertainty to the trade space evaluation.

Physical models are typically modular, where each subsystem is designed separately, from first principles or using physical rules-of-thumb. [102] Physical models offer higher fidelity (10-20% error) and are particularly useful for planetary surface vehicles, which are more deeply affected by the environment and concept of operations that orbiters and flybys. Most NASA centers possessing an

integrated design center develop their own physical model. However, a few models are also openly available in the public literature; these are presented in Table 10.

**Table 10: Parametric models of planetary surface vehicles available in the public literature**

Author	Model
Lamamy [24], [103], [104]	Rover model
Cunio [105]	Hopper model
Bailey [106]	Lunar lander model
McCloskey [107]	Walking & hybrid (walking + roving) vehicle model
Hong [108], [109]	Power model for rovers

The limitation with these models is that they only allow for the design of one vehicle at a time. In collaborating systems, especially if the vehicles are fractionated, mass often shifts from one vehicle to another. For example, if one system is recharging another, the first system will be larger, whereas the second will be much smaller. However, both vehicles will need additional infrastructure to enable the sharing of power. When exploring the trade space of multi-vehicle systems, there is therefore a need to add options to these physical models to account for the mass changes produced by function sharing.

### 1.3.2.3 Path-Planning Tools

Path-planning tools allow the mission designers to understand how multiple assets can be used on the surface of a planet and how they can work together to achieve the mission goals. Moreover, the availability of environment information, such as the illumination properties, communication visibility and slope profiles can help the designer to best utilize the vehicles' resources.

Traditional path planning, such as that performed during the Apollo lunar missions, aimed at maximizing scientific return by first establishing the locations of scientific interest. Traverses were then planned by hand, to meet the science requirements without violating the given constraints, using photomosaics and topographic maps from previous missions. This led to a great deal of uncertainty in the mission duration and traverse energy requirements, and did not allow for any in-situ path re-planning. More recently, the Mars Exploration Rovers (MERs) *Spirit* and *Opportunity* also heavily relied on ground station support to perform their traverses. [110] Although they did benefit from the use of some decision support aids, these were used for temporal scheduling, rather than path planning. The rovers' every move was planned from the ground and uploaded as a batch of commands to each of the rovers. This inevitably led to inefficiencies in the use of the rovers' time and energy, since the evolution of the environment during the traverse was not formally taken into account. Furthermore, in both these examples, when changes in the traverse were needed, neither the Apollo astronauts nor the Mars rovers had any self-contained computational ability to re-plan their journey. They were reliant on data from the ground operation center, which in turn led to more delays, risks and reduced exploration efficiency.

Although the current approach to planetary surface operations has been successful thus far, the operation of multiple coordinated assets on a planetary body will require much more pre-mission planning and on-board autonomy in order to maximize the science return. To this end, the thesis will build upon a path-planning tool, the Surface Exploration Traverse Analysis and Navigation Tool (SEXTANT), which was developed at MIT. The development of SEXTANT began at MIT in 2001. The first implementation of SEXTANT was called the Geologic Traverse Planner, developed by Carr [111]. With this tool, the user selected ordered waypoints over a terrain digital elevation model, and the Geologic Traverse Planner drew a straight-line path between the waypoints. Márquez [112], [113] then created a new tool, which greatly expanded upon the capabilities of Carr's Geologic Traverse Planner. The goal of this system, called the Planetary Aid for Traversing Humans (PATH), was to experimentally investigate the effects of two different levels of automation on a user's performance and situational awareness. Development of PATH was continued by Lindqvist [114], who united the optimization capabilities of PATH with the mapping features of the ArcGIS geographical information system (GIS) software suite. In this integrated mission planner, ArcGIS served as the interface, allowing the user to view the terrain and specify waypoints directly on a two- or three-dimensional (2D or 3D) terrain map. Essenburg [115] then combined the functionality of both into one program, called Pathmaster. This tool improved the user interface for the PATH algorithms, making it easier to plan traverses and view the desired information. The main Pathmaster interface was a 3D elevation map over which the user could modify obstacles and waypoints and see the generated traverse. The Pathmaster interface was then expanded and modified by Johnson [116], [117] to serve as the current basis of the SEXTANT interface. In particular, Johnson added the ability for SEXTANT to calculate the illumination properties during the traverse, thus enabling the computation of the thermal load on suited astronauts and the power properties of solar powered rovers, over the entire traverse.

This thesis will enhance SEXTANT to allow it to be used as a simulation tool for *fractionated* and *spatially distributed heterogeneous* planetary surface vehicles. Path planning tools are primarily used to assist in the planning and operations of multi-vehicle missions. However, such tools can also contribute in the design of planetary surface assets themselves. In current system design procedures, the specific details of operations are often an after-thought, where the path taken and the vehicle operations are adapted in order for the constraints from the vehicle design to be met. This lack of feedback loop between the detailed concept of operations and the vehicle design often leads to lower operational efficiency and decreased science return. Rapid path-planning tools such as SEXTANT allow for different traverses to be investigated during the design phase of the mission, giving the designer an understanding of the main challenges associated with exploring particular regions of a planetary body. The impacts of changing certain design parameters, such as the size of the batteries or the speed of the vehicle, can also be easily

investigated. Thus, this tool enables the designer to use the properties of the environment during the mission to inform and validate the design of the vehicle.

#### 1.3.2.4 Gap Analysis 2

From the literature that has been explored in this section, it can be observed that, although there is a range of tools available for the modeling of planetary exploration missions, none of them explicitly allow for the design of multi-vehicle systems. They do not account for the effect of *collaboration* within the system on the mission properties, and do not enable architectures where multiple different *types* of spacecraft, which are *temporally* or *spatially distributed*, are used to achieve the mission goals, to be considered in the trade space exploration process. This thesis therefore builds upon available tools to enable the exploration of multi-vehicle architectures.

## 1.4 Overview of Thesis

The remainder of this document presents the framework developed for evaluating multi-vehicle architectures against their monolithic counterparts and provides case studies as examples of when and how multi-vehicle architectures are beneficial for planetary exploration. Chapter 2 provides the details of the framework developed, as well as a description of all the evaluation metrics. Chapter 3 contains the first two case studies, the first being based on the MERs and the second on MSL. This chapter investigates the effects of spatial distribution on a system. Chapter 4 introduces the path-planning tool SEXTANT and demonstrates how it can be used to evaluate the performance of spatially distributed multi-vehicle systems in their operational environments and to obtain more accurate estimates of vehicle properties. Chapter 5 investigates the effects of spatial distribution through the Europa exploration case study. Chapter 6 combines both spatial and temporal distribution in the MSR case study. Finally, Chapter 7 summarizes the conclusions of this research, the contributions that have been made, and the suggestions for future work in this arena.

Overall, the thesis provides missions designers with a framework for evaluating multi-vehicle architectures. It also demonstrates how this framework can be used to rapidly evaluate such systems against monolithic vehicles to provide an understanding of how different types of distributed systems behave. The metrics developed within the framework are shown to successfully address the hypothesis put forward in Table 5 and it is demonstrated that metrics that are not mass-based can provide valuable insights into the advantages and limitations of multi-vehicle systems. For example, even though multi-vehicle systems do suffer from an inherent mass penalty (each platform has a minimum mass), through



the many case studies they are shown to be able to provide higher science benefit and increased robustness to failure as compared to the monolithic equivalent, and sometimes do so at a lower cost. Finally, the application of the framework in the case studies presented in Chapters 5 and 6 is shown to yield valuable results for the Europa and Mars Sample Return design teams and led to recommendations being made for these ongoing missions.



# Chapter 2

## FRAMEWORK AND METRICS

### 2.1 Overview of Framework

This chapter describes the general framework developed to enable the evaluation of architectures with multiple distributed vehicles of different type in early mission concept design. An overview is shown in Figure 5. It consists of five different steps, with the fifth step being optional. These are: (1) problem decomposition; (2) trade space generation; (3) trade space evaluation; (4) trade space visualization and exploration; and (5) mission concept simulation. The first four steps are described in detail in this chapter; the fifth step is discussed in Chapter 4.

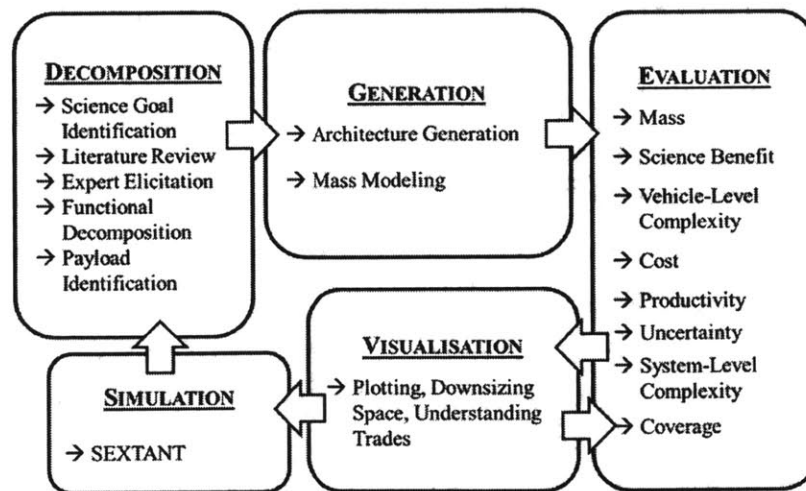


Figure 5: Overview of framework

## 2.2 Functional Decomposition and Trade Space Generation

The first two stages of the process are the problem decomposition and trade space generation. An overview of the process required to complete these steps is presented in Figure 6.

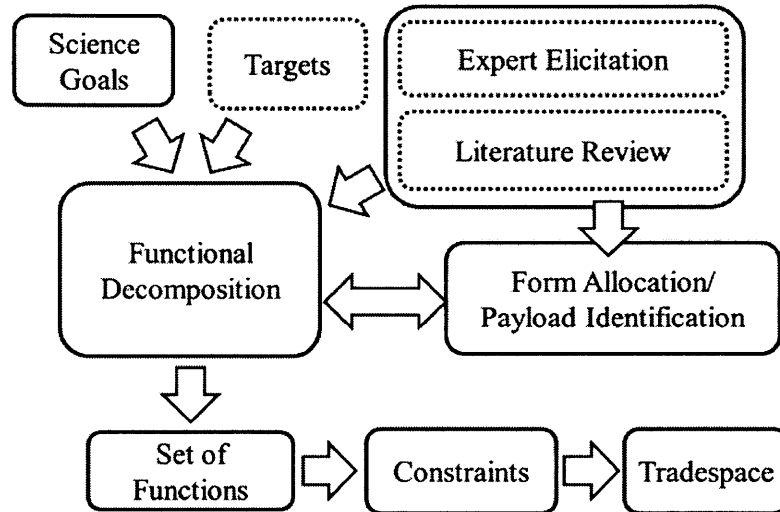


Figure 6: Overview of the problem decomposition process

### 2.2.1 Functional Decomposition

The first step of the problem decomposition process is to identify the science and technology demonstration or engineering goal(s) for the mission. The science goal(s) can be decomposed into science objectives and then into specific investigations. By going through the concept of operations required to achieve the goals, a functional decomposition can then be performed. This entails identifying all the *functions* the vehicle must perform in order to achieve the science and technology demonstration goals and the way they will achieve these functions (i.e. the *form*). Functions are the activities, operations and transformations that cause, create or contribute to performance (i.e. to meeting goals). In the case of the science-related functions, science investigations can then be mapped directly to science instruments.

If different types of vehicles are being considered in the trade space, this must be repeated for each type (note that it is possible that some types cannot accomplish all the goals). This process is very similar to that of forming a science traceability matrix, except that this matrix allows for more than one vehicle type, with each form being type-specific.

During this decomposition process, consulting the literature and conversing with expert scientists can help identify different types of technologies or payload. In many cases, more than one instrument can achieve a particular science goal. Interviewing a range of scientists can help provide an understanding of

the advantages and limitations of all the instruments, as well as how they are operated. This information is eventually used during the architecture evaluation process. Consulting the literature, or past studies for a similar target (if available), can also help identify what technologies have previously been considered for this problem (e.g.: solar power vs. Advanced Stirling Radioisotope Generator (ASRG)). The functional decomposition process is therefore somewhat iterative. Once it is complete, the output of this step is a set of functions the vehicle must perform, as well as different payloads and technologies (i.e. forms) that can achieve these tasks, along with the relative value of each of these forms.

### 2.2.2 Trade Space Generation

Generally, when generating a trade space, the full enumeration of the possible function combinations is performed. This typically generates very large trade spaces. In order to reduce the size of the trade space and limit the space being explored to architectures that make physical sense, the functions derived in the functional decomposition process are categorized into different types of functions. Functions can all be classified into two distinct categories: Value Delivery (VD) functions, that provide the primary value associated with the mission objectives (science or technology goals), and supporting functions. The forms associated with VD functions are mostly science instruments. Supporting functions are functions that do not directly provide value, but are needed for value to emerge. Examples of supporting functions are “long-range traversing” and “generating energy”. The difference between these two types of functions is shown in the Object-Process Diagram (OPD) [118] shown in Figure 7.

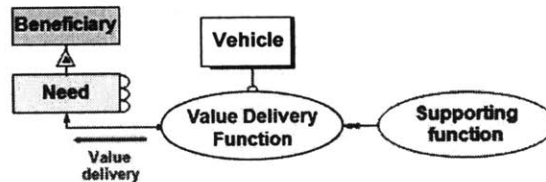


**Figure 7: OPD showing the difference between value delivery and supporting functions**

Supporting functions can be further separated into Essential Supporting (ES) functions, which every vehicle has to have in order to operate, and Supplying Supporting (SS) functions, which one vehicle can theoretically provide to another. In other words, SS functions can be shared from one vehicle to another, and ES ones cannot. Often, whether a function is essential or not is dependent on the technology available. Moreover, sharing a function often leads to losses in efficiency in achieving that particular function, but can increase the overall system efficiency. For example, “generating energy” could be transformed into the SS function of “transferring energy” where one vehicle would generate additional energy and transfer it to another. This would rely on a technology able to transfer energy from one system to another being available (e.g.: energy beaming or safe docking). Energy beaming leads to additional losses, but if one vehicle were to beam energy to another, the latter would not need to carry an on-board

source of power generation. It would be lighter and less complex, thus possibly leading to a more efficient overall system. The difference between these two categorizations is shown in Figure 8.

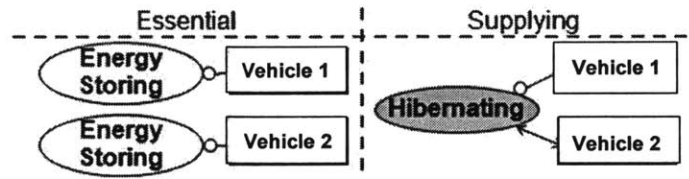


Figure 8: OPD showing the difference between ES and SS functions

After the functions have been derived and categorized, the architecture trade space can be generated. Only SS and VD functions can be split across vehicles. ES functions must be present on each vehicle. The space is generated by setting a minimum and maximum number of vehicles and generating the possible combinations of forms associated with the SS and VD functions. In order to limit the size of the space, constraints can be imposed on the trade space, such as enforcing that certain functions be on the same vehicle (if the payload is highly integrated for example) or that two functions be on separate vehicles (to increase redundancy/productivity). This process of functional decomposition and categorizing the functions is explicitly demonstrated in Chapter 3 to illustrate the process.

Upon the completion of the architecture trade space generation, the architectures need to be evaluated against each other, to understand the trades that occur when replacing single vehicle systems with multi-vehicle ones. This evaluation process is described in the next section.

## 2.3 Trade Space Evaluation

In order to compare multi-vehicle systems to monolithic systems on a one-to-one basis, a set of evaluation metrics was developed. These metrics include: mass, science benefit, complexity, cost, productivity, mission success, coverage and uncertainty. Although not all metrics are used in every single case study, they are all required to evaluate the hypotheses described in Chapter 1. This section details the purpose of each of these metrics, how they were derived and how they are defined in general terms.

### 2.3.1 Mass

The mass of a system has traditionally been one of the leading cost drivers and metric by which architectures have been evaluated. Even though mass is not believed to be the only driver in the cost and science return of multi-vehicle architectures, it is still an important metric since it drives procurement and launch vehicle costs for example. The system mass must therefore still be considered in the evaluation process. As explained in Chapter 1, there are two types of mass models: physical models and parametric models. Typically, physical models offer higher fidelity, but this comes at the cost of increased

computational complexity and cost. Mass models are case study specific, since they are dependent on both the target planetary body and the type of vehicle being considered in the trade space exploration. The different models used are therefore discussed on a case-by-case basis.

### 2.3.2 Science Benefit

In all cases thus far, missions to other planetary bodies in the solar system have primarily been used for technology demonstration and for performing science. Since the return from such missions cannot be calculated in monetary terms, a metric was developed to reflect the relative perceived benefit between a range of different architectures. The science benefit metric is unitless and identifies the ability of each architecture to meet the mission's science and technology goals. For a given cost, a higher science benefit leads to a higher expected return for the overall mission. Many science benefit-type metrics are available in the literature. [24], [106], [119], [120], [121], [122] However, it was found that many of these are too complex to enable efficient computation (and often overly complex considering the lack of specificity in requirements for planetary exploration missions). On the other hand, the simpler metrics do not allow for synergies between instruments or the value of instruments on different types of platforms to be accounted for. Additionally, none of these metrics explicitly allow for the variation of the prioritization of each goal, nor do they enable the evaluation of the benefit returned in a multi-vehicle, collaborative system. A new metric, based on these previously developed metrics, was therefore developed and is defined in Equation 1.  $B_j$  is the benefit associated with an individual platform (or vehicle), and  $B$  is the benefit of the system as a whole.

$$B_k = K_{seq_k} \sum_{j=1}^n E_{j,k} \sum_{i=1}^m V_{i,j,k}$$

$$B = \sum_{k=1}^p W_k \cdot B_k$$

**Equation 1**

Where each of the following terms are explained in further detail in the remainder of this section:

- $V_{i,j,k}$  is the instrument value
- $E_{j,k}$  accounts for synergies between instruments
- $K_{seq_k}$  accounts for synergies between platforms
- $W_k$  is the weighting given to the science objective  $k$ .

$V_{i,j,k}$  is the perceived benefit provided by instrument  $i$ , on a platform  $j$ , for a given science objective  $k$ , based on the scale given in Table 11.

**Table 11: Value weightings scale**

Weighting	Meaning
0	Does not address science investigation
1	Touches on the science investigation
2	Partially addresses the science investigation
3	Addresses most of the science investigation
4	Fully addresses the science investigation
5	Exceeds the science investigation

However, having a duplicate of a given instrument in an architecture will not necessarily provide twice as much science benefit. Typically, the second instrument will provide less net value, except in cases where the two instruments can interact positively or when having more of the same type of data is more valuable than having data from a different instrument. Therefore, in cases where instruments are allowed to be duplicated across an architecture, the  $V_{i,j,k}$  value becomes a curve which can be read from to determine the additional value of the duplicate instrument in the architecture  $m$  is the number of instruments on a platform.

$E_{j,k}$  is a look-up table with entries that account for the added benefit that arises when there are synergies between instruments. This look-up table can either be in the form of a matrix where the entries are weightings for beneficial instrument interactions, or it can contain a set of rules defining increases in value when certain instruments are on a given platform.  $n$  is the number of platforms (or spacecraft).

$K_{seq_k}$  accounts for the increase in value that occurs if the new vehicle can work in combination with a functionality that has already been deployed. This can be used is when adding a vehicle as part of an independent, non-coordinated system (as defined in Chapter 1). The weighting can then help account for the additional value that is obtained by having to vehicles on a planet. For example, if vehicle A with a seismometer is landed in region C, and an identical vehicle B is then landed in region D a short period of time later, the value of the A-B system is more than double that of the A system, since the interaction of the two vehicles will provide additional science benefit.  $K_{seq_k}$  can also account for the increase in benefit that occurs when information from a precursor mission leads to a decrease in uncertainty about the science to be done at the target. For example, a precursor mission can help establish exactly which measurements should be taken, and in which range. This can reduce either the uncertainty associated with the potential benefit of instruments and/or it can increase the expected benefit of a given instrument.

$W_k$  is the weighting given to the science objective  $k$ . Each  $W_k$  is a number between 0 and 1 and the sum of all  $W_k$  is 1.  $p$  is the number of science goals for the mission.  $W_k$  values can be varied during the trade space exploration to understand the effect of the prioritization of mission objectives on the relative



value of the architectures. [101] This aspect of the metric directly enables the evaluation of how the priority assigned to an objective affects the choice of the architectures. The benefit values can be derived directly from the science traceability matrix, the literature or through interviews with the science definition team of the mission.

The science benefit metric can be validated by comparing the results to the relative values of existing point design studies (from Decadal Survey white papers, for example [6]), or by performing an additional round of expert interviews to ensure that the results obtained accurately reflects the scientists' understanding of the system.

### 2.3.3 Complexity

This thesis puts forward the idea that the potential benefits of multi-vehicle systems cannot be demonstrated through the use of traditional mass metrics and mass-based cost metrics. One argument is that the cost of a system is also correlated to its complexity. [123] Complexity is typically a symptom of highly integrated systems, where complexity emerges due to interactions between instruments, components or subsystems. The more demands are put on a system, the more complex it is likely to be. This thesis argues that in some cases, several systems that share a set of goals are less complex, easier to build and test, and less costly than one larger system acting on its own, even though the combined mass of the multi-vehicle system may be higher.

In order to illustrate this shift in complexity, two complexity metrics were developed and are described in this section:

- A) A *vehicle-level complexity metric* that evaluates the *design complexity* of each individual vehicle within an architecture, depending on the subsystems and instruments that each vehicle possesses.
- B) A *system-level complexity metric* that evaluates the interactions (if any) between each vehicle within an architecture. This metric reflects the *operational and structural complexity*.

#### 2.3.3.1 Existing Complexity Metrics

Historically, approaches have been developed to measure the complexity of both hardware and software systems [124], [125], [126], [127]. A range of complexity metrics, and methods for developing such metrics, are available in the systems architecture literature. Meyer [128] proposes a very simple way of calculating system complexity, where the number ( $N_p$ ) and types ( $N_t$ ) of parts, as well as the number of interfaces ( $N_i$ ) are each added up, and then multiplied together, giving the following complexity metric:

$$Complexity = (N_p * N_t * N_i)^{1/3}$$

Equation 2

The main issue with this “part-counting” metric is that it treats different parts and interfaces as being equal. However, in the work at hand, the difference between these is a key to improving the way planetary surface exploration is conducted.

Dori [118] describes complexity as “an attribute of a thing that determines whether it is simple or non-simple”. Although this description has no mathematical equivalent, it does portray that complexity can be something that is *perceived*. Essentially, the level of complexity is dependent on engineers’ ability to deal with it, and thus also depends on the level of expertise.

Suh [129], on the other hand, describes complexity as “a measure of uncertainty in achieving the specified functional requirements”. Indirectly, this means that the more information is needed to achieve functionality, the more complex the system will be. While on the surface this seems to be a reasonable description of complexity, it does not account for “clever engineering designs”, or the fact that there are several ways of achieving the same functional requirements.

Crawley [27] defines three types of complexity: essential complexity, which is the minimum amount of complexity required to deliver functionality; perceived complexity, which is the complexity perceived by the designer and/or user; and actual complexity. In order for a system to be successful, the perceived complexity must be below the human limits of comprehension, and the actual complexity should be as close to the essential complexity as possible. Many [130], [131], [132] have followed on from this initial work on complexity and have identified three dimensions of complexity, which are all positively correlated: functional complexity, which relates to customer requirements; organizational complexity, which relates to cost and schedule; and structural complexity, which is driven by functional complexity and in turn drives organizational complexity.

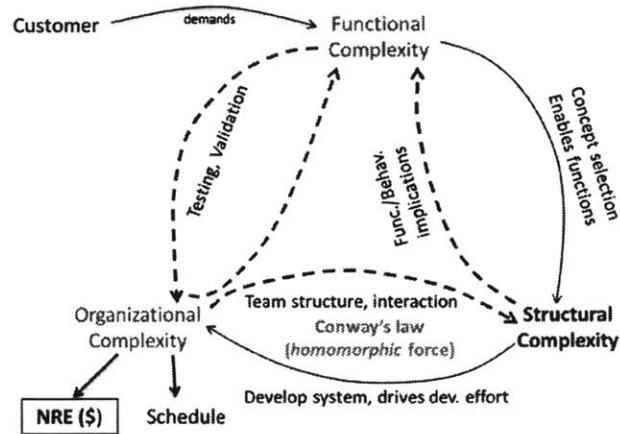


Figure 9: Three types of complexity [133]

In this particular case, we are interested in the structural complexity of the system. Within this type of complexity, Crawley [27], Sussman [134], Biedermann and Lindemann [135], [136] identified 5 measures

of complexity: the number and type of components, the number and type of connections, and the dependency structure (i.e. how the connections are arranged within the system). Kreimeyer and Lindemann [131] identified several quantifiers of the dependency structure of a system, including centrality/bus architecture; number and length of cycles; reachability; nesting depth; and entropy content, to name but a few.

Within these, Sinha [137] converged on the *graph energy* (i.e. the energy of the connectivity matrix, which is a binary matrix identifying the connections between each node in a system) as a measure of topological complexity. Sinha developed a structural complexity metric which, at the top level, can be written as:

$$C = C_1 + C_2 \cdot C_3$$

**Equation 3**

Where :

- $C_1$  is the complexity of the components of a system.
- $C_2$  is the complexity due to pair-wise component interactions.
- $C_3$  is the complexity due to topological formation (i.e.: due to the dependency structure).

More specifically, Sinha's complexity metric can be written as:

$$C(n, m, A) = \sum_{i=1}^n \alpha_i + \left( \sum_{i=1}^n \sum_{j=1}^n \beta_{ij} A_{ij} \right) \gamma E(A)$$

**Equation 4**

Where:

- $\alpha_i$  is the complexity weighting for component i.
- $\beta_{ij}$  is the weighting for the connection between component i and j.
- A is the binary connectivity matrix, where  $A_{ij}$  is 1 if two components are linked, and 0 if they have no interaction.
- $\gamma$  is a normalizing factor (1/n).
- $E(A)$  is the sum of the singular values of the A matrix:

$$E(A) = \sum_{i=1}^n \sigma_i$$

**Equation 5**

One of the biggest challenges in this equation is finding the correct weighting factors. Sinha proposes the use of the estimate cost of components. Alternatively, a variation of the complexity metrics discussed

earlier can be used as a starting point for these weighting factors. This thesis proposes the use of a set of weightings based on parameters that drive complexity and cost, as explained in the next sections.

### 2.3.3.2 Vehicle-level Complexity

The vehicle-level complexity metric accounts the  $C_1$  component of Sinha's complexity metric, where each vehicle is considered as one of the nodes or components of the system. Sinha uses cost to account for this component. However, it has already been established that no non mass-based cost metric exists to accurately be used in this part of the evaluation process. Therefore, the vehicle-level complexity metric was designed to account for the effects of mass, technology used, information gained from sequences of missions, vehicle type and conflicts between instruments or technology choices. These aspects have historically been shown to drive the cost of a mission. [138], [139] The vehicle-level complexity metric is defined in Equation 6. Complexity is calculated for all the vehicles and the whole sequence of missions. In the evaluation process, it can be normalized by the baseline vehicle's complexity or averaged for each architecture.

$$vehicle\ level\ complexity = K_{seq} \sum_{j=1}^m F_j \cdot E_j \cdot Mass_j \sum_{i=1}^n CW_{i,j}$$

**Equation 6**

Where:

- $CW_{i,j}$  is the complexity weighting for each instrument or technology choice  $i$  on a platform  $j$ . This weighting is based on the concept of cost-risk subfactors, which are normally used to assign additional budget reserves. [139] They are characteristics of a mission that are believed to drive complexity and cost.  $CW$  weightings vary depending on the mission/case study.
- $E_j$  is an additional weighting that accounts for conflicting requirements between instruments or technology options. Each time two components have conflicting requirements (based on the  $CW_{i,j}$  categories),  $E_j$  increases by two to five percent. (based on [138])  $E_j$  is essentially read from an upper triangular weighted connectivity matrix or a look-up table for the instruments, where each entry has a minimum value of 1.
- $F_j$  accounts for the difference in complexity between different vehicle types.
- $K_{seq}$  is the reduction in complexity that occurs when information from a precursor mission leads to a decrease in uncertainty for a subsequent mission.  $K_{seq}$  is a number between 0 and 1, and decreases as knowledge increases.
- $m$  is the number of instruments.
- $n$  is the number of platforms (or spacecraft) in an architecture.

An example of the  $CW$  weighting scheme used in Chapters 3 and 4 is shown in Table 12.

**Table 12: CW allocation scheme for instruments and key technologies**

Category	Levels	Weighting
TRL	1-4	+2
	5-6	+1
	7-9	0
Special Positioning/ Mechanism	Yes	+1
	No	0
Cleanliness Requirement	Yes	+1
	No	0
Data Rate	> 100kbps	+1
	< 100kbps	0
Thermal Requirement	Active	+1
	Passive	0
Power Level	> 10W	+1
	< 10W	0

### 2.3.3.3 System-level Complexity

Because spatially distributed vehicles explore collaboratively to accomplish the mission goals, the vehicle interactions cannot be ignored. Even if the vehicles do not interact in any way (e.g. if they do not share samples, or share power to name but a few), the vehicles have to interact with each other in order to avoid collisions since they are exploring the same site. The system level complexity is based on the  $C_2 \cdot C_3$  component of Sinha's equations. It illustrates the added system complexity that arises from this interaction and is defined in Equation 7.

$$\text{System - Level Complexity} = \frac{\varepsilon * (\sum_{j=1}^n \sum_{i=1}^m \beta_{i,j} A_{i,j})}{n}$$

**Equation 7**

Where:

- $n$  is the number of vehicles.
- $m$  is the number of functions on vehicle  $n$ .
- $\beta_{ij} * A_{ij}$  is the weighted connectivity matrix that describes the interactions between each vehicle.
- $\varepsilon$  is the graph energy, defined as the sum of the eigenvalues of the connectivity matrix  $A_{ij}$ .

The weighting  $\beta_{ij}$  is allocated to each incoming and outgoing link between two vehicles (directionality is important in cases where one vehicle provides a functionality to another) based on the types of interactions between the two vehicles, as commonly identified in a Design Structure Matrix (DSM). [136] These interactions are shown in Table 13. The weighting of a connection from one vehicle to another is the number of types of interactions there are between the two vehicles. It is to be noted that although the system-level complexity metric aims at demonstrating the effect of distribution on testing and operational cost, the correlation between system-level complexity and cost may not be linear. As discussed in Chapter 7, further testing is required to establish this correlation.

**Table 13: Types of interactions between vehicles**

Label	Type of Interaction
A	Mechanical Contact
B	Information Transfer
C	Mass Transfer
D	Energy Transfer

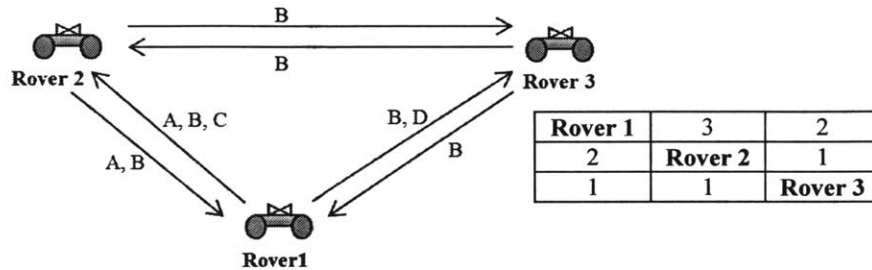


**Figure 10: Example of interactions between a 3-rover system.**

The table shows the weighting on the connection between two rovers (e.g. the connection from Rover 1 to Rover 2 has a weighting of 3)

### 2.3.4 Cost

Another architecture evaluation metric is cost. Because the complexity metric is correlated to both mass and interactions within the system, to first order, it can be correlated to cost for spacecraft and landers. However, depending on the mission, the cost estimate must also include launch vehicle costs, the cost of sending a “dead” weight to its destination and Entry, Descent and Landing (EDL) system costs, for example. The correlation between cost, complexity and mass must therefore be established for each case study and be anchored based on the (known) cost of the monolithic option for the mission. If the costs of other designs are available in the literature, they can also be used to help anchor the correlations.

Alternatively, a ground-up or parametric cost model can be used to estimate the cost of a mission.

### 2.3.5 Productivity

One of the other important aspects of planetary exploration missions is the ability of an architecture to achieve the goals (i.e. its ability to successfully complete the mission goals) and its productivity during the mission (i.e. the amount of science done). The performance of different architectures with respect to these metrics is non-trivial, especially since redundancy and emerging behaviors can affect them, and must therefore be carefully evaluated. One of the advantages of distributed systems is that they provide an opportunity to increase the mission reliability through the duplication of subsystems. In turn, this increases the productivity of the mission, since a more reliable system can operate for longer without failure. Reliability is defined as the probability that a system will be in a functional state at the end of the

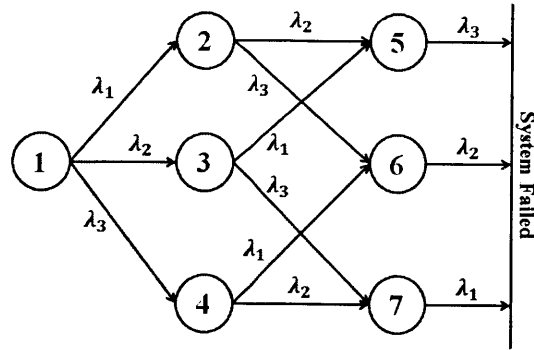
nominal mission. There are two distinct ways to increase a system's reliability: the component reliability can be increased, or redundancy can be added. In complex systems, reliability is therefore achieved by carefully trading component reliability with redundancy. Spatially distributed systems in particular intrinsically lend themselves to increased redundancy, which also means that higher risks can be taken in terms of component reliability to achieve the same system reliability as a monolithic system.

Although reliability is a key factor when designing a system, the ability of this system to continue to function in the event of a failure is also important, and this concept was explored in detail by Agte et al. [140], [141] In order to design a system that has as high productivity as possible, the system must be modeled and productivity must be analyzed in each possible state. A state is defined as the functional system that remains in the event of failure. Modeling the productivity of a system in each state requires two aspects: a method to model the productivity of a system given the system parameters, and a Markov, or state-transition, model of the initial system. [142]

A Markov chain, first developed by Andrey Markov, is a system which transitions from one state to another among a finite number of states. [143] It is a random process where, by definition, the next state of the system only depends on the current state and not the events that have occurred before it. It is commonly used to evaluate the performance of a system throughout its lifetime: as a system suffers a failure, its performance decreases with time. Therefore, a Markov chain can be used to evaluate the probability of the system being in different partially degraded states over its lifetime. More recently, Markov chains were shown to be useful tools for evaluating the performance of aerospace systems, and in particular distributed and non-safety critical aerospace systems, by Wertz. [72], [144] The Markov framework developed by Wertz to evaluate the performance of distributed interferometers is adapted in this thesis to evaluate the performance of spatially distributed systems over time. An overview of how Markov chains are built and evaluated is provided in the remainder of this section, and further detail can be found in any probabilistic systems analysis textbooks. [145]

#### **2.3.5.1 The *A*-matrix**

In Markov theory, it is assumed that the system starts in a state where all components are working (this is the initial state). The system then transitions from state to state (via intermediary states) when components fail, until complete system failure occurs (which is the final state). Given that these transitions will each occur at given rates rate ( $\lambda_i$ ), a state-transition matrix, also called the *A* matrix, can be computed. An example, where there are only 3 components that can fail, of a trivial state diagram, or Markov model, and its corresponding *A* matrix are shown in Figure 11.



$$A = \begin{bmatrix} -\lambda_1 - \lambda_2 - \lambda_3 & 0 & 0 & 0 & 0 & 0 & 0 \\ \lambda_1 & -\lambda_2 - \lambda_3 & 0 & 0 & 0 & 0 & 0 \\ \lambda_2 & 0 & -\lambda_1 - \lambda_3 & 0 & 0 & 0 & 0 \\ \lambda_3 & 0 & 0 & -\lambda_1 - \lambda_2 & 0 & 0 & 0 \\ 0 & \lambda_2 & \lambda_1 & 0 & -\lambda_3 & 0 & 0 \\ 0 & \lambda_3 & 0 & \lambda_1 & 0 & -\lambda_2 & 0 \\ 0 & 0 & \lambda_3 & \lambda_2 & 0 & 0 & -\lambda_1 \end{bmatrix}$$

**Figure 11: Example of a Markov Model and the Corresponding  $A$  Matrix**

For distributed systems in this thesis, it is assumed that the system is degraded when VD functions fail. There are multiple types of failures that could lead to the loss of a VD function, and these must be accounted for when setting up the state transition diagram. As an example, the loss of the ability of the system to provide a generic VD function ‘X’ can be due to any combination of the following events:

- Loss of the payload or technology providing ‘X’ in the system
- Loss of communication on a vehicle providing the ‘X’ function
- Loss of mobility of a vehicle providing the ‘X’ function (only if mobility is required for that VD function to be performed)
- Loss of power on a vehicle providing the ‘X’ function
- Total loss of long-range communication of the system
- Total loss of path-planning ability of the system

The system has completely failed when none of the VD functions can be achieved anymore. For a given case study, the effects of failures of different functions on the VD functions must first be established. The  $A$  matrix can then be automatically generated using a method developed by Wertz. [144]



### 2.3.5.2 Determining the Probability of Being in Each State at Each Time

Once the  $A$  matrix has been defined, if  $P(t)$  is defined as the vector of probabilities of being in each state of the system at a particular time, the  $A$  matrix is defined as:

$$\frac{dP(t)}{dt} = AP(t)$$

**Equation 8**

The probability of being in any given state over time is calculated using numerical integration. [146] In this method, the  $A$  matrix must be transformed into a discrete time matrix, called  $M$ .

$$M = I + A\Delta t$$

**Equation 9**

In Equation 9,  $\Delta t$  is the duration of the time step (set by the user) and  $I$  is the identity matrix. By integrating Equation 8, the probability of being in each state at a given time,  $P(t, :)$ , can be evaluated:

$$P(t, :) = e^{At}$$

**Equation 10**

$t$  can then be broken into the time at the end of the previous time step plus the length of the time step:

$$P(t, :) = e^{A((t-1)+\Delta t)} = e^{A\Delta t} e^{A(t-1)}$$

**Equation 11**

The first term in Equation 11 is a Taylor series approximation for the  $M$  matrix:

$$e^{A\Delta t} \cong I + A\Delta t = M$$

**Equation 12**

And the second term in Equation 11 is essentially the previous row of the  $P$  matrix:

$$e^{A(t-1)} = P(t-1, :)$$

**Equation 13**

From the earlier description of a Markov chain, it is known that the first state and therefore the first row of the  $P$  matrix,  $P(1, :)$ , is the initial condition, where the probability of being in the first state (where all functions are working) is 1, and the probability of being in any other state is zero. Consequently, the rest of the  $P$  matrix can be found by multiplying the probability of being in each state from one time step before by the  $M$  matrix.

$$P(t, :) = P(t-1, :) * M$$

**Equation 14**

Consequently, the rows of  $P$  correspond to time steps, and the columns of  $P$  correspond to states. Once the system has been evaluated over the desired lifetime, the state transition curves (i.e. the columns

of  $P$ , or the probability of being in a given state over time) can be plotted in order to illustrate the behavior of the system over time.

As has been explained so far, the state-transition matrix is not only dependent on how many functions exist within the system, but also on how they are distributed across the system. For given levels of reliability, architectures can therefore be compared to each other. A generic two-rover architecture with 5 instruments and a total mass similar to that of its single vehicle equivalent was used to demonstrate the use of this metric. Its state transition curves and that of the single rover are shown in Figure 12.

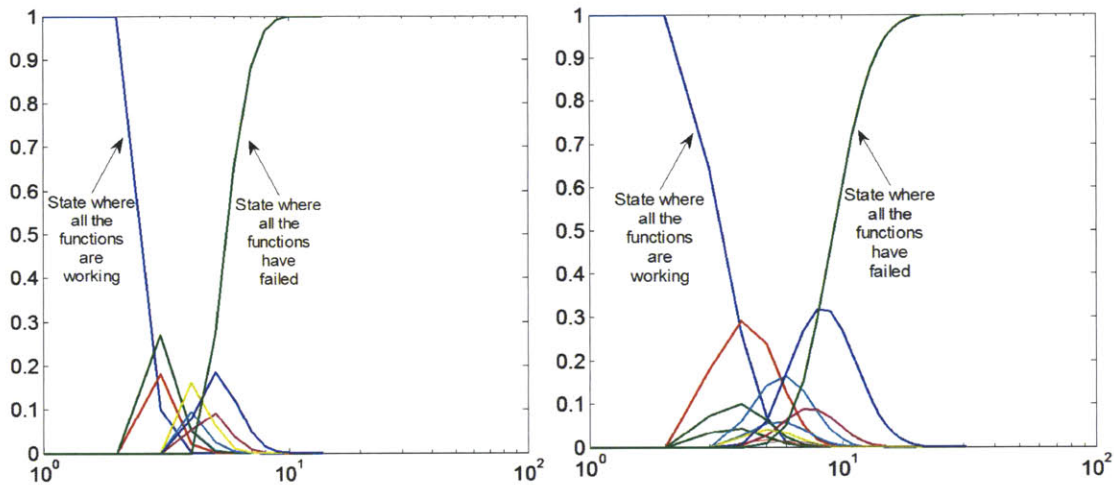


**Figure 12: State transition curves for the 1- (left) 2-rover (right) architectures.**

**The y-axis gives the probability of being in a given state, and the x-axis is normalized mission time.**

In both of these plots, the blue line dropping from 1 to 0 represents the first state, where all VD functions are working. The green line going from 0 to 1 represents the last state, where all VD functions have failed. All the other curves represent intermediate states, where parts of the system have failed but the system as a whole is still able to operate and perform some science. It can be seen that the 2-rover system degrades more gracefully over the mission lifetime (the blue curve is more shallow and the system spends more time in the intermediary states). This could be leveraged by performing tasks with instruments that have high failure rates first, and undertaking the subsequent tasks once the system has degraded.

In the special case where there is no functional redundancy in the system (this can occur in temporally distributed systems, or in spatially distributed systems where the vehicles are non-coordinated) and where the system cannot operate in a degraded state (i.e. if a failure occurs, the Markov chain ends), the Markov chain breaks down to a simple single-string chain of events and the lifetime components for each of the systems can be separated into a direct multiplicative term. This simplification can therefore be used to measure the probability of the system completing certain tasks successfully or for assessing the probability of the system being in its nominal state at a given time. The use of simplification will be

explored in Chapter 6, which conducts a case study for a Mars Sample Return mission and where the desire is to evaluate the ability of the system to achieve the “binary” goal of returning a sample (i.e. either the sample is returned or it is not).

### 2.3.5.3 Calculating the Total Productivity

The total productivity of the system can be calculated in a similar way to that proposed and validated by Lamamy et al. [103], by calculating the total time each instrument is operational for during the lifetime of an architecture. This is illustrated in Equation 15.

$$Productivity = \int_{lifetime} \sum_{all\ states} \left( P_i(t) * \sum_{all\ VD\ functions} DS_{state} \right)$$

**Equation 15**

Where *DS* is the duty cycle of each of the operational value delivery functions (i.e. the duty cycle of each instrument) in a given state, and is defined by the user when setting up the problem. Essentially, the productivity metric calculates the total number of days during which each value delivery function is expected to be operational over the lifetime of a given architecture.

### 2.3.6 Coverage

An important aspect of planetary exploration is the coverage provided by the mission. Typically, the larger the number of sites visited and the larger the area explored at each site (i.e. the wider the path width), the greater the data return is for planetary surface vehicles. For orbiters and fly-by missions, these parameters correspond to greater coverage and resolution respectively. A coverage metric was therefore developed to encompass these properties, using concepts from multi-attribute utility. Since the two parameters are independent, the metric can be formulated as:

$$Coverage = \frac{\sum_1^n sites \alpha * fn(area\ and/or\ resolution) + \beta * fn(sites\ visited\ or\ coverage)}{Baseline\ mission\ coverage}$$

**Equation 16**

The value associated with the number of sites explored and their area is a function that is dependent on size. Typical functions for these properties are shown in Figure 13.

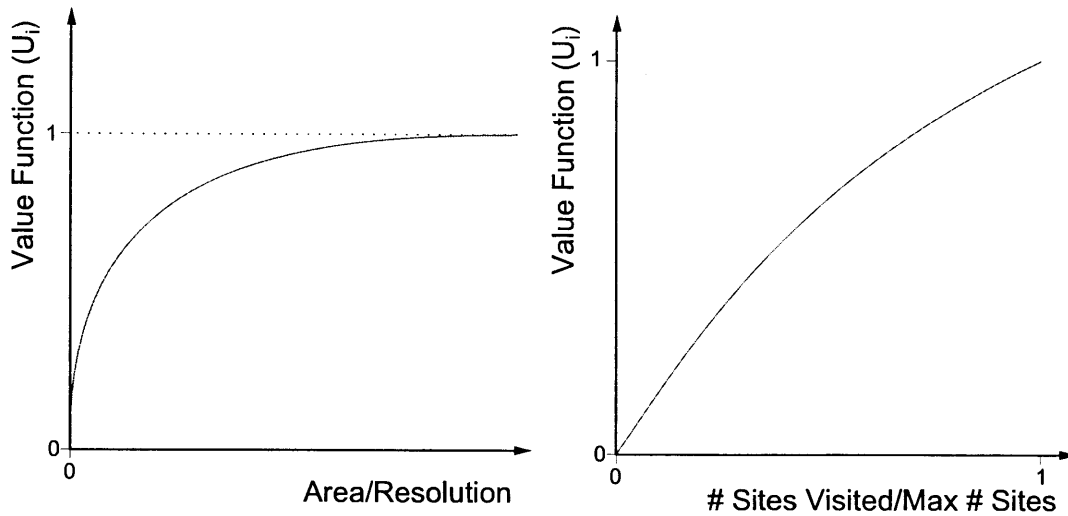


**Figure 13: Value functions for the number of sites visited and their area**

The  $\alpha$  and  $\beta$  weightings are used to prioritize one feature or another, depending on how they affect the mission goals. For orbital assets, the coverage and resolution can be obtained from the orbital parameters of the mission. In the case of planetary surface vehicle, a multi-vehicle path-planning tool must be used to evaluate the properties of the mission. Such a tool, called SEXTANT, was developed as part of this thesis and is described in Chapter 4.

### 2.3.7 Uncertainty and Risk

Another important factor in decision-making is the risk associated with a given architecture. In this thesis, risk is defined as the uncertainty associated with the science benefit, complexity and cost metrics. It illustrates disagreements in the effectiveness of instruments in achieving the science goals, or uncertainties in technology and in integration difficulty. All these aspects have historically been shown to be associated with increased mission cost and schedule delays.

Each of the aforementioned metrics includes a set of weightings derived either from science goals, existing designs or expert opinions. Uncertainty in the metrics arises in differences in expert opinions. Each architecture therefore carries a certain amount of uncertainty. An example of a typical trade space is shown in Figure 14.

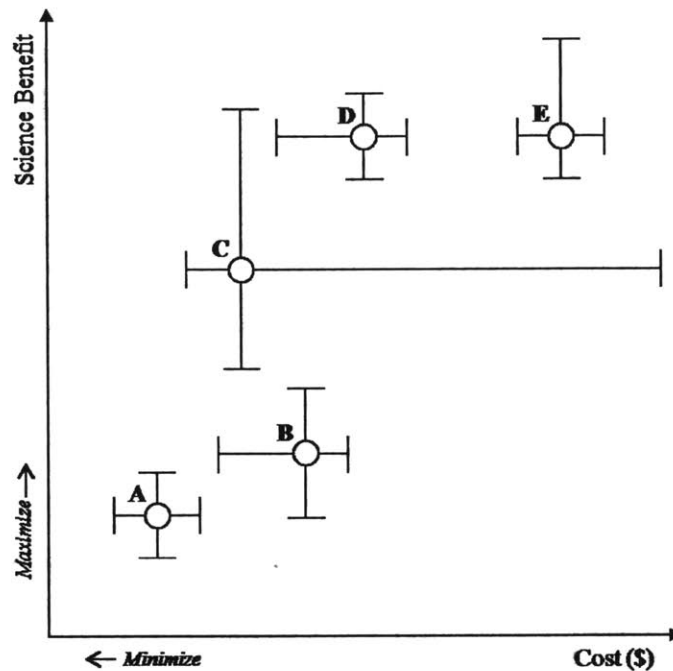


**Figure 14: Example trade space with error bars showing uncertainty range**

There are two possible issues that arise from uncertainty. First, uncertainty can affect which architectures are perceived as being optimal. In Figure 14, if the uncertainties are ignored, architecture A, C and D would be chosen as the “best” architectures. However, once the error bars are added, although A is still a better choice over architecture B, it is unclear which of architecture C, D and E is the best choice. This example demonstrates that, at times, the architectures that may seem optimal in fact run the risk of being worse than seemingly less optimal options. A metric to account for this risk is detailed in section 2.3.7.2.

Another challenge is the risk that arises from having uncertainty in a design. In Figure 14, architecture C has much greater uncertainty than any other design. Even though it has the potential of providing a large amount of science return at low cost (and it is one of the “optimal” architectures), it may not be a preferred architecture due to the inherent risk: the uncertainty could lead to a greater cost than anticipated, and possibly even a lower science return for that cost.

### 2.3.7.1 Pareto Optimality

Before considering how risk affects the set of “best” architecture, the criteria for an optimal architecture must be defined. Since there are multiple metrics, that could all either be minimized or maximized, there is no single optimal architecture for a given case study. The solution in fact consists of a

set of “best” solutions, also known as the Pareto set. [98] The Pareto set is the set of solutions for which no improvement in any objective can be made without worsening another objective.

In order to formally define Pareto set, some terms from the field of multi-objective optimization must first be defined. The *design vector*,  $\mathbf{x}$ , is the set of all variables that can be changed to specify an architecture. It essentially encompasses the decisions that the architect must make in order to define an architecture. An example of a design vector for a rover is:

$$\mathbf{x} = \begin{bmatrix} \text{Number of instruments} \\ \text{Type of instruments} \\ \text{Type of comm system} \\ \text{Number of wheels} \\ \text{Lifetime} \\ \dots \end{bmatrix}$$

An *objective function*,  $\mathbf{J}(\mathbf{x}, \mathbf{p})$  maps the design vector,  $\mathbf{x}$ , to figures of merit. In the studies presented in this thesis, these figures of merit consist of a set of the metrics presented thus far. An example of an objective function is:

$$\mathbf{J}(\mathbf{x}, \mathbf{p}) = \begin{bmatrix} \text{System mass} \\ \text{Science Benefit} \\ \text{Vehicle – level complexity} \\ \text{Productivity} \\ \dots \end{bmatrix}$$

The metrics in the objective functions are in some cases competing, and there typically will not be a single architecture that performs best for all the components of the objective function. This is why the concept of Pareto front is important. Within a trade space of architectures, there are three types of solutions:

*i) Weakly dominated solutions*

For two objective vectors:  $\mathbf{J}^1 = \mathbf{J}(\mathbf{x}^1)$  and  $\mathbf{J}^2 = \mathbf{J}(\mathbf{x}^2)$  with  $n$  elements,  $\mathbf{J}^1$  weakly dominates  $\mathbf{J}^2$  if and only if:

$$\begin{aligned} J_i^1 &\leq J_i^2 \quad \forall i, i \in \{1, 2, \dots, n\} \\ \text{and } J_j^1 &< J_j^2 \quad \forall \text{ for at least one } j, j \in \{1, 2, \dots, n\} \end{aligned}$$

**Equation 17**

*ii) Strongly dominated solutions*

If all elements of  $\mathbf{J}^1$  are more favorable than the corresponding elements of  $\mathbf{J}^2$ , then  $\mathbf{J}^1$  strongly dominates  $\mathbf{J}^2$ :

$$J_i^1 < J_i^2 \quad \forall i, i \in \{1, 2, \dots, n\}$$

**Equation 18**

*iii) Non-dominated solutions*

Finally, if neither  $\mathbf{J}^1$  nor  $\mathbf{J}^2$  dominate each other, the solutions are non-dominated. These are the bases for Pareto optimality. In a set of non-dominated solutions (referred to as a Pareto set), no improvement to any element of the objective vector can be made without a penalty in a different element of the objective vector. A solution,  $\mathbf{J}^*$  is non-dominated if there exists no solution,  $\mathbf{J}$ , such that:

$$\mathbf{J}_i \leq \mathbf{J}_i^* \forall i, i \in \{1, 2, \dots, n\}$$

and  $\mathbf{J}_j < \mathbf{J}_j^* \forall$  for at least one  $j, j \in \{1, 2, \dots, n\}$

**Equation 19**

In order to demonstrate the concept of Pareto optimality, a set of architectures and their values for two metrics,  $J_1$  and  $J_2$ , is shown in Figure 15. In this example, architectures A, C and D form the Pareto set. Architecture B is strongly dominated by architecture A and architecture E is weakly dominated by architecture C.

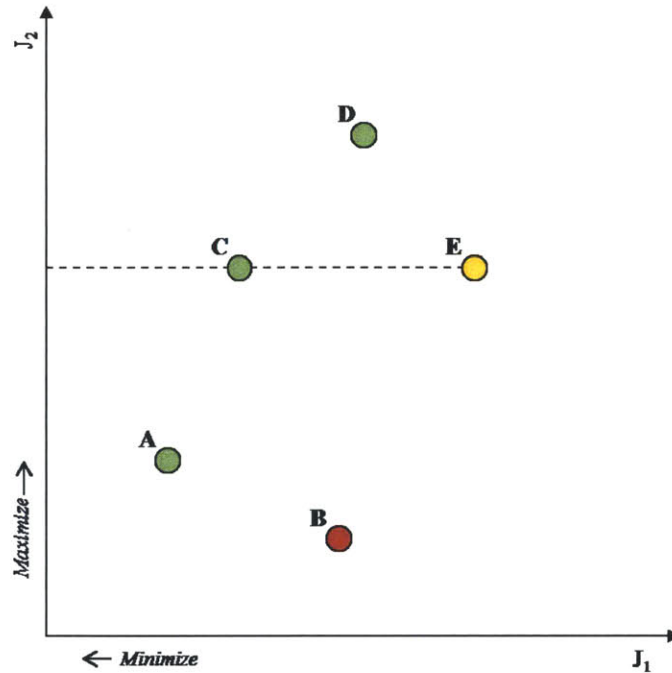


**Figure 15: Example of non-dominated, weakly dominated and strongly dominated architectures**

### 2.3.7.2 $\epsilon$ -Pareto Optimality

As explained earlier in this section, the uncertainty associated with each of the points within a trade space can lead to points that are not in the Pareto set to have the potential to be optimal architectures. In order to find these architectures, the concept of  $\epsilon$ -dominance and  $\epsilon$ -Pareto set are introduced. [106], [147] For two objective vectors:  $\mathbf{J}^1 = \mathbf{J}(\mathbf{x}^1)$  and  $\mathbf{J}^2 = \mathbf{J}(\mathbf{x}^2)$  with  $i$  elements,  $\mathbf{J}^1$   $\epsilon$ -dominates  $\mathbf{J}^2$  with some uncertainty  $\epsilon_i > 0$  if and only if:

$$(1 + \epsilon_i)J_i^1 \leq J_i^2 \quad \forall i, i \in \{1, 2, \dots, n\}$$

$$\text{and } (1 + \epsilon_j)J_j^1 < J_j^2 \quad \forall \text{ for at least one } j, j \in \{1, 2, \dots, n\}$$

Equation 20

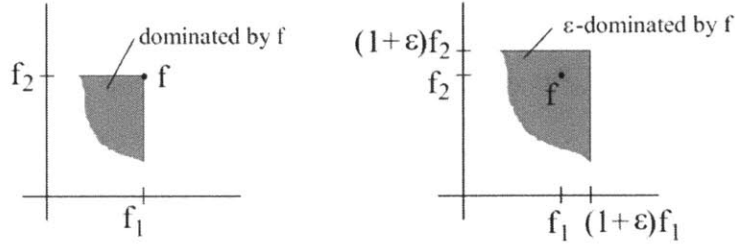


Figure 16: Plot illustrating the concept of  $\epsilon$ -dominance [147]

The  $\epsilon$ -Pareto set can therefore be found by through a pairwise comparison of all designs to check for  $\epsilon$ -dominance. Any designs left at the end of the comparison that were not found to be  $\epsilon$ -dominated during the process are part of the  $\epsilon$ -Pareto set.

### 2.3.7.3 Uncertainty Estimation and Risk

Even if an architecture is both on the Pareto and the  $\epsilon$ -Pareto set, it may still not be a desirable architecture. This can occur if there is a large amount of uncertainty, which translates into design risk, associated with the architecture. Looking at architecture C in Figure 14 for example, this architecture performs well, but runs the risk of having a higher cost for a lower return than architectures D and E.

As explained earlier, the cost, complexity and science benefit include a certain range in value due to both uncertainties in models and disagreement between experts. Depending on the sample size, the range or standard deviation of the values for each architecture can be used to evaluate the risk associated with the. Architectures can thus be excluded from the list of potentially interesting architectures by imposing a cap on either the range or the standard deviation of the data. Alternatively, the range or standard deviation can be used as an additional metric (that can be translated to risk for each of the metrics) that can be plotted against in the evaluation process.

One of the advantages of temporal distribution is that it might help reduce the uncertainty associated with the vehicle-level complexity and the value of instruments. This is mirrored through the effect of the  $K_{seq}$  (introduced in Equation 1 and Equation 6) term in both of their equations.



### **2.3.8 Summary**

The metrics described in this section are comparative rather than absolute. This means that they are most useful if they can be normalized by a baseline value, which is typically the monolithic design alternative.

The metrics can be validated in different ways. In particular, mass and cost can be validated using the properties of existing designs. Vehicle-level complexity is also correlated to cost. System-level complexity is a structural complexity metric (and is also correlated to testing and operations costs), and the productivity metric is based on Markov models. These are both commonly used metrics in other fields. Science benefit is a metric that portrays perceived value, which is improved by an increased number of expert opinions. The benefit metric is only as useful as its inputs are, and can be validated by obtaining feedback on the results from the expert interviewees. Examples of how the metrics can be validated are shown in the case studies in the subsequent chapters.

It is expected that the science benefit, missions success and cost metrics will be the most important in the analysis process. This is because they are applicable to both spatially and temporally distributed systems, and they illustrate attributes and trends that are not intuitive. It is also important to note that these metrics are not all orthogonal. For example, the complexity and cost metrics are intended to be heavily correlated. Care must therefore be taken during the analysis process to ensure that appropriate conclusions are reached.

## **2.4 Trade Space Visualization**

Once the architectures have been generated and the metrics have been calculated, the architecture space must be visualized in order to enable the exploration of the trade space. A software tool was developed to do this (see Appendix C). Given a set of goals, instruments, weightings and constraints, the tool generates the trade space of possible architectures and calculates the relevant aforementioned metrics for each architecture. The results are displayed on a graphical user interface (GUI), an example of which is shown in Figure 17. On this screen, any metric can be plotted against any other. The user can then downsize the space using the down-selection option. This allows the user to interactively explore the trade space. Once the final few architectures have been chosen, the tool can display the state transition plots for each of the final architectures (examples of which were given in Section 2.3.5).

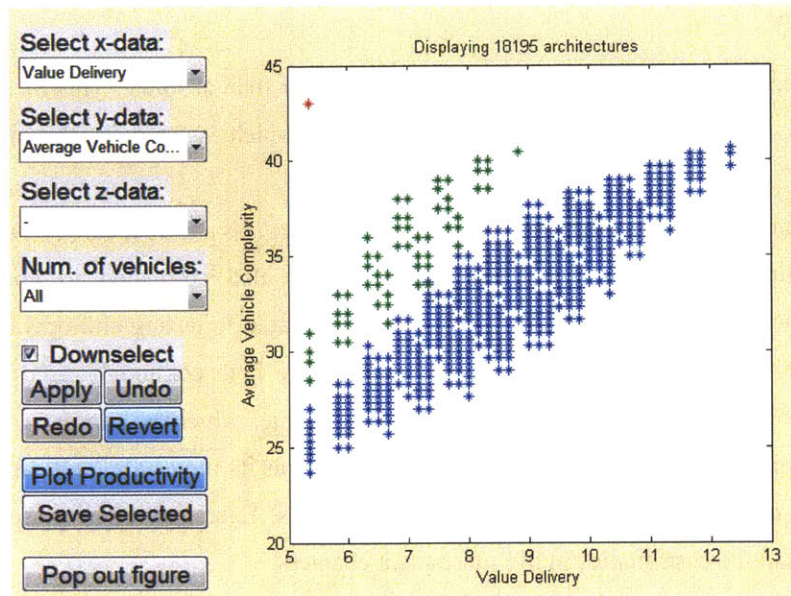


**Figure 17: Example of a display of a 3-vehicle trade space in the GUI developed for the visualization of architectures.**

For case studies involving orbital assets and planetary surface assets (Chapters 5 and 6), the software was customized to optimize performance for the given problem (i.e. either a science- or engineering-driven mission). Although the underlying framework remains the same, some of the metrics (e.g. mass and cost) and visualization aspects differ slightly (e.g. options to vary the science goal weightings, to down-select the Pareto and  $\epsilon$ -Pareto front, and to identify the different types of vehicles in an architecture are added). These slight variations of the software were developed and are also available.

## Chapter 3

# SPATIALLY DISTRIBUTED SYSTEMS FOR MARTIAN SURFACE EXPLORATION

### 3.1 Introduction

In the past ten years, three roving missions have been successfully landed and operated on Mars: the two Mars Exploration rovers (MERs – Spirit and Opportunity) and the Mars Science Laboratory (MSL - Curiosity) rover. Two of these rovers (Curiosity and Opportunity) are still active today. The MERs are identical 185kg rovers, each carrying 15kg of payload, that were landed on opposite sides of the red planet. Together, including the five mission extensions, the MERs cost approximately FY2003 USD\$820M. [148] MSL, on the other hand, is a 900kg rover with 150kg of payload. [149] It was landed on Mars two years behind schedule and nearly 400% over budget, running a bill of approximately FY2012 USD\$2.5 billion. [150] The increase in mass and complexity between the two missions was found to be due to the increased science demands levied on MSL, as well as the increased complexity in its landing system and scientific instruments.

As the exploration of Mars and other planetary surfaces continues and becomes more ambitious, and considering the recent trend in planetary science budgets, there is a need for a change of paradigm in the way planetary surface missions are performed. This thesis proposes the concept of *task distribution*, both spatial and temporal. This chapter explores the effects of *spatial distribution*, using the metrics developed and described in Chapter 2. The aim of this chapter is to identify how different types of function sharing in spatially distributed system affect the system, as measured by the metrics developed. This will then

provide mission designers with an understanding of how spatial distribution can help enhance mission properties, and what the limitations are.

This chapter starts with a case study based on the MERs' science goals. It methodically explores the trades between different system features, to uncover trends in mission properties. This is followed by a short investigation of the effects of adding small micro-rovers to a larger planetary surface mission. The final section of the chapter consists of an MSL-redesign study that looks at possible multi-vehicle alternatives to the MSL rover, and how they perform given MSL's mission goals and instruments.

## 3.2 Mass Metric

In the following two case studies, the metrics described in Chapter 2 are used to evaluate the properties of spatially distributed systems. In addition to these, a physical mass model was specifically developed to estimate the mass of the rovers in these architectures. The model consists of nine sub-systems, along with a payload system, that are called by a master script in an iterative manner to obtain a model that meets the input requirements. The model inputs and outputs are detailed in Table 14 and the interactions between the subsystems in the modeling tool are highlighted in Table 15.

**Table 14: Inputs and outputs to the rover modeling tool**

<b>Inputs</b>	<b>Outputs</b>
# Sortie Days	Navigation System Mass
Planet	Comm. System Mass
Bandwidth	Comm. System Power
Data Rate Needed	Structure Mass
# Wheels	Wheel Size & Mass
Chassis Material	Wheel Load
Sinkage	Sprung Mass
% Time Spent on Slope	Steering Mass
Max Slope Angle	Turning Radius
Wheel Slip	Level Power
Drive Type	Slope Power
Motor Type	Power Mass
Power Source	Solar Array Size
Payload Mass	Total Power
Payload Power	Thermal System Mass

**Table 15: Connection between each subsystem**  
**Boxes shaded in represent feedforward and feedback links between subsystems**

Comm								
	Chassis							
		Thermal						
			Wheels					
				Steering				
					Terrain			
						Drive		
							Power	
								Suspension

**Table 16: Overview of the assumptions used for the design of each sub-system**

Sub-System	Assumption
Payload	Mass, power and duty cycle for all instruments given as an input by the user
Communications	Mass and power calculated using the link budget equation and mass correlations
Chassis	Modeled as a simple ladder frame
Thermal	Thermal balance equation evaluated, heat is rejected using radiators and is input using radioisotope heater units (RHUs)
Wheels	Diameter and width of wheels are sized for a specific sinkage and soil bearing pressure
Steering	Assumes Ackerman steering (models the mass of a steering motor required for each set of wheels that are steerable), a steer-by-wire system, and additional mass for mechanisms
Terrain	Terrain properties are used to measure driving resistances
Drive	Resistances are used to measure torque and motor power
Power	Power of other subsystems are used to measure energy requirements and to size the subsystem
Suspension	Assumed to be 12% of the rover mass, from historical data

Details of the modeling tool can be found in Appendix A, and a brief overview of the modeling assumptions for each subsystem is shown in Table 16. The modeling tool was validated against existing rover designs and was found to have estimates within 20% of the actual masses of these rovers (details are shown in Appendix A).

Since the evaluation of the architecture space occurs in the early stages of the design process, the system mass is used to categorize the architecture. Any architecture having a mass within  $\pm 30\%$  of the mass of the monolithic vehicle is assumed to be part of the same *class* of architectures (30% is a standard margin in Pre-Phase A design). In this work, a mission *class* is a set of mission that fall within a certain mass (e.g. 0 – 100kg, 100 – 300kg, 300 – 600kg, 600 – 900kg...) or cost (e.g. <\$350M, \$350-\$700M,

\$700M - \$1.5B, > \$1.5B...) range. They identify types of mission that would typically be competed against each other in proposals. The assumption is that systems of the same class can be launched on the same launch vehicle and can be landed with the same Entry Descent and Landing (EDL) system. Architectures of the same class can therefore directly be traded against each other. The rest of the architecture trade space can also be divided up into classes, in order to evaluate the potential science return per dollar.

### **3.3 “Multi-MER” System Case Study**

#### **3.3.1 Overview of MER Goals and Designs**

The Mars Exploration Rovers (MERs) represent NASA’s first steps in achieving the goals of the Mars Exploration Program. These goals are to:

- Determine whether life ever arose on Mars,
- Characterize the climate of Mars,
- Characterize the geology of Mars,
- Prepare for Human Exploration.

The MER mission particularly concentrated on achieving the geology goals, and the rovers were equipped with a full suite of geology instruments [148]. Since the MERs had a fairly straightforward design, with a limited suite of instruments, their design is used in this case study, which aims at uncovering the main trends and trades between the metrics described in Chapter 2, and at informing mission designers of the effects of function sharing and spatial distribution on planetary surface missions.

Table 17 presents a full functional decomposition of the MER design, which is the starting point for the analysis.

When generating the different trade spaces, the duplication of instruments on a vehicle was not constrained. Additionally, only vehicles with science benefit greater than or equal to that of a single MER were considered. During the first iteration of the evaluation process, it was found that separating the instruments that are mounted on the robotic arm created extra mass (due to the need to have another arm) for little return. Therefore, the instruments indicated by an asterisk in Table 17 were assumed to be part of one instrumentation “group” that could be duplicated but not separated. In the rest of this section, the trade space of multi-vehicle options is explored and specific trends are discussed.

**Table 17: Functional decomposition of the MER design  
(instruments with an asterisk (\*) must be mounted on a robotic arm) [148]**

Function	Form	Category
Imaging	Panoramic Camera	VD
Detecting infrared emissions	Mini-Thermal Emission Spectrometer (Mini-TES)	VD
Moving Payload	Robotic Arm	VD
Determining abundance and composition of iron-bearing minerals	Mössbauer Spectrometer*	VD
Detecting x-ray emissions	Alpha-Particle X-Ray spectrometer (APXS)*	VD
Scraping outer layers of rock	Rock Abrasion Tool (RAT)*	VD
Imaging close-up views of rocks and soil	Microscopic Imager*	VD
Navigating	Navigation cameras	ES
Short-distance traversing	Mobility system	ES
Long-distance traversing	Mobility system	ES or SS
Energy generating	Solar panels	ES or SS
Energy storing	Batteries	ES
Payload carrying	Vehicle	ES
Thermal protecting	Thermal system	ES
Surviving the Martian night	Thermal system	ES
	Power system	ES or SS
Transmitting data	Rover-to-rover communication system	ES
	UHF Communications to an orbiter	SS
	Direct to Earth communication	SS

### 3.3.2 Most Significant Trades

In this initial trade space exploration, it was assumed that the instruments described in Table 17 were distributed across several vehicles. In addition to this, the long-range communication ability was also distributed across the rovers. This means that each rover in these architectures is equipped with the ability to communicate with other rovers on the surface. The rovers considered here are therefore all *coordinated* (i.e. they are all in the same region at a given time) and *dependent*. In this initial part of the case study, only 2- and 3-rover architectures were investigated.

#### 3.3.2.1 System Mass vs. Average Vehicle-level Complexity Trade

The first trade investigated the relationship of mass with the average vehicle complexity of the system. The mass model described in Section 3.2 and the complexity weightings provided in Chapter 2 were used to evaluate the architectures. The result is shown in Figure 18. Because only vehicles with greater capability than the MER baseline are considered, the mass of the monolithic vehicle (shown in red) is the lowest of the trade space. However, it can be seen that it also has the highest complexity.

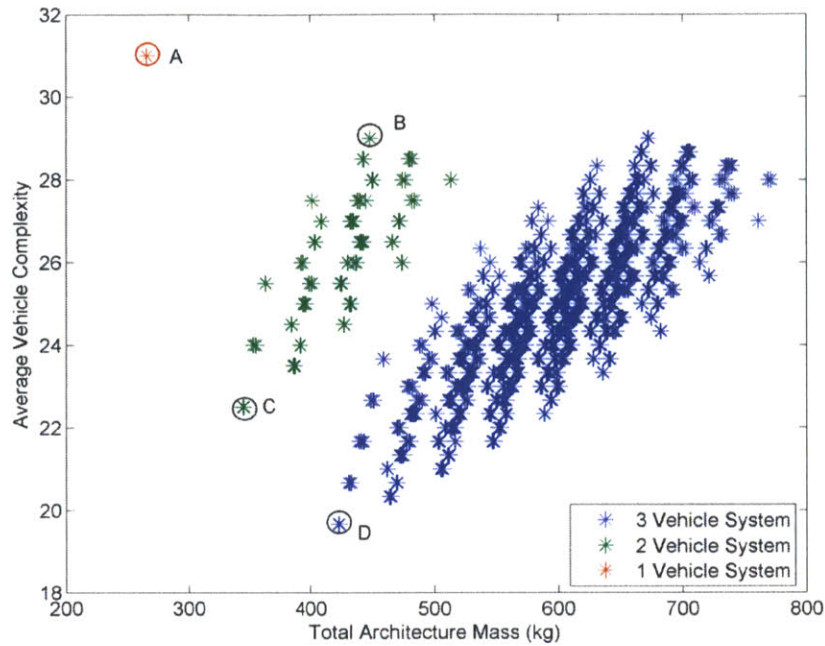


**Figure 18: Mass vs. vehicle-level complexity trade**

**Table 18: VD and SS functions possessed by the vehicles in the architectures circled in Figure 18**

Label	Vehicle 1	Vehicle 2	Vehicle 3
A	All functions (monolithic)	-	-
B	PanCam, Mini-TES, DTE Comm.	Arm, M-Spec, APXS, RAT, MicroCam, UHF Comm.	-
C	All payload, DTE Comm.	All payload, UHF Comm.	-
D	Arm, M-Spec, APXS, RAT, MicroCam, UHF Comm.	PanCam, DTE Comm.	Mini-TES

The general trend depicted in Figure 18 is that, in spatially distributed systems, complexity is traded for mass. In the multi-vehicle architectures, the instruments are spread across several vehicles, and thus each of the vehicles is itself less complex than the monolithic vehicle. On the other hand, there is an inherent mass cost that is associated with any rover, even if it does not carry any instrumentation. Therefore, in general, architectures with lower vehicle-level complexity have greater mass. However, increased mass does not necessarily mean that the cost of the system will be greater, since the vehicles in these more massive architectures are less complex and thus have a much lower development cost. The effect of these architectures on the science benefit is explored in the next section. It is to be noted that having similar vehicles in an architecture, such as architecture B, can help reduce the cost of this additional mass, since the same platform can theoretically be used for both vehicles. Moreover, there are several architectures that have a mass within 30% of the monolithic vehicle and therefore can be viewed as being part of the same vehicle “class” as the monolithic, as described earlier.



### 3.3.2.2 Science Benefit Trade

The next major trade is that of science benefit. In the last section, it was demonstrated that multi-vehicle systems typically have lower system-level complexity, at the cost of increased total system mass. Here, the science benefit is plotted against both the mass and the average vehicle-level complexity, in Figure 19 and Figure 20 respectively. The weighting scheme for the science benefit metric was based on the science traceability matrix for the MERs, with all goals weighted evenly. [149]

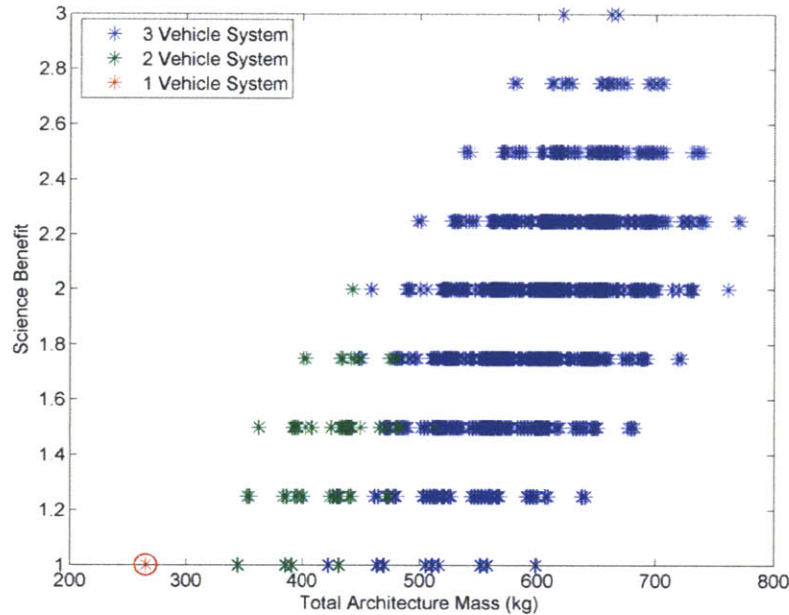


Figure 19: Science benefit vs. total mass

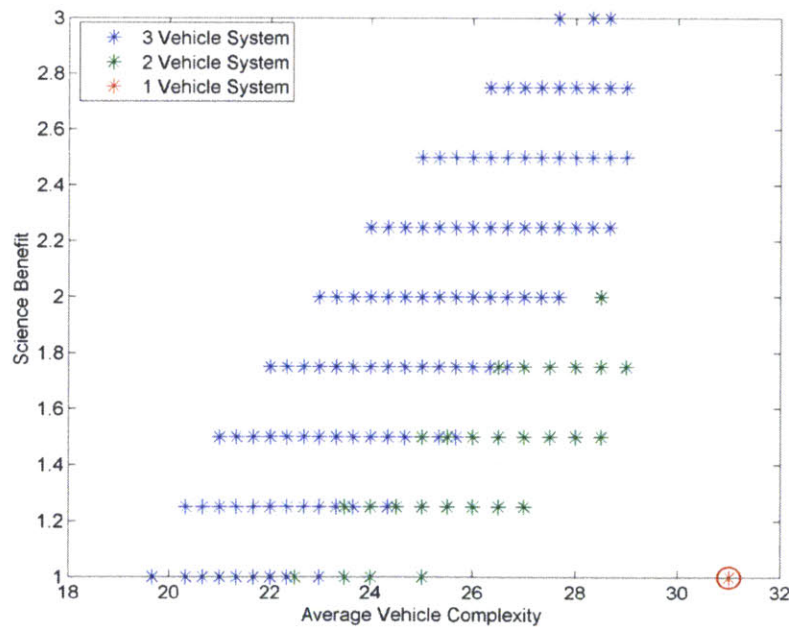


Figure 20: Science benefit vs. average vehicle-level complexity

From these figures, it can be observed that, in distributed planetary surface systems, mass is traded for value in a non-linear manner. When looking at the architectures on the Pareto front, a certain percentage increase in mass corresponds to a higher percentage increase in science return. This is because there are instruments that can be duplicated across vehicles at a very low marginal cost in a multi-rover system (for example, adding cameras). Although the benefit of duplicating instruments does not correspond to double the benefit of that particular instrument (there are diminishing returns of adding more instruments), there is a low mass cost to adding these instruments, which results in this non-linear relationship between mass and science benefit. The limitation, however, is that thus far only vehicle-level complexity has been evaluated. The next section deals with the effect of interactions between vehicles.

### 3.3.2.3 Vehicle-Level vs. System-Level Complexity Trade

A selected number of architectures with high science benefit were down-selected. In Figure 21, their vehicle-level complexity is plotted against their system-level complexity. These complexities were calculated using the schemes presented in Chapter 2.

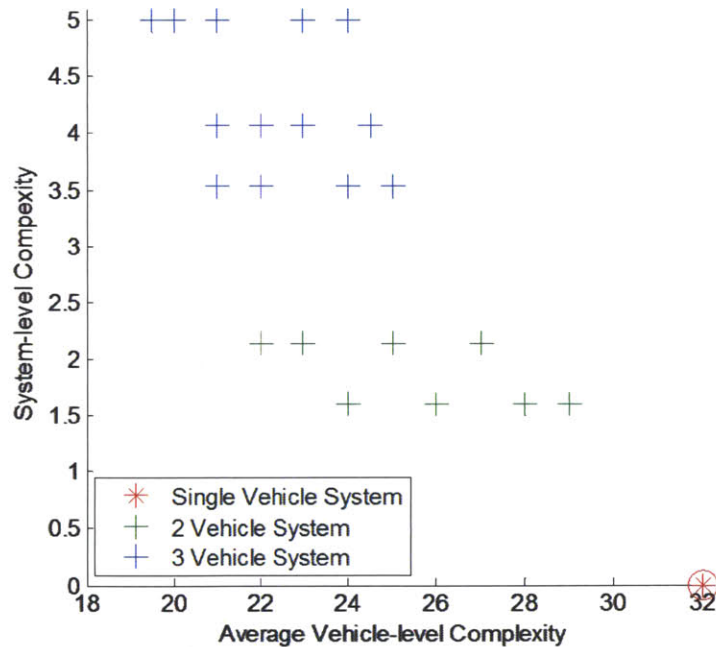


Figure 21: Vehicle- vs. system-level complexity

Because these are systems of coordinated, dependent vehicles, their system-level complexity is non-zero (i.e. there are interactions between vehicles). However, since the vehicles only have to interact with each other in terms of communication and collision avoidance, their system-level complexity is relatively low. In general, it can be seen that the multi-vehicle systems have higher system-level complexity, but

their vehicles have lower complexity. This means that development time and individual vehicle testing, for example, are traded for testing of the system as a whole. Furthermore, design cost is traded for the cost of the implementation of the collision avoidance and navigation system for the architecture. In order to make a decision on the trade of between vehicle- and system-level complexities, a designer would need to understand the impact of system-level complexity on system cost by evaluating the cost of the implementation of the multi-vehicle navigation system for a specific mission.

### 3.3.2.4 Reliability and Redundancy Trade

Thus far, it has been demonstrated that spatially distributed systems enjoy higher science return and lower vehicle-level complexity, at the cost of somewhat increased system mass and system-level complexity. This section explores the effect of increasing the number of vehicles on the productivity of the system, using the Markov model formally defined in Chapter 2.

The first step of the evaluation involved assuming a 99.9% reliability for every component, with exponential decay in performance over time and a lifetime of 80 days (i.e.: every subsystem, or function defined in Table 17). The expected productivity curves for the monolithic architectures under this assumption are presented in Figure 22. The two most important curves (all functions working and system failed) are marked. All the other curves on these plots are intermediary states (not all intermediary states are shown for clarity), where part of the system is broken down but science is still being performed.

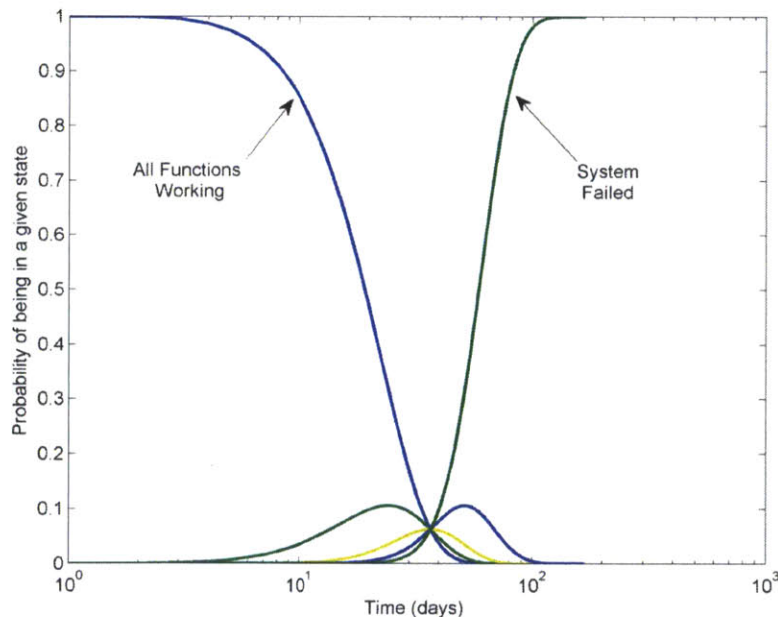


**Figure 22: State transition curves of the monolithic system with baseline reliability**

A two-vehicle and a three-vehicle architecture with the same science benefit value as the monolithic rover were chosen for comparison. The same reliability value was assumed for all components, except

that the emerging benefits of having multiple rovers were accounted for. For example, the failure modes described in Chapter 2 were used and implemented in the state-transition matrix. Additionally, a few emergent properties from having coordinated dependent spatially distributed vehicles were considered. It was assumed that the long-range communication system had not failed until all long-range communication systems across the architecture had failed (loss of a single long-range communication system still resulted in reduced productivity, but not mission failure). The same was assumed for the path-planning system: since the vehicles are assumed to be in the same region, if one vehicle loses its path-planning ability, then theoretically it could be provided path-planning information from another vehicle via short-range communication and by using vision navigation from its cameras. Finally, the probability of failure of the mobility system was assumed to be reduced due to the fact that one vehicle could theoretically help another get “unstuck” if such a failure happened (this is the failure that almost led to the demise of the Spirit MER). The productivity plots for these architectures are shown in Figure 23 and Figure 24.

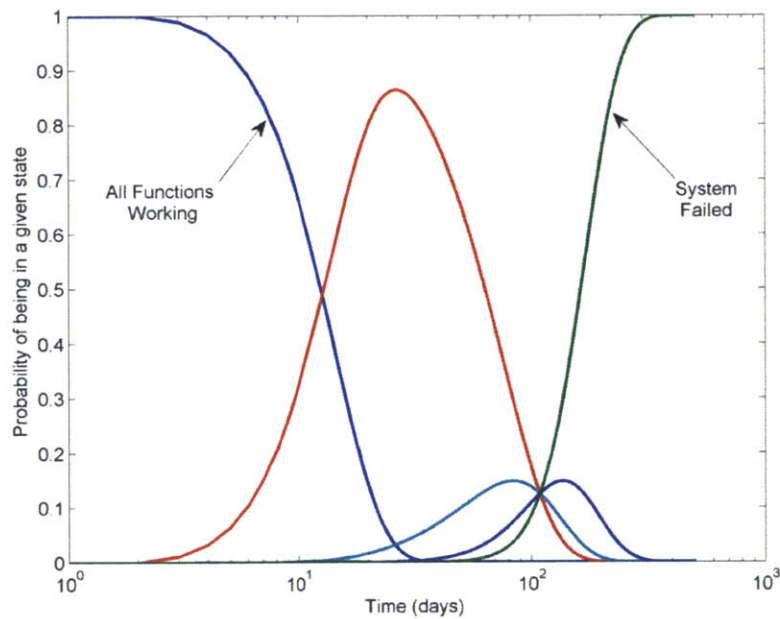


**Figure 23: State transition curves of a 2-vehicle architecture with baseline reliability**

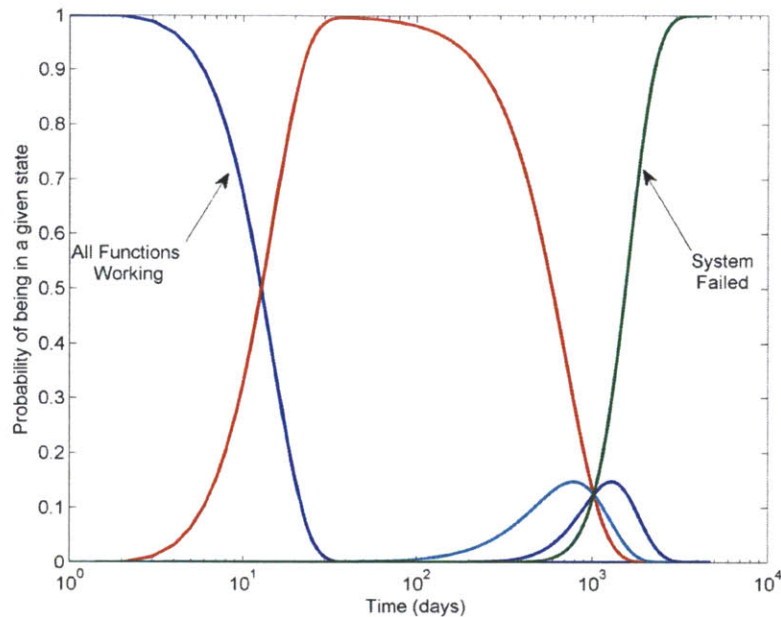


**Figure 24: State transition curves of a 3-vehicle architecture with baseline reliability**

It can be seen from these plots that the multi-rover architectures have greater productivity (i.e. larger areas under the curves that indicate states in which the system is still operational) and a longer lifetime. Additionally, the “all functions working” curve (i.e. the blue curve) has a shallower gradient as the number of vehicles increases. This indicates that the systems degrade more gracefully as the number of vehicles increases. Therefore, this shows that in *coordinated* multi-vehicle systems, mass and system level complexity is also traded for greater mission productivity and lifetime. As will be shown in Section 3.3.8, non-coordinated systems still have benefits in productivity, but these are not as pronounced as for coordinated vehicles since they cannot take advantage of the emergent properties of having a multi-vehicle system.

Another aspect to consider is that component reliability can be traded for productivity in multi-vehicle systems. The reliability of the 3-rover system components was decreased until its mission lifetime became similar to that of the monolithic vehicle. The resulting state curves are shown in Figure 25. In this exercise, the reliability of the components in the 3-vehicle architecture were reduced by almost an order of magnitude (to 99%). This means that, due to redundancy of components and the emergent properties they enjoy, multi-vehicle systems can achieve the same lifetime as the monolithic equivalent without having components that are as reliable (and therefore may be cheaper).

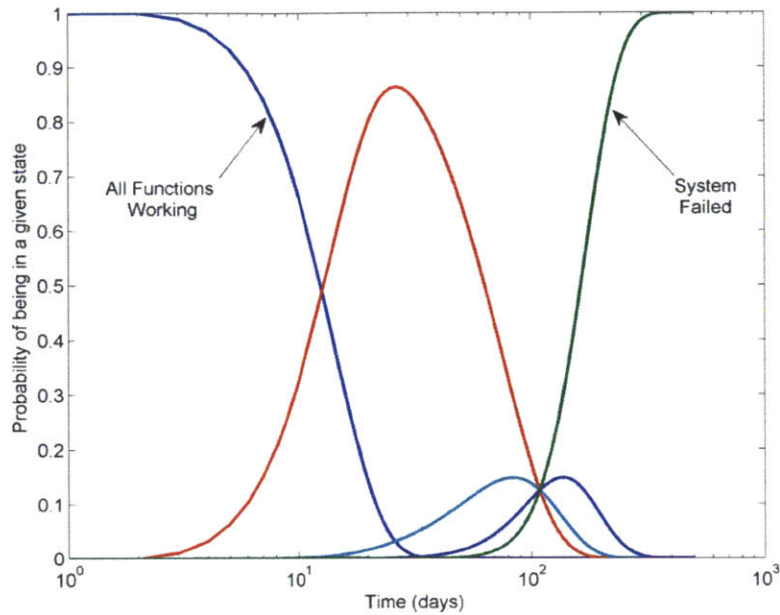


**Figure 25: State transition curves of a 3-vehicle architecture with reduced reliability**

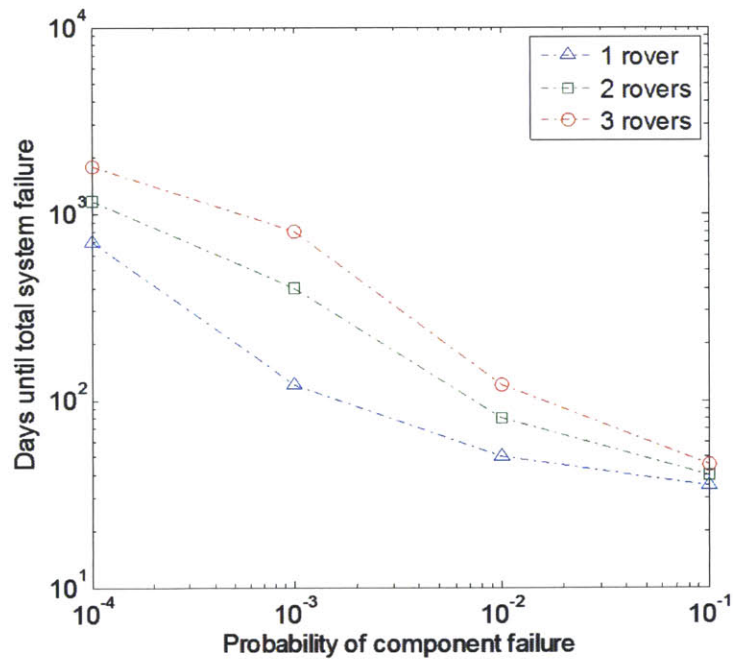


**Figure 26: Sensitivity analysis of productivity for multi-rover systems**

A sensitivity analysis was performed to ensure that this general trend held true for a range of probabilities of failure. Figure 26 shows the time to total failure for each of the three architectures as the probability of failure varies. It can be seen that the trend holds true as the probability of failure varies: the higher the number of rovers, the longer the system survives. It is to be noted that as the probability of

failure becomes very high, the advantage of having multiple vehicles decreases due to the rapid state transition rates. However, a probability of failure of 10% is very high and sits at the edge of the envelope of what would be acceptable for flight. Furthermore, due to the parallelization of tasks enabled by having multiple distributed vehicles, the productivity of the 2- and 3- rover systems is also significantly greater than that of the single rover system during their respective lifetimes.

### **3.3.2.5 Conclusions**

In this section, it has been shown that, for spatially distributed systems where the vehicles are coordinated and dependent, and where only architectures that have greater value than the monolithic baseline are considered, the following trends emerge:

- System mass increases, due to the inherent mass cost of any vehicle, as the number of vehicles increases
- Vehicle complexity decreases and science benefit increases as mass increases
- System-level complexity increases as the number of vehicle increases due to the interactions between vehicles
- The overall productivity of the system increases as the number of vehicles increases due to inherent redundancies in the system as well as emergent properties of multi-vehicle systems in terms of mobility, communication and navigation.

### **3.3.3 Effects of Sharing Supplying Supporting (SS) Functions**

In the last section, only the “communications” Supplying Supporting (SS) function was shared across the vehicles. In this section, the effects of sharing each of the four SS functions identified in Table 17 are explored for a range of two vehicle architectures from the trade space in Figure 18. General trends are identified to help a mission architect understand what the effects of sharing different SS functions are on the system.

### **3.3.4 Hibernation**

The first SS function investigated is the “hibernation” function. This is the power required for a rover to survive the Martian night (the thermal system is assumed to be an ES function). This function would be shared via power transfer from one vehicle to another during the night. (This could be done by beaming if the vehicles are far apart or, more efficiently, by inductive coupling if the vehicles come together, which is the case considered here.) This reduces the solar array area and battery size required by the vehicle receiving power, but it increases that of the other vehicle. If the second vehicle is already large and the marginal increase on its power requirement is small, or if it possesses RTGs, then this leads to reduced

overall vehicle-level complexity. However, sharing this function leads to greater system level complexity, since the vehicles have to be in close proximity (<1 meter) for this inductive coupling to be successful. A set of two-vehicle architectures where the vehicles do not share hibernation were compared to identical architectures where one vehicle supplies energy to the other. The total system mass for each of these is plotted against the nighttime power requirement in Figure 27.

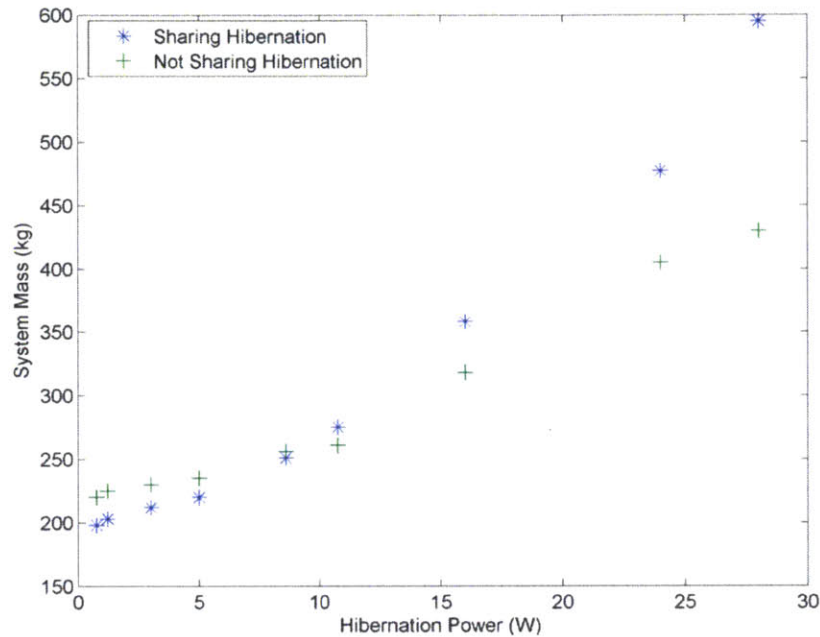


**Figure 27: System mass against nighttime power requirement**

As can be seen from Figure 27, sharing the hibernation function is only beneficial if the smaller vehicle’s nighttime power requirement is low and the overall gain from sharing this function is also low, in the case of a Martian mission. However, in the case of Lunar missions, the nighttime requirements are much greater (the lunar night lasts two Earth weeks), and therefore it is expected that for small vehicles, sharing the hibernation function will be significantly more beneficial. Consequently, this trade will be explored again in the case study in Chapter 4.

### 3.3.5 Energy Generating

The concept of sharing “energy generating” is similar to that of sharing the “hibernation” functionality. However, in this case, the vehicle receiving the energy must still carry a full set of batteries due to the fact that it will not always be within power transfer distance. This reduces the benefits of sharing the “energy generating” SS function. Once again, a range of 2 vehicle architectures that do not share the “energy generating” function are compared to identical architectures that do, in Figure 28.



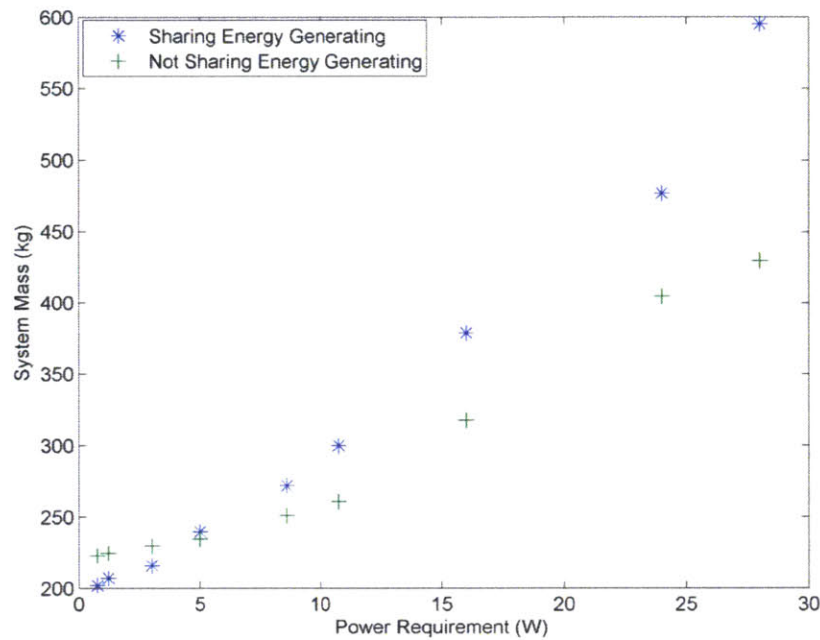


**Figure 28: System mass against power supply requirement**

Figure 28 shows that sharing the “energy generating” function is only beneficial when the vehicle receiving has very low power requirements, which in turn leads to a significant reduction in its complexity. In other words, if the power requirement ratio (i.e. the power requirement for the vehicle receiving energy/the power requirement of the supply vehicle) is very low, the marginal increase in complexity and mass for the supply vehicle is low. Alternatively, again, if nuclear power (i.e. RTGs or ASRGs) are required to power the supply vehicle, it may already produce enough additional energy to power a smaller vehicle. Therefore, it is likely that sharing the “energy generating” function would only be beneficial in cases where the monolithic vehicle is much bigger than the MERs, or when very small vehicles such as micro-rovers are flown, as is explored in Section 3.4.

### 3.3.6 Communication

Sharing the “long-range communicating” function was found to be extremely beneficial in reducing the mass and complexity of the system. Since coordinated vehicles are being considered, the vehicles must already be in frequent communication visibility of each other to provide context and achieve the science goals, and they all already possess short-range communication ability to communicate with each other. Consequently, sharing the communication function does not increase the system-level complexity. However, long-range communication does significantly drive the power requirements for Martian rovers and thus sharing this function across several vehicles (while making sure that there is enough bandwidth to communicate all the science data being produced) provides significant advantages in terms of vehicle

mass and complexity reduction, as well as increased redundancy (leading to higher lifetime). In the case of exploration near craters, as will be shown in Chapter 4, there are additional visibility advantages to sharing the long-range communication functionality across multiple vehicles.

### **3.3.7 Long-Range Traversing**

The final SS function to be investigated is that of long-range traversing. There are two ways of sharing this functionality, and the method used is dependent on the weight ratio between the carrying vehicle and the secondary vehicle. The first method involves having a large vehicle towing another. This method is better suited to 2-vehicle systems that have a mass ratio that is large (i.e. the two vehicles have similar masses). It can be useful if the mobility system of a vehicle breaks down, because the larger system can then tow it to a new location, thus still enabling useful science to be performed. The towing ability adds mass and complexity to the system however, so there must be a careful trade with the desire to extend a mission's lifetime.

The second way to share the long-range traversing ability is if a large vehicle can carry one, or several, significantly smaller rovers, which can then be deployed at specific sites on the surface. This allows the design of the mobility system of the smaller rovers to be much simpler. Additionally, it can enable them to traverse across large obstacles that they would otherwise not be able to surmount on their way from the landing site to their final destination. It is to be noted that if a vehicle carries another, then the additional system-level complexity cost of sharing the hibernating and energy generating function is minimal, since the vehicles already have a docking mechanism or can be connected via a tether. This last concept is explored further in Section 3.4.

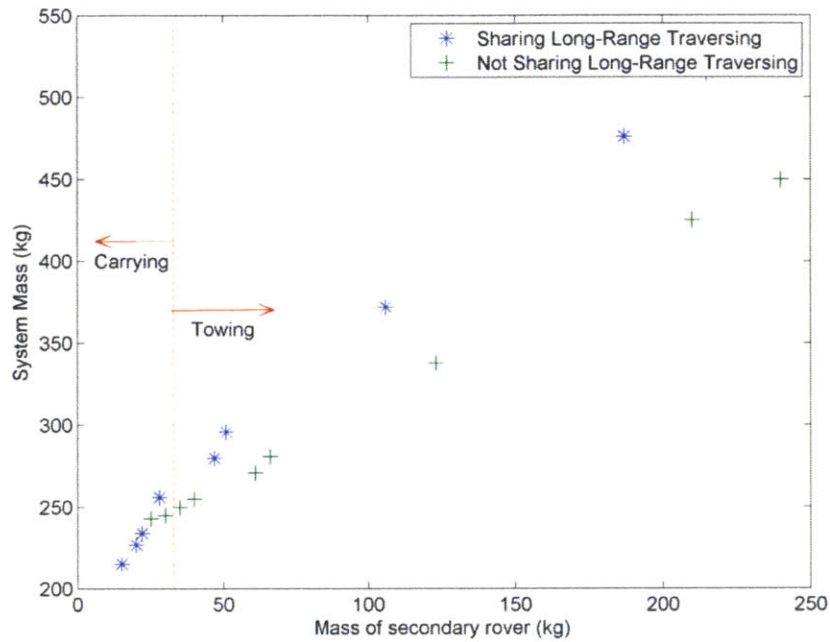


**Figure 29: Effects of carrying/towing a vehicle on system mass**

Figure 29 shows the effect of sharing the “long-range traversing” function on the overall system mass. It can be seen that in cases where the vehicle being towed is large, the process of sharing this function has a negative impact on mass. However, for very low mass vehicles, sharing this function seems to be very promising.

### 3.3.8 Effects of the Different Types of Spatial Distribution

The analysis thus far has only considered dependent, coordinated systems, where vehicles stay in the same region and stay in communication range of each other. In Chapter 1, two other types of spatial distribution were identified. Independent, coordinated vehicles explore the same region at any given time, but they do not share supplying supporting (SS) functions and therefore do not have to be in communication range of each other at all times. Finally, non-coordinated, independent vehicles are identical vehicles (or identical vehicle sets) that are landed in different regions of the planet. This allows the system to perform science experiments in different regions of the planet and obtain a global understanding of the scientific phenomena. This section explores the effect of these different types of spatial distribution, summarized in Table 19, on the system properties.

**Table 19: Different types of spatial distribution**

	<b>Coordinated</b>	<b>Non-Coordinated</b>
<b>Dependent</b>	Vehicles are always in communication visibility.	N/A
<b>Independent</b>	Vehicles do not have to be visible to each other at all times, but are always in the same region.	Vehicles do not have to be visible to each other, and are not in the same region.

In order to uncover the trends associated with these three different types of spatial distribution, the analysis performed in Section 3.3.2 was repeated for the two types of independent systems. The case study was also repeated with different instruments, and with different targets. Together, ten different cases were run for each type of distribution, and general trends were observed. In particular, the difference in the behavior of the metrics depending on the type of spatially distributed system was noted. The average trend lines for each of the metrics and type of system are shown in Table 20, Table 21 and Table 22, and are subsequently explained.

**Table 20: Effects of different types of spatial distribution on science benefit and productivity**

	Science Benefit	Productivity
<b>Coordinated Independent</b>	<p>Science Benefit</p> <p>1</p> <p>Number of Vehicles</p>	<p>Days (Cumulative)</p> <p>100</p> <p>1</p> <p>Number of Vehicles</p>
<b>Coordinated Dependent</b>	<p>Science Benefit</p> <p>1</p> <p>Number of Vehicles</p>	<p>Days (Cumulative)</p> <p>100</p> <p>1</p> <p>Number of Vehicles</p>
<b>Non-Coordinated Independent</b>	<p>Science Benefit</p> <p>1</p> <p>Number of Vehicles</p>	<p>Days (Cumulative)</p> <p>100</p> <p>1</p> <p>Number of Vehicles</p>

**Table 21: Effects of different types of spatial distribution on system mass and mission coverage**

	Mass	Coverage
<b>Coordinated Independent</b>	<p>Mass (kg)</p> <p>Number of Vehicles</p>	<p>Number of sites visited</p> <p>Number of vehicles</p>
<b>Coordinated Dependent</b>	<p>Mass (kg)</p> <p>Number of Vehicles</p>	<p>Number of sites visited</p> <p>Number of vehicles</p>
<b>Non-Coordinated Independent</b>	<p>Mass (kg)</p> <p>195</p> <p>1</p> <p>Number of Vehicles</p>	<p>Number of sites visited</p> <p>Number of vehicles</p>

**Table 22: Effects of different types of spatial distribution on vehicle- and system-level complexity**

	Vehicle-Level Complexity	System-Level Complexity
<b>Coordinated Independent</b>		
<b>Coordinated Dependent</b>		
<b>Non-Coordinated Independent</b>		N/A

### **3.3.8.1 Science Benefit**

The science benefit of a system is seen in Table 20 to increase as the number of vehicles in an architecture increases. However, there is a diminishing return in increasing the number of vehicles. This is because, if the suite of possible instruments that achieve a mission goal is set, even though increasing the number of times a given instrument appears in an architecture increases redundancy and the quantity of measurements being taken over the lifetime, the science benefit does not necessarily increase in a linear manner with quantity. As explained in Chapter 2, doubling the occurrence of an instrument in most cases does not double the science benefit, especially in systems exploring the same region.

In general, the science benefit slope for coordinated dependent vehicles is the shallowest because in these systems, each vehicle has lower functionality than for the other types of spatially distributed systems (on the other hand, coordinated dependent systems have a higher science benefit to mass ratio, as is discussed in Section 3.3.8.3). Finally, the diminishing return effect for non-coordinated, independent vehicles is less acute. This is because these vehicles operate in different regions, which in turn leads to variability in science and thus a higher science benefit.

### **3.3.8.2 Productivity**

As expected, the productivity increases with the number of vehicles for all types of spatial distribution. However, coordinated dependent vehicles have lower productivity at low vehicle numbers than coordinated independent vehicles. This is because, when there are only a few vehicles, systems with coordinated dependent vehicles have lower redundancy (each vehicle has lower functionality). However, as the number of vehicles increases, dependent vehicles tend to have higher productivity and a longer lifetime because these vehicles can interact with each other, which lead to beneficial emergent behaviors, as was explained in Section 3.3.2.4.

In the case of non-coordinated vehicles, if the number of vehicles doubles, the total productivity only doubles, because the vehicles are in different regions and cannot interact with each other in a beneficial manner (i.e. there is no inherent redundancy in the system).

### **3.3.8.3 Mass**

Unsurprisingly, mass increases in a linear manner as the number of vehicles increases. The correlation plot for coordinated dependent vehicles has the lowest gradient again because, typically, each vehicle has lower capability and more functionality is shared between vehicles in this type of system. The correlation plot for non-coordinated vehicles on the other has the highest correlation since the vehicles are in different regions and cannot share any functionality.



#### **3.3.8.4 Coverage**

Coverage increases as the number of vehicles increases. However, this is due to different reasons for each of the types of spatial distribution. For coordinated vehicles (both dependent and independent), as the number of vehicles increases, the area explored at each site or in each region increases (i.e.: the “footprint” of the system increases). Furthermore, the expected lifetime increases as the number of vehicles increases due to redundancy, and therefore the number of sites visited also increases.

For non-coordinated vehicles, the vehicles are landed in completely different regions. Therefore, although the lifetime of each vehicle does not increase, the number of sites visited increases linearly as the number of vehicles increases.

#### **3.3.8.5 Vehicle-level Complexity**

As predicted in Chapter 1, the vehicle-level complexity decreases as the number of vehicles increases in a spatially distributed system. However, each type of system exhibits very particular trends. In systems with coordinated dependent vehicles, functionality is increasingly shared and spread out as the number of vehicles increases. Therefore, on average, the vehicle-level complexity decreases dramatically as the number of vehicles first increases. However, a minimum level of complexity is eventually reached and the trend curve eventually flattens out.

Although they demonstrate a similar behavior, systems with coordinated independent vehicles do not enjoy as dramatic a reduction in vehicle-level complexity because they do not share SS functions.

Non-coordinated vehicles, however, do not share functionality and therefore the vehicle-level complexity does not necessarily reduce as the number of vehicles is increased. However, since the vehicles in non-coordinated systems are very similar, there is a significant learning curve effect, which in turn reduces the average vehicle-level complexity (i.e. the CW weightings decrease as duplication occurs, up to a certain level) since more is understood about the system every time a new vehicle is built, and vehicle testing does not have to be repeated.

#### **3.3.8.6 System-level Complexity**

In systems with coordinated dependent rovers, the interactions between the vehicles can affect system-level complexity exponentially, depending on how the system is structured. Coordinated independent vehicles do not have such high levels of interaction, but there is a need for coordination of the system and collision avoidance. Therefore, the trend slope of independent vehicles is much shallower than for the systems with dependent rovers.

In both cases, the red dashed lines in Table 22 shows the trends given by the system-level complexity metric developed. However, it is expected that as the number of vehicles increases, the system will

become a swarm, and swarm control techniques will be used. This would reduce the system's complexity because adding a vehicle in a swarm has low marginal cost compared to that calculated by the system-level complexity metric. This expected behavior is illustrated by the blue dashed line in Table 22 but is not captured by the framework.

Non-coordinated vehicles do not suffer from system-level complexity because they are operated independently at different sites.

### **3.4 The Addition of Micro-Rovers to a System**

Part of the analysis presented in the last section has demonstrated that sharing SS functions, particularly the "long-range traversing" function, is particularly advantageous in spatially distributed systems where the secondary vehicle(s) is (are) significantly smaller and less power intensive than the monolithic vehicle. To investigate this finding further, this section explores the concept of adding very small vehicles (i.e. micro-rovers) to a larger rover such as the Mars Science Laboratory (MSL) as part of a Martian surface exploration mission.

Extreme and benign terrains require vastly dissimilar wheel designs. Consequently, a wheeled robot, operating alone, is incapable of efficiently exploring both terrains. [151] A unique solution to this issue was proposed in Murphy et al. [152]: using a marsupial robotic team. In the marsupial relationship, a larger "mothership" rover transports and deploys a team of smaller, "passenger," robots. [153] Despite the potential for a MSL-sized planetary rover to greatly increase its science return by carrying a small team of micro-rover passengers, a marginally similar concept has only been proposed once, by Mathews and Nesna. [154] Most of the current work in the field of marsupial robotics has been focused explicitly on terrestrial applications [155], [156], [157], [158] and the viability of planetary marsupial teams with micro-rover passengers remains understudied.

Planetary micro-rovers, generally having a mass of between one and ten kilograms, [159] are a low cost, low mass, and low complexity alternative to conventional, MER and MSL-sized rovers. A team of these rovers can perform high-risk tasks, keeping the mothership rover out of danger. If the micro-rovers are equipped solely to return samples to the instrument suite of the mothership for analysis (that is, to essentially act as an extension to the robotic arm), the loss of a single micro-rover would minimally compromise the mission's science goals. This type of expendability would enable robotic exploration of areas previously thought too dangerous for flagship missions.

Rover Name	Total Mass	Dimensions (l*w*h)	Instrument/Payload Mass	Power	Power Source	Velocity
Axel	39kg (can be scaled down)	84x152x84 cm	Can carry up to 10 kg instruments. can collect/return 2x soil samples on hills 0-40deg	20 W	Battery (8hr), can be charged via tether	MAX 10 cm/sec
Nanokhod	2.55kg (w/payload cab) or ~12kg (w/ coring attachment)	30x20x20 cm	1100g	2W average, 3W peak	Tether to lander	.14 cm/sec
SRR	7.2 kg	88x55x36 cm	4 deg freedom arm (.7m total reach)	1-1.5 hr	Battery pack (no recharging mechanism)	MAX 21 cm/sec
Shrimp	3.1 kg	60x15x23 cm	UNKNOWN	UNKNOWN	Battery	UNKNOWN
SpaceCat	<4 kg total	20x30x20 cm	<2 kg	2W average, 3W peak	Tether?	UNKNOWN
FASTER	14.8 kg	83x50x40 cm	3.6 kg	100W average, 500 W peak	LiPo recharge battery	<1.25 cm/sec
Cliff-Bot/TRESSA	8 kg		UNKNOWN	UNKNOWN	UNKNOWN	
Sojourner	10.5 kg	60x48x30 cm	UNKNOWN	Solar/battery	.22sqm solar/150 W-hr batteries	.667 cm/sec
MICRO5	5 kg	55x53x25 cm	UNKNOWN	~10W (EST)	Solar (peak 27W). NiCd battery	1.5 cm/sec
Rover Name	Locomotion	Science/Uses	Terrain Traverse			
Axel	2 rounded wheels	Sampling on steep slopes	Can lower over 90deg drops & drive down			
Nanokhod	2 tracks	Operations in a ~10 meter radius around stationary lander, Alpha-Particle-X-Ray-Spectrometer, Close-Up Imager, Moessbauer-Spectrometer, payload cab can be replaced by a corer/sampler that can deposit samples in the lander for further analysis	Can climb obstacles 10 cm tall, 24deg slopes			
SRR	4 wheels	Returning samples from science rover to Mars Ascent Vehicle	Can reconfigure its height by adjusting "shoulders" that allow it to modulate ground clearance and COG			
Shrimp	6 wheels (1 Front, 4 Middle-2x2, 1 Rear)	Can traverse rugged terrain well.	Can climb obstacles 22 cm tall (2x wheel diam), 40deg slopes			
SpaceCat	6 Wheels (2 sets of three wheels arranged in a triangle), all powered. The groups of wheels can also be lifted, giving the rover a primitive walking capability	No specific science goals specified. Minimum requirements for project indicate that the rover should be able to operate within a 10 meter radius of the lander	Can "step" over objects by tipping the top wheel onto the obstacle (max 10 cm tall)			
FASTER	2 helical wheels (rear) and 2 wheel legs (front)	Scouting in front of large rover to allow large rover to travel faster	Can climb 25deg on firm soil, 15deg on soft soil			
Cliff-Bot/TRESSA	4 independently driven/steered wheels	Sampling on steep slopes (4x detachable scoops), color microscopic imager, raman spectrometer, reflectance spectrometer	lowered by 2x Anchorbots, 70 deg soil, 85 deg rocky			
Sojourner	6 independently driven wheels	Alpha Proton X-ray Spectrometer	Can climb obstacles 13 cm tall (1x wheel diam)			
MICRO5	5 wheels (4 drive wheels-2x2, 1 wheel to support the weight of the rover when one set of wheels is off the ground)	Geology by photo images. Element Analysis, Wide Area Investigation, Investigation by Manipulator	Can climb obstacles 13 cm tall (1.3x wheel diam), 30deg slopes (hard surface), 20deg slopes (soft surface)			
Rover Name	Advantages	Disadvantages				
Axel	Can reach places its host rover can't, poses little risk to larger rover, un/rewinds its own tether (protects tether from abrasion)	Low energy efficiency b/c of paddle wheels (can't travel long distances on its own).				
Nanokhod	Versatile instrument options, with room for a fourth instrument in the payload cab. The option to swap the entire payload cab out for a core sampler that can return samples to the lander for analysis expands the science missions that the rover can be used for	The rover is limited to brief periods of operation per day because the rover contains no WEB to protect its delicate electronics. As a consequence, the rover can only operate when the outside temperatures are well within the limited ranges of the on board electronics. If one of the track motors fails, the rover is rendered inoperable. VERY slow.				
SRR	Can actuate shoulders to make rover more stable on uneven terrain, can travel very quickly	Does not have any way of surviving more than a single sol				
Shrimp	Can travel over obstacles much larger than its wheel diameter	Though it can climb obstacles on a flat surface, it has limited potential to operate in craters				
SpaceCat	Can travel over extreme terrain well, wheel design is innovative	Science goals not well developed				
FASTER	Can travel over extreme terrain well, provides a safer environment for larger rover	Lower efficiency because of paddle wheels				
Cliff-Bot/TRESSA	Can do more science than the Axel rover, despite weighing less and being smaller, more versatile in its cliff traversing abilities due to the fact that the two tethers provide it horizontal stability as well as the ability to descend steep faces	Can not hang from its tethers, two tethers=two times the area to get snagged on obstacles				
Sojourner	Utilized innovative rocker-bogie suspension system	Solar panel could not recharge on-board battery, which restricted the rover to day operations once battery was depleted				
MICRO5	The science goals of MICRO5 are far better developed than most of the other micro-rover proposals	Though the rover uses an innovative suspension system (PEGASUS), the PEGASUS suspension system is less effective than the rocker-bogie system (only 1.3x diam vs 1.5x diam)				

While micro-rovers are capable of operating alone while carrying a single small experiment or instrument, power and communications constraints preclude this class of rovers from operating for extended periods of time without a supporting entity. Numerous mission concepts for individual and teams of micro-rovers have been developed, and overview of which is provided in Table 23. Wilcox proposed a concept where a team of several hundred “nanorovers” would excavate sites on the Moon or Mars. [23] The FASTER micro-rover, introduced by Sonsalla et al., [161] was designed to measure characteristics of the terrain ahead of its mothership, removing rover operators’ uncertainty in the terrain ahead. The rover operators would then be able to adjust the mothership rover’s speed based on the terrain, allowing FASTER’s mothership to travel faster without the risk of getting trapped in soft sand, which is the fate that the MER Spirit suffered. [162] TRESSA, a heterogeneous team of three rovers (two larger ‘Anchorbots’ and one Cliffbot micro-rover) was shown to be capable of exploring cliff faces up to 85°. [163], [164], [165] However, with the exception of Cliffbot, no other planetary micro-rover put forward in the literature has been shown to be able to explore extreme terrains.

Craters hold the key to understanding whether water currently exists on Mars. The HiRISE instrument onboard the Mars Reconnaissance Orbiter (MRO) first observed seasonally recurring dark patches on the walls of craters in 201. [166] These patches, called Recurring Slope Lineage (RSL), are of unknown composition, though one of the preeminent theories proposes that the observed flows are brine, which would explain the mixture’s ability to exist seasonally as a liquid despite Martian temperature and pressure. [167] Samples analyzed from these dark patches could drastically change scientists’ understanding of the habitability of Mars. Additionally, rock and soil samples collected from exposed strata on crater walls and cliff faces, provided they have not been exposed to prolonged ionizing radiation, are equivalent to samples obtained via drilling. [168]

Current drilling systems are limited; MSL can drill to a depth of only 5 cm, [169] and although the ExoMars rover is planned to drill down to 2 meters, [170] no other rover with a deep drill has ever been designed past pre-phase A studies and such drills heavily drive the mass and complexity of rovers. Assuming that a micro-rover with sampling capabilities similar to the Cliffbot is developed, the micro-rover would be able to access samples from exposed strata that could only be accessed otherwise by drilling 20m [163] into the Martian surface. This is 400 times deeper than MSL is capable of drilling and 10 times deeper than ExoMars’ ability. A small team of versatile micro-rovers could be transported from crater to crater by a rover like MSL, returning samples from various locations in the crater. MSL’s existing suite of instruments would be sufficient for analysis of the samples, and the team of micro-rovers would act as MSL’s “extended robotic arm,” a role for micro-rovers first introduced by Bertrand et al. [171] This was judged to be the most valuable use for a team of micro-rovers if they were added to the current MSL design.

Since no micro-rover design with appropriate properties exists in the literature, a study was performed to design a micro-rover weighing 9.5kg, DRACO (Deployable Rover to Augment sample-Collection Operations), that could be added to MSL. [160] It is to be noted that the rocker-bogie suspension system, typically used by NASA in its rover designs, is poorly suited for extreme terrains. Rocker-bogie rovers need additional motors to steer their wheels and are susceptible to tipping because of their higher center of gravity. These rovers have a high ground clearance, making them unsuitable for fitting underneath or within mothership vehicles.

A CAD rendering of the DRACO system is presented in Figure 30, and a full report on its design, the tools used to estimate its properties and further CAD files are available (see Appendix C). DRACO possesses a robotic arm for sample collection and handling and a pair of cameras. It relies on the mothership vehicle for data handling, long range traversing and communication to the Earth (these are therefore SS functions in this example). One of the main features of this micro-rover is that it would be attached to its mothership vehicle using a tether. It was found that the tether system helped reduce the mass of the micro-rover, since the tether can be used to transfer energy and data. The tether system also enables certain mission concepts, such as cliff scaling which is shown in Figure 31.

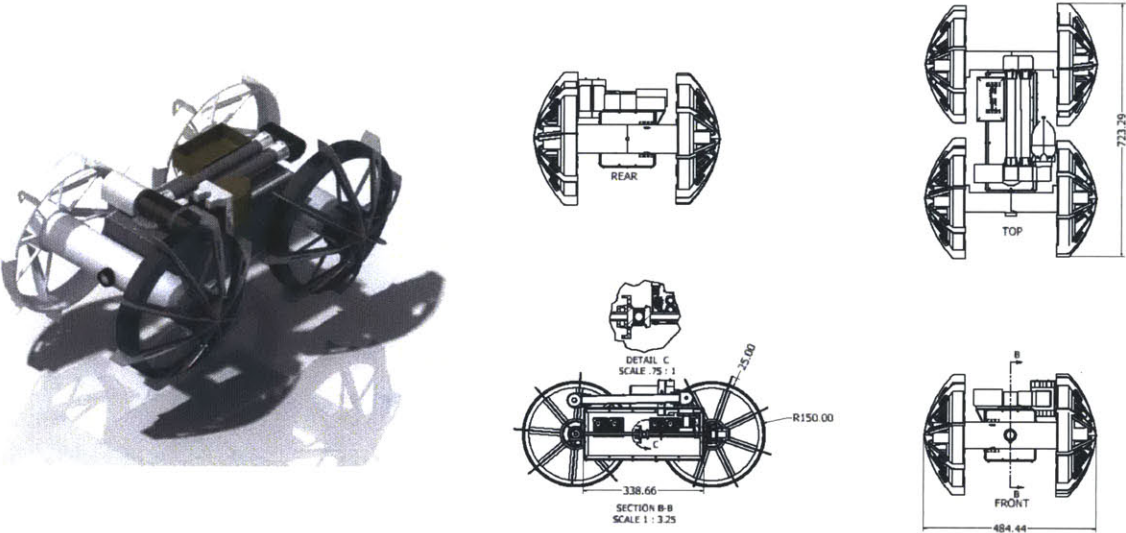


**Figure 30: DRACO micro-rover (chassis is ~ 30cm x 20cm in dimension)**

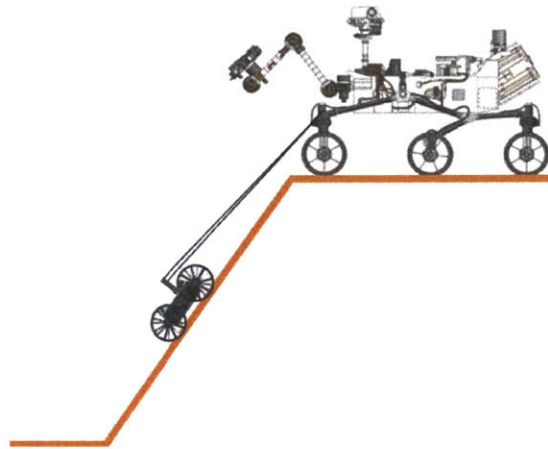


**Figure 31: Micro-rover concept of operations (not to scale)**

Adding two of these rovers to the MSL system would add 30kg to the system (including the deployment mechanism), as well as increasing its complexity by approximately 10%, due to the extra tether mechanisms involved in the design (assuming the micro-rover system has a TRL of 3 in the complexity metric, and that it is modeled as an additional instrument). On the other hand, it would significantly increase MSL's coverage: not only would the system cover more ground, as shown in Figure 32, but it would also be able to access areas of higher scientific interest, as explained earlier. In turn, being able to access these samples would yield greater science benefit as this would enable new science goals (such as the detection of brine, as discussed earlier) to be achieved.

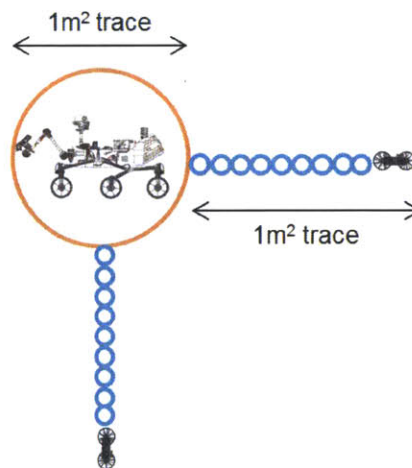


**Figure 32: Adding 2 micro-rover systems could increase the coverage by up to 200% at each site of interest.**

Micro-rover concepts are not currently fully integrated into the framework and tools due to the lack of historical data on such systems. The library of concepts is too slim, and the concepts that have been put forward have not been sufficiently tested. There is therefore a limited understanding of the abilities of such systems to perform in Martian environments. For example, the rover designed in this section was sized using the terramechanics equations presented in Appendix A. While these equations have been shown to be well optimized for large (>50kg) rovers, some of the resistance equations only offer first order estimates for smaller rovers. These must therefore be developed further and correlated with physical test data before they can reliably lead to accurate mass estimates. As further research is performed in this field, these types of systems could easily be added to the tools developed in this thesis.

### **3.5 Mars Science Laboratory (MSL) Case Study**

In this proof of concept case study, which was used to test how the framework can be used to rapidly obtain an understanding of the trades for spatially distributed systems for a given problem, the design of the Mars Science Laboratory (MSL) is used as the baseline monolithic system. MSL is a highly integrated and complex 930kg rover. After a 2-year delay and significant budget overruns, it successfully landed on the surface of Mars on August 6<sup>th</sup> 2012. Even though the design of the rover can be deemed to have been successful, this case study attempts to uncover where the trade between a multi-vehicle architecture and a monolithic system lies in the case of MSL. The overarching science goal for MSL is to explore and quantitatively assess a local region on Mars' surface as a potential habitat for life, past or present. [2] The four primary science objectives are to:

- 1) Assess the biological potential of at least one target environment
- 2) Characterize the geology of the landing region at all appropriate spatial scales
- 3) Investigate planetary processes of relevance to past habitability
- 4) Characterize the broad spectrum of surface radiation

The functions for MSL were derived and classified based on these goals. The list of functions from the functional decomposition is presented in Table 24.

In this case study, energy generation was classified as ES (and thus is not fractionated) and it was assumed that MMRTGs provide power if the rover requires more than 100W of power from its payload (if it required less than 100W, solar panels are assumed). Some restrictions were imposed for the instrumentation. For example, the MastCam had to be accompanied by the ChemCam. Additionally, the APXS and MAHLI had to be on the same vehicle, to avoid duplication of the robotic arm. Similarly, CheMin and SAM were made to be on the same vehicle, to contain the analysis of samples to one vehicle. This led to the 7 groups of instruments shown in Table 25.

**Table 24: Functional decomposition for the MSL case study**

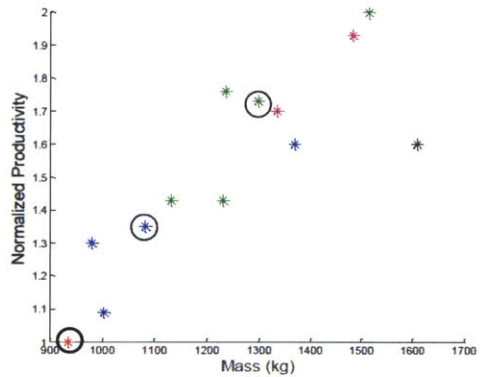
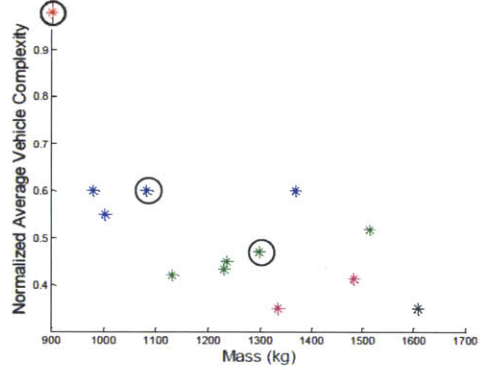
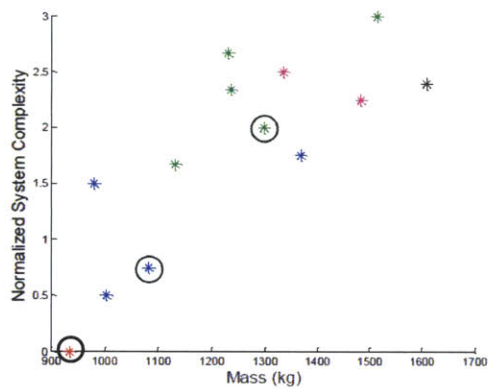
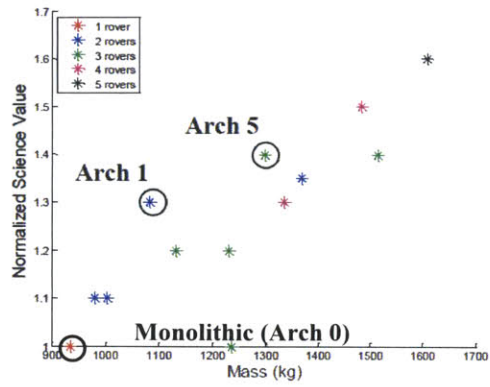
Function	Form	Category
Imaging	Mast Camera (MastCam)	VD
	Mars Hand Lens Imager (MAHLI)	VD
Detecting and identifying molecular species	Chemistry & Camera (ChemCam)	VD
	Alpha Particle X-ray Spec. (APXS)	VD
Identifying and characterizing minerals and compounds	Chemistry & Mineralogy (CheMin)	VD
Exploring molecular & elemental chemistry relevant to life	Sample Analysis at Mars (SAM)	VD
Characterizing spectrum of energetic particle radiation	Radiation Assessment Detector (RAD)	VD
Studying the atmosphere	Rover Environment Monitoring Station (REMS)	VD
Measuring H- & OH- bearing materials in shallow subsurface	Dynamic Albedo of Neutrons (DAN)	VD
Traversing	Mobility System	ES
Energy Generating	MMRTGs or Solar Panels	ES
Energy Storing	Batteries, power management system	ES
Payload Carrying	Vehicle	ES
Thermal Protecting	Thermal System	ES
	Rover-to-rover communication system	ES
Transmitting data	UHF communication to an orbiter	SS
	Direct to Earth communication	SS
Navigating	Path-planning system, HazCam, NavCam	ES

**Table 25: Instruments onboard MSL used in the case study**

Instrument	Acronym	Group
Mast Camera	MastCam	1
Chemistry & Camera	ChemCam	1 & 6
Alpha-Particle X-Ray Spectrometer	APXS	1
Mars Hand Lens Imager	MAHLI	1
Chemistry & Mineralogy	CheMin	2
Sample Analysis at Mars	SAM	2
Radiation Assessment Detector	RAD	3
Rover Environmental Monitoring Station	REMS	4
Dynamic Albedo of Neutrons	DAN	5
Hazard Camera (stereo)	HazCam	1 & 7
Navigation Camera (panoramic)	NavCam	1 & 7

This study would have led to a very large trade space of architectures, but patterns were rapidly identified in the architecture set to help constrain the trade space and downsize it. Twelve architectures that had consistently high Pareto rank and are representative of the trade space were found, as shown in Figure 33. The two best performing architectures in this subset (apart from the monolithic) are circled. Note that all the values shown in Figure 33 are normalized by the value for MSL.





Arch ID	Rover ID	Payload Groups	Mass (kg)
0	1	1, 2, 3, 4, 5, 7	935
1	1	1, 2	790
	2	3, 4, 5, 6, 7	293
2	1	1, 2	790
	2	3, 4, 5, 7	213
3	1	1, 3, 4	745
	2	2, 4, 6, 7	622
4	1	1, 3, 4	745
	2	2, 4, 7	235
5	1	1, 2	790
	2	3, 4, 7	266
	3	5, 6, 7	241
6	1	1, 2	790
	2	3, 4, 7	186
	3	5, 7	156
7	1	1, 3, 4	745
	2	2, 5, 7	540
	3	6, 7	228
8	1	1, 3, 4	745
	2	2, 7	300
	3	4, 7	190
9	1	1, 2	790
	2	3, 7	172
	3	4, 7	190
	4	5, 7	182
	5	6, 7	273
10	1	1, 2	790
	2	3, 7	172
	3	4, 7	190
	4	5, 7	182
11	1	1, 2	790
	2	5, 7	202
	3	6, 7	282
	4	3, 4, 7	208
12	1	1, 2	790
	2	5, 7	202
	3	3, 4, 7	238

Figure 33: Details and evaluation of twelve representative architectures

A few general observations can be derived from the results. First, it can be seen that architectures with more vehicles have higher productivity, higher science benefit and lower average vehicle-level complexity, but they generally have higher mass and higher system-level complexity. This is in line with the results found in Section 3.3.8.

The main sources of uncertainty in the results presented are the reliability of the components and the inaccuracies in the mass metric (which was found to be accurate within  $\pm 20\%$ ). A similar sensitivity analysis to that performed in Section 3.3.2.4 was performed and it was found that this general trend held true for productivity as the reliability varied. Furthermore, it was found that the uncertainty in the mass had a negligible effect on the architectures and the trends related to mass also held true. Finally, since this case study was a redesign of an existing mission, the science benefit and the system level complexity were calculated based on existing science traceability matrices and engineering designs, and known costs. Therefore, these metrics do not have any significant uncertainty associated with them. However, the case study in Chapter 5 will demonstrate how uncertainty in these metrics can affect the Pareto front.

The general trends observed are due to several factors. First, multi-vehicle architectures can cover a larger area during the mission duration, which leads to higher science return. Additionally, the inherent redundancy present in multi-vehicle systems leads to greater robustness to failure and thus to longer mission durations. Each vehicle in the system carries a smaller amount of payload, which means that many of them can operate on solar power. This in turn leads to a lower vehicle mass, and a higher power-to-weight ratio. These vehicles can thus travel at a higher speed and cover more terrain than their heavier counterparts.

In the architectures in Figure 33, it can be seen that if instrument groups 1 and 2 are on different vehicles, the productivity increases but the system-level complexity also increases dramatically. This is because the instruments in group 1 are used to collect a sample, and those in group 2 analyze the sample. If they are on different vehicles, mass transfer must occur between the vehicles, which leads to increased system-level complexity. The increased productivity occurs from the fact that, if on a single vehicle, group 1 and group 2 instruments must operate at different times (and thus have low duty cycles) due to power limitations. If they are on different vehicles, collection and analysis can occur concurrently, thus increasing productivity.

Despite the increase in mass described earlier, there are a number of architectures that fall within 30% of the mass of MSL, and can be assumed to be part of the same mission class. In particular, architectures 1 and 5 performed very well. One interesting point about architecture 5 is that two of the rovers are very alike (both have solar panels and approximately the same mass). This makes the vehicle design simpler than if both vehicles were significantly different and could lead to potential economies of scale.

In this case study, the monolithic vehicle still performs very well in most metrics, and has the lightest total mass. This is due to the fact that many of the MSL instruments were designed to be highly integrated with each other and the vehicle. This is particularly true of the instruments in groups 1 and 2, and therefore limits the amount of VD functions that can be fractionated. Because of the choice of instruments, there are no architectures composed of several very light (<100kg) vehicles that can perform the same task as the monolithic, and at least one larger (>500kg) vehicle is needed in each architecture. If this analysis had been done in the early stages of the mission design, there would have been a trade between instrument complexity, science value and productivity. A more distributed system would have been able to meet the mission goals with different instruments (e.g. with multiple smaller drills and more surface samples) and with a higher productivity, while potentially sacrificing some of the quality of the measurements (which would have been reflected in the  $V_{i,j,k}$  weighting).

### 3.6 Conclusion

The purpose of this chapter was to demonstrate the use of the framework developed in Chapter 2 for exploring the trade space of spatially distributed systems for different missions. Additionally, the general effects of spatial distribution on the system properties were evaluated.

First, a case study based on the Mars Exploration Rovers (MERs) uncovered general trends between mass, science benefit, vehicle-level complexity, system-level complexity, productivity and reliability. This same case study was then used to demonstrate the effect of sharing Supporting Supporting (SS) functions on the system. It was shown that sharing the long-range communication system across several vehicles was always beneficial to the system, but that sharing other functions, such as hibernating and energy generating, are dependent on the size and requirements of the vehicles. Finally, this case study also explored the differences between coordinated versus non-coordinated, and dependent versus independent, spatially distributed systems on the mission properties. The trends evaluated in this case study, including the observed increase in system productivity, mass, system-level complexity and science benefit as the number of vehicle increases and the effects of fractionating different functions, can therefore inform designers on the effect of certain design decisions on the properties of a spatially distributed mission before they even go through the design process.

Then, a short case study investigated the marginal benefit of adding very small rovers, or micro-rovers, to the system. The advantages of micro-rovers are that they are small and lightweight, have low complexity designs and can benefit from economies of scale. In addition, since they are low cost, they can be used for tasks that have higher risks. It was found that micro-rovers can significantly increase the area explored, including areas that are too risky for the main mothership vehicle to explore, and during that process can also help find areas of high scientific interest towards which the main vehicles can then be

directed to, as well as providing additional context in science missions. The example micro-rover system put forward essentially acted as an extended arm for MSL that could collect samples in risky environments for MSL to analyses. As miniaturization of instruments develops further, it is hoped that such systems could be used for performing additional science measurements in planetary surface missions.

The chapter closed with a case study based on the Mars Science Laboratory Design (MSL). This end-to-end rapid case study demonstrated that, while there are multi-vehicle alternatives to MSL, the instruments that were chosen for MSL were highly integrated and thus benefited from being on the same platform. Consequently, the choice of instrument also plays a key role when choosing a type of architecture. This concept will be evaluated further in Chapter 5. Now that the effects of spatial distribution have been explored in depth, Chapter 4 will present how the traverse of these multi-vehicles systems can be simulated during the early mission formulation process, and how these simulations can help further downsize the trade space and refine the systems' designs.

## Chapter 4

# SEXTANT AS A MULTI-VEHICLE SYSTEM SIMULATION TOOL

### 4.1 Introduction

One of the limitations of the framework presented so far is the lack of information on how well these multi-vehicle systems will perform as compared to the baseline monolithic system in its operational environment. For orbital assets, a range of orbital dynamics tools exist to quickly estimate the performance of vehicles and to help refine their design. However, such high-level, rapid tools do not exist for planetary surface vehicles. To address this issue, a path-planning tool, called the Surface Exploration Traverse Analysis and Navigation Tool (SEXTANT) was adapted to simulate the operational environment of multi-rover systems after the architecture evaluation process has taken place. While it is presently being used only for Moon-based traverses, the tool is very flexible and could easily be adapted to measure traverses on Mars and Earth (Earth maps were in fact used during the validation of the tool).

The history of path-planning tools and of the development of SEXTANT was discussed in Chapter 1. SEXTANT consists of a set of lunar maps, along with a graphical user interface (GUI), which allows the user to select points of interest on the map for the rovers to visit. Given the functionality of each of the rovers, and the functionality needed at each point of interest (i.e. the science that must be performed at each point), SEXTANT can solve the Travelling Salesman Problem for a team of rovers. It then uses an A\* optimization algorithm, based on the work of Hart et al. [172] and adapted for SEXTANT by Johnson [116] to calculate the optimal route of the rovers from point to point in terms of energy expended,

distance or speed. The GUI also allows the user to upload the power and mobility properties of each rover from the architecture evaluation process, which is then used to evaluate the ability of each vehicle to traverse the terrain and their power properties. Finally, SEXTANT can measure the illumination on, and communications link availability of, each vehicle using ephemeris data and elevation data from a given point on the traverse.

This chapter starts by giving details of SEXTANT's features. It then provides a simple case study to demonstrate these features and to highlight the ability of SEXTANT to help refine design estimates in the early design phases. The features that make SEXTANT a particularly powerful tool for multi-vehicle mission planning are then presented. The chapter ends with a case study of a set of rovers for the exploration of the South Pole of the Moon.

## **4.2 SEXTANT Features for Single Vehicles**

SEXTANT has been in development at MIT, under various forms, for approximately 10 years, as detailed in Chapter 1 and was most recently adapted by Johnson. [117] In this section, the important existing features of SEXTANT are first detailed. This is followed by a description of the new features added to SEXTANT that are relevant for any type of system, and a short one-vehicle case study to demonstrate how SEXTANT can be used to refine mass estimate in early mission design phases. Section 4.3 then describes the features that were added to SEXTANT to enable it to simulate a multi-vehicle mission.

### **4.2.1 Overview of Existing Features**

#### ***4.2.1.1 Model of the Lunar Environment***

SEXTANT is fundamentally built upon a set of lunar elevation maps, which are matrices of elevations of equally spaced points on the lunar surface. These maps were obtained from data produced by the Lunar Orbiter Laser Altimeter (LOLA) instrument, which flew on the Lunar Reconnaissance Orbiter (LRO). [173] The LOLA data have been used to produce several elevation maps, at both the southern and northern poles of the Moon. A range of map resolutions are already available, and more maps can be added as more elevation data become available. For a given area, a higher resolution leads to a higher computation time. Thus, low-resolution maps of large areas can be used to quickly simulate long traverses or gain an understanding of the region. These higher resolution maps can be used to evaluate specific parts of a long traverse, or traverses of shorter lengths. Higher resolution maps are particularly advantageous in helping to plan operations, as they reveal large objects such as boulders, or particularly

rough terrains, which are not detectable on low-resolution maps. An example of a 10-meter resolution map of the South Pole of the Moon is shown in Figure 34.

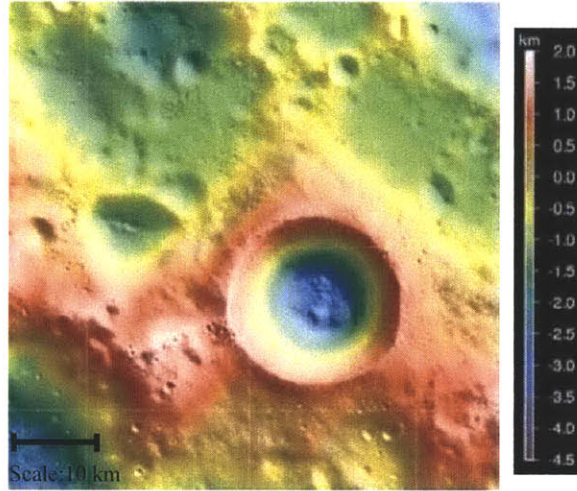


**Figure 34: 60 km<sup>2</sup> map of the South Pole of the Moon, with 10m per pixel resolution**

Using a gradient operation, the magnitude of the local slope at each point can be calculated using the data from the elevation map. The slope data are then stored in a matrix of the same size as that for the elevation data, where each element corresponds to the terrain slope at that location. For each vehicle, the slope data can be used to identify the areas that the vehicle cannot access due to mobility restrictions. Traverses cannot cross through these areas, which are considered as obstacles. To mitigate the limitations in resolution, the user can also manually designate additional areas in which the vehicles cannot travel.

#### 4.2.1.2 Internal Model of Rover Energy and Power

SEXTANT includes an internal rover energy model, which calculates the energy expended by the rover during the traverse. This, combined with the shadowing data and information about the energy used by the payload at each activity point, allows the calculation of the energy profile of the rover, as is shown below. Using the average rover speed ( $v$ ) and the rover mass ( $m$ ), defined using the mass modeling tool detailed in Chapter 3 and in Appendix A, the equations below can be used to calculate the energy expended by each rover. It is to be noted that the energy expended on a slope is different from that on a flat surface. Additionally, it is assumed that each rover uses a baseline amount of energy, even when stationary, which is the idle power that is defined by the user.

$$\text{Energy Rate } (W) = W_{level} + W_{slope}$$

**Equation 21**

$$W_{level} = 0.216 * v * m$$

**Equation 22**

$$W_{slope} = \begin{cases} 0 & \text{for } \alpha = 0^\circ \\ 0.02628 * m * \alpha * (g/1.62) * v & \text{for } \alpha > 0^\circ \\ -0.007884 * m * \alpha * (g/1.62) * v & \text{for } \alpha < 0^\circ \end{cases}$$

**Equation 23**

SEXTANT also possesses a power model, which calculates the amount of power produced by the rover's solar arrays ( $P_{SA}$ ):

$$P_{SA} = V_{sun} I \eta_{SA} A_{SA}$$

**Equation 24**

In this equation, the efficiency ( $\eta_{SA}$ ) is user defined and must be kept the same in SEXTANT and in the mass modeling tool. The solar array area ( $A_{SA}$ ) is derived through the rover tool, which uses information about the terrain and the vehicle's other power requirements to size the solar arrays for average power requirements. Batteries are then used to fulfill peak power requirements and hibernation energy (the energy needed to survive the lunar night). The fraction of the solar disk ( $V_{sun}$ ) that can be seen by the rover is derived from the illumination algorithm. A clear advantage of using SEXTANT to assist in the design of the power system is that it can help identify areas of low illumination in the mission, which in turn can lead to the decision to increase the size of the batteries (or other energy storage system, such as fuel cells) to deal with the low illumination environment.

#### **4.2.1.3 Shadowing**

In addition to its enhanced ability to plan traverses for multiple vehicles jointly exploring a planetary surface, SEXTANT can calculate some of the key mission parameters. Johnson [117] designed an algorithm to calculate the shadowing at every point on the traverse. Since this function forms the baseline for optimizing the vehicles' energy profile during the traverse, and since a similar methodology is used to calculate the link availability for each rover, a brief overview of the function is given here.

To account for the movement of the Sun in the sky during the traverse, SEXTANT calculates the Sun's position at each time step. By default, this time step is set at 120 minutes, during which time the Sun moves by  $1^\circ$ . A smaller time step would give a more accurate result, but would also lead to increased computation time. The traverse between each AP is divided into a series of intermediate Path Points (PPs) and the time at which each rover arrives at a PP is rounded to the closest multiple of this time step. This leads to a series of unique times, at which the Sun position is calculated. The position of the Sun at each of these times with respect to the Moon's center of mass is then calculated. A coordinate transformation must also be performed to obtain the elevation and direction of the Sun from each PP at the given time.



SEXTANT must then determine whether or not the Sun is visible at each time. This is performed using the horizon method, which was used for the Moon most recently by Mazarico et al., [174] with the LOLA data. There are two distinct steps in the method. First, a database of 720 separate horizon maps is constructed. Each map shows the elevation of the horizon in a certain direction for all points on the terrain map. Each of these horizon maps is in a direction that varies  $0.5^\circ$  from the surrounding maps. It is to be noted that the horizon database only needs to be constructed once, and does not need to be recalculated as the Sun's position changes. The second step in the horizon method requires referencing specific horizon maps in the direction of the Sun to determine whether or not the Sun is visible for a PP. Once the horizon elevation has been calculated for each PP, it is compared to the elevation of the Sun. From the surface of the Moon, the solar disk has an apparent diameter of  $0.52^\circ$ . Because the Sun is not a point source, it can either be: fully visible, partially visible or not visible at all. In turn, the percentage of the solar disk visible at each point is calculated by SEXTANT as a value between 0 and 1. The shadowing for each path stage is determined as the average between the two PPs at either end of the stage. Figure 35 demonstrates the shadowing on a vehicle over a sample traverse.

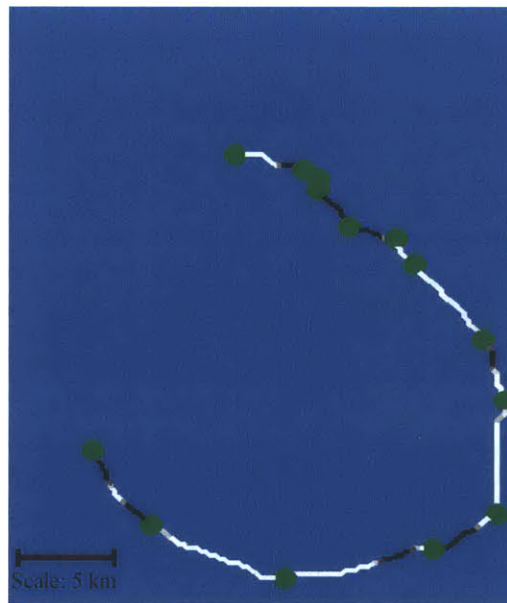


**Figure 35: Shadowing on the vehicle throughout the mission duration.**  
Along the path, when the line is white, the full solar disk is visible; a shade of grey indicates that the solar disk is partially visible; and the Sun is fully obscured when the line is black.

#### 4.2.2 New Single Vehicle Features

This section describes the additions that were made to SEXTANT and that apply to the vehicles themselves. The details of the SEXTANT additions that help evaluate multi-vehicle systems are detailed in Section 4.3

#### 4.2.2.1 Energy Profile

Once the shadowing at each point on the traverse has been calculated, the energy consumption rate can be compared to the energy produced by the solar panels. If the solar panels do not produce enough energy to power the vehicle, energy from the batteries is used. When the solar panels produce more energy than needed, the batteries are charged. Using this simple energy allocation algorithm, the battery levels on the rover can be calculated for the whole traverse. SEXTANT then possesses the ability to check whether the batteries are sufficient to meet the power requirements throughout the mission. If they are not, SEXTANT attempts to add waiting time at any point along the traverse in areas of high illumination to recharge the batteries. If a viable solution is found, then SEXTANT gives the user the option to choose this modified path. Otherwise, it informs the user that the chosen path does not have a solution for the power system. The user can then either change the traverse or increase the size of the batteries through the rover modeling tool, again highlighting the trade between operations requirements and design. Figure 36 demonstrates SEXTANT's ability to add waiting times to ensure that the vehicle has enough energy during the traverse.

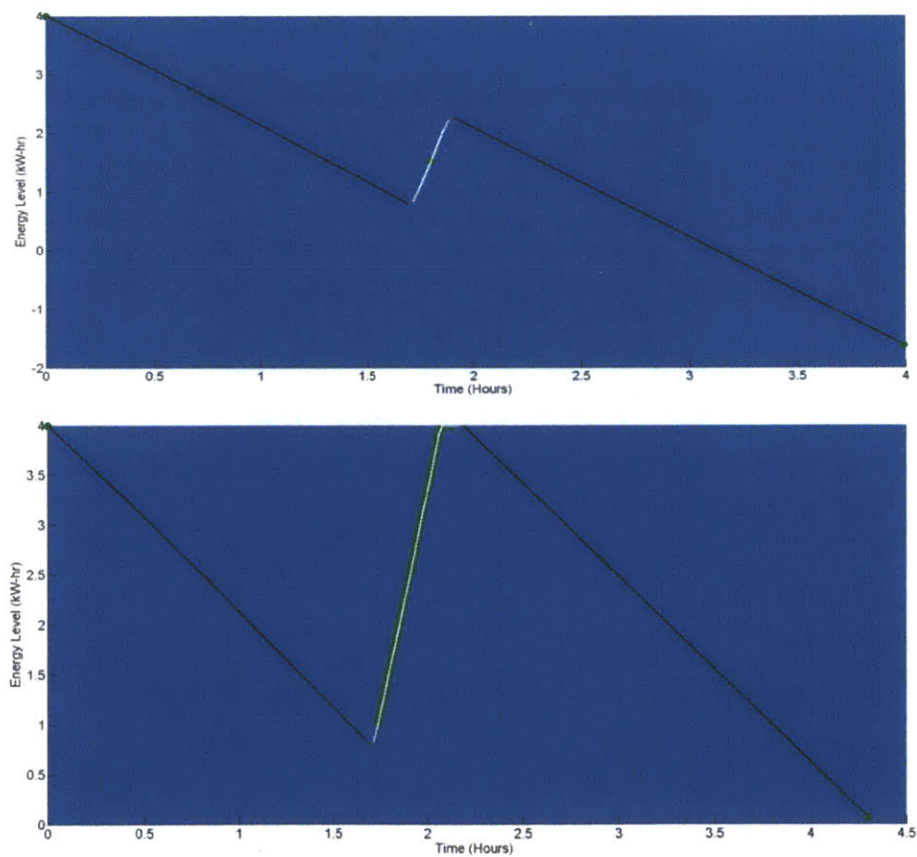


**Figure 36: Rover energy levels before waiting times are added (top) and after (bottom). Areas in light green indicate when the rover is stationary.**

#### 4.2.2.2 Link Availability

Using the same methodology as for the shadowing and energy profile, the ephemeris for the Earth can replace that of the Sun, and the time available for direct data transmission through the Deep Space Network (DSN) can be calculated. In this case, it was assumed that at least 30% of the Earth had to be visible in order for successful transmission to occur. This number can be changed by the user as desired, and can even be replaced by specific ground station coordinates for added accuracy. SEXANT can then measure the percentage of the traverse during which communication with Earth can occur, as is shown in Figure 37. Using that number and the total mission duration, this information can inform the design of the communication architecture between several vehicles to ensure that all vehicles can receive, relay and transmit all the necessary data in an efficient manner during a mission.

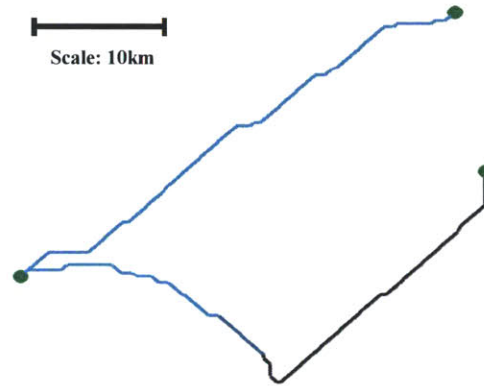


**Figure 37: Communication link availability.**

**The lighter blue color corresponds to high visibility, the darker blue represents lower or no visibility.**

#### 4.2.3 Single-Vehicle Case Study

One of the targets of high scientific interest on the Moon is its South Pole, due to its relative age, the large number of craters existing in that area, and the possible presence of significant quantities of water ice. [6] In order to demonstrate how SEXTANT can be used in conjunction with the mass-modeling tool to rapidly obtain an accurate estimate of a feasible rover design, a mission near the Shackleton crater was modeled. This area is interesting because it is particularly treacherous due to areas of high and low illumination, and to long nights. The first step was to establish the length of the traverse, from one point of interest to the next. Figure 38 shows the chosen traverse, which was found to be 16.5km long, with approximately 60% of the traverse being on a slope, the latter having a maximum inclination of 15°.

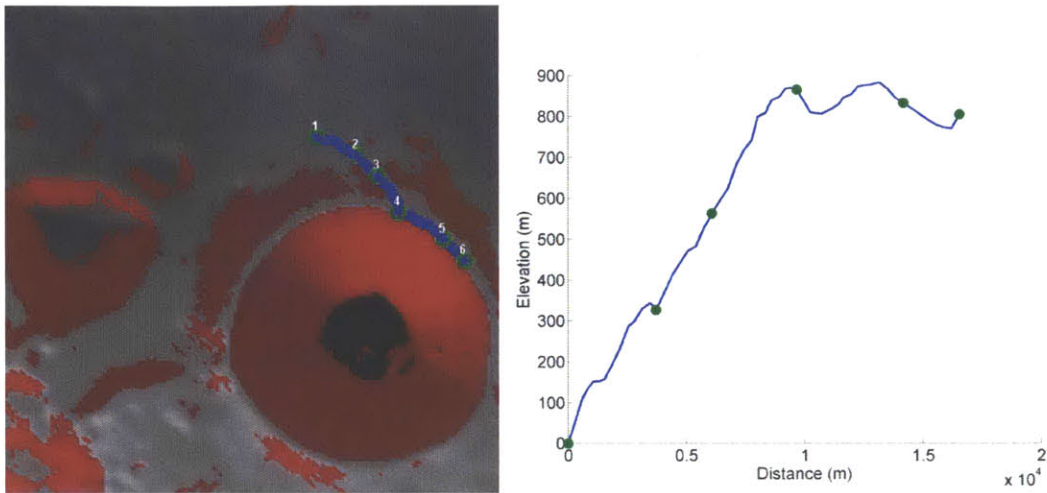


**Figure 38: Chosen example traverse (left) and corresponding elevation during the traverse (right)**

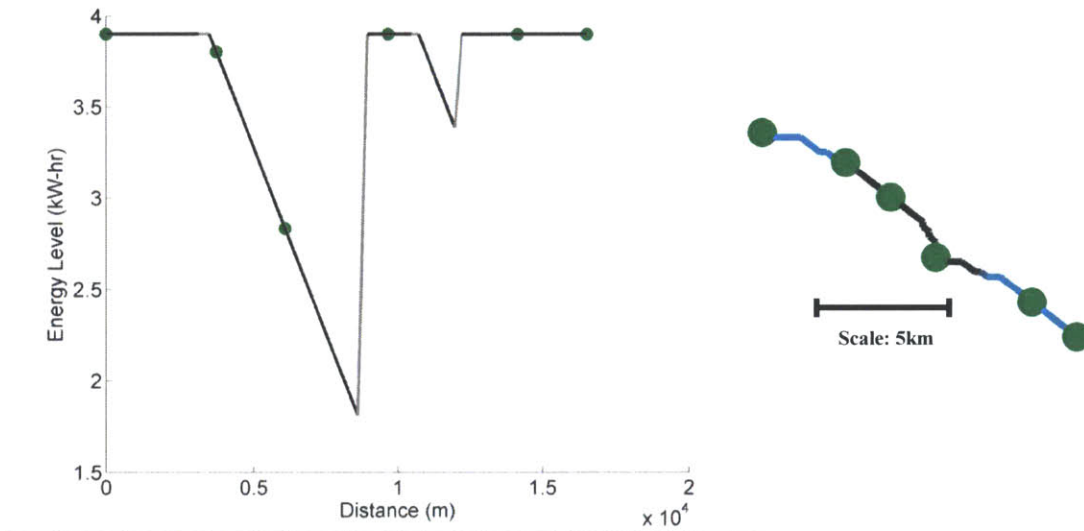


**Figure 39: Energy level (left) and Earth visibility (right) of the rover during the traverse.  
Cyan line: Earth is fully visible; Black line: Earth is not visible; Shade: partial Earth visibility.**

To complete the mission, the rover was given a suite of instruments with a mass of 15kg and needing 30W of power. This instrument suite includes an X-ray spectrometer, a thermal spectrometer, a camera and a mass spectrometer to analyze the composition of the volatiles in the southern hemisphere atmosphere. The data requirement was found to be 60 Megabits per day. Using data from the Mars Exploration Rovers as the baseline, the total link duration with Earth per day was estimated to last 15% of the day, which involves a 5 Kb/sec link. Using the mass modeling tool and these assumptions, the mass of a rover able to perform this traverse while travelling at a speed of 0.25 km/hour was found to be approximately 150kg, with 26kg of batteries, assuming 10% sun visibility (again, this is a standard assumption in early mission design).

With this information, the properties of the rover were modeled in SEXTANT to establish the feasibility of the design. In this case, the rover was found to be overdesigned due to the conservative assumptions made. It was estimated to be able to complete the mission in 55 days of continuous operations (not accounting for downtimes at night), without ever running out of power, as can be seen in Figure 39. It is to be noted that with the way rover operations is currently conducted, rover systems are only operated from 5 to 10% of the day. A real traverse could therefore take years under these assumptions. Consequently, the case considered here is an extreme case in terms of resource usage. In addition, the rover was found to have link visibility with Earth for 56% of the mission, with the shortest link availability in a given day being just under 30% of the day.

Armed with this new knowledge, the required data rate was manually reduced to 3.5 Kb/sec, and the mass of the batteries was reduced to 10kg. This new design still meets the power and distance requirements, but this time the vehicle's mass is only 120kg: a 20% reduction from the initial design. This new design is still conservative and includes a 30% margin on all subsystems. This demonstrates that the operations modeling tool can assist in rapidly obtaining higher accuracy estimations of the vehicle size in the early stages of the design, without having to perform complex simulations. Conversely, the tool can demonstrate the challenges involved with a particular traverse, and can help the designers perform the trade between the sites to be visited and the design of the vehicle.

When modeling two vehicles, SEXTANT can also help identify which tasks would be performed better if they were shared between two vehicles. For example, in Figure 40, a second rover was added to the traverse. The maximum separation between the rovers was kept within 500 meters and it was assumed that the rovers were always within communication visibility of each other. It can be seen that, under the chosen design, there is always one vehicle able to communicate back to Earth. This means that if both rovers have a long-range communication system, the whole mission will always be in communication with Earth. This will be true even if more rovers are added, as long as these are also always in visibility of one of the two rovers.

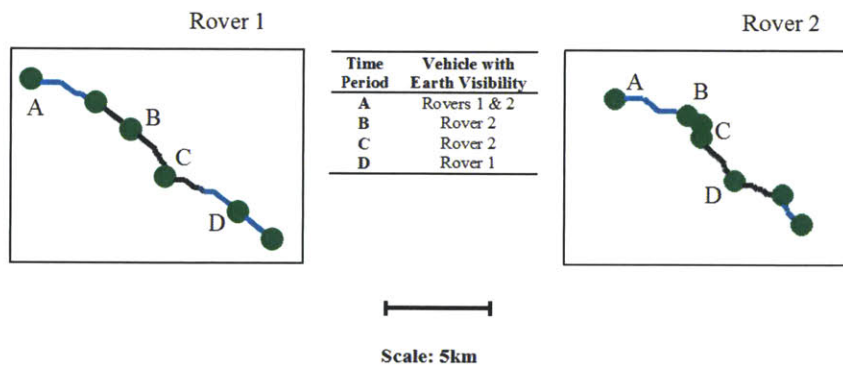


**Figure 40: Evaluating the opportunity for multiple rovers to share communication systems**

## 4.3 SEXTANT Features for Multi-Vehicle Systems

### 4.3.1 Collision Avoidance

Spatially distributed systems, and in particular coordinated vehicles, involve vehicles interacting together as part of a larger system, to provide more value to the stakeholders than they would have done individually. When multi-vehicle missions are planned, there are often minimum and maximum separation constraints between the vehicles to ensure communication visibility and avoid collisions, as well as to impose meeting points. The key difficulty is that path planning must be performed both in the time and space domains in order to ensure that the optimal path is computed within these constraints. Rather than optimizing paths for all the rovers at once, which would require far more complex optimization techniques, the path planning is done sequentially. The first rover plans its path without considering the other rovers. Then each successive rover plans its path such that it does not conflict with its predecessors. The definition of a conflict depends on the constraints being enforced.

In the examples below, the rovers are required to be at least 2 meters apart at all times, to ensure that they do not collide with each other. Figure 41 shows the setup for a simple traverse with three rovers travelling from start to goal waypoints. The rovers start very close to each other, with rovers 1 and 2 (blue and yellow, respectively) only 1 meter apart. Figure 41 also shows the paths computed for each of the vehicles under the given constraints. Due to the temporal logic, all three rovers are able to navigate through the same passage without violating the two-meter collision avoidance buffer. The distances between all the rovers are shown in Figure 42. Line 1 at the top of the figure shows that rovers 2 and 3 (yellow and purple, respectively) start 4 meters apart and remain about six meters apart for the duration of the traverse. Similarly, the middle line (Line 2) shows that rovers 1 and 3 start four meters apart and remain approximately three and a half meters apart until the end of the traverse, where they diverge. Finally, the bottom-most line (Line 3) shows the distance between rovers 1 and 2. Since the rovers start in violation of the two-meter requirement, rover 2 does not leave its starting position until the time when rover 1 is at least two meters away. This is indicated by the sudden jump in the line from one meter to approximately two and a half meters in Figure 42.

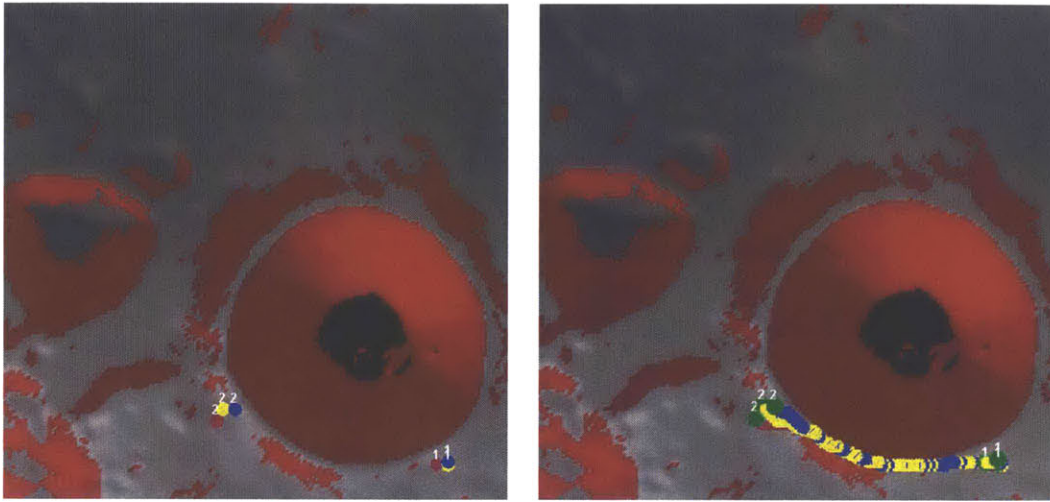


**Figure 41: Start & end waypoints for three rovers and collision-free paths generated by SEXTANT**

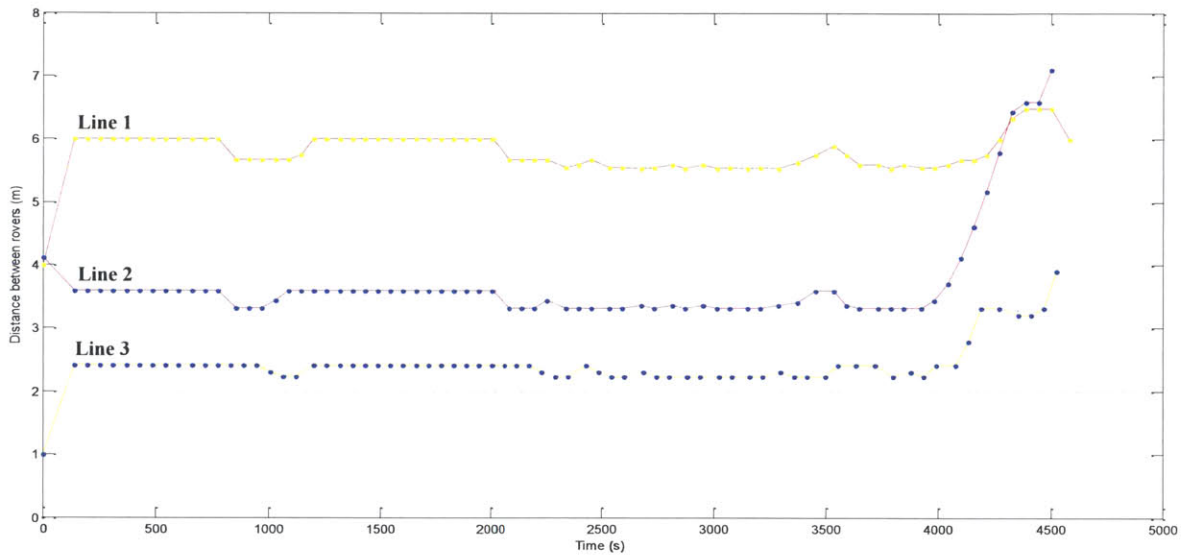


**Figure 42: Distance between all pairs of rovers over the course of the traverse.  
Line 1: distance between rovers 2 and 3; Line 2: distance between rovers 1 and 3; Line 3: distance between rovers 1 and 2.**

Figure 43 shows a more complex scenario with six rovers, each with three waypoints. Again, all the rovers are able to traverse the same narrow passages to reach their waypoints. The distances between rovers are shown in Figure 44. The increased number of rovers results in a severe increase in the number of rover pairs checked, but as in Figure 42, all pairs of rovers remain at least 2m apart over the course of the entire traverse (all rovers were started more than 2m apart in this case).

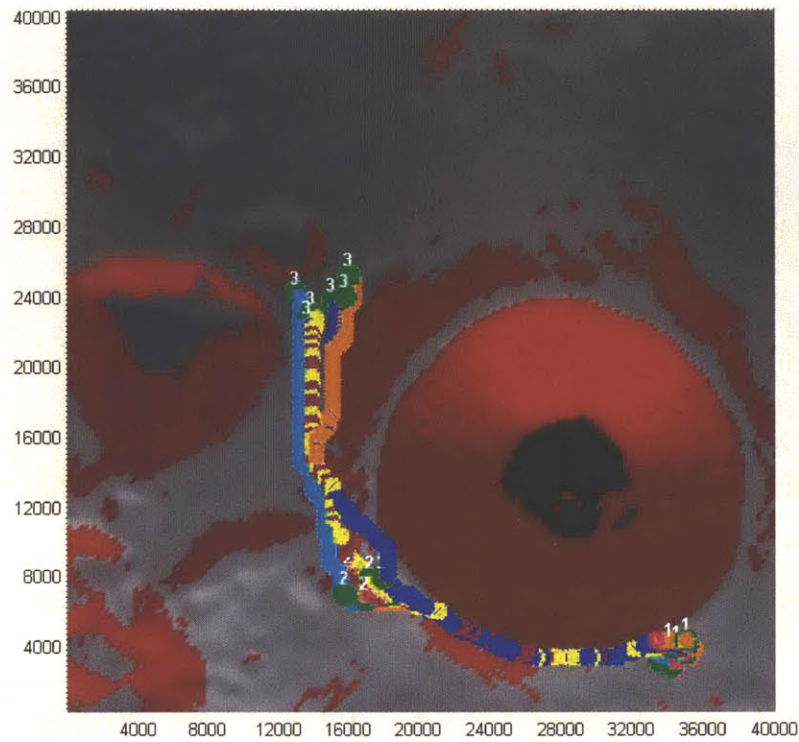


**Figure 43: Collision-free traverse for six rovers (axes are in meters)**

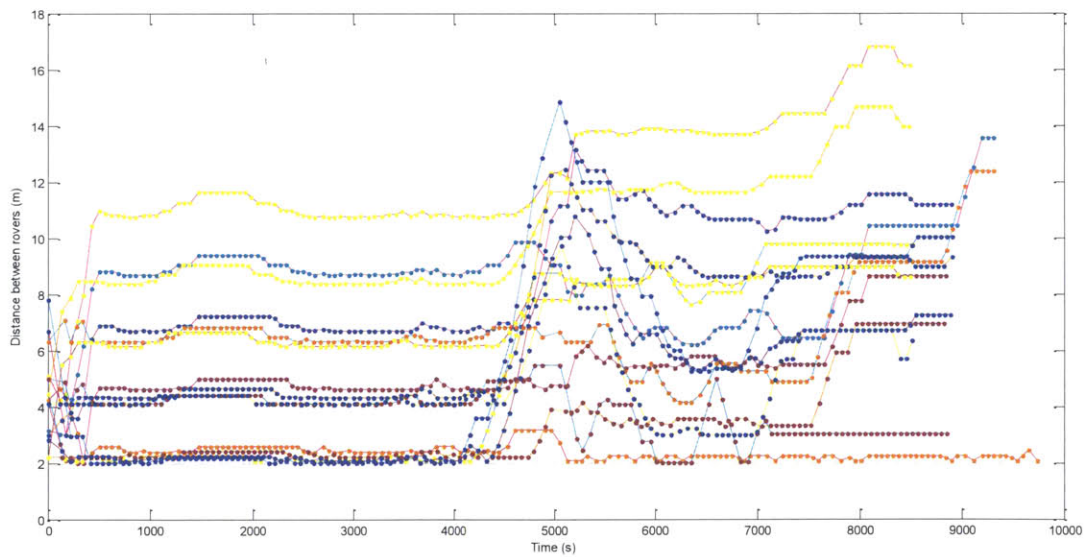


**Figure 44: Distance between all pairs of rovers – always remain greater than 2m**

Depending on the constraints imposed between the vehicles, this algorithm could help the users identify how much margin should be added on the vehicles' power systems and data storage capacity, for example. It is to be noted that the paths taken by each of the rovers (except rover 1) has deviated from the optimal path to prevent collisions from occurring, which means that the illumination and link availability properties have also changed. In this particular case, adding the collision avoidance criteria led to the



rovers taking a non-optimal path and to a ~10% increase in the total mass of the system due to the higher energy requirements. This particular example thus demonstrates that SEXTANT, in combination with the mass-modeling tool, can be used to evaluate the effects of the environmental constraints on the design of a team of vehicles.

One of the powerful features of this approach is that it takes into account both temporal and spatial constraints. It can therefore be used to add meeting points for vehicles, to allow for one vehicle to re-power another for example, or to transfer a sample. This often leads to one vehicle having to stop at the meeting point to “wait” for another to arrive. If so desired, using more Activity Points, the user can choose to change the path taken by the vehicle before the meeting point to minimize the wait time of the rover prior to the rendezvous and maximize the amount of science performed.

### 4.3.2 Traveling Salesman Problem

The second significant augmentation to the SEXTANT software undertaken in the work for this thesis is the capability of high-level assignment of vehicles to Activity Points (APs) to perform a set of pre-specified tasks. In Johnson’s version of SEXTANT, the user would manually specify APs for each vehicle in turn. SEXTANT would then find the corresponding traverse for each rover. In this new version, the user specifies tasks to be executed at each AP (e.g.: take a picture, pick a sample, etc.), instead of selecting a particular rover to visit that AP. The user then picks any architecture from the architecture evaluation software described in Chapter 3. Thus, the user is allowed to evaluate the performance of several different architectures without manually executing the additional step of choosing activity points for each vehicle to visit. The tasks to be performed at the activity points can be constructed by selecting any combination of functionalities available across all vehicles in the selected architecture.

This capability is enabled by an underlying static vehicle routing algorithm. The objective of this algorithm is to determine, for each vehicle, the APs to be visited and the order in which these APs are to be visited. The inputs to this algorithm are: a list of tasks to be performed at each activity point (user-input through a GUI), descriptions of the functionalities required to perform each task (also user-input through a GUI), and descriptions of the functionalities available on each rover for the selected architecture (from the architecture evaluation and selection process). This algorithm is also capable of combining functionalities from different vehicles to perform tasks.

The problem of static vehicle routing is a combinatorial optimization problem, and it is formulated and solved as a graph search problem. Three problem elements are considered: “*Objects*”, “*Predicates*” and “*Actions*”. “*Objects*” is a collection of entities in the system, defined as:

$$\begin{aligned} \text{Vehicles: } \mathcal{R} &= \{r_1, r_2, \dots, r_{N_R}\} \\ \text{Tasks: } \mathcal{T} &= \{\tau_1, \tau_2, \dots, \tau_{N_T}\} \end{aligned}$$

$$\begin{aligned} \text{Functionalities: } \mathcal{F} &= \{f_1, f_2, \dots, f_{N_F}\} \\ \text{Activity Points: } \mathcal{W} &= \{w_1, w_2, \dots, w_{N_W}\} \end{aligned}$$

In the above collection of sets,  $N_R$ ,  $N_T$ ,  $N_F$ , and  $N_W$  are, respectively, the number of rovers, tasks, functionalities and activity points involved in the static routing problem.

“*Predicates*” is a set of logical statements that take elements from “*Objects*”. The “*predicates*” of interest are:

$$\begin{aligned} &Has(r, f) \\ &Needs(\tau, f) \\ &At(r, w) \\ &ToDo(\tau, w) \end{aligned}$$

In these predicates, the variable  $r$  is an element of the rest of vehicles  $\mathcal{R}$ , which belongs to the “*Objects*” collection. Similarly, the variable  $f$  is an element of the set  $\mathcal{F}$ , the variable  $\tau$  is an element of the set  $\mathcal{T}$ , and the variable  $w$  is an element of the set  $\mathcal{W}$ . For given arguments, each predicate can either be true or false. For example, the predicate  $Has(r, f)$  is true if the vehicle has the functionality  $f$ , otherwise it is false.

The initial and goal conditions of the static vehicle routing problem can be formulated by specifying the truth values at the initial and goal conditions of certain predicates. For example, a general equation for the initial condition is formulated as follows:

$$\left( \bigwedge Has(r_k, f_l) \right) \wedge \left( \bigwedge Needs(\tau_k, f_l) \right) \wedge \left( \bigwedge At(r_k, w_l) \right) \wedge \left( \bigwedge ToDo(\tau_k, w_l) \right)$$

**Equation 25**

Equation 25 is read as: “*The vehicles  $r_k$  have functionalities  $f_l$ , the tasks  $\tau_k$  need the functionalities  $f_l$ , the vehicles  $r_k$  are at activity points  $w_l$ , and the tasks  $\tau_k$  are yet to be performed at the activity points  $w_l$ ,*” where the indices take on appropriate values. Similarly, the goal condition may be formulated as follows:

$$\bigwedge \neg ToDo(\tau, w)$$

**Equation 26**

This expression is read as: “*None of the tasks remain to be performed at any activity point.*”

Finally, “*Actions*” is a set of activities that can change the truth values of the aforementioned predicates. The activities of interest in the static vehicle routing problem are:

$$\begin{aligned} &Go(R, W_k, W_l) \\ &Do(\tau, w) \end{aligned}$$

In these actions,  $R$  is a subset of  $\mathcal{R}$ .  $W_k$  and  $W_l$  are subsets of  $\mathcal{W}$ . Each action is associated with some pre-conditions that must be true before the action can be executed, and some effects that change the truth values of the aforesaid predicates. The pre-condition for the action  $Go$  is:

$$\left( \bigwedge_{m=1}^{N_R} At(r_m, W_k^m) \right)$$

**Equation 27**

Here,  $W_k^m$  is the  $m^{\text{th}}$  element of the set  $W_k$ , and the precondition is read as: “Each rover in the set  $R$  must be present at an activity point in the set  $W$ .” Similarly, the pre-condition for the action  $Do$  is as follows:

$$ToDo(\tau, w) \wedge \bigwedge_{k=1}^{N_F} \left( Needs(\tau, f_k) \wedge \left( \bigwedge_{l=1}^{N_R} (At(r_l, w) \wedge Has(r_l, f_k)) \right) \right)$$

**Equation 28**

The pre-condition is read as: “The task  $\tau$  is yet to be done at activity point  $w$ , and for each function  $f_k$  required to do the task  $\tau$ , at least one rover  $r_l$  present at the activity point  $w$  has the functionality  $f_k$ .” The effects of the predicates on the truth values of each of these actions are follow simple logic. For example, if the predicate  $At(r_l, w_1)$  is true, which implies that the predicate  $At(r_l, w_2)$  is false (a rover cannot be present at two different activity points at once), then the pre-condition for the action  $Go(r_l, w_1, w_2)$  is satisfied and this action can be executed. The effect of this action is that  $At(r_l, w_2)$  becomes true, and  $At(r_l, w_1)$  becomes false.

Following the definitions of “Objects”, “Predicates” and “Actions”, and the formulation of the initial and goal conditions using elements from “Objects” and “Predicates”, the static routing problem can be formulated as a graph search problem. The vertices of this graph are obtained by associating a vertex with every possible combination (logical conjunctions) of truth values of the predicates. Note that some combinations are impossible (e.g.:  $At(r_l, w_1) \wedge At(r_l, w_2)$  is not a valid combination). As previously explained, actions change the truth values of predicates. Hence, actions are associated with edges of this graph. The satisfaction of preconditions and effects are various combinations of vertices in the graph determine the manner in which these actions are associated with edges. Furthermore, several problem-specific observations may be used to significantly prune unnecessary vertices and edges of this graph to make the graph search tractable. Finally, standard techniques such as the A\* algorithm may be used to search this graph.

The result of this graph search is a sequence of actions to be taken so that the truth values of the predicates change from the initial condition to the desired goal condition. This sequence of actions represents the solution of the static vehicle routing problem. It proves, for each vehicle, the APs to be visited by that vehicle, and the order in which they are to be visited.

## 4.4 Lunar South Pole Case Study

In this section, the science and technology goals for the exploration of the Moon are first detailed. A subset of these goals are then chosen to be the basis for a case study. A few interesting architectures from the architecture evaluation process are identified. The section then concentrates on demonstrating how the performance of these vehicles can be evaluated using the features of SEXTANT described thus far.

### 4.4.1 Science Definition

Recent exploration of the Moon has revealed a geochemically complex surface and polar volatiles (e.g., hydrogen or ice), leading to significant unanswered questions about the Earth-Moon system. Furthermore, it is believed that now-quiescent bodies like the Moon and Mercury preserve evidence of the early histories of the terrestrial planets. Two general scientific goals for lunar exploration were identified by the Planetary Science Decadal Survey [6]: understanding the origin and diversity of terrestrial planets and understanding how the evolution of terrestrial planets enables and limits the origin and evolution of life. Here the specific objectives related to each scientific goal are presented, as well as the measurements required to attain meet these objectives.

#### 4.4.1.1 *Understanding the Origin and Diversity of Terrestrial Planets*

The following presents the three fundamental objectives associated with the goal of understanding the origin and diversity of terrestrial planets, as well as the key lunar investigations that need to be performed in order to achieve this goal.

- 1) Constraint of the bulk composition of the terrestrial planets to understand their formation from the solar nebula and controls on their subsequent evolution
  - Sample return of crust and mantle materials from the Moon
  - Characterization of the Moon's lower mantle and core
- 2) Characterization of planetary interiors to understand how they differentiate and dynamically evolve from their initial state
  - Determining the locations and mechanisms of seismicity and characterization of the lunar lower mantle and core.
  - New analysis of the ages, isotopic composition, and petrology (including mineralogy) of existing lunar samples, of new samples from known locations, and of remotely sensed rock and regolith types
  - Continued development of new techniques to glean more information from samples will form the basis of knowledge for the detailed magmatic evolution of the Moon.

- 3) Characterization of planetary surfaces to understand how they are modified by geologic processes.
- Global characterization of planetary morphology, stratigraphy, composition, and topography, modeling the time variability and sources of impacts on the inner planets
  - Continued analysis of sample geochronology to help provide constraints on the models
  - Development of an inventory and isotopic composition of lunar polar volatile deposits to understand their emplacement and origin, modeling conditions and processes occurring in permanently shadowed areas of the Moon

#### ***4.4.1.2 Understanding How the Evolution of Terrestrial Planets Enables and Limits the Origin and Evolution of Life***

The following presents the three fundamental objectives that will help understand how the evolution of terrestrial planets enables and limits the origin and evolution of life, as well as the key lunar investigations that need to be performed in order to achieve this goal.

- 1) Understanding of the composition and distribution of volatile chemical compounds;
- Determination of the state, extent, and chemical and isotopic compositions of surface volatiles, particularly in the polar regions on the Moon
  - Determination of the inventories and isotopic compositions of volatiles in the mantles and crust of all the terrestrial planets
  - Determination of the fluxes of volatiles to the terrestrial planets (e.g., by impact) over time.
- 2) Understanding of the effects of internal planetary processes on life and habitability;
- Constraint of the styles, timescales and rates of volcanism and tectonism on the Moon through orbital and in situ investigations;
- 3) Understanding of the effects of processes external to a planet on life and habitability.
- Investigation of loss rates of volatiles from the Moon to interplanetary space, in terms of solar intensity, gravity, magnetic field environment, and atmospheric composition.

#### ***4.4.1.3 South Pole – Aiken Basin Sample Return***

The Planetary Science Decadal Survey identified the exploration and sample return from the Moon's South Pole-Aitken (SPA) as having being one of the highest priority activities for solar system science. The high priority allocated to this mission stems from the fact that it would address most of the objectives detailed above. Though recent remote-sensing missions provide much valuable new data from orbit about the diversity of materials and the geophysical context of this important basin, completely achieving all these science objectives requires precision of age measurements to better than  $\pm 20$  million years and accuracy of trace elemental compositions to the parts-per-billion level, which is only achievable via

sample return. The principal scientific reasons for undertaking a South Pole-Aitken Basin Sample Return mission are as follows:

- Determination of the chronology of basin-forming impacts and constraint of the period of late heavy bombardment in the inner solar system, and thus addressing of fundamental questions of inner solar system impact processes and chronology;
- Elucidation of the nature of the Moon's lower crust and mantle by direct measurements of its composition and of sample ages;
- Characterization of a large lunar impact basin through "ground truth" validation of global, regional, and local remotely sensed data of the sampled site;
- Elucidation the sources of thorium and other heat-producing elements in order to understand lunar differentiation and thermal evolution;
- Determination of ages and compositions of far-side basalts to determine how mantle source regions on the far side of the Moon differ from regions sampled by Apollo and Luna.

To maximize the likelihood of achieving these objectives, the return of at least 1kg of rock fragments has been set at a goal.

#### **4.4.2 Trade Space Generation and Architecture Selection**

From the scientific goals identified in the previous sections, the following activities to be performed by the planetary surface vehicles can be derived:

- 1) Sample collection (min 1kg of samples) and appropriate sample packaging for return
- 2) Distribution of geological instrumentation at multiple sites
- 3) Direct analysis of lunar soil at several sites
- 4) Travel on the poles of the Moon and in permanently shadowed areas

The functions required to achieve these goals are dependent on both the scientific goals and the concept of operations. The functions required to complete the aforementioned activities, which are necessary to meet the scientific goals set out by the Planetary Science Decadal Survey, are detailed in Table 26.

This case study concentrates on activities (3) and (4) since these follow directly from the shorter case studies from Section 4.2.3. The maximum number of vehicles was set to three and the functions chosen to be separated across vehicles are given in Table 27.

**Table 26: Functional decomposition**

	Activity	Function	Category
Scientific Goal	1) Sample Collection and Preparation	Drilling	V
		Acquiring	V
		Curing	V
		Storing	V
		Transferring	V
		Long-range traversing	V
	2) Distribution of geological instrumentation at multiple sites	Off-loading	V
		Long-range traversing	V
	3) Direct analysis of lunar soil at several sites	Drilling	V
		Acquiring	V
Analyzing		V	
4) Travel on the poles of the Moon and in permanently shadowed areas	Lunar Shadow Thermal Protecting	ES	
Technical Goals	1) Travel on Moon	Long-range Traversing	V
		Short-Range Traversing	ES
	2) Perform Scientific Activities	Energy Generating	SS
		Energy Storing	ES
		Payload Carrying	SS
	3) Survive Lunar Days	Lunar Day Thermal Protecting	ES
	4) Survive Lunar Nights	Hibernating	SS
	5) Transmit Data	Short-Range Communicating	ES
Long-Range Communicating		SS	

**Table 27: Functions considered in the case study**

Function	Form	Label
Analyzing via spectroscopy	Laser-induced spectroscope, with arm	Spec
Analyzing via radar	Ground penetrating radar	Rad
Observing	Athena Pancam/Mini TES	Cam
Long-Range Communicating (1)	Comm Direct to Earth	Comm1
Long-Range Communicating (2)	Comm via a low altitude orbiter	Comm2
Hibernating	Additional power to survive lunar night	Hib

This case study focuses on the use of SEXTANT in the loop, and in particular on the use of the traveling-salesman ability. Three very different architectures that performed well during the architecture evaluation process were therefore selected in order to provide an interesting case study for the path planning tool. These architectures are provided in Table 28 and their properties are shown in Table 29.

**Table 28: Architectures of interest  
Functions are defined in Table 27.**

N° rovers/ Arch Label	Rover 1 Functions	Rover 2 Functions	Rover 3 Functions
Monolithic	Spec, Rad, Cam, Comm1, Comm2, Hib	-	-
2	Rad, Cam, Comm1	Spec, Cam, Comm2, Hib	-
3	Spec, Cam, Comm2, Hib	Rad, Cam, Comm1, Hib	Cam

**Table 29: Architecture properties (normalized, 2 significant figures)**

N° rovers/ Arch Label	Total Mass (kg)	Science Benefit	Vehicle-level complexity (max)	System-level Complexity
Monolithic	180	1	1	0
2	240	1.2	0.74	3.0
3	310	1.4	0.74	4.0

One important feature to note is the effect of sharing the hibernation function on the overall system mass. In Chapter 3, it was found that sharing this function was only beneficial when the secondary vehicle’s average power requirements were very small. Figure 45 shows the mass of selected two-vehicle architectures that do not share the hibernation system, and of identical pairs of vehicles that do share this functionality. It can be seen that for this particular application, sharing the hibernation function is significantly more valuable than for the Martian case study. In fact, in addition to the reduction in complexity of the vehicle receiving the hibernation power, there is a mass advantage to this approach as long as its nighttime average power requirement is lower than 15 Watts.

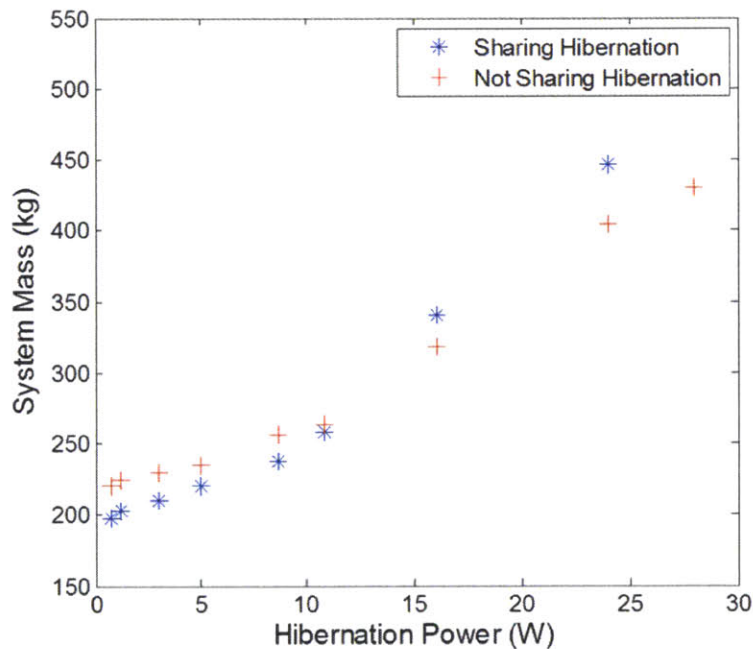


**Figure 45: System mass against nighttime power requirement**



### 4.4.3 Mission Path-Planning using SEXTANT

Once a set of architectures has been selected, it is important to compare how each architecture performs in the mission environment. To this end, the three architectures are “tested” on an 11km traverse at the South Pole of the Moon, around the Shackleton crater area. The points to be visited during the mission are shown in Figure 46 below.

To demonstrate the full potential of SEXTANT, it is assumed that the following payload are used at the following points:

- Points 1 and 2: Ground-penetrating radar and camera
- Point 3, 4 and 5: Spectrometer, ground-penetrating radar and camera
- Point 6: Camera only

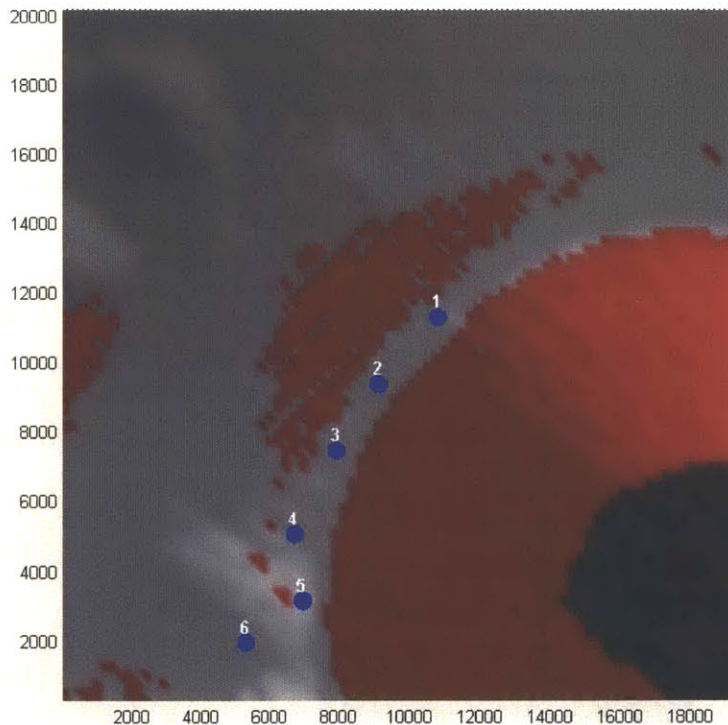


**Figure 46: Points to be visited during the traverse (axes are in meters)**

Using the routing tool in SEXTANT, the paths and traverse times (in terms of *operational hours*, this only includes times when the vehicle is moving and excludes time for check-out, maintenance, hibernation, etc.) shown in Table 30 were found for each vehicle. The resulting paths, assuming an optimization to minimize mission time are also shown in Figure 47, Figure 48 and Figure 49.

In the one rover case shown in Table 30, it was assumed that the rover could be landed at any point. It can therefore be seen that the optimal path for a one rover vehicle is to traverse directly from one end of

the path to the other, since the rover must visit each site. Overall, the rover takes 70 hours of operations to perform this traverse and the science activities required at each point.

In the two- and three-rover case, the paths are very different. It is assumed that all vehicles must be landed at the same site, and in this case this site was chosen to be at point 4. Because of this, the traverse becomes much less efficient. When looking at their route, the vehicles, and in particular the vehicle with the most capability (Rover 1 in both cases) can be seen to travel back and forth between points. This in turn increases their traverse time. On the other hand, each individual vehicle does not need to perform as much science at each point, since the payload is spread across multiple vehicles. In this case, this attribute reduces the operational time required. It is also to be noted that, although the total mission duration for these three systems may be similar, the cost of operating two or three rovers simultaneously is not the same as that of operating a single rover. This was reflected in their system-level complexity.

**Table 30: Route for each of the down-selected architectures**

Number of rovers	Rover Number	Rover Functions	Route	Operational Hours
<i>Monolithic</i>	Rover 1	Spec, Rad, Cam, Comm1, Comm2, Hib	1 → 2 → 3 → 4 → 5 → 6	70
2	Rover 1	Rad, Cam, Comm2, Hib	4 → 5 → 6 → 4 → 3 → 2 → 1	70
	Rover 2	Spec, Comm1	4 → 5 → 3	50
3	Rover 1	Spec, Cam, Comm2, Hib	4 → 6 → 4 → 5 → 4 → 3	85
	Rover 2	Rad, Comm1, Hib	4 → 3 → 2 → 1	50
	Rover 3	Cam	4 → 3 → 4 → 5	20

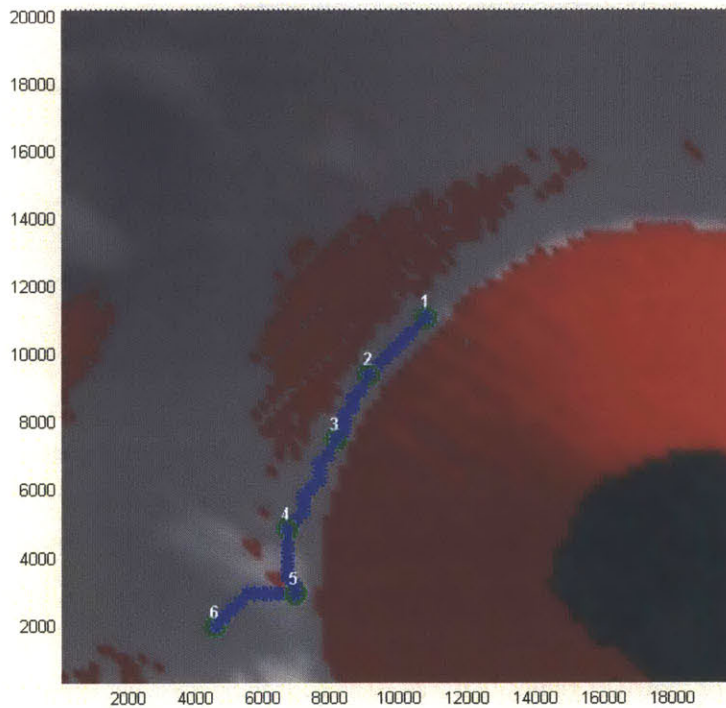


**Figure 47: Path for single-vehicle architecture (axes are in meters)**

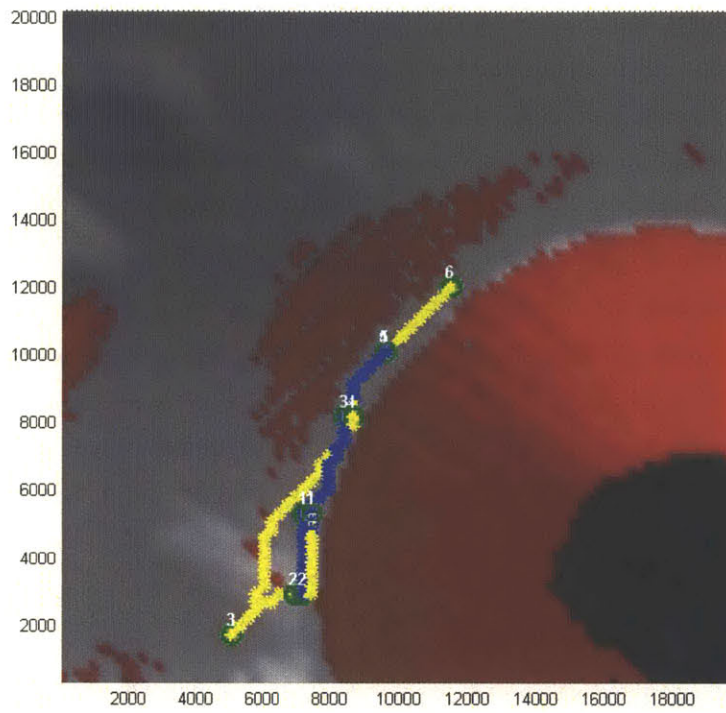


**Figure 48: Paths for the two-vehicle architecture (axes are in meters)**

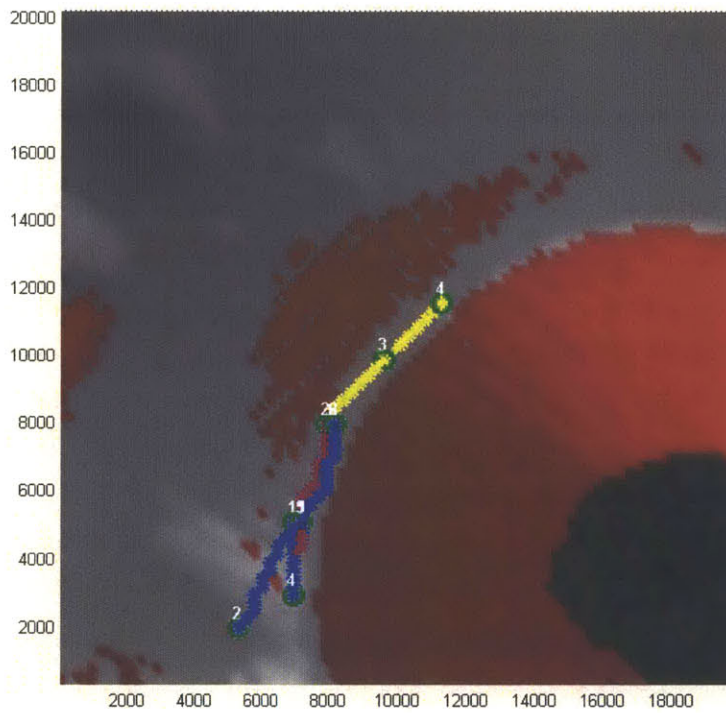


**Figure 49: Paths for the three-vehicle architecture (axes are in meters)**

The figures and information given in the table allow a mission design to understand some more subtle properties of these multi-vehicle architectures. As can be seen by the operational time, assuming that the operation of the rovers can be parallelized, the time taken to perform the mission is the same for the one and two rover architectures, but the two rover architecture is obviously more productive during that time (both vehicles can collect data). However, the three vehicle architectures takes ~20% longer to complete the mission. This is because of the requirement for one of the vehicles that can provide hibernation to be close to the vehicle that does not have hibernation (in order to enable it to survive the lunar night). The route and paths demonstrate that this causes one of the vehicles to go back and forth between the points. This could be avoided by letting the third vehicle “die” during the lunar night. Although this would reduce the productivity of the third rover, it may in fact lead to an increase in productivity for the first rover, since it will be spending less time performing proximity operations with the third rover. In this case study, the two vehicle architecture appears to perform best: it covers more terrain for a given mission duration and is less massive than the three vehicle architecture. It has increased productivity and science benefit (assuming the goals are evenly weighted), as well as reduced vehicle-level complexity. This, however, does come at the cost of increased system-level complexity (due to one vehicle providing the hibernation function to another) and of a 35% increase in mass as compared to the monolithic system.

## 4.5 Conclusion

This chapter has introduced the Surface Exploration Traverse Analysis and Navigation Tool (SEXTANT) and has detailed how it can be used to simulate a multi-vehicle mission and evaluate the performance of multi-vehicle architectures. First, an overview of the existing features of SEXTANT was provided. This was followed by a detailed description of the new features that were added to SEXTANT to allow it to better evaluate the properties of each vehicle throughout a mission. A short single-vehicle case study was also provided to illustrate how these features can be used. Following this, a description of two capabilities that were added to SEXTANT to enable it to better simulate a multi-vehicle mission was given. The first is a “collision avoidance” algorithm, which ensures that vehicles are always within a minimum (or maximum) distance of each other, or to make sure that they meet at certain points during their traverse. The second feature is a traveling-salesman algorithm, which looks at the tasks to be performed at each point on a traverse and the properties of each vehicle to decide on the routing of each vehicle in an architecture. Finally, the chapter ended with a case study demonstrating the aforementioned features of SEXTANT.

# Chapter 5

## TEMPORAL DISTRIBUTION FOR THE EXPLORATION OF EUROPA

### 5.1 Introduction

Planetary bodies in the outer solar system are believed to hold fundamental clues to help us understand how the solar system evolved. In particular, moons such as Europa, Titan and Enceladus may harbor habitable environments and possibly even life. Despite the great successes of missions such as Cassini, Galileo and Voyager, our understanding of these bodies is still limited. Thus, the 2013-2022 Planetary Science decadal survey identified Europa as a high-priority target for exploration. [6] Unfortunately, the excitement of the potential discoveries involved with exploring outer solar system planetary bodies is somewhat tempered by recent budget cuts and a desire to reduce the risk and complexity associated with large flagship missions. There is therefore a need to reconcile ambitious long-term scientific goals with limited annual budgets and increasing pressures for short project durations and rapid scientific returns.

The theme of this thesis is to address this issue by replacing these large missions with distributed missions. Thus far, the case studies have investigated the effects of *spatial distribution* on the overall mission properties. In this case study, the concept of architectures involving sequences of missions, that is to say *temporally distributed* missions, is investigated. It is hypothesized that temporally distributed missions have the potential to reduce risk and to increase the ability to achieve demanding scientific goals under stringent budget constraints. To understand the trade associated with this change in paradigm, the

framework described in Chapter 2 is used to rapidly generate and explore a trade space of multi-mission architectures, and to help demonstrate how the prioritization of mission goals affects the design space. The current science goals for the exploration of Europa are used as the basis for the case study.

This chapter first presents the science goals at Europa, and the potential instruments that could be flown to address them. Current proposed mission designs are also presented. Details of the architecture generation and evaluation process, including a description of the weightings used in the previously described evaluation metrics, are then given. The trade space is then thoroughly explored to identify candidate mission architectures at Europa, and the effects of uncertainty and risk on the choice of architectures are also addressed. The chapter concludes with an analysis of the trades that occur when moving away from large flagship missions towards sequences of smaller missions.

## **5.2 Science at Europa**

### **5.2.1 The Importance of Europa**

Europa is the sixth closest moon to Jupiter and the smallest of the Galilean satellites. It is primarily made of silicate rock and it has an iron core and an icy surface. The latter is believed to be one of the smoothest, and thus newest, surfaces in the Solar System. Most notably, Europa is thought to possess an ocean with twice the volume of Earth's ocean and to have a thin ice shell. This, in combination with the possibility that there may be an active core-ocean exchange, makes Europa a particularly interesting scientific target. Consequently, a mission to Europa would be the first step in understanding the potential for icy satellites as abodes for life. The 2013-2022 Planetary Science Decadal Survey identified Europa as being the second most important target for planetary exploration, after a Mars sample return mission. [6] It encompasses the motivation for Europa exploration under the fundamental science question: "Where are the habitable zones for life in the solar system, and what are the planetary processes responsible for producing and sustaining habitable worlds?" Thus, the overarching goal for a mission to Europa was identified as being: "*Explore Europa and investigate its habitability.*"

### **5.2.2 Mission Goals and Payload Identification**

The first step in deriving the trade space of possible architectures for missions at Europa is to decompose the given overarching goal into science objectives and to derive the investigations associated with these objectives. In this case study, the scope of the trade space is limited to only address the four objectives selected for the Europa Habitability Mission (EHM). These are detailed in Table 31 and can be roughly labeled as exploring the ocean, ice shell, composition and geology of Europa.

The main challenge in trying to choose a mission to achieve these objectives is that each investigation can be performed by different instruments, and from different platforms. In each of these cases, the quality and quantity, and thus the scientific value, of the measurements made are different. Additionally, the engineering complexity, and therefore the mission cost, varies depending on the chosen instrument suite and platform. All the instruments addressing each of the science investigations, on any of the following three platforms: flyby, orbiter or lander, must therefore first be identified, as shown in Table 31. Note that in this chapter, INMS stands for Ion and Neutral Mass Spectrometer. Furthermore, a “flyby” mission is a vehicle in orbit around Jupiter that does multiple close proximity flybys of Europa, as shown in Figure 50. This has the advantage of providing extended periods of observation at Europa, while minimizing the radiation exposure and  $\Delta v$  requirement.

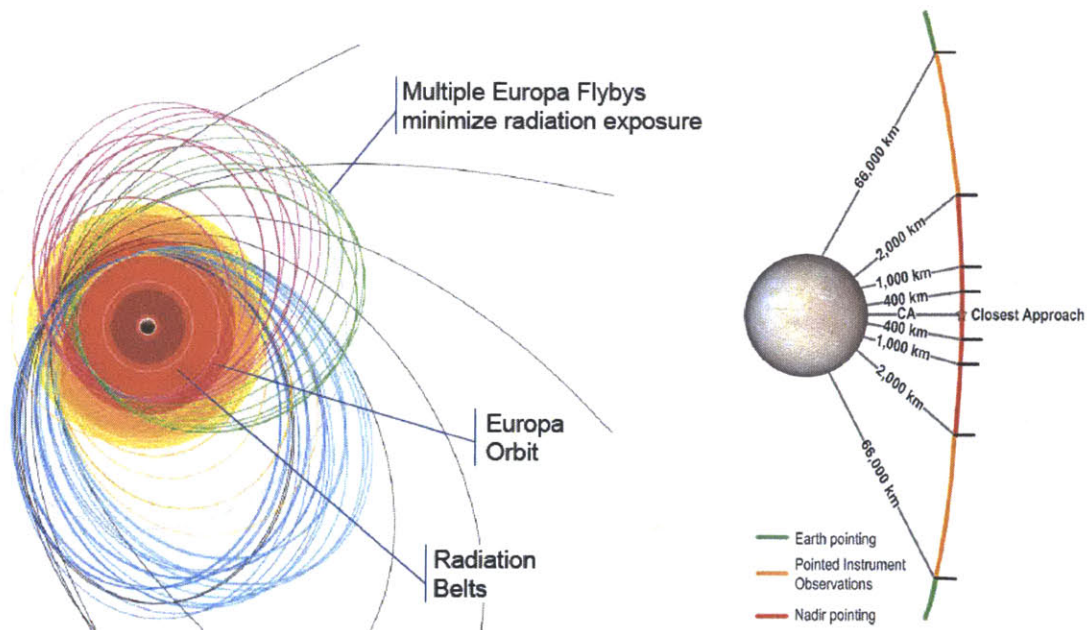


**Figure 50: In-orbit trajectory for the Clipper flyby mission [9]**

In this study, the possible instruments were limited to those that were put forward for the Jupiter Europa Orbiter (JEO) and those that are currently being suggested for EHM, details of which are given in the next section. This constraint was imposed to limit the size of the trade space generated.

**Table 31: Europa science traceability matrix**

Science Objective	Science Investigation	Fly-By	Orbiter	Lander
Characterize the Ocean and the Deeper Interior	Determine amplitude and phase of gravitational tides	-	Comm & laser altimeter	-
	Determine induction response from ocean at multiple frequencies	-	Magnetometer	Magnetometer, Multi-band Seismometer Package
	Characterize surface motion over tidal cycle	-	Comm & laser altimeter	Magnetometer, Multi-band Seismometer Package
	Determine dynamical rotation state & amplitude of libration	-	Comm & laser altimeter	-
	Investigate core and rocky mantle	-	Comm, laser altimeter & magnetometer	-
Characterize the ice shell and any subsurface water, and the nature of surface-ice-ocean exchange	Characterize distribution of any shallow subsurface water	Radar sounder, Topographic Imager	Radar sounder, wide-angle camera & laser altimeter	Magnetometer, Multi-band Seismometer
	Search for ice-ocean interface	Radar sounder, Topographic Imager	Radar sounder, wide-angle camera & laser altimeter	Magnetometer, Multi-band Seismometer Package
	Correlate surface features and subsurface structure to investigate processes governing among the surface, ice shell & ocean	Radar Sounder, IR spectrometer, Topographic Imager	All	Site Imager, Microscopic Imager
	Characterize the physical properties of the regolith and possible links to the interior	Radar Sounder, IR spectrometer, Topographic Imager	All	Site Imager, Microscopic Imager
Determine global surface compositions and chemistry, especially as related to habitability	Characterize surface organic & inorganic chemistry	IR spectrometer, INMS	IR spectrometer, INMS	Mass Spectrometer, Raman spectrometer
	Relate compositions to geological processes especially communication within the interior	IR spectrometer, INMS	Radar sounder, IR spec, cameras, thermal instrument, laser altimeter	Mass Spectrometer, Raman spectrometer
	Assess the effects of radiation on surface materials, albedo, sputtering and redox chemistry	IR spectrometer, INMS	IR spectrometer, INMS, camera, particle & plasma instrument, thermal spec.	Mass Spectrometer, Raman spectrometer
	Characterize the nature of exogenic materials	IR spectrometer, INMS	IR spectrometer, INMS, camera, particle & plasma instrument	Mass Spectrometer, Raman spectrometer
	Search for compositional indicators of past or present life	IR spectrometer, INMS	IR spectrometer, INMS, camera, particle & plasma instrument	Site Imager, Microscopic Imager
Understand the formation of surface features, including sites of recent or current activity, and identify & characterize landing sites	Characterize magnetic, tectonic and impact features	-	Cameras, laser alt., radar, magnetometer	-
	Search for areas of recent or current geological activity	Topographic Imager	IR Spectrometer, Thermal Instrument, Medium- and Narrow-angle camera	Multi-band Seismometer package
	Investigate global and local heat flow	Radar sounder	Thermal Instrument	
	Assess relative surface ages	Topographic Imager	Cameras, thermal instrument, IR spectrometer	Site Imager
	Assess processes of erosion and deposition	-	Thermal instrument, narrow-angle camera, magnetometer	Site Imager
	Understand the processes that determine the composition, structure and dynamics of the Jovian atmosphere as a type of a gas giant planet	IR Spectrometer, INMS	IR spectrometer, Thermal Instrument, Cameras	-
	Study the interactions between Jupiter's radiation environment (magnetosphere) and its satellites	IR Spectrometer, INMS	Magnetometer, Particle & plasma instrument, cameras	-



## 5.2.3 Review of Proposed Designs

### 5.2.3.1 Past Studies

In the past fifteen years, over a dozen Europa mission concepts have been investigated by the Jet Propulsion Laboratory (JPL). [175] In 1997, JPL's concurrent engineering design team, Team X, developed a point design for an all-solar mission to Europa. This design had a 42kg payload mass, including a 15kg surface package, leading to a wet mass of 3530kg with a launch on a Titan IV. The following year, this design was re-examined, under the assumption that the spacecraft could launch on a Shuttle, with an Inertial Upper Stage. The payload was reduced to 20kg, and the wet mass decreased to 2925kg. Despite this decrease, the study was not able to reduce the size of the spacecraft enough for it to fit on the Shuttle.

In 2001, the in-depth point design of a 30-day mission at Europa was undertaken. The mission used a Radioisotope Power System (RPS) and had a 27kg science payload. Overall, the design had an estimated wet mass of 1790kg. The study paid particular attention to the assessment of the radiation environment around Jupiter. In that same year, follow-up studies were performed to assess the alternatives to the Europa Orbiter study. Trades were performed in the trajectory (direct vs. indirect with planetary flyby gravity assists), the overall system (baseline vs. minimum mass) and type of mission (flyby vs. orbiter). Although the alternatives did result in cost savings, this was at the expense of potential scientific return.

In 2002, a study was also performed to develop a low cost (< \$1B) 30-day mission to Europa, with the aim of developing it into a New Frontiers proposal. The spacecraft had 6 instruments, including an ice-penetrating radar, totaling a mass of 17kg.

The Jupiter Icy Moons Tour (JIMT) Studies were also performed in 2002. These were composed of three independent studies. The first was a reactor-powered mission, which used a nuclear fission power system and advanced ion propulsion, with a single launch vehicle architecture. The spacecraft had a payload of 490kg and a total flight mass of 21000kg. The second study was also reactor-powered but it used multiple launches to low-Earth orbit (LEO) and on-orbit assembly techniques. In this case, the fuel tank and science module, which had a payload allocation of 500kg, were launched first on a heavy Evolved Expendable Launch Vehicle (EELV). The power and propulsion modules were then launched on a Shuttle, and solar electric propulsion (SEP) was to be used for the initial spiral out of LEO. The third study investigated a non-reactor-powered option, which could have one or more flight systems to attain the same science objectives as the first two studies. Five options were identified for further study, three of which relying solely on SEP:

1. Three identical vehicles in orbit around Jupiter, with multiple fly-bys of the icy moons.
2. Three identical vehicles, with one orbiting each of the three icy moons.
3. One large spacecraft using Nuclear Electric Propulsion (NEP), orbiting each of the three icy moons for several weeks in sequence before moving on to the next.
4. Two identical spacecraft, which would each sequentially orbit two of the moons.
5. A SEP/Radioisotope Electric Propulsion (REP) mothership that would deliver a dedicated orbiter at each of the three icy moons.

The fourth option was found to be the most advantageous and was developed further. Each spacecraft had a payload of 273kg, and also each carried a 132kg lander, each with 6 instruments, to be delivered at Europa and Ganymede. Notably, the design mostly used existing technologies in order to lower mission risk and cost.

The Jupiter Icy Moons Orbiter (JIMO) studies followed on directly from the first of the JIMT studies (the single launch option). In this study, the payload allocation grew to 1500kg, leading to a launch mass of more than 36000kg. The project was cancelled after the successful completion of Phase A, due to changes in programmatic priorities.

In 2005, the Europa Geophysical Explorer (EGE) study used a Venus-Earth-Earth gravity assist trajectory to bring 150kg of payload to Europa's orbit for a 30-day mission. The total mass of the vehicle was approximately 7230kg.

In 2006, the Europa Explorer (EE) study developed a 90-day mission with a payload allocation of 180kg, as well as an additional 340kg of "unallocated mass" for a possible lander or additional science payload. The system had a wet mass of 6988kg and also used a gravity assist trajectory along with a traditional chemical propulsion system and Multi-Mission Radioisotope Thermoelectric Generators (MMRTGs). This study enjoyed a marked improvement from the past studies due to major advances in radiation-hardened component technologies. A follow-on study investigated the possibility of using solar power instead of MMRTGs to achieve the same mission goals. However, this study found that the size of the solar arrays and of the gimbals and reaction wheels needed for an orbiter that could survive Europa eclipses would be impractical.

The EGE concept was also updated in 2006, as part of the Enhanced Europa Geophysical Explorer (EEGE) study. This study performed a trade space analysis to investigate the impact of using different radioisotope power systems, as well as a range of different launch dates, trajectories and launch vehicles.

In 2007, NASA commissioned the Europa Explorer Flagship study, as a further development to the 2006 EE study. The system had a payload of 205kg and the design was refined to reduce the number of MMRTGs to six (instead of 8 in the EE study). In addition to the baseline implementation, the study also investigated a floor mission that achieved a baseline set of goals, at a lower cost. In parallel to this study,

a solar-powered Europa Orbiter design study was carried out. In contrary to the 2006 solar-powered EE study, this design used a continuous illumination orbit around Europa to reduce the excess solar array area. The study was limited but concluded that this option may be feasible, but at reduced scientific return due to the change in the Europa orbit geometry.

In addition to these orbiter and flyby designs, another dozen studies were performed during that time to investigate the design of Europa landers. A large number of lander designs were investigated, ranging from a simple probe to mobility systems such as submarine vehicles and cryobots. However, none of the Europa mission studies have ever baselined a lander as part of their mission architecture, even though many have highlighted that such a lander would provide significant science, above and beyond the science objectives noted in the last section. The reason for excluding landers from these architectures is that landers were believed to cause a high impact on the cost and risk associated with this type of mission.

#### **5.2.3.2 The Jupiter Europa Orbiter (JEO)**

The Jupiter Europa Orbiter concept was developed in the period of 2008 to 2009, and was the NASA component of the Europa Jupiter System Mission (EJSM). [119] This was a joint mission with the European Space Agency (ESA), where ESA was to provide the Jupiter Ganymede Orbiter (JGO). In addition to investigating the objectives detailed in Table 31, JEO also aimed at studying the Jupiter system as a whole. JEO was to be built to withstand the radiation environment in Europa's orbit, and aimed to carry the following ten instruments and perform radio science, for extensive mapping of Europa:

- 1) Laser Altimeter
- 2) Ice Penetrating Radar
- 3) VIS-IR Imaging Spectrometer
- 4) UV Spectrometer
- 5) Ion and Neutral Mass Spectrometer (INMS)
- 6) Thermal Instrument
- 7) Narrow Angle Camera
- 8) Wide and Medium Angle Camera
- 9) Magnetometer
- 10) Particle and Plasma Instrument

On its way to Europa, JEO was to tour the Jovian system, making observations of Jupiter and of its environment. The estimated total dry mass of JEO was found to be 1367kg, including 106kg of payload, and its wet mass was estimated to be approximately 4700kg. The total cost of the mission was estimated by JPL to be \$3.8B in real year costs, and was later independently reviewed by the Aerospace Corporation and estimated to cost up to \$4.7B. Although the 2013-22 Planetary Science Decadal Survey

[6] found Europa to be a priority target with “*exceptional science merit*,” it also indicated that the cost and risk involved with JEO was excessive, and that the mission needed to be re-evaluated. The JEO mission was therefore cancelled and the European component of EISM, JGO/Laplace, is now known as the JUPiter ICy moons Explorer (JUICE).

### 5.2.3.3 *The Europa Habitability Mission (EHM)*

Following the recommendations of the Decadal Survey, JEO was split into two smaller, more focused missions. [9] These, in addition to a lander concept, are still under investigation at the time of writing. The first mission consists of a spacecraft, called Clipper, in a Jovian orbit performing multiple flybys of Europa. The mission concentrates on, in order of importance, the ice shell, composition, and geology objectives, detailed in Table 31. The Clipper baseline mission currently supports four instruments, and is estimated to cost \$1.9B. The second mission is a 30-day mission with a spacecraft in orbit around Europa, also carrying four instruments and performing radio science, to address the ocean and geology objectives. This mission was estimated to cost \$1.6B. A third concept, that of a Europa lander, was recently added to the study. This late addition emerged from a study performed in the summer of 2011 at JPL that proposed a concept with two simple landers, each with 40kg of payload, as the baseline for a Europa mission with an estimated cost of \$1.8B. [176] The current EHM lander concept is also a stand-alone mission, consisting of a soft lander with a drill and sample handling system, and an orbiter acting as a communication relay, with a reconnaissance camera. The mission would spend an initial 30 days in Europa orbit to perform landing site observation, and then 32 days (9 eurosols) on the surface of the moon. The baseline model possesses seven instruments, addressing, to some extent, all four science objectives for Europa and is estimated to cost \$2.8B. The instruments put forward for all three of these missions are detailed in Table 32.

**Table 32: EHM instrument suite**

<b>Flyby</b>	<b>Orbiter</b>	<b>Lander</b>
Ice Penetrating Radar	Laser Altimeter	Mass Spectrometer
Topographic Imager	Magnetometer	Raman Spectrometer
Shortwave IR Spectrometer	Langmuir Probe	Magnetometer
Ion and Neutral Mass Spectrometer (INMS)	Mapping Camera	Multi-Band Seismometer Package
		Site Imaging System
		Microscopic Imager
		Reconnaissance Imager

Overall, the current versions of Clipper and the lander mission were both found by the study team to have excellent science return, beyond what the orbiter can offer. However, the risk associated with the lander was found to be much greater than for the flyby mission. Consequently, Clipper is currently the preferred mission.

## 5.3 Architecture Generation and Evaluation Metrics

### 5.3.1 Architecture Generation

Table 33 shows all the instruments that were used to generate the trade space in this study. It is to be noted that most instruments can be flown on either the flyby or the orbiter (although their scientific return is different on each platform, as explained later) except the laser altimeter. In order for the laser altimeter to completely achieve the ocean objective, it must measure the tidal flexing of Europa by taking measurements over the same point above the surface of Europa for a whole revolution of Europa around Jupiter. This can only be achieved from an orbiter.

**Table 33: Instruments considered for the trade space exploration of possible Europa missions**

Flyby or Orbiter		Lander
Radar Sounder (IPR)	Laser Altimeter	Multi-Band Seismometer
Topographic Imager	Magnetometer	Site Imager
IR Spectrometer	Thermal Spectrometer	Mass Spectrometer
INMS	Langmuir Probe	Raman Spectrometer
Wide-angle Camera	Narrow-angle Camera	Magnetometer
Stereo Imager	Imager	Microscopic Imager

Instead of generating the full trade space of possible combinations of instruments on all platforms, some constraints were imposed to the space to limit its size. For example, floor instruments had to fly first on any sequence and instruments could not be duplicated across the flyby and the orbiter. Furthermore, the lander in this study was assumed to be a soft lander, accompanied by an orbiter with a reconnaissance imager, acting as a communication relay between the lander and Earth. This architecture was chosen because it is the same as that in the EHM study. Additionally, it was assumed that each mission in a multi-mission architecture flies *sequentially* and that one mission can inform the other. This is not always necessary (for example the EHM flyby and orbiter missions are completely independent of each other and

could even be flown at the same time) but is assumed to allow for the evaluation of the impacts of temporal distribution.

It is also important to understand that not all instruments are required to at least partially achieve all the objectives. Often, one instrument will simply provide a higher resolution measurement of the same phenomena as another. For example, a significant amount of the ocean goal can be achieved by only using radio science. However, the laser altimeter gives more accurate results, and also allows additional properties to be calculated. The trade between the complexity of the payload suite and the science return of each architecture is explored using the metrics discussed in the next section.

### 5.3.2 Evaluation Metrics

Once the trade space of possible mission architectures has been generated, a set of metrics is needed for the evaluation of the design space. These were discussed in Chapter 2. Five of the metrics detailed in that chapter are used for the trade space exploration of temporally distributed options at Europa: science value, complexity, mass, cost and uncertainty. Each of these metrics is discussed in this section.

#### 5.3.2.1 Science Benefit

The science value metric identifies the ability of each instrument to answer the major science questions (i.e. the amount and quality of information each instrument provides to the scientist, measured based on the overall scientific goals). As a reminder, assuming that vehicles in a sequence will not survive until the next vehicle arrives (due to the radiation environment at Europa), it is defined as:

$$\text{Science Benefit} = \frac{\sum_{j=1}^m W_j (\sum_{k=1}^p E_{j,k} \sum_{i=1}^n V_{i,j,k})}{\text{Baseline Value}}$$

**Equation 29**

In this equation,  $V_{i,j,k}$  is the value of instrument  $i$ , for a given science objective  $j$  and for a given platform  $k$  (flyby, orbiter or lander), based on the scale given in Table 4. The  $E_{j,k}$  value for each pair of instrument is read from a look-up table where the weightings account for the synergies between instruments.  $W_j$  is the weighting given to the science objective  $j$  and  $W_j$  is a number between 0 and 1. The sum of all  $W_j$  is 1. In this study, the  $W_j$  values are varied during the trade space exploration to understand the effect of the prioritization of mission objectives on the relative value of the architectures. The value is calculated for the whole sequence of missions and the baseline value is a normalization factor. In this case, the science value for JEO was used as the baseline.

**Table 34: Value weightings scale (adapted from [119])**

Weighting	Description
0	Does not address science investigation
1	Touched on science investigation
2	Partially addresses science investigation
3	Addresses most of science investigation
4	Fully addresses the science investigation
5	Exceeds science investigation

### 5.3.2.2 Complexity and Mass

While the science value metric evaluates the impact a suite of instruments has on the science performed, the complexity metric accounts for the engineering challenges associated with each architecture, and is ultimately correlated with the development and building costs of the vehicles in each architecture. This cost has traditionally been estimated from the mass estimate for each vehicle. However, such mass-based cost estimates have often proven to be inaccurate since, in particular, they do not account for the cost of instrument development. [4] The complexity metric was defined in Chapter 2 and is expanded below for this particular case study, along with its associated weightings.

$$Complexity = \frac{\left( \begin{aligned} &[\sum(E * \sum_{i=1}^n CW_i)_{fb} * Mass_{fb}] \\ &+ [\sum J_{orb} * (E * \sum_{i=1}^n CW_i)_{orb} * Mass_{orb}] \\ &+ K * [\sum J_{lan} * (E * \sum_{i=1}^n CW_i)_{lan} * Mass_{lan}] \end{aligned} \right)}{Baseline\ Complexity}$$

**Equation 30**

**Table 35: Weighting scheme for the complexity metric**

Category	Levels	Weighting
TRL	1-4	+2
	5-6	+1
	7-9	0
Special Positioning	Yes	+1
	No	0
Pointing Requirement	< 1 arcsec	+1
	Other	0
Data Rate	> 1000kbps	+1
	< 1000kbps	0
Power Level	> 15W	+1
	< 15W	0
Radiation Sensitivity	High	+1
	Low	0

In Equation 30,  $CW$  is the complexity weighting for each instrument  $i$ , calculated using the scheme in Table 5. This weighting is based on the concept of cost-risk subfactors, which are normally used to assign additional budget reserves. [139] They are characteristics of a mission that are believed to drive

complexity and cost.  $CW$  ranges from 0 to 7 for each instrument.  $E$  is an additional weighting that accounts for conflicting requirements between instruments. Each time two instruments conflict in the categories in Table 5,  $E$  increases by five percent.  $E$  is looked up from an upper triangular weighted connectivity matrix for the instruments (each entry in the upper half of the matrix has a minimum value of 1).  $J$  accounts for the difference in complexity between flybys, orbiters and landers. It is set at 2 for a lander.  $K$  is the reduction in complexity that occurs when information from a precursor mission leads to a decrease in uncertainty for a subsequent mission.  $K$  is a number between 0 and 1, and decreases as knowledge increases. For the lander,  $K$  is inversely proportional to the resolution of the surface maps available. Again, complexity is calculated for the whole sequence of missions and is normalized by JEO's complexity. In this metric, the sources of uncertainty in the complexity metric arise from the values of  $E$ ,  $J$  and  $K$ .

The mass of each vehicle is calculated using a basic parametric mass model developed with the assistance of engineers familiar with deep space missions. It assumes that Advanced Stirling Radioisotope Generators are used (ASRGs), and that for a mission at Europa, the mass of some of the subsystems, such as the thermal, guidance and navigation, command & data handling (CDH) and communication subsystems are approximately constant. The dry mass, used in the complexity metric, can then be calculated by summing the subsystem masses, the mass of the number of ASRGs needed to meet the power requirements, the mass of any additional mechanical components (e.g.: a boom, a launch vehicle adapter, a landing system) and the instrument mass. The mass of the radiation shielding is assumed to be 30% of the vehicle mass and a 30% margin is added to the total dry mass. Using the dry mass estimates available for JEO and the EHM vehicles, this simple parametric tool was found to provide estimates within 15% of the masses estimated by JPL for these four vehicles. The wet mass was also calculated, using the following Equation 31 and the values in Table 6 where, in case of the lander, the  $\Delta v$  is broken up between a carrier and a separate lander, each having different propulsion systems.

$$\Delta v = I_{sp} g_o \ln \frac{m_o}{m_1}$$

**Equation 31**

**Table 36:  $\Delta V$  and ISP values for wet mass estimation (adapted from [9])**

<b>Vehicle</b>	<b><math>\Delta V</math> (m/s)</b>	<b><math>I_{sp}</math> (s)</b>
Flyby	1675	325
Orbiter	2275	325
Carrier	2870	325
Lander	1767	250



Once the complexity metric has been calculated, the science benefit can be plotted against it to demonstrate the trades between different architectures. Figure 51 shows where the EHM spacecraft lie on the trade space. The cost estimates for the systems presented in this figure are known, and it was found that the complexity ratios calculated for these spacecraft were closely correlated to their cost ratios, thus validating the metric described in this section. Figure 52 portrays the whole trade space evaluated, with all goals evenly weighted. The uncertainty portrayed through the error bars in Figure 51 was derived from the range differing opinions expressed during interviews with experts which led to uncertainties in the values used in the aforementioned equations (i.e. from uncertainties in  $CW_i$ ,  $J$  and  $K$  for the complexity metric and in  $V_i$  for the science value metric). The effects of this uncertainty of technical risk are explored later in this chapter. There are a few key conclusions that can be drawn from these figures. First, it can clearly be seen that the EHM combined orbiter and flyby concept provides nearly the same value at JEO, but is less complex and also less risky. Additionally, under these weightings, the flyby and lander provide much more value than the orbiter, but the lander does so at a higher complexity and risk. Figure 51 therefore independently and numerically confirms the conclusions drawn by the Europa Science Definition Team (SDT). Additionally, while some of the landers sit very close to the Pareto front on Figure 52, the uncertainty associated with them if no precursor mission precedes their design leads to very high mission risk. An example of this is shown for the lander in Figure 51.

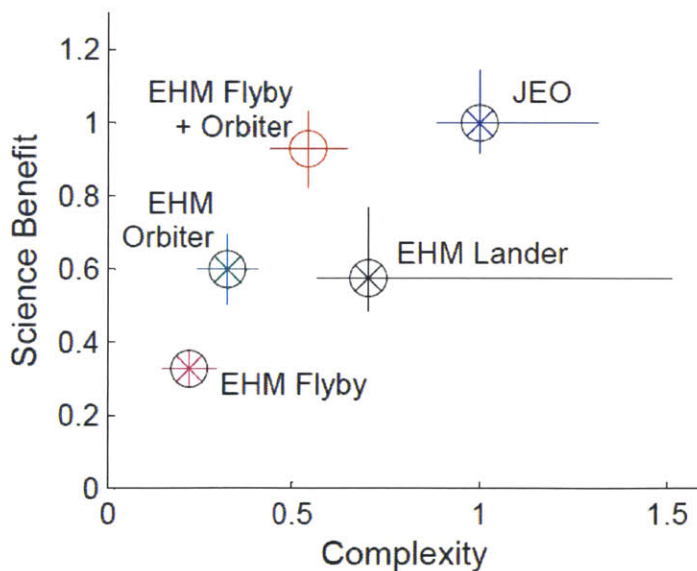
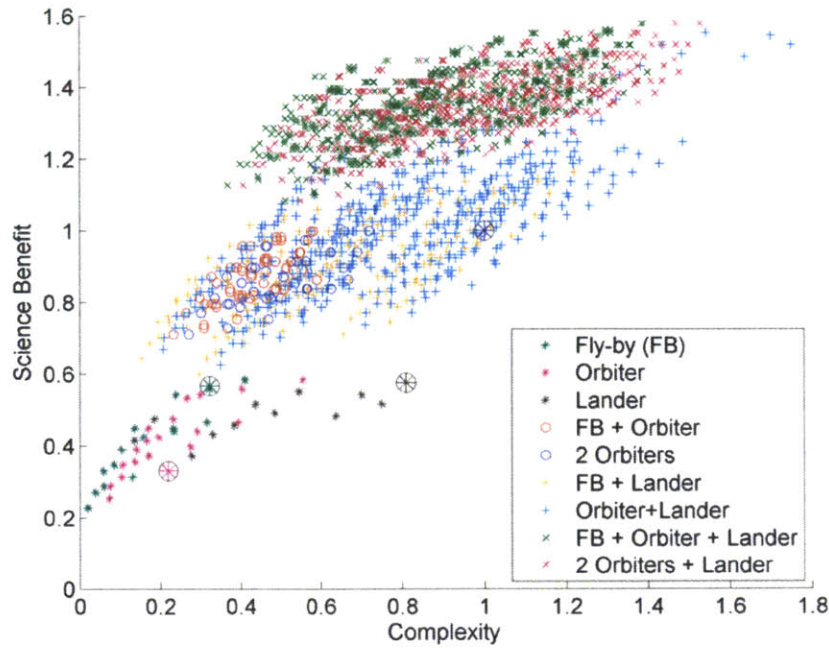


Figure 51: Science benefit vs. complexity for the EHM concepts



**Figure 52: Science benefit vs. complexity for the trade space explored (evenly weighted objectives)**

### 5.3.2.3 Total Cost

To first order, system complexity can be assumed to be correlated to development cost. However, the complexity metric described in Equation 30 does not account for all the costs involved with sending a set of missions to Europa. First, the metric does not account for the launch costs involved with requiring a number of missions to achieve the science objective. Additionally, the metric is heavily based on the complexity of the instruments, and how they affect the cost of the spacecraft. Although it is true that instruments drive spacecraft cost, there is also a baseline cost involved with sending any spacecraft to Europa.

To account for both of these additional costs, a cost metric was derived from the complexity metric, with the normalized inherent costs added onto the complexity value for each architecture. It assumes that each mission is launched separately at a cost of \$350M per launch. Additionally, the cost of sending an “empty” orbiter to Europa was estimated to be \$700M, and that for a flyby was \$600M, based on historical data and the rule-of-thumb derived from correlations in past studies by JPL’s Team-X shown in Equation 32.

$$Fixed\ Cost = \frac{2}{5} * \left(1 - \frac{m_{inst}}{m_{dry}}\right) * Total\ Cost$$

**Equation 32**

These numbers are intended to be conservative estimates. Due to the inherent uncertainty in this crude cost metric, these costs could likely be reduced with more detailed study of a given mission concept.

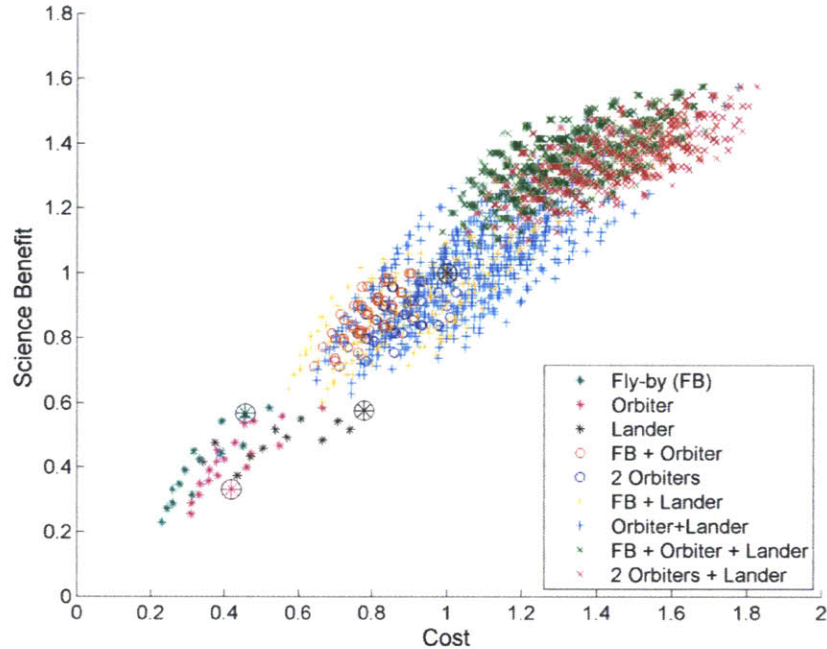


**Figure 53: Science benefit vs. cost (normalized) for the trade space explored (evenly weighted objectives)**

Figure 53 demonstrates that including these costs causes the multi-vehicle architectures to shift along the x-axis, while the Pareto front remains mostly unchanged, as compared to Figure 52. In Section 5.4, the cost metric will be used when exploring the trade space in order to account for the inherent costs involved with sending any mission to Europa.

## 5.4 Trade Space Exploration

One of the key challenges in early mission design is understanding how the prioritization of the science goals affects the chosen architecture. Additionally, it is important to identify the science requirements that drive cost. This section demonstrates how the framework developed in this thesis can help answer these questions. In all the following trade space figures, the EHM baseline concepts presented in Figure 51 are shown as larger points so that they can be easily identified. The JEO baseline is always plotted at (1,1) since it serves as the baseline for the study. It is to be noted that all the orbiters and flybys in the analysis were assumed to carry a medium-angle camera in addition to the instruments discussed for each architecture.

### 5.4.1 Evaluation of the EHM Design

Figure 51 demonstrated the complexity-value relationship for the three EHM concepts, as compared to JEO, with all goals evenly weighted. Under this assumption, the flyby mission provides a much greater return per dollar. However, the objectives for the EHM mission were not evenly weighted but prioritized in the following order: ocean, ice shell, composition and finally geology. Changing the relative weighting of these goals has a significant effect on the value of each of the EHM concepts as compared to JEO, as demonstrated in Figure 54. For each arrow in this figure, the weighting of a given goal is first set to zero, and the rest of the available weights are spread evenly between the other three goals. The weighting of the goal associated with a particular arrow is then gradually increased, until it reaches 1 (and the weightings on the other three goals is then zero).

Figure 54 demonstrates that the EHM orbiter mission is primarily focused on achieving the ocean objective for Europa, with the secondary objective being geology. This is again in accordance with the original intention of the Europa SDT. Similarly, it can be seen that the flyby mission deals with composition, ice and geology particularly well. Figure 54 thus demonstrates how the framework can be used in the early phases of the mission formulation process in discussions between the SDT and the engineering team, and to numerically illustrate the effects of prioritizing certain objectives over others.

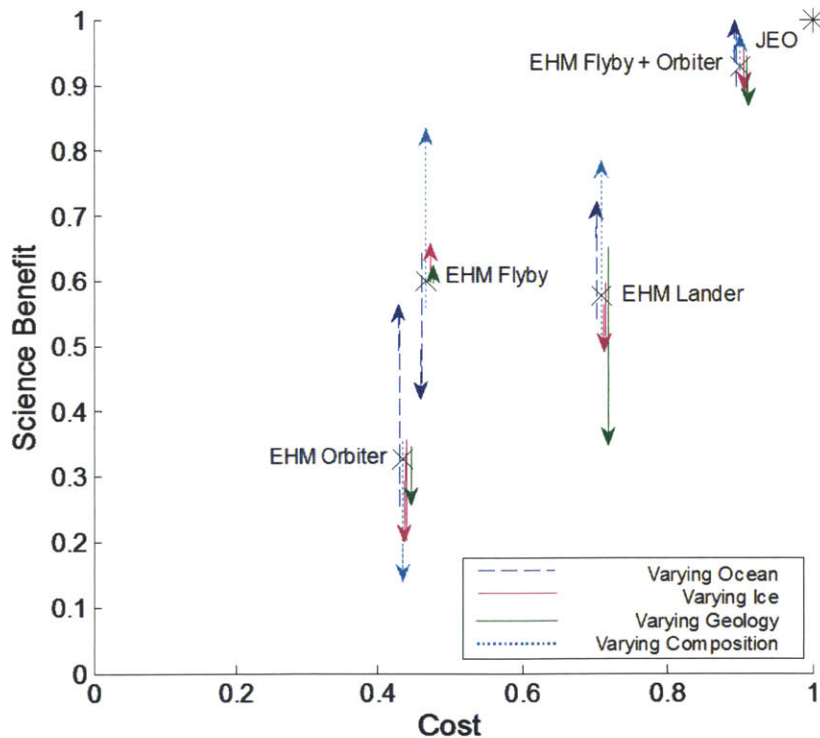


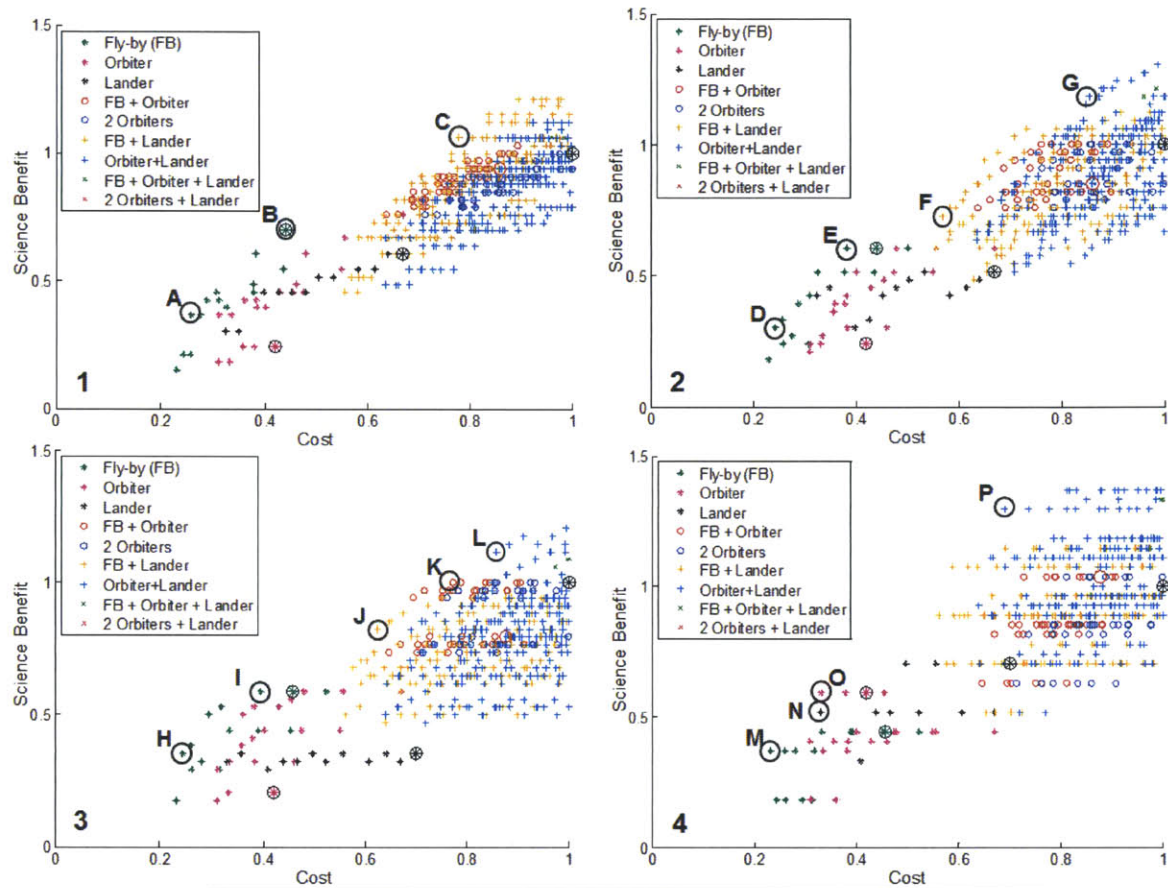
Figure 54: Existing designs' sensitivity to objective weightings ( $W_j$ )

## 5.4.2 Focused Missions

When dealing with missions to the outer solar system, another consideration is whether there are any opportunities for focused, low-cost missions that can still provide high science return. In order to address this, the trade spaces for each of individual science objectives were generated and investigated. In addition to allowing for low-cost missions to be identified, looking at each objective separately helps identify whether any of the goals have conflicting requirements with the others and how that affects cost.

Figure 55 shows the trade space for all four science objectives. Looking at the composition goal (labeled 1), the EHM flyby mission (labeled B), performs very well and sits on the knee of the Pareto front. Within that same goal, there is a large cost increase in order to have a valuable lander as the second mission. This is because it is assumed that the sample for the mass spectrometer must come from below the surface due to radiation induced space weathering on the surface. Therefore, a drill and robotic arm, or a melting device, is associated with the mass spectrometer, which greatly increases its complexity. For the composition, ice shell and geology objectives (labeled 1, 2 and 3 respectively), the flyby missions offer a good low cost alternative, and the best options in the high-value areas are mostly flyby and lander combinations. The ocean objective (labeled 4), however, requires an orbiter due to the laser altimeter, as explained earlier. This leads to a very different Pareto front for this particular goal, as compared to the other three.

This analysis has therefore uncovered that the ocean goal heavily drives the design of a Europa orbiter. In the EHM study, this goal was identified as being the top priority science goal by the STD, which in turn led to the orbiter design being nearly as valuable to the flyby in the STD's analysis. If a similar measurement to that made by the altimeter could be made by a different instrument, if it could be performed with acceptable reliability by a flyby mission, or if the priority of that objective was reduced, the cost of a high value mission to Europa would be significantly reduced since the flyby mission would be able to achieve a high science benefit score. The results also demonstrate some of the similarities between the instruments needed to achieve the objectives. For example, the IR spectrometer, magnetometer and camera combination on a flyby performs well for all objectives, and is an attractive combination for a low-cost mission.



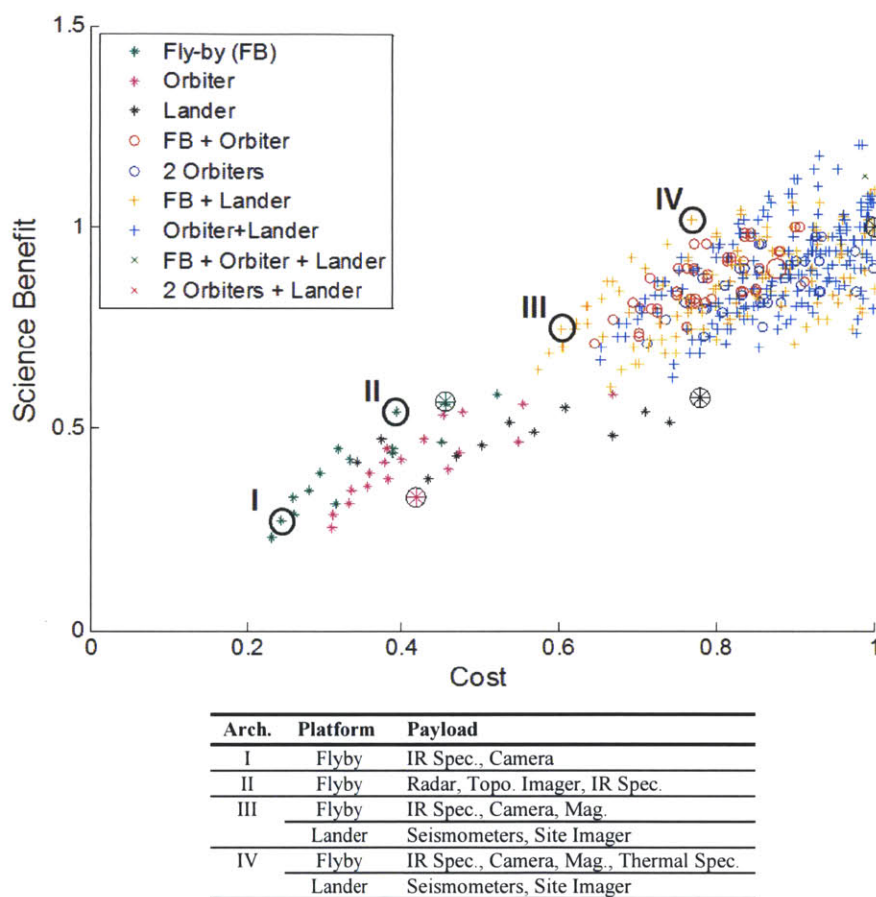
Goal	Arch.	Platform	Payload
1: Composition	A	Flyby	IR Spec., Camera
	B	Flyby*	Radar, Topo. Imager, IR Spec., INMS
	C	Lander	Mass Spec., Site Imager
2: Ice Shell	D	Flyby	Thermal Spec., Camera
	E	Flyby	Radar, Topo. Imager, Thermal Spec.
	F	Lander	Thermal Spec., Camera
	G	Orbiter	Seismometers, Site Imager
3: Geology	H	Orbiter	Radar, Topo. Imager, Laser Alt., Mag.
	I	Lander	Seismometers, Site Imager
	J	Flyby	Thermal Spec., IR Spec., Camera
	K	Flyby	Thermal Spec., IR Spec., Camera
	L	Orbiter	Radar, Topo. Imager, Laser Alt., Thermal Spec., Mag.
4: Ocean	M	Lander	Seismometers, Site Imager
	N	Flyby	Camera, Mag.
	O	Orbiter	Laser Alt., Camera, Mag.
	P	Orbiter	Radar, Topo. Imager, Laser Alt., Mag.

Figure 55: Trade space evaluation for focused missions.

Architecture B (with a flyby indicated with an asterisk) is the flyby mission that was baselined by JPL for EHM.

### 5.4.3 General Missions

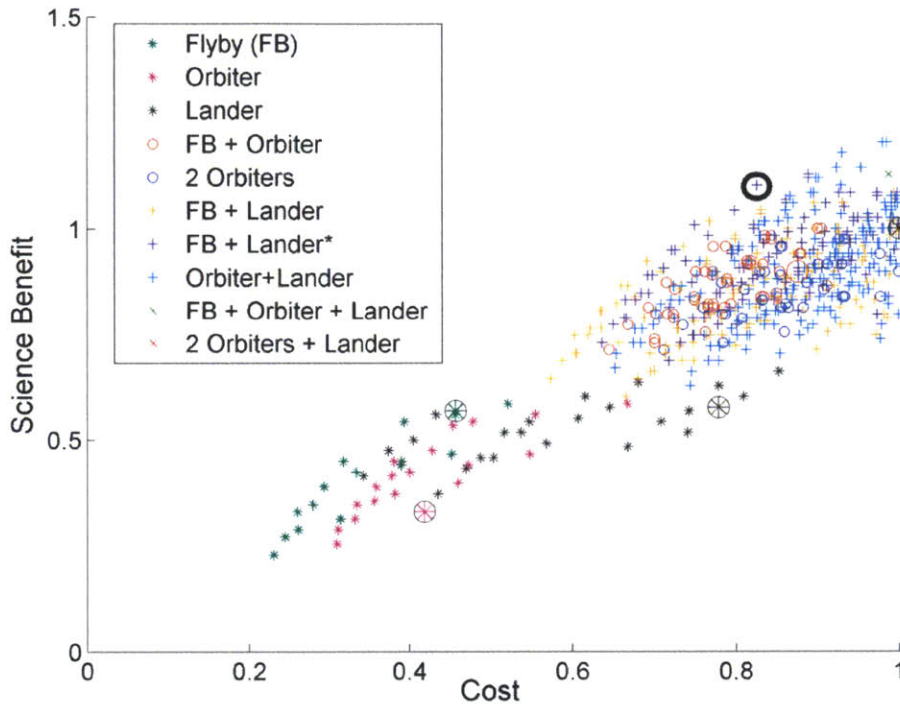
The next step in the trade space analysis process is to identify architectures that perform well no matter what the weightings on the mission objectives are. Figure 56 shows all the architectures having a cost lower than or equal to that of JEO, assuming that the mission objectives are evenly weighted.



**Figure 56: Trade space evaluation for evenly weighted goals**

By comparing Figure 56 to Figure 55, it can immediately be seen that, for a given science benefit, the cost of a general mission is greater than that of a focused mission. This demonstrates that, if a low cost mission is desired, having focused science goals will provide a higher return per dollar. Looking at the Pareto front in Figure 56, it can be seen that the EHM flyby mission floor (labeled II) sits on the knee of the Pareto front and is a good option for an investment on the order of ~\$2B. Within the low cost mission options, a flyby mission with an IR spectrometer and a camera again performs very well, and is estimated to have the potential to be achievable for less than \$1B. Such a mission would therefore fit within a New Frontiers class budget. If higher value is to be achieved, the most promising combination is a flyby mission followed by a simple lander mission.

Under the current assumptions, a campaign of missions with a science return greater than that of JEO is almost unachievable without an orbiter as part of the sequence. This is again due to the fact that the laser altimeter must be flown on an orbiter in order to achieve most of the ocean goals. One way to circumvent this issue is by allowing the orbiter hosting the lander to carry a laser altimeter in addition to its communication system and reconnaissance camera, leading to the trade space shown in Figure 57.



Platform	Payload
Flyby	Radar, Topographic Imager, IR Spec., INMS
Lander	Seismometers, Site Imager, Mass Spec., Magnetometer
Carrier	Reconnaissance Imager, Laser Altimeter

**Figure 57: Addition of a laser altimeter on the carrying orbiter**

Adding architectures with a more capable carrier expands the space and leads to an understanding of the marginal science return for this particular case. In Figure 57 for example, it can be seen that a mission with at least 20% greater science return than JEO could be achieved at approximately 80% the estimated cost of JEO (circled). This mission consists of the EHM flyby mission (Clipper), followed by a simple lander and a carrier orbiter with a reconnaissance imager and a laser altimeter. In this case, cost and science benefit are traded for speed at which science benefit is returned: the sequence is cheaper than the flagship and will mostly likely provide greater science benefit due to the value of in-situ measurements, but its overall timeline is also longer than that of a flagship mission, which would answer all mission objectives at once.



## 5.5 Effects of Uncertainty and Risk

As explained in Chapter 2, the uncertainty and risk metrics are used as secondary metrics to evaluate the perceived risk associated with architectures that have been down-selected. They mirror the differing opinions associated with the weightings in the science benefit, complexity and cost metrics. In the graphs presented in this section, the error bars represent the range in science benefit and complexity values, caused by disagreements between experts during interviews. Therefore, the error bars are correlated to the spread in agreement (or disagreement) between the interviewees. The values are again comparative and not ultimate, and should be interpreted with care. In this section, the insights provided by these metrics on the choice of instruments and platform, as well as on the effects of temporal distribution, are explored.

### 5.5.1 Effects of Instrument Choice on Uncertainty

One of the first insights that the uncertainty metric can provide is an understanding of how particular instruments can affect the uncertainty associated with a given architecture. An example of this is presented in Figure 58, where the uncertainties associated with two very similar flyby missions are compared.

In Figure 58, the two flybys are identical in every way, except from the fact that the second architecture includes an Ion and Neutral Mass Spectrometer (INMS). This is not only a fairly power intensive instrument, but it was also discovered during expert interviews that there are disagreements in the science community on the accuracy of the results that can be obtained from such an instruments. An INMS was flown on the Cassini orbiter, which was initially judged to be successful. However, it has recently been argued that, due to the speed at which the particles enter the INMS on an orbiter or flyby, the properties (composition and structure) of the particles that are measured by the INMS are changed before they even enter the instrument. Thus, there are disagreements on whether flying an INMS at such high speed actually provides accurate results.

The impacts of these disagreements are shown in Figure 58. First, the INMS increases the complexity of the flyby architecture due to its mass and power contribution. It also increases the uncertainty in that complexity metric, due to its difficulty in integration, required positioning and data rate. Most importantly, because of the uncertainty in the accuracy of the results produced by existing orbiting INMS, the expected science benefit provided by the INMS is also highly uncertain. In fact, this figure shows that there is a risk that, even if the INMS is added, it could provide the same value as the flyby without the INMS, but at an increased cost and complexity.

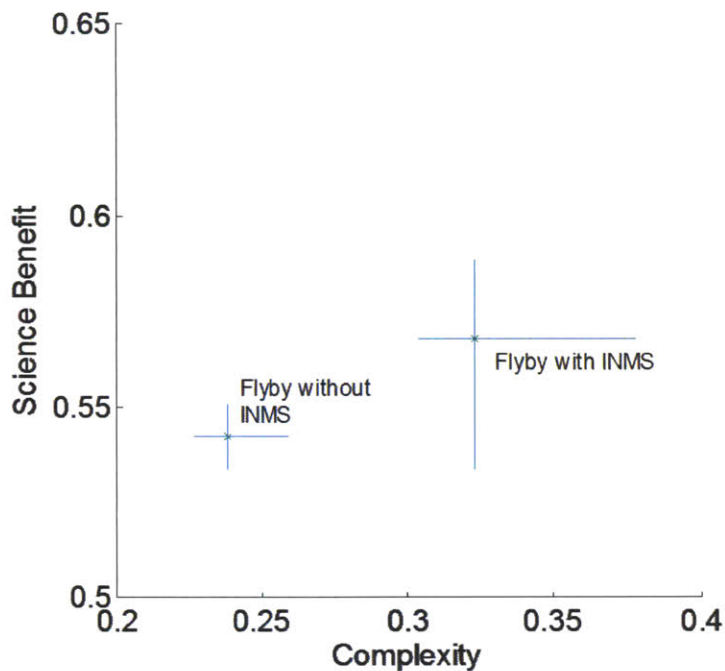


**Figure 58: Effect of instrument choice on uncertainty**

This type of observation would discourage a science and engineering team from including the INMS in the chosen architecture without investigating the problem further. In fact, at the time of writing, the inclusion of this instrument is being re-considered for the baseline EHM flyby due to these risks and a new instrument (a simpler dust and particle detector) is being considered to take its place in the strawman payload for the Clipper mission.

### 5.5.2 Effects of Platform Choice on Uncertainty

The metric can also help demonstrate the difference in the uncertainty associated with different platforms. This is portrayed in Figure 59, where the uncertainty associated with different platforms in 1-vehicle architectures is plotted.

At first glance, it can be seen that the lander carries far greater uncertainty, both in terms of the science benefit and the complexity, than either of the other two platforms. This is due to the fact that very little is known about Europa and its surface. In turn, this leads to uncertainties in exactly what should be measured to answer the science questions being posed, which means that, without learning more about the surface, there is uncertainty in the potential return of the mission. The instruments flown could simply measure the wrong phenomena once landed on the surface. Most importantly, very few pictures of the surface of Europa are available, and these also have limited resolution. This makes it very difficult to design a soft lander for Europa. For example, pictures of Europa from Galileo show ridges and lines on

the surface of the planet. Although these appear to be large scale features, it is unclear what the surface looks like on a smaller scale. It could be flat, it could have similar smaller ridged features, or it could even have cracks leading deep down into the ice layer or even the ocean. This lack of knowledge makes the design of the lander highly complex, as portrayed in Figure 59.

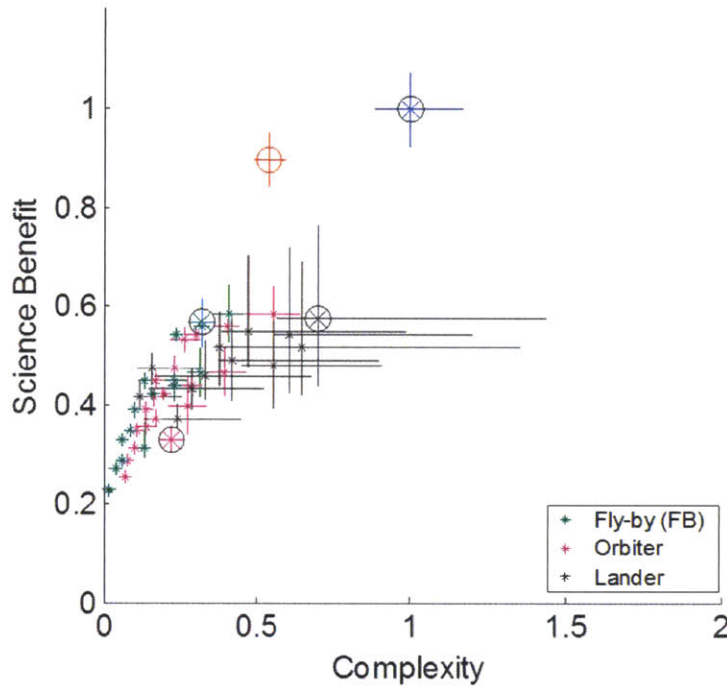


**Figure 59: Effect of platform choice on uncertainty**

A more subtle difference between flyby and orbiter missions can also be observed in Figure 59: in general, the flyby architectures have lower uncertainty in their complexity than the orbiter architectures. This is due to the challenging high radiation environment that orbiter missions encounter. Because the flyby missions' orbits around Jupiter are typically highly eccentric, they only spend part of their time in proximity of Europa, which somewhat relaxes the radiation hardening and the  $\Delta v$  requirements for these spacecraft, as compared to the orbiter. The flyby missions can therefore be seen, through this metric, to carry lower technical risk.

### 5.5.3 Effects of Temporal Distribution on Uncertainty

As discussed earlier in this section, flying a lander as the first mission to Europa carries enormous uncertainty due to the lack of information about the surface of Europa and its constitution. This uncertainty is reduced once more is known about the surface, by way of a precursor flyby or orbiter mission for example. The uncertainty metric can help illustrate the subsequent reduction in the perceived risk associated with the lander, both in terms of the complexity and the science benefit of the mission.

This is demonstrated in Figure 60. In this case, an architecture consisting of a lander alone, and one with a flyby/lander sequence are plotted together. It can be seen that the flyby “precursor” helps reduce the uncertainty in the complexity of the lander because more accurate and higher resolution data will be available about the surface of Europa through the flyby. It also helps reduce the uncertainty in expected science return, because greater knowledge about the moon can also help focus the science questions and calibrate the instruments appropriately.

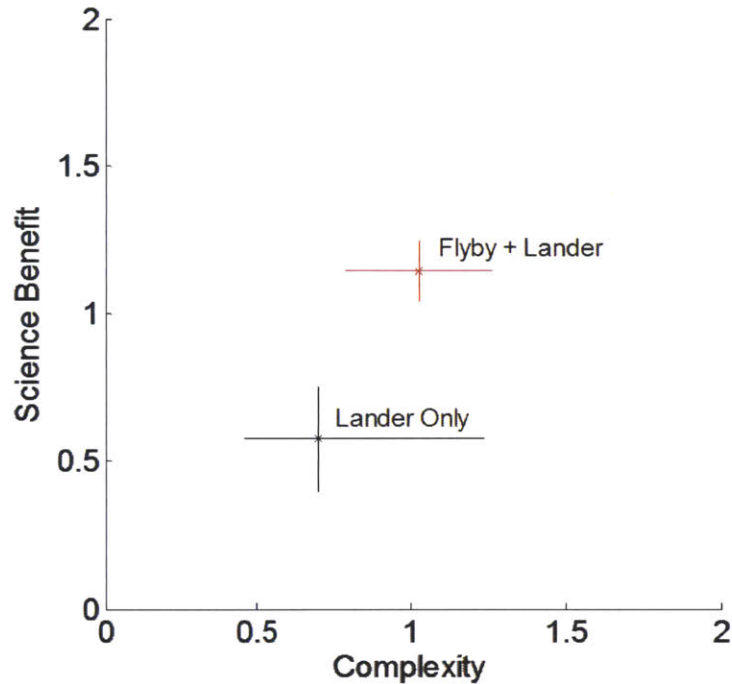


Figure 60: Effect of temporal distribution on uncertainty

#### 5.5.4 General Effects on Trade Space

The  $\epsilon$ -Pareto front, a concept introduced in Chapter 2, for architectures with normalized maximum complexity values smaller than 1 and uncertainty smaller than 30% in both metrics is presented in Figure 61. This corresponds to low-uncertainty, low-complexity architectures. It can be seen that, in the 1-vehicle architectures, flyby missions mostly dominate, due to their low complexity and the range of science questions they could answer. There are some orbiters that appear in the  $\epsilon$ -Pareto front, but these typically have a larger range in possible value and thus may be less desirable since a larger range implies a higher risk, both in terms of cost and return. It is also noteworthy that, from the existing designs proposed by the Europa study group [6], [9], only the EHM flyby can be found in the  $\epsilon$ -Pareto front.

When looking at the 2-vehicle architectures, the  $\epsilon$ -Pareto front is much more populated, or “fuzzy.” This is due to significant overlaps in error bars, which occur from uncertainty in metrics, or disagreements between experts. In particular, the ratio of orbiter-lander to flyby-lander combinations appears much

larger than the orbiter to flyby architecture ratio in the 1-vehicle case. This was found to be due to the laser altimeter carried by the orbiter in the first of the 2-mission sequence in the 2-vehicle architectures. This laser altimeter was judged by experts to have the potential to provide very accurate information about the surface of Europa, thus reducing the potential complexity of the landing system. Nonetheless, the orbiters themselves are more complex than the flybys, and they also have a lower potential science benefit for a given complexity (assuming evenly weighted goals). Consequently, there is a careful trade between sending a simpler mission (flyby) and then a slightly more complex lander, or sending a slightly more complex mission (orbiter) in the hope that the subsequent lander would be less complex.

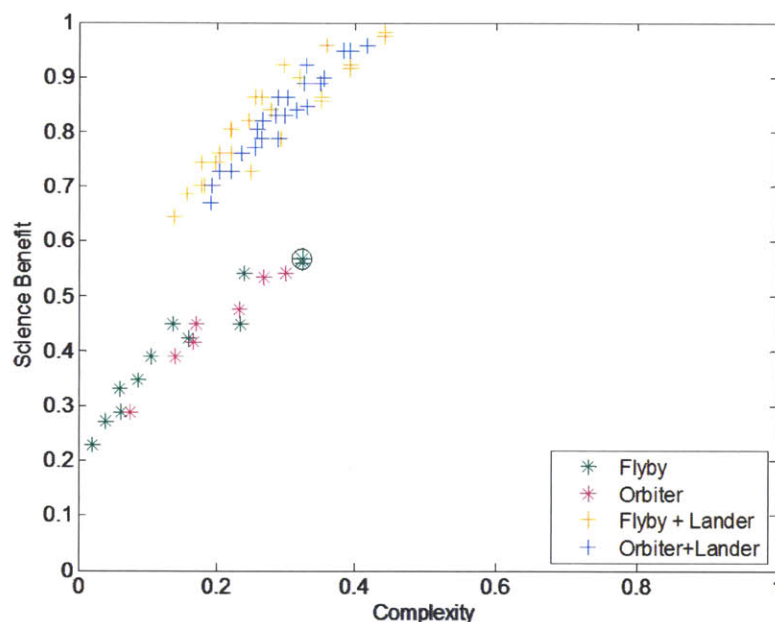


Figure 61:  $\epsilon$ -Pareto front

Finally, the numerical uncertainty (i.e. the range in potential values) of the complexity and science benefit can also be used as a secondary metric to downsize architectures. The complexity and science benefit range for architectures discussed in Section 5.4 are presented below. The numbers again re-iterate the advantages of only flying a lander as the second of a 2-mission sequence.

Table 37: Value ranges for select architectures, normalized by the JEO ranges

Architecture	Platform	Complexity Range	Science Benefit Range
EHM Flyby	Flyby	0.4	0.5
EHM Orbiter	Orbiter	0.2	0.25
EHM Lander	Lander	1.8	1.4
<i>JEO</i>	<i>Orbiter</i>	<i>1</i>	<i>1</i>
I (from Figure 56)	Flyby	0	0.1
II (from Figure 56)	Flyby	0.2	0.1
III (from Figure 56)	Flyby+Lander	0.6	0.8
IV (from Figure 56)	Flyby+Lander	0.8	1.0

## 5.6 Conclusion

The framework developed in this thesis was applied to the case of the exploration of Europa to demonstrate that it allows for the rapid exploration of the multi-mission trade space for missions where the science goals are plentiful, varied, and sometimes at odds with one another. The case study highlights the trade between mission cost, risk and return. It also demonstrates that the framework could help structure conversations between science and engineering teams by quantitatively demonstrating the relative effects of mission architecture choices and the weighting of science priorities on the science return and cost of a mission. Furthermore, it could aid in evaluating the marginal return of adding a particular instrument to a mission. This framework promotes synergy between instruments and helps systematically identify valuable combinations of instruments early on in the design process. It also allows a science definition team to rapidly explore a large portion of the trade space of possible missions and to understand how the prioritization of science goals affects the design space, helping to guide the selection of a mission concept that maximizes the science return for the funds available.

Finally, the analysis undertaken has highlighted the trade between the flagship and the sequential approaches to planetary exploration. While flagship missions offer very high value as part of a comprehensive effort, are more conducive to “unexpected” discoveries due to their large suite of instruments, and may possibly have a lower total cost than a whole campaign would, they also can carry high risk and complexity, have long timelines until the first science results are returned, and often have to deal with conflicting science goals that are hard to resolve. Conversely, sequences of missions deal with the science objectives in smaller, more manageable chunks. This leads to smaller missions that could more easily fit into a limited annual budget and be developed more quickly, returning science results earlier. In the sequential approach, the risk of science loss from a failure on any one mission is lower. In addition early missions can inform the design of a subsequent mission, leading to the potential of higher science value and lower complexity for later missions in a sequence. However, in sequences, science has to be prioritized, an often difficult task.

When it comes to choosing between a flagship mission or a sequence of missions, the answer is highly dependent on the programmatic priorities and the economic climate. Although a sequence of small missions spread over several years could lead to a lower program cost per year and a shorter time to first science return than a flagship mission, a sequence of missions could also lead to a longer time for full science return and a higher total cost. This puts these missions more at risk of being cancelled due to changes in government and programmatic interests, and this factor must be carefully weighed when taking choosing between temporally distributed systems and large flagship missions.

## Chapter 6

# SPATIALLY AND TEMPORALLY DISTRIBUTED SYSTEMS FOR MARS SAMPLE RETURN

### 6.1 Introduction

The concept of Mars Sample Return (MSR) was first considered by NASA during the Apollo era, [177] just over half a century ago, and it was again identified in the 2013-2022 Decadal Survey [6] as being the mission with the highest importance for the decade ahead. Although in-situ missions can allow for the exploration of some of the questions posed by a MSR campaign, the latter would enable carefully selected samples to be analyzed using a large range of instruments on Earth by the Mars science community as a whole, and is thus highly preferable. Due to its complexity and cost, such a campaign would inherently contain multiple systems interacting together on the surface of Mars and in orbit, which would be launched separately to achieve the sample return goal. MSR must therefore be treated as a *spatially and temporally distributed* system. Over the years, dozens of different MSR concepts have been studied. The most recently studied campaign consists of four components: (1) a caching rover, (2) a sample fetch and ascent vehicle, (3) a return vehicle, and (4) an Earth processing facility. Although the Mars 2020 rover [11] was recently announced as a vehicle that will fulfill the caching component of such

a campaign, steps (2) and (3) in the sample return process are still very loosely defined. Most importantly, the types of vehicles that will be used to perform these tasks, how the required functionality will be spread among them, the number of launches required to fly them, and the ordering in which such missions should be sent to Mars are trades that are not yet fully understood. Consequently, this chapter explores the multi-vehicle sample return trade space, and seeks to demonstrate the effects of the main architectural decisions involved in steps (2) and (3) of MSR, using the framework put forward by this thesis.

The chapter starts by providing a short overview of the concepts that have been investigated for MSR in the past decade, highlighting the main features of the sample return concept currently considered as well as the open trades in its architecture. This is followed by a thorough decomposition of the functionality required to perform the retrieval, ascent and return components of the sample return mission. An overview of the specific metrics used to evaluate it, which are refined from the metrics presented in Chapter 2, is provided. The remainder of the chapter explores the sample return trade space and the ability of the framework to demonstrate the effects of the main architectural and technology choices on the mission's return on investment. Finally, eight key recommendations for the MSR campaign are drawn from the analysis presented.

## **6.2 History of Mars Sample Return**

### **6.2.1 Why Sample Return?**

In 2006, fifty-five important future Mars science goals were identified by the Mars Exploration Program Analysis Group (MEPAG). [178] In their 2008 report, the Next Decade Science Analysis group (ND-SAG) concluded that nearly half of the MEPAG science goals could be addressed by a Mars sample return mission. [179] It found that MSR was the campaign that could provide the greatest science return from Mars. The 2008 ND-SAG report was written following a 2007 National Research Council (NRC) report, which indicated that sample return was the highest priority in astrobiology, and that current and upcoming missions (up to and including the Mars Science Laboratory) would provide enough information to enable the selection of an appropriate landing site for MSR. [180] Furthermore, the ND-SAG report was supported by the 2013-2022 Planetary Science Decadal Survey, which indicated that a MSR caching mission is the single most important solar system exploration priority for the upcoming decade. [6]

While many of the MEPAG goals can be achieved through in-situ missions and the analysis of Mars meteorites, some goals could simply not be achieved without MSR. There are four primary reasons why MSR is of such high value to science: (1) complex sample preparation, (2) instrumentation that would not be suitable for flight to Mars, (3) instrument diversity and (4) the fact that Mars meteorites are useful for answering only some, but definitely not all, of the questions. Consequently, although recent publications



have challenged this assumption, [181] the planetary science community generally agrees that the answers to the questions posed by the MEPAG can only be elucidated via a MSR campaign.

## 6.2.2 Overview of Past and Current Designs

Although MSR has been studied for decades, the foundation for the concept that has been considered for the past fifteen years was first established in 1998, in a study in partnership between NASA and the Centre National d'Études Spatiales (CNES). [182] The architecture consisted of a mobile caching vehicle to collect the sample, a Mars Ascent Vehicle (MAV) to bring the sample to orbit and a return vehicle to carry the sample back to Earth's vicinity. The mission was cancelled in 1999, following the failure of the Mars Climate Orbiter and the Mars Polar Lander missions. In 2001, four teams, involving more than 20 institutions, along with the Jet Propulsion Laboratory's (JPL) concurrent engineering team, Team X, were tasked to explore a range of concepts for Mars Sample Return. These were mostly multi-launch architectures, ranging in cost between FY2001 USD \$1.5B and \$3.0B, but the concepts put forward varied significantly. [183] Concepts explored during these studies included the use of Solar Electric Propulsion (SEP), aerobraking and aerocapture, double vehicle redundancy on the surface, and return to Earth orbit instead of direct entry. In 2002, cuts in government funding reduced the Mars Exploration Program's budget. This led to the creation of a MSR Science Steering Group, which proposed a de-scoped "first" MSR mission, called the "Groundbreaking Approach." [184] This mission consisted of a simple grab-and-go lander, and forewent the mobile component of the sample caching process, in order to significantly reduce the cost of the mission to approximately FY2002 USD \$1B.

In 2008, following the 2007 NRC Report, [179] the ND-SAG and the International Mars Exploration Working Group (IMEWG) developed a set of requirements for the samples to be collected at Mars. These were incorporated into the International Mars Architecture for Return of Samples (iMARS), and formed the basis for the requirements of the Mars 2020 rover, which will be discussed in the next section. These studies recommended that the sampling targets be carefully selected, and that supporting *in situ* science was essential to provide context on the provenance of the samples. [185] It was also established that the ESA and NASA goals for sample return were very much in line. This led a collaborative 2-rover 2018 mission to be put forward in 2009 by the 2-Rover International Science Working Group (2R-iSAG). [186] This mission included a European rover, ExoMars, and a NASA rover, MAX-C (the Mars Astrobiology Explorer-Cacher), to be landed at the same site, thus providing complementary science. The NASA portion of the mission was cancelled soon after due to reduced budget, but the ExoMars is still scheduled as an orbiter and rover mission sequence to be launched in the 2016 and 2018 launch opportunities.

The past decade has also seen the development and demonstration of several enabling and supporting technologies for MSR, through the successful landing of two landers (Pathfinder and Phoenix) and four

rovers (Sojourner, Spirit, Opportunity and Curiosity) as well as two orbiter missions (Mars Odyssey and Mars Reconnaissance Orbiter) by NASA. Technology demonstrations at Mars have included the development of guidance and navigation algorithms for precision landing, the use of the sky crane to land masses of up to 1000kg on the surface of Mars, the use of aerobraking to reduce orbiters' fuel requirements for Mars Orbit Insertion (MOI). Additionally, autonomous rendezvous techniques were demonstrated in Earth orbit by the Department of Defense (DoD) and re-entry of samples from deep space were performed as part of the Stardust and Genesis missions.

### 6.2.3 2011 MSR Baseline

In 2011, analyses performed for the Planetary Science Decadal Survey [6] further established that the caching rover and the MAV needed to be landed separately, unless significant technology improvements were made to land higher masses on Mars. This separation was also found to provide necessary additional time for the caching rover to perform in-situ science and carefully select samples. In turn, this led to the creation of the aforementioned four-step architecture. The 2011 architecture contained three flight elements: a caching rover launched in 2018, a chemical propulsion orbiter launched in 2020 and a lander and fetch rover launched in 2022. [187] The fourth step is the Mars Returned Sample Handling facility (MRSF) on Earth. In this architecture, the lander and orbiter components of the campaign were on separate launches, with a total timeline (from first launch to Earth return) of 5 years. Together, the campaign was estimated to cost between FY2015 USD \$5B and \$6B. Since this architecture is the latest to have been formally published, in the remainder of this work the vehicles put forward for the fetch, ascent and return part of the 2011 architecture are used as the baseline against which the rest of the architectures in the trade space are compared (note that different launch dates are baselined). The details of this baseline are presented in Table 38.

**Table 38: Baseline architecture**

<b>Platform</b>	<b>Properties</b>
Orbiter	Chemical propulsion, return to Earth; launched in 2024
MAV	2 stage solid and liquid combination, 500km orbit, dual-string; launched with lander
Lander	5km landing ellipse, dual-string; launched in 2026
Fetch Rover	10km range, dual-string; launched with lander
EEV	44kg; launched with orbiter

## 6.2.4 Mars 2020 Rover

In July 2013, the Mars 2020 rover Science Definition Team (SDT) released its preferred science objectives for the rover mission. [11] The team specified four mission objectives:

- 1) Explore an astrobiologically relevant ancient environment on Mars to decipher its geological processes and history, including the assessment of past habitability
- 2) Assess the biosignature preservation potential within the selected geological environment and search for potential biosignatures.
- 3) Demonstrate significant technical progress towards the *future return of scientifically selected, well-documented samples* to Earth.
- 4) Provide an opportunity for contribute Human Exploration & Operations Mission Directorate (HEOMD) or Space Technology Program (STP) participation, compatible with the science payload and within the mission's payload capacity.

In addition to these goals, the SDT defined a 2020 launch, a one Mars year (~690 Earth days) mission, and a set of cost limits for the different components of the mission. Overall, the SDT found that all four of these objectives can be achieved by a “single rover carrying a modest but highly capable payload that includes the capacity to produce a returnable cache,” containing 31 samples. The rover is therefore expected to contain a system to collect samples for caching, a caching system, a mechanism for maintaining sample integrity, methods for sample processing, encapsulation and transfer, and the rock surface preparation capabilities needed for optimal science measurements.

In order to generate a relevant trade space, this work takes the Mars 2020 rover SDT requirements as input assumptions to the ascent and return parts of a potential MSR campaign. It assumes that a 500g sample, which is encased in a 5kg container, is be left at a known stationary position on the surface of Mars, by a rover such as the Mars 2020 rover.

## 6.2.5 Current Trades for Retrieval, Ascent and Return

Although the scientific community now has a good understanding of the process that must occur in order to leave a relevant set of samples in a cache on the surface of Mars, the architecture of the systems bringing the sample back from the surface of Mars to the surface of the Earth is still being traded. One of the main challenges with choosing an architecture is that each architectural decision for a given vehicle heavily impacts the design of the rest of the system. The first step in understanding the potential set of systems that could achieve the return of cached samples to Earth is to define all the necessary tasks, called functions, which need to be performed in order for the return to be successful. These are shown in the first column of Table 40. For each of the possible platforms, the way the platform can achieve a particular

function, called the form, is then identified. It can be seen in Table 40 that no single platform is able to achieve all the required functions on its own, hence the need for a multi-vehicle campaign that is both spatially and temporally distributed. In addition to the different types of vehicles that can be used, and the different ways in which the functions can be spread amongst these vehicles, the functional decomposition also uncovers open trades in terms of the functions needed and the different forms that can achieve them. These open trades are highlighted in green in Table 40.

The functional decomposition led to the identification of eight important trades that will be evaluated in this case study. They are presented in Table 39 and will be explored in order throughout this chapter. These trades consider: using different technology options, such as Solar Electric Propulsion (SEP), a large rover carrying the MAV and precision landing, whether or not to use redundancy, whether or not to return the sample directly to the Earth, mission sequencing, and launch dates. The enumeration and evaluation process part of the framework are described in the next section.

**Table 39: Summary of main trades explored**

#	Name	Description
1	Rover Range	Shorter rover range means smaller landing ellipse, reduced mission time but higher propellant use
2	MAV Capability	Single vs. dual string
3	MAV Mobility	Stationary on lander with fetch, or on rover
4	Direct Return	MAV to escape, no orbiter option
5	Orbiter Propulsion	Chemical vs. solar electric
6	MAV Target Orbit	500km, 2-day elliptical or escape
7	Sequencing	Orbiter first vs. lander first
8	Orbiter Destination	Earth surface vs. lunar orbit

**Table 40: Functional decomposition of the Fetch, Ascent and Return part of a MSR campaign; cells in light green represent open trades.**

Platforms	Orbiter	Lander	Rover	MAV	EEV
<b>Sample Retrieval</b>					
Precision Landing on Mars Surface	-	EDL System with TBD precision	EDL System with TBD precision	-	-
Traversing on Mars Surface (up to 10km each way, shorter range means higher precision)	-	-	Mobility System: Single or Dual String	-	-
Sample Acquisition	-	-	Robotic Arm	-	-
Sample Transfer	-	Robotic Arm	Robotic Arm	-	-
Sample Containment	-	-	-	Sample Bay	-
Contingency Sampling	-	Robotic Arm	Robotic Arm	-	-
<b>Reach Mars Orbit</b>					
Provide $\Delta V$ to reach TBD orbit	-	-	-	Propulsion: # Stages, Type of fuel	-
Provide Guidance to reach TBD orbit	-	-	-	GNC System: Single or Dual String	-
Sample Positioning	Sensors	-	-	Sensors (Single or Dual String)	-
Return Vehicle Rendezvous	Guidance System & Prop	-	-	Guidance System & Prop	-
Return Vehicle Sample Transfer	Robotic Arm	-	-	-	-
Sample Protection/Sealing	Sample Bay	-	-	-	-
<b>Return to Earth Vicinity</b>					
Provide $\Delta V$	Propulsion: Chemical or SEP	-	-	Propulsion: # Stages, Type of fuel	-
Track Orbit	Sensors	-	-	Sensors	-
Contain Sample	Sample Bay	-	-	Sample Bay	-
Retain Sample Integrity	Sample Bay Packaging	-	-	Sample Bay Packaging	-
Jettison Contaminated s/c Parts (at Mars or near Earth)	Separation System	-	-	Separation System	-
<b>Return to Earth Surface</b>					
Survive Thermal Environment	-	-	-	-	Heat Shield
Survive Hard Landing	-	-	-	-	Robust Structure
Contain Sample	-	-	-	-	Sample Bay
Retain Sample Integrity	-	-	-	-	Sample Bay Packaging
<b>Essential Supporting Activities</b>					
Communication to Earth	Comm.	Comm.	Comm.	Comm.	Comm.
Inter-vehicle Communication	Comm. to Surface	Comm. to surface, comm. to rover	Comm. to lander, comm. to orbiter	Comm. to orbiter	Comm. to orbiter
MAV platform	-	Chassis	Chassis	-	-

## 6.3 Architecture Generation and Evaluation Metrics

### 6.3.1 Architecture Generation

Once the functional decomposition has been performed and the key trades of interest have been identified, the full trade space of sample return options can be generated. As explained in Chapter 2, there are several steps involved in this process. First, the viable combinations of vehicles can be identified from Table 40. Only combinations that fully address all the required functions are valid combinations. Next, the different form and function options (identified in green in Table 40) must be enumerated, leading to the trade tree shown in Figure 62.

This figure also shows constraints between different technology choices: only combinations that are connected by arrows are valid architectures. Two constraints are worth noting. First, only the single-string MAV is able to reach very high altitudes. In this study, three destination orbits were considered: a 500km (baseline) orbit, a highly elliptical 2-day orbit and sending the MAV to escape. In the 500km case, a 3-axis stabilized 2-stage MAV is assumed, where the dual-string MAV has a dual-string attitude control system and command and data handling system, both running during operations. The MAV going to the higher orbits has a different design (in order for there to be a viable design that does not violate the maximum landed mass constraint). It consists of a two-stage MAV where one stage is spin-stabilized. The second constraint is for the return to the Moon option: only SEP orbiters were able to achieve this return orbit without more than doubling their propellant requirement.

Finally, the enumeration process can be repeated for different launch years. In this analysis, the launch years considered were 2022, 2024, 2026 and 2028. When the analysis is performed, the sequence (orbiter first or lander first) is defined and a launch year is chosen by the user for the first vehicle being launched. The subsequent launch date is chosen automatically by the model such that the arrival of the second vehicle at Mars is at the earliest possible time after the arrival of the first vehicle. At the end of this process, a set of valid architectures, where each architecture consists of compatible vehicles, is generated.

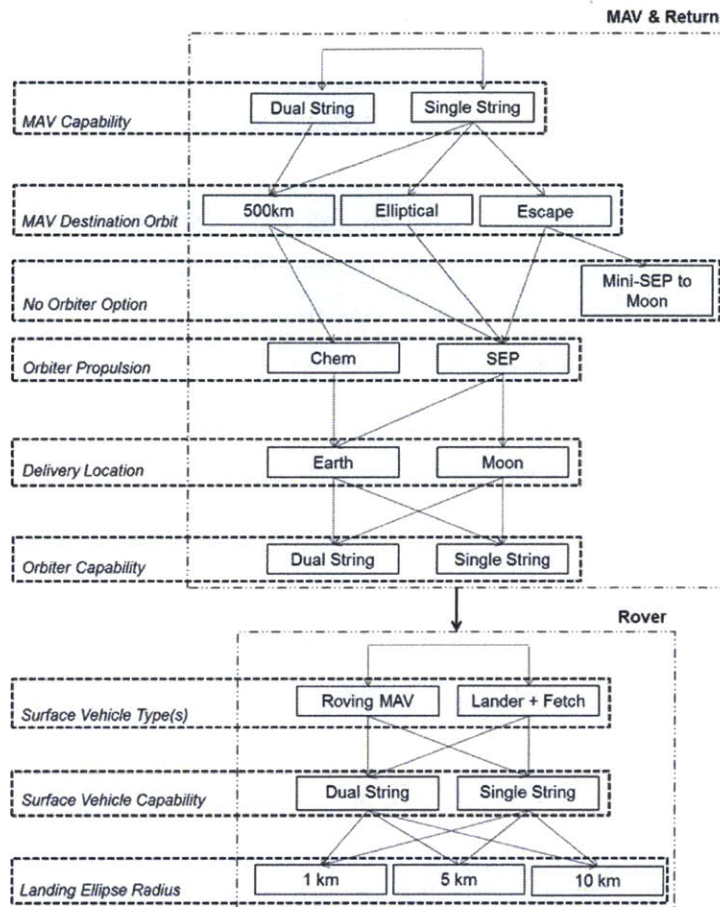


**Figure 62: Basic trade tree of technology options explored**

### 6.3.2 Evaluation Metrics

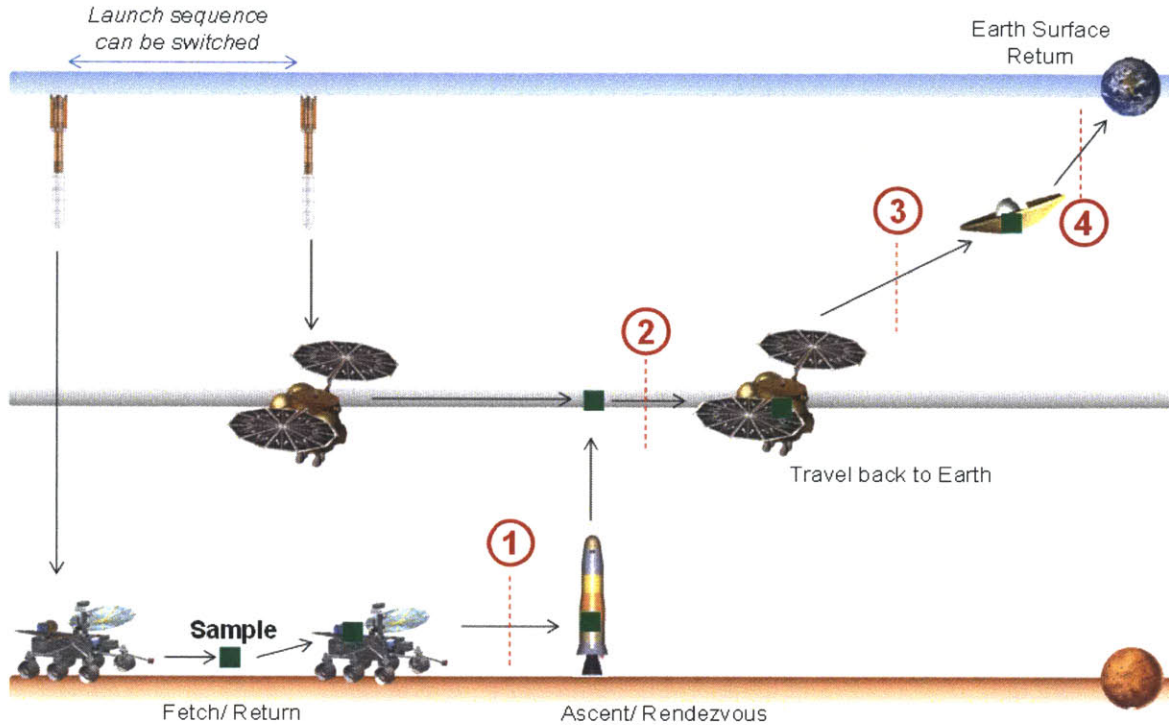
Now that the architectures have been enumerated, the metrics developed in Chapter 2 can be used to evaluate each multi-vehicle architecture and compare them to each other and the baseline. These metrics enable the comparison of the relative engineering value of each architecture against its relative cost, which in turn demonstrates the relative return on investment for each trade explored. Four of the metrics described in Chapter 2 are used in this case study: probability of mission success (derived from the productivity metric), mass, complexity and cost. The remainder of this section provides a reminder of the metrics, an overview of the models used within the metrics and specific details on exactly how they are used.

### 6.3.2.1 Mission Success

Chapter 2 discussed how the productivity metric, which is a Markov model for the system, can be used to evaluate the state of the system over time. In this particular case study, the specific metric of interest is the ability of the mission to complete a set goal: returning a sample from the surface of Mars to the Earth-Moon system. Additionally, there is no redundancy in the system and it is assumed that the system cannot operate in a degraded state. The system was assumed to only fail due to lifetime degradation or by its inability to achieve key tasks involved in the ascent and return portion of a sample return mission. This dramatically decreases the complexity of the Markov state-transition matrix because there are now only two possible states: the system is either operational or not. Furthermore, the desire is only to know the probability of the system being in its initial (i.e. functioning) state at the end of the mission: this is the mission success metric. Because only the end-state matters, the lifetime degradation can be de-coupled from the ability of the system to perform given tasks or complete events during the mission. This metric is therefore directly derived from the Markov model described in Chapter 2, which has been simplified due to the assumptions made in this case study.

The first step in evaluating the probability of mission success for this study involves understanding the events that must occur in order for the mission to succeed. These can be directly derived from the functional decomposition of the system. They can then be arranged into a timeline, describing the mission at a high-level. In a mission, some events are independent of each other, and others are dependent and form a chain of events. This sequence is portrayed in Figure 63 based on the functional decomposition performed in Table 40, and only one of the possible orderings is shown in Figure 63. Four key events were identified in the sample return process. These are the events that describe the overarching goal of a particular vehicle in an architecture and mark the end of the life of that vehicle. Each vehicle must survive until the end of its key event. For example, the key event for the fetch rover is “transferring the sample cache into the MAV.” Thus, the number of *temporally distributed* vehicles in the system is equal to the number of key events. The key events are also shown in Figure 63 and also represent “safe states” for the sample.





Event #	Description of Key Events
1	Transfer sample into MAV
2	Transfer sample into orbiter
3	Release EEV <i>or</i> Enter lunar orbit
4	Land sample on Earth

**Figure 63: Event sequence for returning a sample back to Earth (not to scale)**

Under the given assumptions, the ability of the system to successfully complete these key events depends on two factors: (1) every function leading to this event (called “coin toss” events, such as launch, orbit insertion, landing, etc.) must occur successfully, and (2) the vehicles necessary for the key function to occur must still be operational until all its functions have been performed.

In the case of independent “coin toss” events, their probability of success can be multiplied directly with each other. For dependent events, the conditional probability for events must be used, as defined by Bayes’ Law:

$$P(A|B) = \frac{P(B|A) * P(A)}{P(B)}$$

**Equation 33**

$$P(A \cap B) = P(A|B) * P(B)$$

**Equation 34**

The conditional probability of an event (i.e. the probability of an event being successful given that all other events in the chain were successful) is in fact often easier to measure than its absolute probability. The probability of “coin toss” events being successful is based on historical data from similar systems or their closest analogies. For example, the probability of an Atlas V launch being successful is 0.95. However, for Mars Orbit Insertion (MOI), we know from historical data that given that we have successfully launched and arrived in the Mars vicinity (let’s call this event L), then the probability of success of MOI (let’s call this event M) given that the launch and travel were successful is  $P(M|L)$  and is 0.83 (since 1975, NASA and ESA have launched 8 orbiters, 7 of them successfully travelled it to Mars vicinity but 1 of them failed during MOI, so  $P(M|L)$  is  $6/7 = 0.83$  and  $P(L) = 7/8$ ). For dependent events, it is important that this conditional value be used, and not  $P(M) = 6/8$ , which is the probability of a successful MOI given that the vehicle has been built. As another example, the probability of a rover successfully retrieving a sample given that it has landed on a planetary surface and is functional can be tested in the lab to be 0.99.

The conditional probability of success of the most important events is shown in Table 41. In the case where no such data exists, an optimistic conditional probability of success of 0.99 is assumed. Additionally, it is assumed that single string systems have a probability of failure (one minus the probability of success) twice as high as dual string systems. Finally, the “Earth Re-entry” event was assumed to have a conditional probability of success of 1. This is because the planetary protection requirement for a MSR imposes that the mission must have 99%  $6\sigma$  reliability in its ability to contain the sample and not contaminate the Earth. [188] It can quickly be seen that even though the probability of success of each event can be very high, since the total probability is a product of individual probabilities, the ability of an architecture to complete a mission degrades severely as the number of key events increases.

**Table 41: Conditional probability of success of the most important events**

Event		Probability of Success
Launch		0.95
MOI	Chemical	0.86
	SEP	0.96
Landing		0.86
MAV Launch		0.90
Lunar Capture (SEP)		0.96
Earth Re-entry		1

The probability of each event in a chain being successful is conditional on the vehicle being functional at each event. The probability of each of the platforms being functional until they are last needed is modeled by an exponential decay in performed where the 25% percentile lifetime is based on

the historical lifetime of similar systems. This probability is described by Equation 35 and Equation 36. The lifetimes used are again based on historical data, and are shown in Table 42. For example, the average lifetime of a rover is eight years (based on the Spirit and Opportunity rovers [148]).

$$P(t) = e^{-\lambda t}$$

Equation 35

$$\lambda = -\ln(0.25)/\tau_{25\%}$$

Equation 36

**Table 42: Historical lifetime of platforms**

Type of Vehicle	25 <sup>th</sup> percentile lifetime ( $\tau_{25\%}$ , yrs.)
Orbiter	20
Rover	8
Lander	8
MAV	5

Bayes' Law can be used to show that the probability of a vehicle being functional at each of the events in a chain is equivalent to the vehicle being functional at its last event:

$$\text{Prob. functional at event } A = \tau_1$$

$$\text{Prob. functional at event } B \text{ given functional at event } A = P(\tau_2|\tau_1)$$

$$P(\tau_2|\tau_1) = \frac{P(\tau_1|\tau_2) * P(\tau_2)}{P(\tau_1)} = \frac{1 * P(\tau_2)}{P(\tau_1)}$$

$$P(\tau_2 \cap \tau_1) = P(\tau_2|\tau_1) * P(\tau_1) = \frac{1 * P(\tau_2)}{P(\tau_1)} * P(\tau_1) = P(\tau_2)$$

Equation 37

The mission success metric can therefore be simplified down to Equation 38.

$$\text{Mission Success} = \prod_{\text{all event chains}} \text{Prob. Event Chain Success} * \text{Prob. Platforms Functional}$$

Equation 38

A 2-event chain can be used as an example to illustrate this.

- Pick up the sample, given that rover is functional, has P(K)
- Transfer the sample, given that rover is functional, has P(T)

From laboratory experiments, it may be known that the rover is able to pick up a sample 99% of the time, given that it is fully functional. It could also be tested that, *given that it has a sample on board* (i.e. that K has occurred successfully), the rover can transfer the sample 99% of the time. Therefore:  $P(T|K) = 0.99$ , and  $P(T \cap K) = P(T|K) * P(K) = 0.9801$ ; but P(T) is *not* 0.999. This means that, given that the dependent values of probability are used, then the probability of the mission being successful can be

calculated using direct multiplication. Furthermore, if an early event in the chain is unsuccessful, then no other event in the chain can be successful. For example, if the pick-up event (K) (or any event earlier in the sequence) is not successful, then  $P(T) = 0$ . This simplification is an artifact of this metric being designed to be used for an engineering mission with a single “binary” goal (either the mission is successful or it is not, there is no partial achievement) and no redundancy; for science missions or missions with redundant vehicles, partial success is been allowed and the full set of Markov chains must be used, as described in Chapter 2. Looking at the probability tree (where  $P(nK)$  is the probability of the pick-up not being successful, etc.) illustrates this concept:

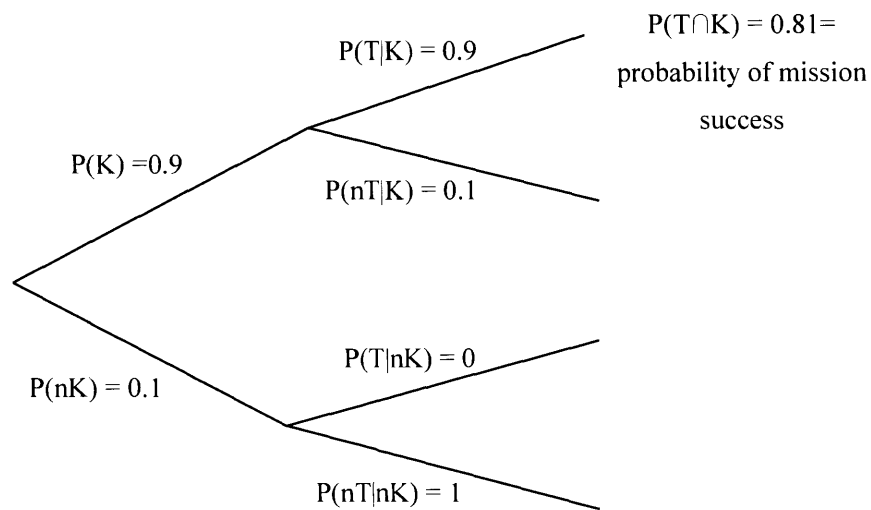


**Figure 64: Example probability tree**

### 6.3.2.2 Mass

One of the main differentiators among the architectures is their mass. The latter is driven by several factors, including the chosen technology option, the type of propulsion system, the trajectory, the level of redundancy and the launch year. In turn, the mass of the system and the excess velocity at launch ( $C_3$ ) drives the number of launches for the system, the travel time and the overall cost. Moreover, there are clear dependencies between the masses of the different vehicles in an architecture. For example, the mass of a lander is driven by its payload, which includes a fetch rover and a MAV. Similarly, the amount of fuel required by an orbiter for changes in orbital altitude is dependent on the target launch altitude of the MAV. An overview of these dependencies is given in Figure 65. This figure also shows that the MAV and fetch rover drive the design of the lander or of the roving MAV, which then drives the orbiter design.

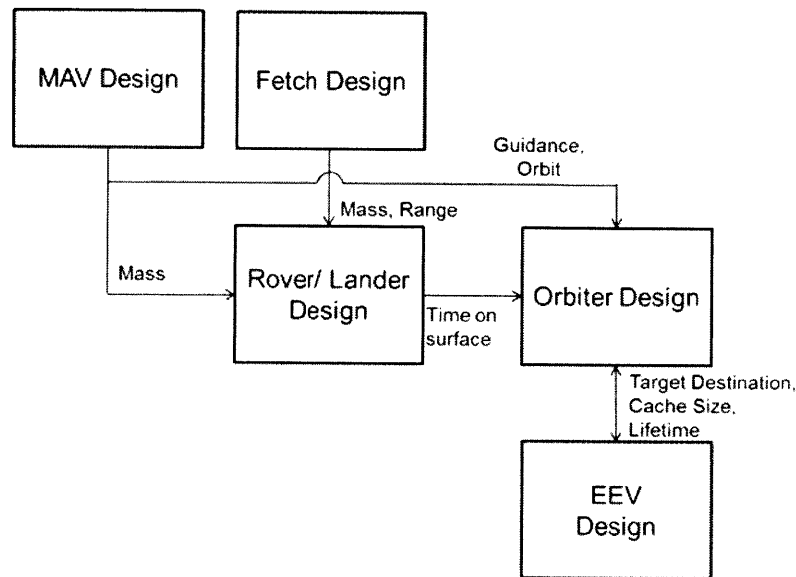


**Figure 65: Overview of interdependencies between vehicles**

The masses of these different vehicles were estimated using a combination of physical and parametric models previously developed for other MSR studies, as well as the rover mass model described in Chapter 3 and in Appendix A. A highlight of the input to these models is provided in Table 43. Furthermore, the assumed  $\Delta V$  requirements for the modeling of orbiters with chemical propulsion are shown in Table 44. Figure 66 provides an example of a low thrust trajectory used for sizing orbiters with SEP. The full set of trajectories used to size SEP orbiters is provided in Appendix B. The estimates obtained from these models were compared to, and found to fall within 15% of, estimates from historical data and previous studies, and thus provide a good basis for comparison.

**Table 43: Overview of mass models**

Type of Vehicle	Model Highlights & Input
MAV	Physical model based on $\Delta v$ requirements; <i>Input</i> : n° of stages, level of redundancy, target altitudes, Mass Equipment Lists (MELs)
Fetch Rover	Physical model based on system type and technology choices; <i>Input</i> : payload, n° of wheels, material type, range, speed.
Lander/ Roving MAV	Parametric model based on payload and trajectory (for EDL); <i>Input</i> : launch year, payload mass, technology choices (a max. EDL mass of 1200kg was assumed)
Chem. Orbiter	Parametric model based on payload & trajectory; <i>Input</i> : launch year, $\Delta v$ requirements, type of MOI, payload mass, technology choices
SEP Orbiter	Set of trajectories and designs obtained for each case, any other orbiter is sized by keeping thrust constant (i.e. keeping the dry mass, power and propellant ratios constant)

**Table 44:  $\Delta V$  requirements for return orbiters with chemical propulsion; starred values indicate that the requirement is trajectory dependent**

Mission Phase	$\Delta V$ (m/s)
Cruise	40
MOI	950*
Aerobraking	140
Rendezvous/ Mission	350
TEI	2200*
Return Cruise	80
<b>Total <math>\Delta V</math></b>	<b>3760</b>

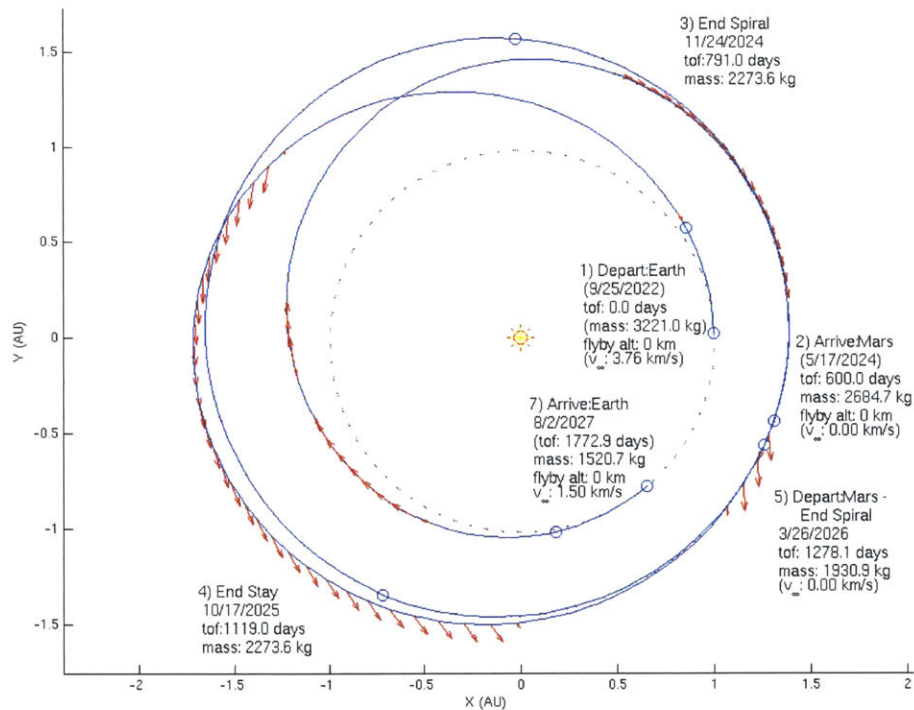


**Figure 66: Example of a SEP trajectory with a 2022 departure and an 11-month stay at Mars (courtesy of Damon Landau)**

### 6.3.2.3 Complexity and Cost

The development and manufacturing costs of each of the architectures has traditionally been estimated from correlations with the mass estimate for each of its vehicles. However, such mass-based cost estimates have often proven to be inaccurate since, in particular, they do not account for the cost of technology development. Chapter 2 therefore put forward a vehicle-level complexity metric to provide a better estimate of the development cost of a new system.

As was discussed in Chapter 5, the main challenge of the complexity metric is to find an appropriate set of weightings to demonstrate the correlation between technology choices and cost. The literature offers a limited number of complexity metrics to illustrate the non-mass driven costs that occur during

development. In particular, Bearden [4] proposed that a range of properties that have historically been shown to drive cost can be used to calculate a complexity index. More recently, a set of cost-risk subfactors was identified from past studies and missions at JPL. [12, 13] These are typically used to assign additional margins in early cost estimates, but were also shown to help provide more accurate cost correlations when used as mass weightings. The weightings used in this case study are taken directly from [138], as it offers the most comprehensive historical overview of the correlation between technology choices and cost.

The complexity metric is defined again in Equation 39, showing only the components of the metric that are relevant to this case study.

$$Complexity = \frac{\sum_j^n F_j * Mass_j \sum_i^m CW_{i,j}}{Baseline Complexity}$$

**Equation 39**

In this equation, *F* is the relative average cost per unit mass of a given platform *j*, and *CW* is the complexity weighting of a given technology choice *i*, derived from the list of cost-risk subfactors in [138]. The most important weightings are provided in Table 45. Additionally, *m* is the number of technology options, and *n* is the number of platforms.

**Table 45: Complexity weightings (CW) applicable to all technologies**

Property		Weighting
Technology TRL	> 6	0
	6	+ 0.05
	5	+ 0.1
	4	+ 0.2
	≤ 3	+ 0.4
Similar concept at Earth?	Y	0
	N	+ 0.05
Additional power/data over baseline?	Y	+ 0.05 per
	N	0
Mechanism?	Y	+ 0.05 per
	N	0

By calculating the complexity of architectures from MSR studies performed for the Decadal Survey [6] and previous studies related to MSR performed by JPL’s early mission concept design team (Team-X), which have known cost estimates (estimated using more involved proprietary cost models), the correlation between complexity and development costs can be found, as shown in Figure 67. This correlation is found to have an *R*<sup>2</sup> of 0.95, which is a significant improvement on the correlation between development cost and system mass (*R*<sup>2</sup> = 0.79).

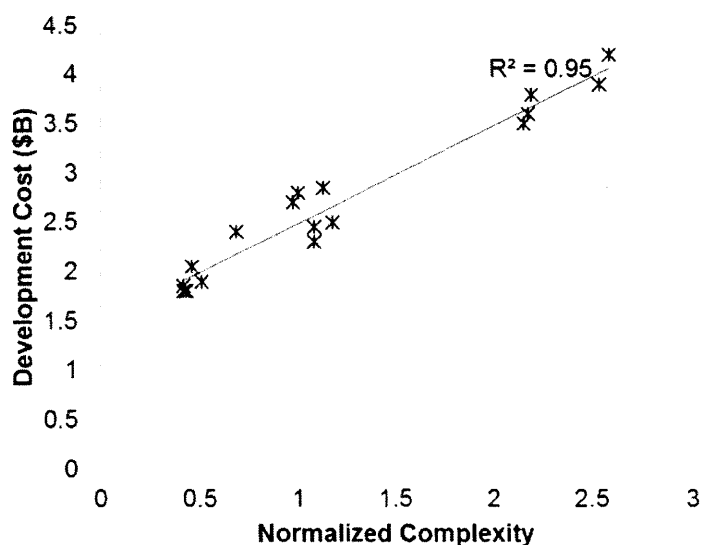


**Figure 67: Correlation between cost and complexity**

The total cost of the system is given in Equation 40.

$$Total\ Cost = Development\ Cost + Launch\ Vehicle\ Costs + Operations\ Cost$$

**Equation 40**

For each architecture, the minimum number and size of launch vehicles needed is used to estimate the launch vehicle costs, and the operations cost is estimated to be FY2015 USD \$60M/year. The baseline architecture, described earlier, is estimated to have a total cost of \$3.8B, which is in line with current JPL estimates.

## 6.4 Trade Space Exploration

Once the trade space has been enumerated and each multi-vehicle architecture has been evaluated, the architectures can be compared against each other. In this section, each of the eight trades introduced at the start of this chapter in Table 39 are evaluated in turn, using the framework developed in this thesis.

The first step of the trade space evaluation process involved investigating architectures that are similar to the baseline. Each point in Figure 68 represents a full architecture, consisting of a lander, a fetch rover, a MAV, a return orbiter with chemical propulsion, and an EEV. The large red star in Figure 68 represents the baseline architecture described in 6.2.3. The metrics for all other architectures are normalized by the metrics of baseline. As a reminder, the baseline consists of a lander, a dual-string fetch rover, a dual-string MAV and a return orbiter with chemical propulsion. The baseline is assumed to have an orbiter launch in 2024 and a lander launch in 2026. These launch dates are kept constant for the



normalization process, even if different launch dates are being considered for a particular evaluation step, in order to enable the effects of changing dynamics between different launch opportunities to be shown. The  $C_3$  and  $\Delta v$  requirements for both chemical and solar electric propulsion change between each launch window due to the eccentricity of the orbit of Mars. These changes affect the launch vehicle requirement and the trade between using the different types of propulsion and therefore must be account for in the model.

Figure 68 shows that in a family of similar platform combinations, the chosen baseline architecture is very well optimized and provides the best marginal return on investment. Exploring the differences between the architectures presented in Figure 68 answers the first two trades described in Table 39.

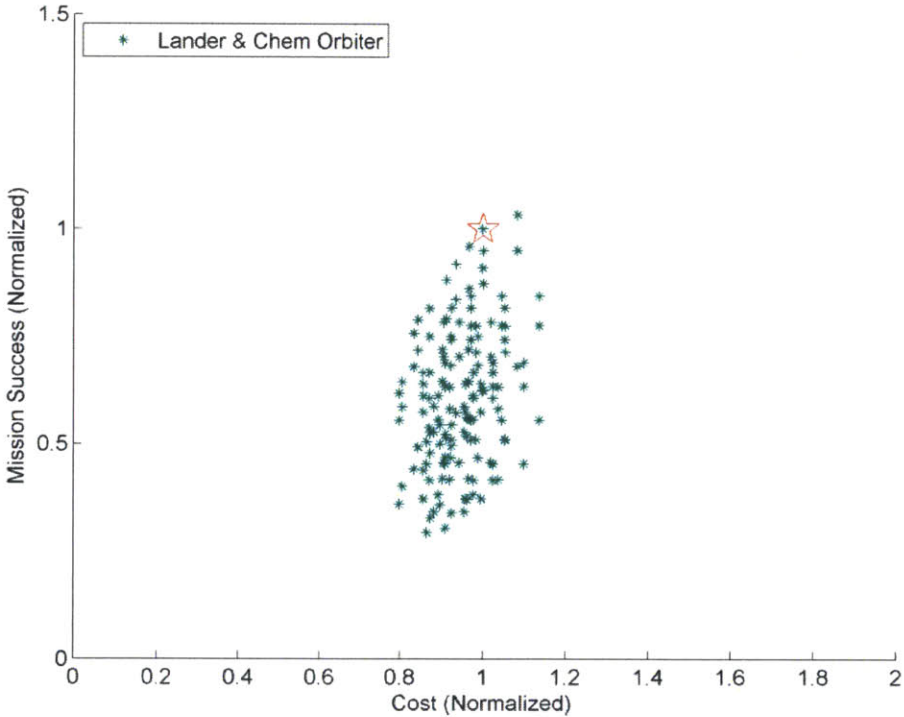


**Figure 68: Architectures with a lander, fetch rover, a MAV and chemical orbiter; assumes an orbiter launch in 2024 and a lander launch in 2026**

### 6.4.1 Trade #1: Rover Range

The first trade presented in Table 39 investigates the effects of different landing ellipses. Three different types of ellipse radii were investigated: a 10km radius (similar to that of the Mars Science Laboratory (MSL)), a 5km radius (the baseline) and a 1km radius (precision landing). Decreasing the landing radius leads to a shorter rover traverse on the surface of Mars, and thus reduces the mission duration and the rover's likelihood of failing. However, decreasing the ellipse size also involves higher guidance cost and increased propellant usage.

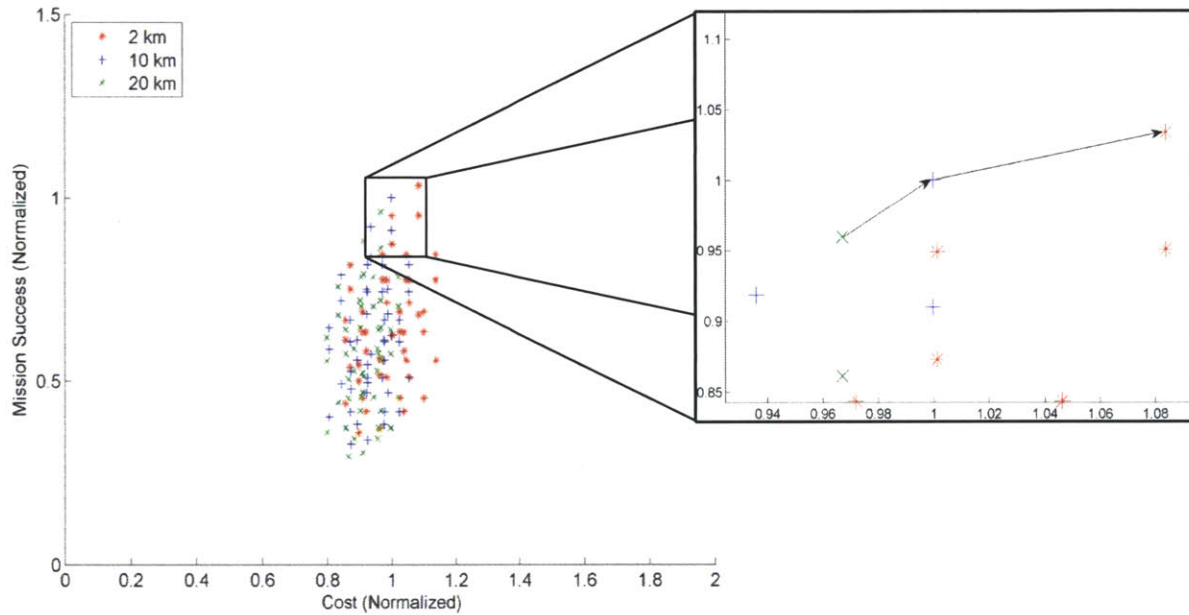


**Figure 69: Effect of changing landing ellipses**

Figure 69 shows that the 5km ellipse size (10km return traverse range) provides the best return on investment. It provides significant increase in mission success, for a small cost investment. Comparatively, the precision landing option (1km ellipse, 2km traverse option) offers little improvement in the mission success metric for a large monetary investment, due to the increased propellant cost and the significant technology investment.

## 6.4.2 Trade #2: MAV Capability

The second trade identified in Table 39 is that of the MAV capability. A dual-string MAV offers high reliability, but its heavy mass also significantly drives the mass and cost of the landed system. Figure 70 demonstrates this trade. It can be seen that low capability, single-string MAVs offer cost savings benefits, but that this comes at the cost of reduced reliability of the overall system. Options with single-string MAVs are unable to provide a better return on investment than the baseline.

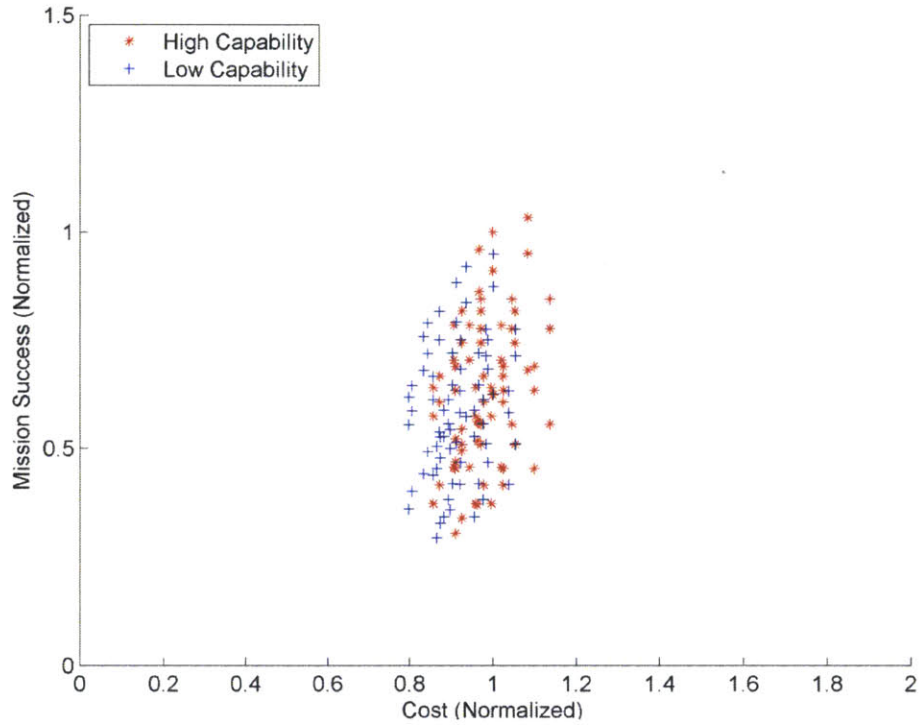
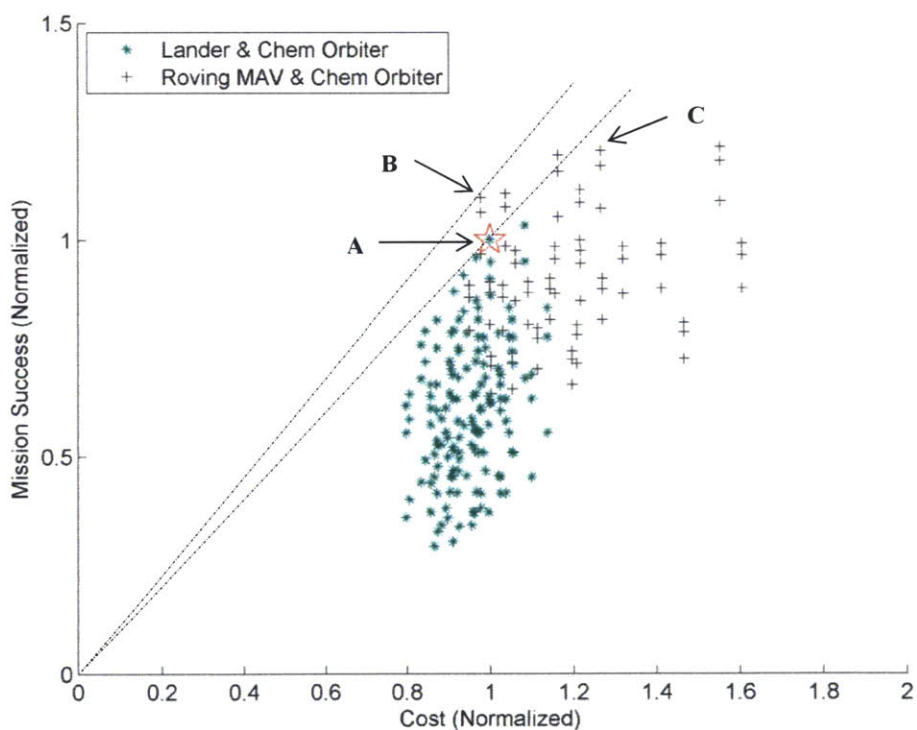


Figure 70: Single- vs. dual-string MAV

### 6.4.3 Trade #3: MAV Mobility

An alternative to using a lander with a stationary MAV and a fetch rover is to have a large rover that can carry the MAV directly to the sample. This reduces the traverse time in half because a return journey from the sample back to the landing site is no longer required. Furthermore, the roving MAV option has reduced system-level complexity because it only involves three vehicles (the rover, the MAV and the orbiter) interacting together as spatially distributed system instead of four (the lander, the fetch rover, the MAV and the orbiter), which in turn also reduces the number of key events in the operational timeline. However, depending on their design, MAVs have masses anywhere between 150 and 400kg (note that the MSL payload mass was 100 kg). Therefore, a roving vehicle larger than any that has ever been flown before would be required to achieve this task. This has a significant impact on the cost of the system for several reasons. Having a larger rover means that a larger heat shield is required. This in turn exponentially increases the propellant needed to land the system. Furthermore, building a rover and heat shield that are bigger than that of MSL increases the complexity of the system, which again affects cost.



Arch	Description
A	Baseline
B	Roving MAV with single-string MAV, rest as baseline
C	Roving MAV with dual-string MAV, rest as baseline

**Figure 71: Comparison of the lander & fetch option to the roving MAV; a gradient between the origin and an architecture point indicates a higher return on investment.**

Figure 71 shows the trade space with the roving MAV options added in. The development and mass impacts on cost can clearly be seen from the increased cost of these options. However, the return on investment for the roving MAV (shown by the gradient of the dotted lines; the greater the gradient (i.e. the higher the slope line), the better the return on investment) is either equal to or greater than that of the lander and fetch options, for similar architectures, while providing a higher probability of mission success. Consequently, the roving MAV option is found to present significant advantages as compared to the lander and fetch option and is a worthwhile technology investment to investigate further.

#### 6.4.4 Trade #4: Direct Return

The framework developed allows for the evaluation of low-cost, exotic solutions for MSR to be included in the trade space and compared directly against more traditional solutions. To demonstrate this, a low cost direct return option concept by Strange et al. [189] was added to the set of architectures, an overview of which is presented in Figure 72. This system consists of a single-string MAV containing a small CubeSat-class return vehicle. This vehicle, equipped with a 50W solar array and 64 micro-electric propulsion (MEP) thrusters, would be able to contain the sample and return it to a retrograde lunar orbit. This would remove the need for a return orbiter but would involve significant risk because both the MAV and the return vehicle would be single string. Moreover, the MEP technology is still at a very low technology readiness level and may not be developed enough by the time of launch to offer long lifetime reliability.

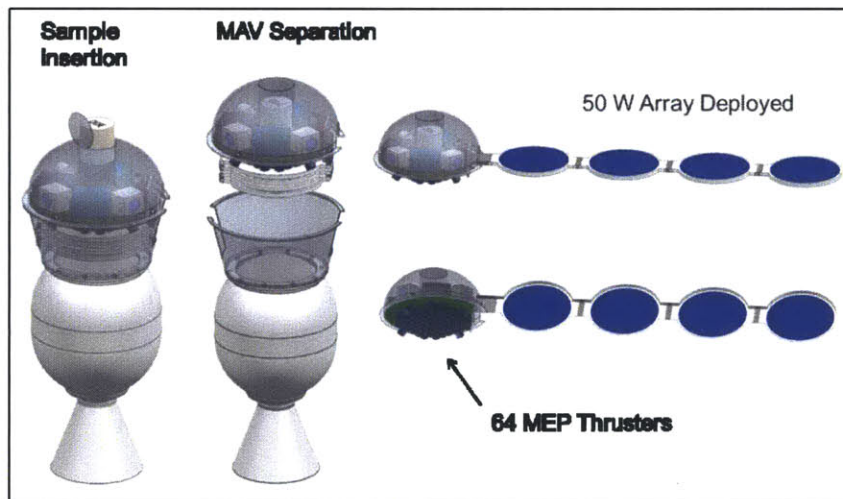
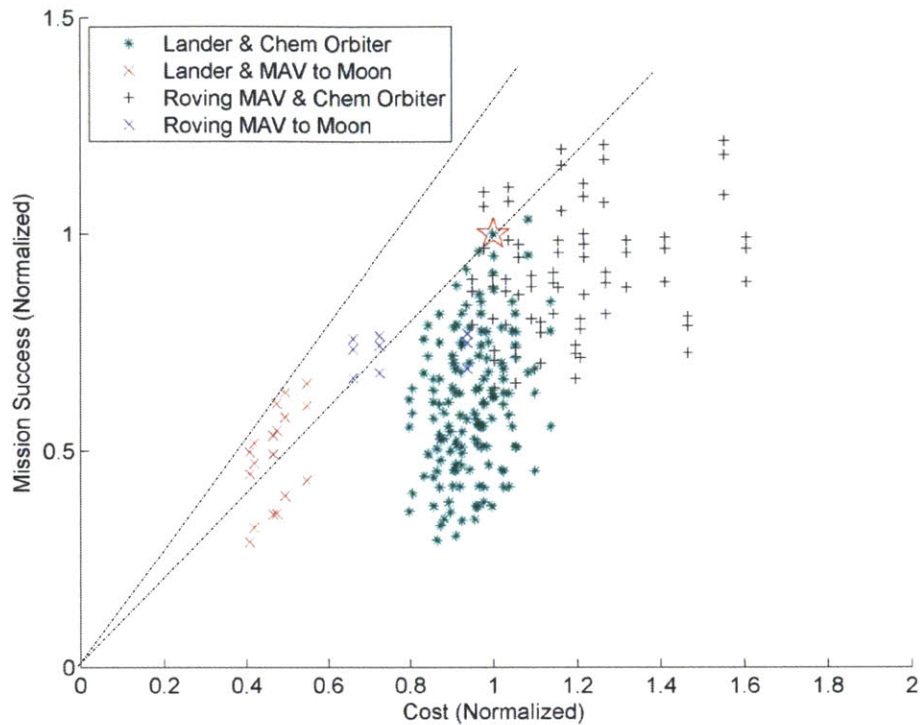


Figure 72: Configuration of the low-cost, direct return option [189]

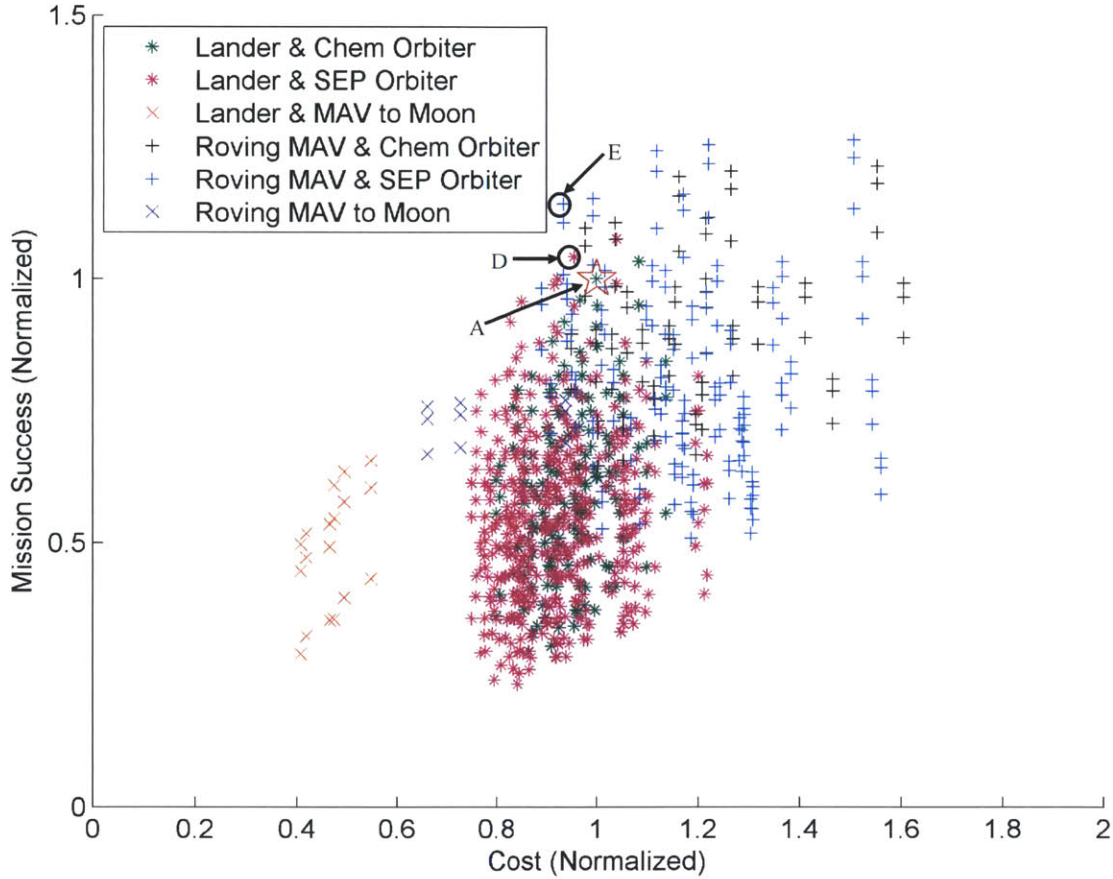


**Figure 73: Trade space with low cost direct return options**

Figure 73 illustrates the trade space with the direct return options, which is the fourth trade evaluated in this paper, included. It can be seen that although this low cost option would cause approximately a 25% reduction in the probability of mission success while reducing the cost of the program by a little over 50% as compared to the baseline. The gradient of the lines in Figure 73 show that these low cost options offer a much better return on investment than the chosen baseline. Their reliability could also be increased by making an additional investment to demonstrate the long-term viability and lifetime of electrospray propulsion. It is to be noted, however, that these architectures would bring back a dirty sample that is not sealed in the Earth-Moon system. This causes two problems: (1) it may violate the planetary protection requirements for such a mission; and (2) the sample would still have to be recovered from the lunar orbit and brought back to Earth.

### 6.4.5 Trade #5: Orbiter Propulsion

Thus far, aside from the low cost direct return options, only architectures with return orbiters using chemical propulsions have been considered. The next trade investigated in this chapter evaluates how SEP could be used for the return orbiters. The trajectories investigated were constrained to have a maximum Earth return  $V_\infty$  of 4.5 km/s to ensure similar re-entry conditions to those with the chemical orbiter, without over constraining the SEP trajectory.



Arch	Description
A	Baseline
D	SEP return orbiter, rest as baseline
E	Roving MAV & SEP return orbiter, rest as baseline

**Figure 74: Full trade space for 2024 orbiter launch**

Figure 74 presents the ascent and return trade space with the SEP orbiter options included. Even though chemical orbiters have shorter trajectory durations (and thus a reduced mission timeline), it can be seen that SEP options strongly dominate over all the chemical orbiter options. This is because SEP orbiters not only enjoy significant benefits in terms of reduced system mass, but they also have virtually

no MOI risk (the trajectories investigated arrive at Mars with a  $V_{\infty}$  of zero and then spiral down to the desired orbits; orbit insertion is no longer a critical event). This trend holds true for all launch years considered. Figure 75 and Figure 76 show a similar pattern in the full trade spaces for the 2022 and 2026 orbiter launch windows respectively. SEP orbiters also enjoy a range of intangible benefits. First, SEP enables missions to have much more flexible launch windows without significantly affecting the performance of the mission. Furthermore, for long (1-2 years) travel times, SEP missions have a lower change in propellant requirements than chemical propulsion missions as the launch date changes, thus rendering SEP missions more flexible and robust to delays. Finally, although there are concerns with the high propellant throughput required to enable a SEP mission to Mars, which are currently negatively impacting SEP options with a low TRL, such systems have been shown to be essential to enable a manned mission to Mars. [190] Therefore, flying a SEP system would also serve as a technology demonstration for a manned mission, which is part of the goals of the Mars Exploration Program. [178]

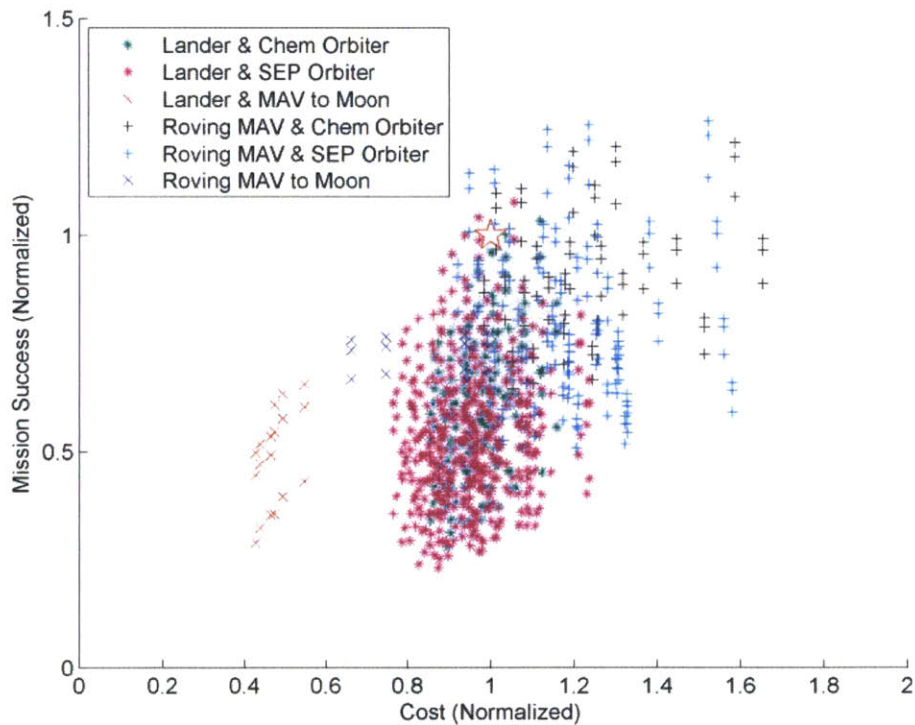


**Figure 75: Full trade space for a 2022 orbiter launch**



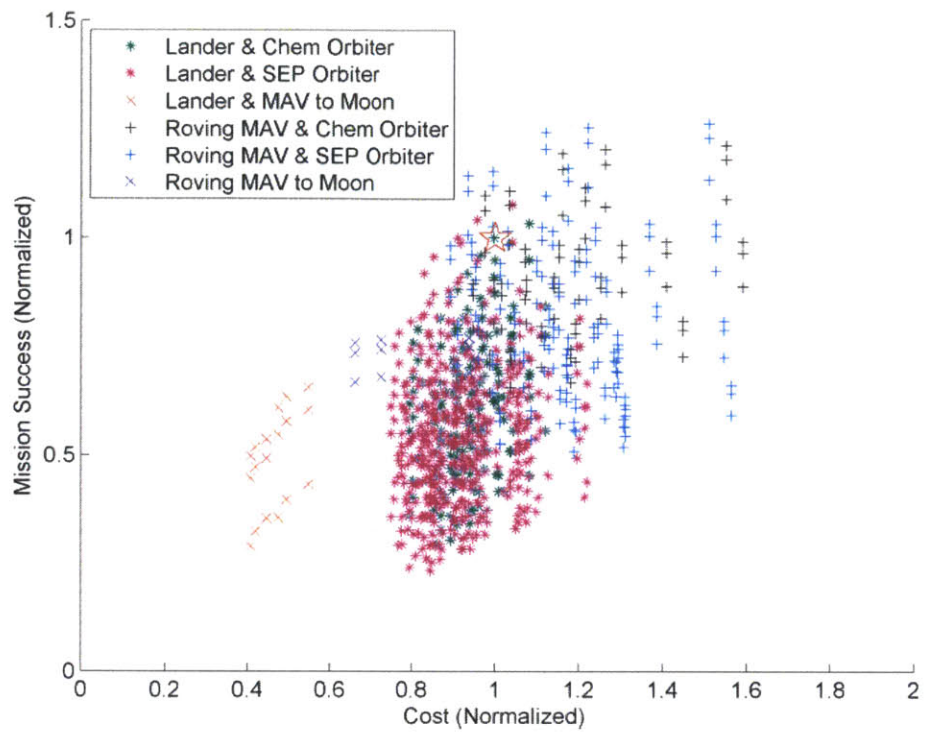


**Figure 76: Full trade space for a 2026 orbiter launch**

### 6.4.6 Trade #6: MAV Target Orbit

Once SEP orbiters are added into the trade space, the target orbit of the MAV becomes an important trade. A significant amount of a SEP orbiter's  $\Delta V$  budget (35% on average) is spent during the spiral down the gravity well at Mars, and back out. That expenditure can be reduced if the MAV is launched to a higher orbiter. However, this means that the MAV has to be heavier, and must carry more fuel, which in turn increases the mass of the landing system and heat shield. Three different MAV destinations were considered: a 500km orbit, a 2-day elliptical orbit and a launch to escape. It is to be noted that the 500km MAV trade space contains both dual and single string systems, whereas the other two destinations are only reached by single-string MAVs (due to landed mass constraints). Furthermore, the MAVs to 500km are two-stage MAV with a solid and a liquid stage, whereas the MAVs to the 2-day ellipse and to escape are two-stage MAVs where one stage is a spin stage. Those two designs must therefore also include a spin table. In addition, the MAV to escape includes a small radio beacon and propellant for an extra 1 km/s of  $\Delta V$  on the orbiter for rendezvous manoeuvres.

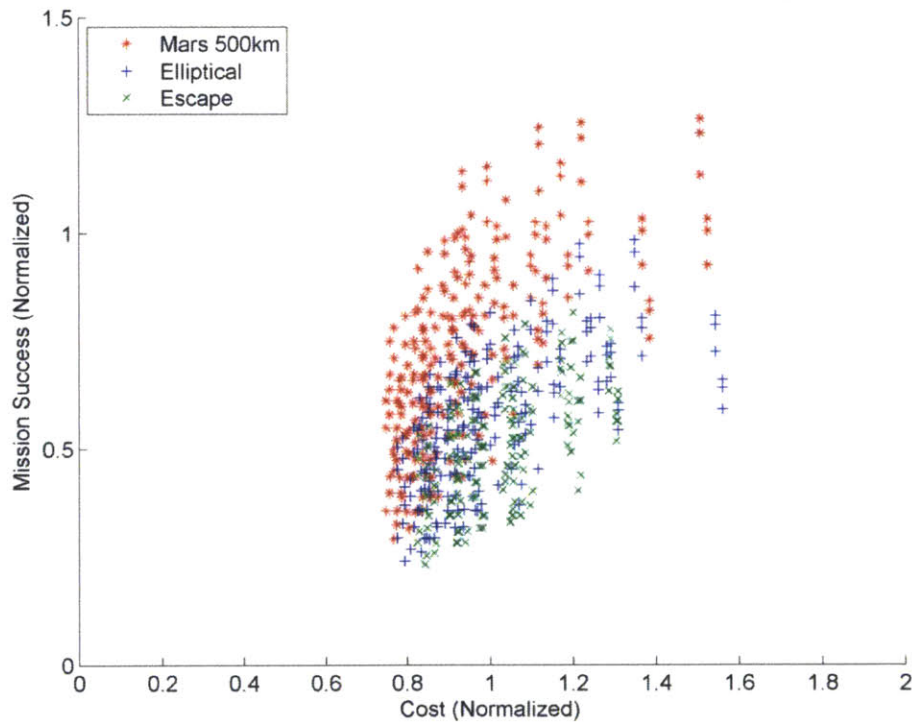


Figure 77: Trade space of different MAV orbit destinations

Figure 77 illustrates that the 500km orbit destination is the most advantageous. In this trade, the reduction of propellant mass on the SEP orbiter was not found to outweigh the increase in mass of the MAV. This is because the mass of the MAV very strongly drives the mass of the rest of the landed system and, in turn, its cost. Furthermore, it can be seen that there is no large difference between sending the

MAV to a high elliptical orbit or to escape. This trade could be made more complete by increasing the number of different target altitudes and MAV designs, in order to find the MAV that offers the highest return on investment.

### 6.4.7 Trade #7: Sequencing

The architectures considered so far all assumed that the orbiter would be launched before the lander. However, the launch sequence for these missions is also part of the trade space. Figure 78 shows the full trade space for a 2024 orbiter launch and a 2026 lander launch, and Figure 79 is the trade space for a 2024 lander launch and a 2026 orbiter launch. It is important to note that the model has an assumption that there will be at least one working relay orbiter at Mars at all times in the 2020s. If this assumption is taken away, the landed assets in the lander first option must have a direct to Earth (DTE) communication system, which is found to increase the cost of the overall architecture by an average of 2%.

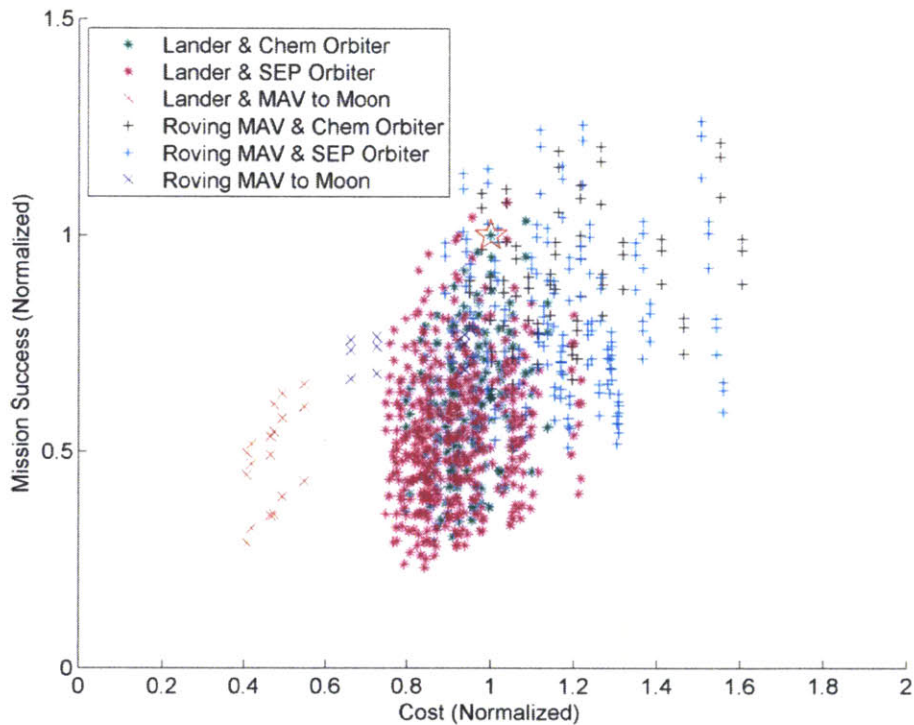
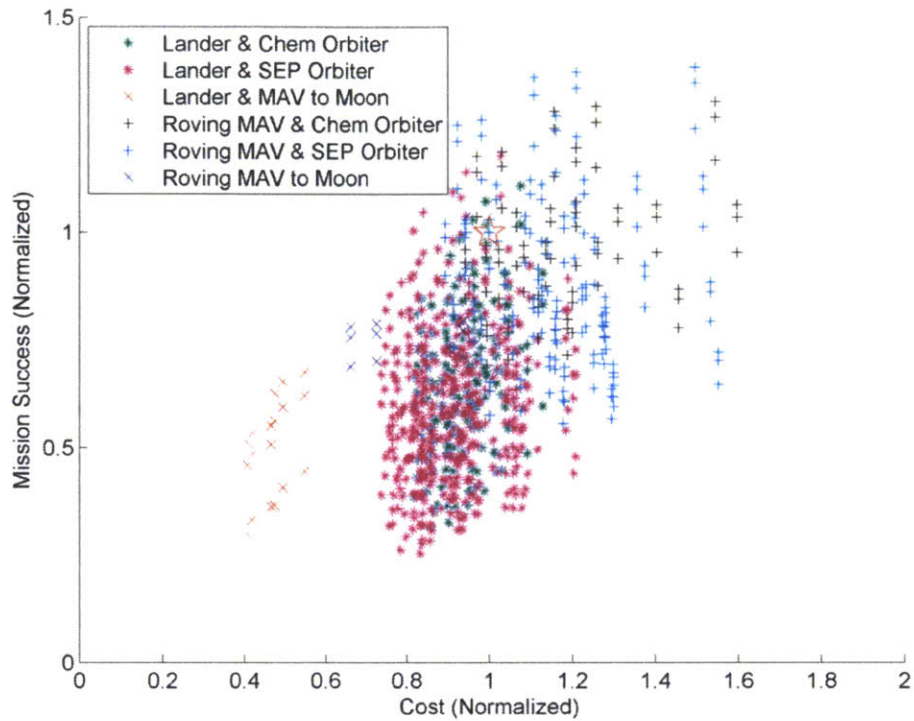


Figure 78: Full trade space, 2024 launch, orbiter first option



**Figure 79: Full trade space, 2024 launch, lander first option**

It can be seen from Figure 78 and Figure 79 that the lander first architectures provide a 5 to 8% increase in mission success probability for a given cost. This is because the landed mission can be completed without having the return orbiter present around Mars. Hence, the time taken to perform the landed mission is the same in both cases, but the orbiter mission is 2 to 3 years longer in the orbiter first case, thus reducing the probability that the system will be alive at the end of the mission. A lander first mission is also more robust to failure: not only is a significant amount of risk retired once the Orbiting Sample (OS) has reached orbit, but if failure that does not destroy the OS occurs during the landed mission, that part of the mission can be re-flown without the orbiter suffering any lifetime degradations. Consequently, if only the MSR goals are taken into account, the lander first option is the most advantageous. However, if the sample return orbiter is used to provide an additional communication relay or to perform scientific investigations while in orbit around Mars, then the orbiter first option may be more beneficial for the Mars Program as a whole.

### 6.4.8 Trade #8: Orbiter Destination

One of the main challenges of Mars Sample Return is meeting the planetary protection requirements for cleaning, sealing and containing the sample. The requirement imposes a 99%  $6\sigma$  reliability on the EEV's ability to contain the sample and on the risk of contamination of the Earth. [188] In this analysis, the probability of the EEV to reenter the sample successfully was set to 1, as explained earlier. However, if this requirement cannot be met with current technology, a clean Mars sample could be returned to a stable retrograde lunar orbit. The sample could then be retrieved using another robotic mission or a manned mission (this last step is not added into the trade space). Returning to a lunar orbit can only be achieved at a reasonable propellant cost by SEP orbiters. The SEP orbiter return trajectory must arrive into the Earth-Moon system at a maximum  $V_\infty$  of 1.5 km/s in order to be captured into a stable lunar orbit using a few gravity assist manoeuvres. This causes the mass of a SEP orbiter returning to the Moon to be greater than that of a SEP orbiter simply delivering the sample to the Earth. As can be seen in Figure 80, returning to the Moon does not increase the reliability of the system, but it does reduce the cost of the overall system by 5 to 10% because the 44kg EEV does not need to be carried all the way to Mars and back. Having an architecture that returns to the Moon instead of the Earth therefore does not provide significant cost savings and is not advantageous, unless the level of reliability of the EEV cannot be proven to meet the planetary protection requirements.

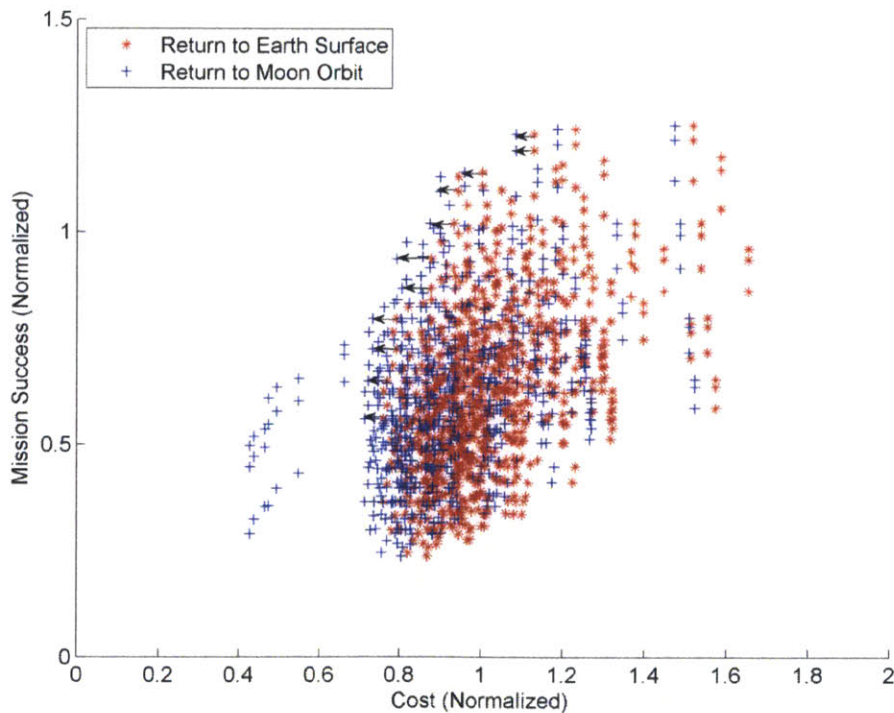


Figure 80: Architectures returning the sample to the Moon

## 6.5 Conclusions

This chapter has detailed a framework to enumerate and evaluate the *spatially* and *temporally distributed* trade space for the fetch, ascent and return part of a MSR campaign. As part of the evaluation process, eight trades were examined, and the following conclusions were reached:

- 1) A 5km radius landing ellipse similar to the ellipse that may be used by Mars 2020 provides the best return on investment.
- 2) Using a low capability, single-string MAV provides significant cost reductions but has a negative impact on reliability.
- 3) The roving MAV concept has a higher cost than the lander and fetch concept, but it also provides a higher return on investment.
- 4) Low cost, direct return options exist, but they have a significant detrimental effect on reliability.
- 5) Initial analysis shows that SEP options could be cheaper and more reliable than orbiters with chemical propulsion.
- 6) Sending the MAV to a low but stable Mars orbit (500km was investigated) is cheaper than sending the MAV to a high orbit and spending less fuel on the orbiter.
- 7) Both the orbiter-first and the lander-first options are very similar: the lander-first option has higher reliability and robustness, but the orbiter-first option may have programmatic advantages.
- 8) If a reliable EEV can be developed, sending the sample to a retrograde lunar orbit does not provide significant enough cost savings to be valuable.

In addition to these specific conclusions, the framework developed in this thesis possesses enough flexibility to enable the exploration of further MSR-related trades, including new technology options or novel approaches to returning the sample. Furthermore, the case study demonstrated that the framework more generally enables the high level exploration of trade space of any *spatially* and *temporally distributed* engineering missions, even though this particular study concentrated on a Mars Sample Return example. This provides engineers with valuable insights on the key trades involved in such missions, and an understanding of how their architectural and technology decisions affect the trade space as a whole.

# Chapter 7

## CONCLUSIONS AND RECOMMENDATIONS

### 7.1 Thesis Summary

The past decade has witnessed exceptional progress in the exploration of the Solar System, and the 2013-2022 Planetary Science Decadal Survey [6] put forward very ambitious exploration goals for the coming decade, including a Mars Sample Return mission and a mission to Jupiter's moon Europa. However, in the current economic climate, planetary science budgets are limited to approximately \$1B to \$1.5B per year, which severely limits the type of concepts that can feasibly be considered. This thesis argued that it may be possible to continue to achieve challenging science goals in the solar system with these constrained budgets by using a *distributed* approach to planetary exploration, where the concept of *task distribution* is used to reduce capability needed by individual vehicles. *Task distribution* involves the spreading of the functions that one monolithic vehicle would accomplish across several vehicles. Two types of distribution were considered:

i) *Spatial distribution*, which entails spreading several heterogeneous vehicles across an area, either on a planetary surface, on orbit or both.

ii) *Temporal distribution*, which is the separation of a large vehicle into a sequence of vehicles of different types that are launched and operated separately to achieve the original mission goal.

Chapter 1 started by analyzing the current state of planetary exploration and of analysis tools for mission design in the early phases of the development process. It identified distribution as a potential

approach for reducing the cost and complexity of missions, while increasing their return or ability to complete the mission. Existing frameworks that were created to analyze multi-vehicle systems were investigated. In particular, two fields were explored in depth: systems of systems (SoS) and distributed spacecraft systems. It was found that the SoS literature mostly provided qualitative models, and that the few quantitative models available mostly concentrated on mapping multi-stakeholder objectives rather than modeling the systems in depth. Conversely, the tools created to analyze distributed spacecraft system mostly modeled homogeneous systems and only dealt with Earth orbiting assets, many of which were only used for communications or were simple single-goal systems (e.g. observation systems). Furthermore, none of the frameworks in the literature were able to deal with *temporal distribution*, or missions with set goals that have binary outcome (i.e. where the mission is either 100% successful, or it is a complete failure; and example of this is a sample return mission: either the sample is returned to Earth or it is not).

Chapter 2 put forward a new five-step framework for the evaluation of multi-vehicle systems which is used in the rest of the thesis. Each of the five steps are:

- 1) Problem decomposition, where a method for defining different types of functions and mapping multiple functions and forms (on a non one-to-one basis) to the mission goals is discussed;
- 2) Trade space generation, where architectures in the trade space consist of multiple heterogeneous vehicles;
- 3) Trade space evaluation, where eight metrics, mass, science benefit, vehicle-level complexity, cost, risk, productivity, system-level complexity, and coverage, are put forward to evaluate both *spatially* and *temporally distributed* systems, eight of which are not mass-based;
- 4) Trade space visualization, where the effects of distribution on the system is illustrated;
- 5) Simulation of down-selected systems through the software tool SEXTANT, where a method that allows for the performance of architectures to be evaluated directly in their operational environment, and therefore to inform the design and architecture selection process, is described.

Chapter 3 explored the concept of *spatial distribution* in depth, and identified different types of spatially distributed systems, as shown in Table 46.

**Table 46: Types of spatially distributed systems**

	<b>Coordinated</b>	<b>Non-Coordinated</b>
<b>Dependent</b>	Vehicles are always in visible (i.e. line of sight) contact.	N/A
<b>Independent</b>	Vehicles do not have to be visible to each other at all times, but are always in the same region.	Vehicles do not have to be visible to each other, and are not in the same region.



In this chapter, multiple case studies investigating the use of spatial distribution for the exploration of Mars were performed. Moreover, trends demonstrating how the types of spatial distribution shown above affect the system were derived, based on the different metrics put forward in Chapter 2. In general, it was found that spatially distributed systems provide higher coverage, science benefit and productivity, degraded more gracefully and had reduced risk as compared to monolithic systems. However, many distributed systems had higher system-level complexity than monolithic vehicles, and they also had higher total system mass. Mass was therefore traded for lower vehicle-level complexity and increased system robustness. The chapter ended with a short case study investigating the redesign of the Mars Science Laboratory into a multi-vehicle system, to demonstrate how the framework and tools developed could rapidly be used to generate and evaluate a trade space. It found several options that could have resulted in a more robust and productive system, but it also showed that the monolithic system was well optimized given the choice of instruments.

Chapter 4 put forward the use of a path-planning tool, SEXTANT, to model the operations of multi-vehicle systems on planetary surfaces. The tool was originally used to model the traverse of astronauts on a surface, and was adapted to deal with multi-vehicle robotic systems. It includes a rover model that optimizes the traverse path based on rover properties, a collision avoidance model that looks at path constraints given that there are multiple vehicles on the surface of the planet that must both avoid and interact with each other, and a travelling salesman solver that helps plan the traverse of a multi-vehicle system based on a set of desired measurements at different sites. Chapter 4 demonstrated that such a tool can be used to compare the performance of a few downsized architectures, and to help refine mass and power estimates for rovers.

Chapter 5 investigated the concept of *temporal distribution*, using the exploration of the Jovian moon Europa as a case study. It took the Jupiter Europa Orbiter (JEO) flagship mission, which was found by the Decadal Survey to be of high value but too complex, risky and expensive to fly, as the baseline, and investigated distributed options that would achieve the goals at a lower cost and risk. In particular, the case study demonstrated the use of the science benefit, mass, complexity and cost metrics, as well as how expert elicitation can be used in the evaluation process. It found that the currently proposed multi-flyby mission Clipper achieved a large portion of the science goals at less than 50% of the cost of the JEO mission. It also found that a multi-flyby mission followed by a lander mission would perform better science than the JEO mission at about 80% of its cost, and showed that low cost missions to Europa are also feasible. A summary of the trade space is provided in Figure 81.

Overall, Chapter 5 found that temporally distributed missions can typically achieve more science than a monolithic flagship mission for the same investment, and benefit from reduced uncertainty in potential science benefit. These missions also offer a shorter timeline before some of the science questions are

answered and require a lower yearly budget. On the other hand, they do involve prioritizing science, which can be difficult for scientists when targets are distant and timelines are very long, and can lead to longer program timelines (i.e. it takes longer for all the science questions to be answered, as compared to the flagship mission), which puts them at greater risk of being cancelled due to changes in political or programmatic priorities.

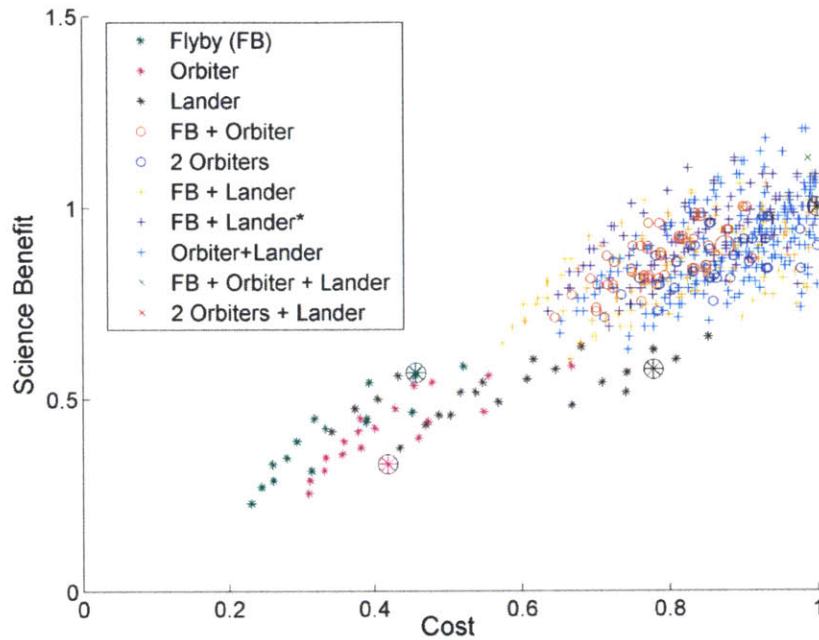


**Figure 81: Full Trade Space for the Europa Case Study.**

**The larger circles at (0.42, 0.33), (0.46, 0.60) and (0.78, 0.58) represent the orbiter, flyby and lander architectures considered by NASA in the 2012 Europa Study [9] respectively and the point at (1,1) is the Jupiter Europa Orbiter presented in the Planetary Science Decadal Survey [6].**

The last large case study of the thesis was presented in Chapter 6. It investigated the use of both *spatial* and *temporal* distribution to achieve the goals of an engineering-driven mission: the ascent and return components of a Mars Sample Return (MSR) mission. This case study mostly investigated the use of the mission success, mass, complexity and cost metrics to evaluate the effects of technology choices and sequencing options on a mission with a binary outcome (success or failure). The case study used the framework put forward in this thesis to investigate eight main trades, and the results obtained were in line with other analysis performed in the Mars Program Formulation office at the Jet Propulsion Laboratory (JPL), thus validating the framework. In particular, it found that options with a Roving Mars Ascent Vehicle (MAV), a Solar Electric Propulsion (SEP) orbiter and a lander-first approach provided the best return on investment. An overview of the trade space for a 2024 orbiter launch and a 2026 lander launch is provided in Figure 82.

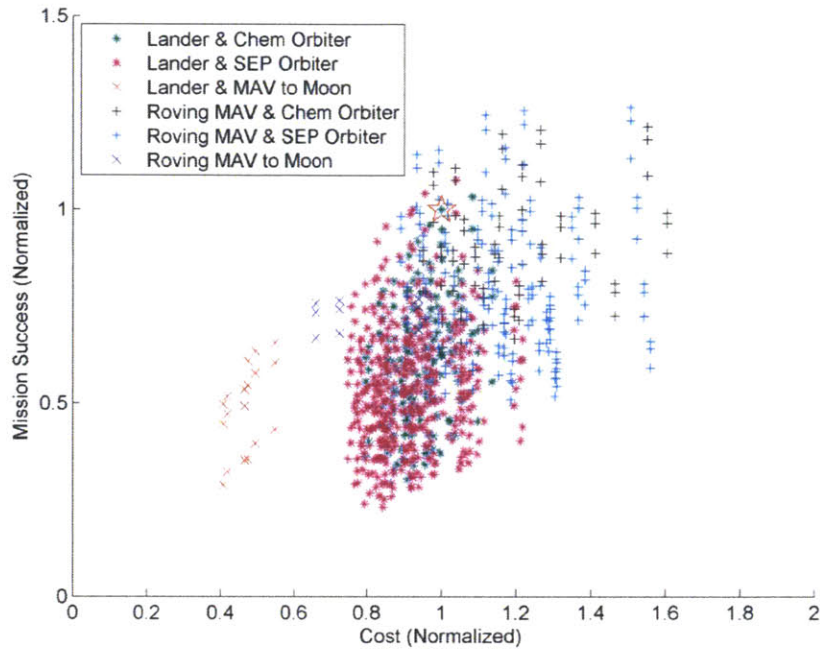


**Figure 82: Full Trade Space for the MSR Case Study.**  
**The large red star represents the architecture studied by NASA in 2011 [187], with a 2024 orbiter launch and a 2026 lander, MAV and fetch rover launch.**

The case studies provided in the thesis showed that the framework developed can be used to evaluate both *spatially* and *temporally distributed* options for planetary exploration missions. In particular, the two longer case studies demonstrated that the framework can be used for both of the possible types of planetary exploration missions: science-driven missions and engineering-driven technology demonstrations missions. The results from these case studies were in line with those found through different analyses performed by the Europa and Mars working groups respectively, and demonstrated that the framework can robustly be used in the early mission concepts/proposal phase of a mission to evaluate a large range of concepts with different types of vehicles, or combinations thereof, and evaluate them against each other on a one-to-one basis without having to go through detailed point designs.

## 7.2 Contributions

This thesis has developed a comprehensive framework for generating and evaluating multi-vehicle architectures for the exploration of the solar system, where the vehicles are of different *types* and are *spatially* and/or *temporally* distributed. A set of short case studies were performed to analyze the effects of spatial distribution on a system. Two longer case studies based on currently studied JPL missions, Europa and MSR, were also undertaken to demonstrate how both types of distribution considered can

help achieve complex and challenging missions. The specific contributions of the research were as follows:

- 1) *To enable the ability to evaluate trade spaces of multi-vehicle architectures for planetary exploration where vehicles are:*

- i. *Of different types*
- ii. *Spatially Distributed*
- iii. *Temporally Distributed*

The thesis developed a framework that can be used to evaluate multi-vehicle systems for any type of planetary exploration mission, whether it be science-driven missions with broad goals or technology-driven missions with set goals and a binary outcome.

- 2) *To provide an understanding of the effects of distribution on the architecture attributes*

The case studies and analysis performed provide the reader with an understanding of how different types of distribution and sequencing affect the properties of a system, and where the trades between the different metrics occur.

- 3) *To enable the simulation of systems of vehicles exploring the surface of a planetary body*

The path-planning tool SEXTANT was further developed to enable the traverse of down-selected architectures on the surface of a planet to be analyzed in order to understand how the system performs throughout the traverse. It also allows a mission designer to plan traverses and the sequencing of measurements, to model the interactions between systems, to measure coverage and to refine the architecture's mass and power estimates.

- 4) *Case-study specific recommendations*

Chapter 5 and 6 undertook case studies of missions that are still in development at the time of writing. The results found in these case studies each led to a set of recommendations on vehicle, payload and technology selections that were shared with the respective working groups. Specifically, Chapter 5 demonstrated that the proposed Clipper mission for Europa was a non-dominated architecture, but that flying the Ion-Neutral Mass Spectrometer (INMS) should be reconsidered. It also concluded that although flying a lander as a first mission to Europa would be too complex, it would be the most scientifically beneficial follow-on mission to a multi-flyby mission such as Clipper. Chapter 6 made several recommendations for a Mars Sample Return (MSR) mission. Most notably, it found that SEP return orbiters always dominated over orbiters with chemical propulsion, and that the concept of a Roving MAV would provide higher return on investment than the current baseline. Furthermore, when dealing with only the MSR goals, the lander first sequence was shown to be preferable.

## **7.3 Recommendations for Future Work**

While the work presented in this thesis was shown to provide a robust framework to evaluate early mission concepts for any type of planetary exploration missions, there are certainly many areas that could be explored in greater depth and with higher granularity in the future, as well as related topics that could be investigated. Some of these areas are detailed in the rest of this chapter.

### **7.3.1 Spatially Distributed Systems**

The case studies in this thesis only scratched the surface of the potential benefits of spatially distributed systems. The following recommendations are made for future work:

- Physical demonstration of multi-vehicle systems: this is the first step in ensuring the feasibility of multi-rover systems and would help evaluate the effect of spatial distribution on system-level complexity.
- Payload miniaturization: the effects of using miniaturized payload on the performance of spatially distributed systems should be investigated.
- Variety in types of vehicles: This thesis looked at a limited number of types of vehicles (flybys, orbiters, rovers, landers and ascent vehicles). Other vehicle options that could be added into the trade space include: hoppers, CubeSats, micro-rovers, gliders and balloons. These can easily be added into the framework as long as the relevant mass and performance models are available.

### **7.3.2 Temporally Distributed Systems**

The framework put forward in this thesis was shown to effectively deal with temporally distributed systems, and to help engineers plan sequences of missions. There are a few remaining areas that could still be explored in this topic:

- Investigation of how technology demonstration missions to other targets can help reduce risk or cost of missions to planets in the outer solar system.
- Inclusion of an analysis of the political implications of sequencing a mission and having longer mission timelines.
- Investigation of campaigns of missions to similar targets, such as asteroids.

### **7.3.3 Framework and Metrics**

Although this thesis provided a comprehensive set of metrics that were shown to enable the evaluation of both science and engineering-driven missions, there are still areas that could benefit from further research:

- A comprehensive suite of physical mass models: currently some models (e.g. the rover model) have much greater granularity than others. In particular, the orbiter models, especially the SEP models, are based on parametric correlations or first order sizing rules. A set of detailed physical models for these systems would help improve the fidelity of the model.
- Another topic that was addressed in this thesis is uncertainty and its link to risk. This assumed that each mission only had one stakeholder: NASA or ESA. A good addition to the framework would be to evaluate how uncertainty affects the likeliness of a mission being selected, by including the government and other agencies as part of the stakeholders.
- Addressing the concept of re-supply or replacement of failed systems, and how that affects cost, value and mission success.

### **7.3.4 SEXTANT**

In this thesis, SEXTANT was shown to be a powerful tool to help simulate mission operations, compare the performance of architectures to each other and refine the mass and power estimates for systems of vehicles. There is still a range of applications that SEXTANT could be used for:

- Higher fidelity analysis of rover properties by including detailed terramechanics equations and models using the high definition maps to obtain detailed surface properties of the traverse.
- Landing site selection based on traverse targets.
- Human-robot interaction: SEXTANT was originally developed to model human traverses. The capability to model astronaut traverses could easily be added back into SEXTANT and the new features could be used to evaluate systems with multiple rovers and astronauts interacting together on the surface of the Moon.

### **7.3.5 Case Study Specific Further Work**

This thesis provided a varied range of case studies to showcase the use of the framework developed. Additional case study related work includes:

- Detailed analysis of instrument selection for Europa: now that the Clipper mission has been chosen, the framework could be used to help further trade the different potential instruments currently being considered for the flyby mission and help evaluate potential follow-on missions.

- Further analysis of MSR concepts: the framework could be continually used in the analysis of the MSR ascent and return components. The current analysis could either be refined as more is known about the potential vehicles, or new concepts or trades could easily be added in to quickly evaluate how they compare to current options and if they are worth pursuing further.
- Performing more case studies: this framework can be used in early mission planning for any planetary exploration mission.





# Bibliography

- [1] NASA, “Mars Program Planning Group,” 2012. [Online]. Available: <http://www.nasa.gov/offices/marsplanning/home/index.html>. [Accessed: 28-Oct-2012].
- [2] NASA JPL, “Mars Science Laboratory: Curiosity Rover,” 2012. [Online]. Available: <http://mars.jpl.nasa.gov/msl/>. [Accessed: 28-Oct-2012].
- [3] Mars Program Planning Group, “Summary of the Final Report,” Pasadena, CA, 2012.
- [4] D. a. Bearden, “A complexity-based risk assessment of low-cost planetary missions: when is a mission too fast and too cheap?,” *Acta Astronautica*, vol. 52, no. 2–6, pp. 371–379, Jan. 2003.
- [5] NASA, “FY2013 Budget,” 2012. [Online]. Available: <http://www.nasa.gov/news/budget/index.html>. [Accessed: 28-Oct-2012].
- [6] The National Academies Press, “Vision and Voyages for Planetary Science in the Decade 2013-2022,” Washington, D.C., 2011.
- [7] NASA, “Solar System Exploration,” 2012. [Online]. Available: <http://solarsystem.nasa.gov/missions/index.cfm>. [Accessed: 28-Oct-2012].
- [8] B. Barley, P. Gilbert, and M. Newhouse, “Life Cycle Cost Growth Study for the Discovery and New Frontiers Program Office,” Huntsville, AL, 2010.
- [9] Europa Study Team, “Europa Study 2012 Report,” Pasadena, CA, 2012.

- [10] MEPAG 2-Rover International Science Analysis Group, “Two rovers to the same site on Mars, 2018: possibilities for cooperative science.,” *Astrobiology*, vol. 10, no. 7, pp. 663–85, Sep. 2010.
- [11] Mars Exploration Program Analysis Group (MEPAG), “Report of the Mars 2020 Science Definition Team,” 2013.
- [12] S. Liu, L. Mao, and J. Yu, “Path Planning Based on Ant Colony Algorithm and Distributed Local Navigation for Multi-Robot Systems,” *2006 International Conference on Mechatronics and Automation*, pp. 1733–1738, Jun. 2006.
- [13] W. Burgard, M. Moors, C. Stachniss, and F. E. Schneider, “Coordinated Multi-Robot Exploration,” *IEEE Transactions on Robotics*, vol. 21, no. 3, pp. 376–386, 2005.
- [14] D. Yingying, H. Yan, and J. Jingping, “Multi-Robot Cooperation Method Based On,” in *IEEE Swarm Intelligence Symposium*, 2003, pp. 14–18.
- [15] Perceptual Robotics Lab, “Cooperative Underwater Navigation,” *University of Michigan*, 2011. [Online]. Available: <http://robots.engin.umich.edu/Projects/OWTT>. [Accessed: 29-Oct-2012].
- [16] GRASP Laboratory, “Multiple Autonomous Robots (MARS),” *University of Pennsylvania*, 2010. [Online]. Available: <http://www.cis.upenn.edu/mars/home.html>. [Accessed: 28-Oct-2012].
- [17] D. T. Cole, A. H. Goktogan, and S. Sukkarieh, “The Demonstration of a Cooperative Control Architecture for UAV Teams,” *Experiental Robotics*, vol. STAR 39, pp. 501–510, 2008.
- [18] Q. Lindsey, D. Mellinger, and V. Kumar, “Construction with Quadrotor Teams.” GRASP Lab, University of Pennsylvania, 2011.
- [19] K. Nonami, S. Masunaga, D. Waterman, H. Aoyama, and Y. Takada, “Mine Detection Robot and Related Technologies for Humanitarian Demining,” no. February, Vienna, Australia: I-Tech Education and Publishing, 2008, pp. 392–422.
- [20] DARPA, “Tactical Technology Office: System F6.” [Online]. Available: [http://www.darpa.mil/Our\\_Work/tto/Programs/System\\_F6.aspx](http://www.darpa.mil/Our_Work/tto/Programs/System_F6.aspx). [Accessed: 30-Oct-2012].

- [21] D. J. Barnhart, T. Vladimirova, A. M. Baker, and M. N. Sweeting, "A low-cost femtosatellite to enable distributed space missions," *Acta Astronautica*, vol. 64, no. 11–12, pp. 1123–1143, Jun. 2009.
- [22] T. Vladimirova, X. Wu, A. Jallad, and C. P. Bridges, "Distributed Computing in Reconfigurable Picosatellite Networks," in *Second NASA/ESA Conference on Adaptive Hardware and Systems*, 2007, no. Ahs.
- [23] B. H. Wilcox, "Snow White and the 700 Dwarves," in *Multi-Robot Systems: From Swarms to Intelligent Automata*, A. C. Schultz and L. E. Parker, Eds. Springer, 2002, pp. 123–130.
- [24] J.-A. Lamamy, "Methods and Tools for the Formulation, Evaluation and Optimization of Rover Mission Concepts," Massachusetts Institute of Technology, 2007.
- [25] E. Retchin, *Systems Architecting, Creating & Building Complex Systems*. Englewood Cliffs, NJ: Prentice Hall, 1991.
- [26] M. W. Maier and E. Retchin, *The Art of Systems Architecting*. New York, NY: CRC Press, 2000.
- [27] E. F. Crawley, *Theory of Systems Architecture*. .
- [28] E. F. Crawley, O. L. de Weck, S. Eppinger, C. Magee, J. Moses, W. Seering, J. Schindall, D. Wallace, and D. Whitney, "The influence of architecture in engineering systems - Engineering Systems Monograph," 2004.
- [29] A. M. Ross, D. H. Rhodes, and D. E. Hastings, "Defining changeability: Reconciling flexibility, adaptability, scalability, modifiability, and robustness for maintaining system lifecycle value," *Systems Engineering*, vol. 11, pp. 246–262, 2008.
- [30] R. D. Neufville and S. Scholtes, *Flexibility in Engineering Design*. MIT Press, 2011.
- [31] D. E. Hastings, A. L. Weigel, and M. A. Walton, "Incorporating uncertainty into conceptual design of space systems architecture," in *ESD Symposium*, 2002.
- [32] W. K. Hofstetter, "A Framework for the Architecting of Aerospace Systems Portfolios with Commonality," 2009.

- [33] O. C. Brown and P. Eremenko, "Application of Value-Centric Design to Space Architectures: The Case of Fractionated Spacecraft," in *AIAA Space 2008*, 2008.
- [34] G. B. Shaw, "The Generalized Information Network Analysis Methodology for Distributed Satellite Systems," Massachusetts Institute of Technology, 1999.
- [35] A. Meilich, "System of Systems (SoS) engineering & architecture challenges in a net centric environment," in *IEEE International Conference on Systems of Systems Engineering*, 2006.
- [36] R. Abbott, "Open at the top; open at the bottom; and continually (but slowly) evolving," in *IEEE International Conference on System of Systems Engineering*, 2006.
- [37] W. H. J. Manthorpe, "The Emerging Joint System of Systems: A Systems Engineering Challenge and Opportunity for APL," vol. 17, no. 3, pp. 305–313, 1996.
- [38] A. Odusd and T. Sse, *Systems Engineering Guide for Systems of Systems*, no. August. 2008.
- [39] Los Angeles Airforce Base, "Military Satellite Communications Systems Directorate," *U.S. Airforce*, 2011. .
- [40] D. W. Robbins, "MILSATCOM Systems of Systems Engineering, Architecture and Integration," in *2nd Annual System of Systems Engineering Center of Excellence (SoSECE) Conference*, 2006.
- [41] W. A. Crossley, "Systems of Systems: An introduction of Purdue University Schools of Engineering's Signature Area," in *Engineering Systems Symposium*, 2004.
- [42] L. A. Wojcik and K. C. Hoffman, "Systems of systems engineering in the enterprise context: a unifying framework for dynamics," in *IEEE International Conference on System of Systems Engineering*, 2006.
- [43] M. Jamshidi, "Introduction to System of Systems," in in *Systems of Systems Engineering*, CRC Press, 2008.
- [44] A. Abel and S. Sukkariéh, "The coordination of multiple autonomous systems using information theoretic political science voting models," in *IEEE International Conference on System of Systems Engineering*, 2006.

- [45] INCOSE, *Systems Engineering Handbook: A Guide for System Life Cycle Processes and Activities*, 2006.
- [46] M. W. Maier, "Architecting principles for systems-of-systems," *Systems Engineering*, vol. 1, no. 4, pp. 267–284, 1998.
- [47] A. P. Sage and C. D. Cuppan, "On the Systems Engineering and Management of Systems of Systems and Federations of Systems," *Information Knowledge Systems Management*, vol. 2, no. 4, pp. 325–345, 2001.
- [48] J. Boardman and B. Sauser, "System of Systems – the meaning of of," in *2006 IEEE/SMC International Conference on System of Systems Engineering*, 2006, no. April, pp. 118–123.
- [49] D. A. DeLaurentis, "Understanding Transportation as a System-of-Systems Design Problem," in *AIAA Space 2005*, 2005.
- [50] A. P. Sage and S. M. Biemer, "Processes for System Family Architecting, Design and Integration," *IEEE Systems Journal*, vol. 1, no. 1, pp. 5–16, 2007.
- [51] H. Eisner, J. Marciniak, and R. McMillan, "Computer-Aided System of Systems (S2) Engineering," in *IEEE International Conference on Systems, Man and Cybernetics*, 1991.
- [52] Department of Defense, *Defense Acquisition Guidebook*. Pentagon, Washington, D.C., 2004.
- [53] C. Keating, R. Rogers, R. Unal, D. Dryer, A. Sousa-Poza, R. Safford, W. Peterson, and G. Rabadi, "Systems of Systems Engineering," *Engineering Management Journal*, vol. 15, no. 3, pp. 36–45, 2003.
- [54] N. S. Andreas, "Space-Based Infrared System ( SBIRS ) System of Systems," in *IEEE Aerospace Conference*, 1997.
- [55] M. L. Butterfield, J. S. Pearlman, and S. C. Vickroy, "A System-of-Systems Engineering GEOSS: Architectural Approach," *IEEE Systems Journal*, vol. 2, no. 3, pp. 321–332, Sep. 2008.
- [56] E. Christian, "Planning for the Global Earth Observation System of Systems (GEOSS)," *Space Policy*, vol. 21, no. 2, pp. 105–109, May 2005.

- [57] D. Chattopadhyay, A. M. Ross, and D. H. Rhodes, "Demonstration of System of Systems Multi-Attribute Tradespace Exploration on a Multi-Concept Surveillance Architecture," in *7th Annual Conference on Systems Engineering Research (CSER 2009)*, 2009, vol. 2009, no. April.
- [58] D. Chattopadhyay, "A Method for Tradespace Exploration of Systems of Systems," Massachusetts Institute of Technology, 2009.
- [59] D. Chattopadhyay, A. M. Ross, and D. H. Rhodes, "Combining Attributes for Systems of Systems in Multi-Attribute Tradespace Exploration," in *7th Annual Conference on Systems Engineering Research (CSER 2009)*, 2009, vol. 2009, no. April.
- [60] D. Chattopadhyay, A. M. Ross, and D. H. Rhodes, "A Framework for Tradespace Exploration of Systems of Systems," in *Conference on Systems Engineering Research*, 2008, no. Ross 2006.
- [61] D. Chattopadhyay, A. M. Ross, and D. H. Rhodes, "A Practical Method for Tradespace Exploration of Systems of Systems," in *AIAA Space 2009*, 2009, no. September.
- [62] N. B. Shah, M. G. Richards, D. A. Broniatowski, J. R. Laracy, P. N. Springmann, and D. E. Hastings, "System of Systems Architecture : The Case of Space Situational Awareness," in *AIAA Space 2007*, 2007.
- [63] N. B. Shah, D. H. Rhodes, and D. E. Hastings, "System of Systems and Emergent System Context," in *Conference on Systems Engineering Research*, 2007.
- [64] G. R. Andrews, *Foundations of Multithreaded, Parallel, and Distributed Programming*. Addison-Wesley, 2000.
- [65] S. Gosh, *Distributed Systems - An Algorithmic Approach*. Chapman & Hall/CRC, 2007.
- [66] N. A. Lynch, *Distributed Algorithms*. Morgan Kauffman, 1996.
- [67] G. B. Shaw, D. W. Miller, and D. E. Hastings, "Development of the Quantitative Generalize Information Network Analysis (GINA) Methodology for Satellite Systems," *Journal of Spacecraft and Rockets*, vol. 38, no. 2, pp. 257–269, 2001.

- [68] C. D. Jilla, "A Multiobjective , Multidisciplinary Design Optimization Methodology for the Conceptual Design of Distributed Satellite Systems," Massachusetts Institute of Technology, 2002.
- [69] M. Maurice and S. Kilberg, "Techsat 21 and revolutionizing space missions using microsattellites," in *15th AIAA/USU Conference on Small Satellites*, 2001, no. Fig 1.
- [70] A. Das and R. Cobb, "TechSat 21 - Space Missions Using Collaborating Constellations of Satellites," in *12th Annual AIAA/USU Conference on Small Satellites*, 1998, pp. 125–129.
- [71] C. A. Beichman, "Terrestrial Planet Finder: the search for life-bearing planets around other stars," in *Astronomical Telescopes & Instrumentation*, International Society for Optics and Photonics, 1998, pp. 719–723.
- [72] J. A. Wertz, "Expected Productivity-Based Risk Analysis in Conceptual Design: With Application to the Terrestrial Planet Finder Interferometer Mission," Massachusetts Institute of Technology, 2006.
- [73] O. P. Lay, S. M. Gunter, L. a. Hamlin, C. a. Henry, Y.-Y. Li, S. R. Martin, G. H. Purcell Jr., B. Ware, J. a. Wertz, and M. C. Noecker, "Architecture Trade Study for the Terrestrial Planet Finder Interferometer," vol. 5905, pp. 590502–590502–13, Aug. 2005.
- [74] P. Molette, C. Cougnet, and P. Saint-Aubert, "Technical and economical comparison between a modular geostationary space platform and a cluster of satellites," *Acta Astronautica*, vol. 12, no. 11, pp. 771–784, 1984.
- [75] O. C. Brown, A. Long, N. Shah, and P. Eremenko, "System Lifecycle Cost Under Uncertainty as a Design Metric Encompassing the Value of Architectural Flexibility," in *AIAA Space 2007*, 2007.
- [76] O. C. Brown and P. Eremenko, "The Value Proposition for Fractionated Space Architectures," 2008.
- [77] O. C. Brown and P. Eremenko, "Fractionated Space Architectures: A Vision for Responsive Space," Arlington, 2008.

- [78] O. C. Brown, P. Eremenko, and P. D. Collopy, "Value-Centric Design Methodologies for Fractionated Spacecraft: Progress Summary from Phase 1 of the DARPA System F6 Program," in *AIAA Space 2009*, 2009, no. September.
- [79] N. P. Diller, "Utilizing Multiple Attribute Tradespace Exploration with Concurrent Design for Creating Aerospace Systems Requirements," Massachusetts Institute of Technology, 2002.
- [80] A. M. Ross, M. G. O'Neill, D. E. Hastings, and D. H. Rhodes, "Aligning Perspectives and Methods for Value-Driven Design," in *AIAA Space 2010*, 2010.
- [81] C. Mathieu and A. Weigel, "Assessing the Flexibility Provided by Fractionated Spacecraft," in *AIAA Space 2005*, 2006.
- [82] C. Mathieu and A. L. Weigel, "Assessing the Flexibility Provided by On-Orbit Infrastructure of Fractionated Spacecraft," in *International Astronautical Congress*, 2005.
- [83] M. G. O'Neill, "Assessing the Impacts of Fractionation on Pointing-intensive Spacecraft," Massachusetts Institute of Technology, 2010.
- [84] M. G. O'Neill and A. L. Weigel, "Assessing Fractionated Spacecraft Value Propositions for Earth Imaging Space Missions," *Journal of Spacecraft and Rockets*, vol. 48, no. 6, pp. 974–986, 2011.
- [85] M. G. O'Neill, "Addressing Cost Growth in Spacecraft Acquisition Programs: A Prescriptive Approach." Massachusetts Institute of Technology, Cambridge, MA, 2010.
- [86] M. G. O'Neill and A. L. Weigel, "Assessing the Impacts of Fractionation on Pointing-Intensive Spacecraft," in *AIAA Space 2009*, 2009.
- [87] J. M. Lafleur and J. H. Saleh, "GT-FAST: A Point Design Tool for Rapid Fractionated Spacecraft Sizing and Synthesis," in *AIAA Space 2009*, 2009, no. September.
- [88] J. M. Lafleur and J. H. Saleh, "Exploring the F6 Fractionated Spacecraft Trade Space with GT-FAST," in *AIAA Space 2009*, 2009.
- [89] T. Huntsberger, P. Pirjanian, A. Trebi-ollennu, H. Das Nayar, H. Aghazarian, A. J. Ganino, M. Garrett, S. S. Joshi, and P. S. Schenker, "CAMPOUT : A Control Architecture for Tightly Coupled



Coordination of Multirobot Systems for Planetary Surface Exploration,” *IEEE Transactions on Systems, Man, and Cybernetics - Part A*, vol. 33, no. 5, pp. 550–559, 2003.

- [90] A. M. Ross, N. P. Diller, and D. E. Hastings, “Multi-attribute tradespace exploration with concurrent design for space system conceptual design,” in *Aerospace Sciences Meeting*, 2003, pp. 6–9.
- [91] A. M. Ross, D. E. Hastings, J. M. Warmkessel, and N. P. Diller, “Multi-Attribute Tradespace Exploration as Front End for Effective Space Design,” *Journal of Spacecraft and Rockets*, vol. 41, no. 1, 2004.
- [92] C. D. Jilla and D. W. Miller, “Assessing the performance of a heuristic simulated annealing algorithm for the design of distributed satellite systems,” *Acta Astronautica*, vol. 48, no. 5–12, pp. 529–543, Mar. 2001.
- [93] C. D. Jilla, D. W. Miller, and R. J. Sedwick, “Application of Multidisciplinary Design Optimization Techniques to Distributed Satellite Systems,” *Journal of Spacecraft and Rockets*, vol. 37, no. 4, pp. 481–490, Jul. 2000.
- [94] W. L. Simmons, “A Framework for Decision Support in Systems Architecting,” Massachusetts Institute of Technology, 2008.
- [95] B. H. Y. Koo, “A Meta-Language for Systems Architecting,” Massachusetts Institute of Technology, 2005.
- [96] B. H. Y. Koo, W. L. Simmons, and E. F. Crawley, “Algebra of Systems: A Metalanguage for Model Synthesis and Evaluation,” *IEEE Transactions on Systems, Man, and Cybernetics - Part A: Systems and Humans*, vol. 39, pp. 501–513, 2009.
- [97] M. G. O’Neill, H. Yue, S. Nag, P. Grogan, and O. L. de Weck, “Comparing and Optimizing the DARPA System F6 Program Value-Centric Design Methodologies,” in *AIAA Space 2010*, 2010.
- [98] V. Pareto, *Manuale di Politica*. Milano, Italia: Societa Editrice Libreria, 1906.
- [99] T. L. Saaty, “Decision Making with the Analytic Hierarchy Process,” *International Journal of Services Sciences*, vol. 1, pp. 83–98, 2008.

- [100] R. L. Keeney and H. Raiffa, *Decisions with Multiple Objectives: Preferences and Value Trade-Offs*. Cambridge University Press, 1993.
- [101] F. Alibay and N. J. Strange, "Trade Space Evaluation of Multi-Mission Architectures for the Exploration of Europa," in *IEEE Aerospace Conference*, 2013.
- [102] J. R. Wertz, D. F. Everett, and J. J. Puschell, *Space Mission Engineering: The New SMAD*. Microcosm, Inc., 2011.
- [103] J.-A. Lamamy, "Enhancing the science return of Mars missions via sample preparation, robotic surface exploration and in orbit fuel production," Massachusetts Institute of Technology, 2004.
- [104] J.-A. Lamamy and D. W. Miller, "Designing the next generation of rovers through a mid-rover analysis," in *9th ESA Workshop on Advanced Space Technologies for Robotics and Automation1*, 2006.
- [105] P. M. Cunio, "Tradespace Model for Planetary Surface Exploration Hopping Vehicles," Massachusetts Institute of Technology, 2012.
- [106] Z. J. Bailey, "A Trade Space Model for Robotic Lunar Exploration," Massachusetts Institute of Technology, 2010.
- [107] S. H. McCloskey, "Development of Legged , Wheeled , and Hybrid Rover Mobility Models to Facilitate Planetary Surface Exploration Mission Analysis," Massachusetts Institute of Technology, 2007.
- [108] S. Hong and J. A. Hoffman, "Design of Power Systems for Extensible Surface Mobility Systems on the Moon and Mars," in *AIAA Space 2008*, 2008, no. September.
- [109] S. Hong, "Design of Power Systems for Extensible Surface Mobility Systems on the Moon and Mars," Massachusetts Institute of Technology, 2007.
- [110] J. S. Norris, M. W. Powell, M. A. Vona, P. G. Backes, and J. V. Wick, "Mars Exploration Rover Operations with the Science Activity Planner," in *IEEE International Conference on Robotics and Automation*, 2005, no. April, pp. 4618–4623.

- [111] C. E. Carr, D. J. Newman, and K. V. Hodges, "Geologic Traverse Planning for Planetary EVA," in *AIAA and SAE International Conference on Environmental Systems*, 2003.
- [112] J. J. Marquez, M. L. Cummings, N. Roy, M. Kunda, and D. J. Newman, "Collaborative Human-Computer Decision Support for Planetary Surface Traversal," 2005, no. September, p. AIAA.
- [113] J. J. Marquez and M. L. Cummings, "Design and Evaluation of Path Planning Decision Support for Planetary Surface Exploration," *Journal of Aerospace Computing*, vol. 5, no. 5, pp. 57–71, 2008.
- [114] L. V. J. Lindqvist, "Multidisciplinary Extravehicular Activity Mission Optimization for Lunar Exploration," Technische Universität München, 2008.
- [115] J. R. Essenburg, "Mission Planning and Navigation Support for Lunar and Planetary Exploration," Massachusetts Institute of Technology, 2008.
- [116] A. W. Johnson, "An Integrated Traverse Planner and Analysis Tool for Future Lunar Surface Exploration," Massachusetts Institute of Technology, 2010.
- [117] A. W. Johnson, J. A. Hoffman, D. J. Newman, E. M. Mazarico, and M. T. Zuber, "An Integrated Traverse Planner and Analysis Tool for Planetary Exploration," in *AIAA Space 2010*, 2010.
- [118] D. Dori, *Object-Process Methodology*. Springer, 2002.
- [119] Jet Propulsion Laboratory and Applied Physics Laboratory, "Jupiter Europa Orbiter Mission Study 2008: Final Report. The NASA Element of the Europa Jupiter System Mission (EJSM)," 2009.
- [120] D. Selva and E. F. Crawley, "A rule-based decision support tool for architecting Earth observing missions," *2012 IEEE Aerospace Conference*, pp. 1–20, Mar. 2012.
- [121] A. Aliakbargolkar, "A Framework for Systems Architecting under Ambiguous Stakeholder Objectives : The Case of the Mars Sample Return Campaign," Pasadena, CA.
- [122] R. C. Moeller, C. Borden, T. Spilker, W. Smythe, and R. Lock, "Space missions Trade Space Generation and Assessment using the JPL Rapid Mission Architecture (RMA) Team Approach," in *2011 IEEE Aerospace Conference*, 2011.

- [123] D. A. Bearden, "A complexity-based risk assessment of low-cost planetary missions: when is a mission too fast and too cheap?," *Acta Astronautica*, vol. 52, no. 2, pp. 371–379, 2003.
- [124] T. J. McCabe and C. W. Butler, "Design complexity measurement and testing," *Communications of the ACM*, vol. 32, no. 12, pp. 1415–1425, 1989.
- [125] B. Edmonds, "What is Complexity? - The philosophy of complexity per se with applicaiton to some examples in evolution," in *The evolution of complexity*, 1995.
- [126] M. N. AlSharif, "Assessing the complexity of software architecture," Florida Institute of Technology, 2005.
- [127] E. Weyuker, "The evaluation of software complexity measures," *IEEE Transactions on Software Engineering*, vol. 14, pp. 1357–1365, 1998.
- [128] M. H. Meyer and A. P. Lehnerd, *The power of product platforms*. Free Press, 1997.
- [129] N. P. Suh, "A theory of complexity, periodicity and the design axioms," *Research in Engineering Design*, vol. 11, no. 2, pp. 116–132, 1999.
- [130] R. Riedl, *Strukturen der Komplexität: eine Morphologie des Erkennens und Erklärens*. Springer, 2000.
- [131] M. Kreimeyer and U. Lindemann, *Complexity Metrics in Engineering Design Managing the Structure of Design Processes*. Munich: Springer, 2011.
- [132] M. Kreimeyer, "Aggregate views to manage complex dependency," *Int. J. Product Development*, vol. 14, no. 1–4, pp. 144–164, 2011.
- [133] J. Denman, K. Sinha, and O. L. de Weck, "Technology insertion in turbofan engine and assessment of architectural complexity," in *13th International DSM Conference*, 2011.
- [134] J. M. Sussman, "Ideas on Complexity in Systems -- Twenty Views," Cambridge, MA, 2000.
- [135] W. Biedermann and U. Lindemann, "On the applicability of structural criteria in complexity management," in *18th International Conference on Engineering Design*, 2011, no. August.

- [136] U. Lindemann, "The Design Structure Matrix (DSM)," 2009. [Online]. Available: <http://www.dsmweb.org/>. [Accessed: 31-Oct-2012].
- [137] K. Sinha, "Structural Complexity and its Implications for the Design of Cyber-Physical Systems," Massachusetts Institute of Technology, 2013.
- [138] C. J. Leising, R. R. Wessen, R. Ellying, L. Rosenberg, and A. Leising, "Spacecraft complexity subfactors and implications on future cost growth," in *2013 IEEE Aerospace Conference*, 2013.
- [139] C. J. Leising, B. Sherwood, M. Alder, R. R. Wessen, and F. M. Naderi, "Recent improvements in JPL's mission formulation process," in *IEEE Aerospace Conference*, 2010.
- [140] J. Agte, N. Borer, and O. de Weck, "Design of Long-Endurance Systems With Inherent Robustness to Partial Failures During Operations," *Journal of Mechanical Design*, vol. 134, no. 10, p. 100903, 2012.
- [141] J. S. Agte, "Multistate Analysis and Design: Case Studies in Aerospace Design and Long Endurance Systems," Massachusetts Institute of Technology, 2011.
- [142] R. A. Howard, *Dynamic Probabilistic Systems: Volume 1, Markov Models*. Mineola, NY: Dover Publications, 2007.
- [143] J. R. Norris, *Markov Chains*. Cambridge University Press, 1998.
- [144] J. Wertz, "Reliability and Productivity Modeling for the Optimization of Separated Spacecraft Interferometers," Massachusetts Institute of Technology, 2002.
- [145] D. Bertsekas and J. Tsitsiklis, *Introduction to Probability*, 2nd. ed. Athena Scientific, 2008.
- [146] P. S. Babcock, "An Introduction to Reliability Modeling of Fault-Tolerant Systems," Cambridge, MA, 1986.
- [147] M. Laumanns, L. Thiele, K. Deb, and E. Zitzler, "On the Convergence and Diversity-Preservation Properties of Multi-Objective Evolutionary Algorithms," Zurich, Switzerland, 2001.
- [148] NASA Jet Propulsion Laboratory, "Mars Exploration Rovers," 2013. [Online]. Available: <http://marsrover.nasa.gov/science/>. [Accessed: 01-May-2013].

- [149] NASA, “Mars Exploration Rovers,” *Solar System Exploration*, 2013. [Online]. Available: <http://solarsystem.nasa.gov/missions/profile.cfm?InFlight=1&MCode=MER&Display=ReadMore>.
- [150] NASA, “Mars Science Laboratory/Curiosity,” *Solar System Exploration*, 2013. [Online]. Available: <http://solarsystem.nasa.gov/missions/profile.cfm?InFlight=1&MCode=MarsSciLab&Display=ReadMore>.
- [151] P. Abad-Manterola, “Axel rover paddle wheel design, efficiency, and sinkage on deformable terrain,” in *2011 IEEE International Conference on Robotics and Automation (ICRA)*, 2011.
- [152] R. Murphy, M. Ausmus, and M. Bugajska, “Marsupial-like mobile robot societies,” in *Third Annual Conference on Autonomous Agents*, 1999.
- [153] H. Hourani, P. Wolters, E. Hauck, and S. Jeschke, “A Marsupial Relationship in Robotics Survey,” *Automation, Communication and Cybernetics in Science and Engineering*, pp. 655–667, 2013.
- [154] J. B. Matthews and L. A. Nesnas, “On the design of the Axel and DuAxel rovers for extreme terrain exploration,” in *2012 IEEE Aerospace Conference*, 2012.
- [155] M. Matusiak, P. Paanajärvi, P. Appelqvist, and M. Elomaa, “A novel marsupial robot society: towards long-term autonomy,” *Distributed Autonomous Robotic Systems*, vol. 8, pp. 523–532, 2009.
- [156] E. Kadioglu and N. Papanikolopoulos, “A method for transporting a team of miniature robots,” in *2003 IEEE/RSJ International Conference on Intelligent Robots and Systems (IROS)*, 2003, pp. 2297–2302.
- [157] A. Drenner, M. Janssen, and N. Papanikolopoulos, “Coordinating recharging of large scale robotics teams,” in *2009 IEEE/RSJ International Conference on Intelligent Robots and Systems (IROS)*, 2009, pp. 1357–1362.
- [158] J. P. Gray, J. R. Mason, M. S. Patterson, and M. W. Skalny, “ROBODEXS: multi-robot deployment and extraction system,” in *SPIE DSS 2012 Conference*, 2012.

- [159] M. Van Winnendael, "Nanokhod microrover heading towards Mars," in *Fifth International Symposium on Artificial Intelligence, Robotics and Automation in Space*, 1999, pp. 69–76.
- [160] C. Dablin and F. Alibay, "Cooperative Planetary Exploration," in *Siemens Competition Report*, 2013.
- [161] R. Sonsalla and M. Fritsche, "Concept study for the FASTER Micro Scout Rover," in *13th Symposium on Advanced Space Technologies in Robotics and Automation*, 2013.
- [162] L. A. Nesnas, "Axel and DuAxel rovers for the sustainable exploration of extreme terrains," *Journal of Field Robotics*, vol. 29, no. 4, pp. 663–685, 2012.
- [163] T. Huntsberger, H. Stroupe, H. Aghazarian, M. Garrett, P. Younse, and M. W. Powell, "Field Report TRESSA: Teamed Robots for Exploration and Science on Steep Areas," *Journal of Field Robotics*, vol. 24, no. 11, pp. 1015–1031, 2007.
- [164] P. Younse and A. Stroupe, "Sample acquisition and caching using detachable scoops for Mars sample return," in *2009 IEEE Aerospace Conference*, 2009.
- [165] P. S. Schenker and T. Huntsberger, "Planetary rover developments supporting Mars exploration, sample return and future human-robotic colonization," *Autonomous Robotics*, vol. 14, no. 2–3, pp. 103–126, 2003.
- [166] L. Ojha, A. McEwan, and C. Dundas, "Recurring slope lineae on Mars: updated global survey results," in *43rd Lunar and Planetary Science Conference*, 2012.
- [167] A. McEwan, L. Ojha, C. Dundas, S. S. Mattson, S. Byrne, J. J. Wray, S. C. Cull, S. L. Murchie, N. Thomas, and V. C. Gulick, "Seasonal flows on warm martian slopes," *Science*, vol. 333, no. 6043, pp. 740–743, 2011.
- [168] L. A. Nesnas, P. Abad-Manterola, J. A. Edlund, and J. W. Burdick, "Axel Mobility Platform for Steep Terrain Excursions and Sampling on Planetary Surfaces," in *2008 IEEE Aerospace Conference*, 2008.
- [169] Jet Propulsion Laboratory, "MSL Science Corner: Sampling System," 2013. [Online]. Available: <http://msl-scicorner.jpl.nasa.gov/samplingsystem>. [Accessed: 01-Aug-2013].

- [170] European Space Agency, “Robotic Exploration of Mars,” 2013. [Online]. Available: <http://exploration.esa.int/mars/>. [Accessed: 01-Aug-2013].
- [171] R. Bertrand, R. Rieder, and M. Van Winnendael, “European Tracked Micro-Robot for Planetary Surface Exploration,” in *ESA Workshop on Advanced Space Technologies for Robotics and Automation*, 1998, no. December.
- [172] P. E. Hart, N. J. Nilson, and B. Raphael, “A Formal Basis for the Heuristic Determination of Minimum Cost Paths,” *IEEE Transactions on Systems, Science and Cybernetics*, vol. 4, no. 2, pp. 100–107, 1968.
- [173] D. E. Smith, M. T. Zuber, G. B. Jackson, J. F. Cavanaugh, G. a. Neumann, H. Riris, X. Sun, R. S. Zellar, C. Coltharp, J. Connelly, R. B. Katz, I. Kleyner, P. Liiva, A. Matuszeski, E. M. Mazarico, J. F. McGarry, A.-M. Novo-Gradac, M. N. Ott, C. Peters, L. a. Ramos-Izquierdo, L. Ramsey, D. D. Rowlands, S. Schmidt, V. S. Scott, G. B. Shaw, J. C. Smith, J.-P. Swinski, M. H. Torrence, G. Unger, A. W. Yu, and T. W. Zagwodzki, “The Lunar Orbiter Laser Altimeter Investigation on the Lunar Reconnaissance Orbiter Mission,” *Space Science Reviews*, vol. 150, pp. 209–241, May 2010.
- [174] E. M. Mazarico, G. A. Neumann, D. E. Smith, M. T. Zuber, and M. H. Torrence, “Illumination Conditions of the Lunar Polar Regions using LOLA Topography,” *Icarus*, vol. 201, pp. 1066–1081, 2011.
- [175] J. Elliot and J. Langmaier, “Assessment of Alternative Europa Mission Architectures,” JPL Publi, Pasadena, CA, 2008.
- [176] N. J. Strange, K. P. Hand, J. R. Casani, H. J. Eisen, and J. O. Elliot, “Low-Radiation Europa Lander Mission Concept,” in *American Geophysical Union Fall Meeting*, 2011.
- [177] B. Harvey, *Russian Planetary Exploration: History, Development, Legacy and Prospects*. Springer, 2007.
- [178] Mars Exploration Program Analysis Group (MEPAG), “Mars Scientific Goals, Objectives, Investigations and Priorities: 2006,” 2006.



- [179] Mars Exploration Program Analysis Group (MEPAG), “Science Priorities for Mars Sample Return,” 2008.
- [180] N. R. Council, “An Astrobiology Strategy for the Exploration of Mars,” Washington, D.C., 2007.
- [181] C. Weisbin, W. Lincoln, D. Papanastassiou, and M. Coleman, “Mars Biosignature Detection Capabilities: A Method for Objective Comparison of in Situ Measurements and Sample Return,” in *AIAA Space 2013*, 2013.
- [182] W. J. O’Neill and C. Cazaux, “The Mars Sample Return Project,” *Acta Astronautica*, vol. 47, no. 2–9, pp. 453–465, 2000.
- [183] R. Mattingly, S. Matousek, and R. Gershman, “Mars Sample Return - Studies for a Fresh Look,” in *2002 IEEE Aerospace Conference*, 2002.
- [184] R. Mattingly, S. Matousek, and F. Jordan, “Mars Sample Return, Updated to a Groundbreaking Approach,” in *2003 IEEE Aerospace Conference*, 2003.
- [185] iMars Working Group, “Preliminary Planning for an International Mars Sample Return Mission,” 2008.
- [186] MEPAG 2-Rover International Science Analysis Group (2R-iSAG), “Two Rovers to the Same Site on Mars, 2018: Possibilities for Cooperative Science,” *Astrobiology*, vol. 10, no. 7, pp. 663–685, 2010.
- [187] R. Mattingly and L. May, “Mars Sample Return as a Campaign,” in *2011 IEEE Aerospace Conference*, 2011.
- [188] Committee on the Review of Planetary Protection Requirements for Mars Sample Return Missions, “Assessment of Planetary Protection Requirements for Mars Sample Return missions,” Washington, D.C., 2009.
- [189] N. J. Strange, A. T. Klesh, C. M. Marrese-Reading, D. Oh, J. K. Ziemer, T. P. McElrath, D. F. Landau, and D. J. Grebow, “Interplanetary Sample Canister for Mars Sample Return,” in *Concepts and Approaches for Mars Exploration Workshop*, 2012.

- [190] N. J. Strange, R. Merrill, D. F. Landau, B. Drake, B. Brophy, and R. Hoffer, "Human mission to Phobos and Deimos using combined chemical and solar electric propulsion," in *47th Joint Propulsion Conference*, 2011.

# Appendix A

## ROVER MASS MODELING

A MATLAB<sup>®</sup> model for calculating the mass, power and dimensional requirements of rovers on the Moon or Mars, based on some initial inputs, was developed. This appendix, which is adapted from a report for a NASA Phase II STTR, contract NNX10CB56C, presents the assumptions and sub-system level modeling involved in the construction of this model.

### A.1 Assumptions

A set of high-level assumptions are made in order to reduce the number of design variables and to simplify the rover model. Additional assumptions are made on the subsystem level and are documented in the appropriate sections of this document.

#### A.1.1 Subsystem Interactions

The model consists of a master script that calls each subsystem's module in sequence. The order in which these modules are run, as well as the flow of information between subsystems is shown graphically in Figure 83. Table 47 gives the list of variables involved in the program.

<b>Comm</b>									
	<b>Chassis</b>								
		<b>Thermal</b>							
			<b>Wheels</b>						
				<b>Steering</b>					
					<b>Terrain</b>				
						<b>Drive</b>			
							<b>Power</b>		
								<b>Dimensions</b>	
									<b>Suspension</b>

Figure 83: N<sup>2</sup> diagram showing subsystem interactions

**Table 47. List of all variables used in the master script**

<b>Name</b>	<b>Units</b>	<b>Description</b>
sortieDays	days	Time of continuous operation before rover is refueled or recharged
Planet		'moon' or 'Mars'
Csize	[m m m]	Crew station size (length, width, height)
commNavMass	Kg	Mass of communication/navigation mass
Pcomm	W	Power needed for comm/nav
nWheels		Number of wheels in rover
chassisFrameLoadMass	Kg	Mass supported by chassis frame
chassisMaterial		Material of chassis frame
chassisFrameMass	Kg	Mass of chassis frame
wheelBase	M	Size of wheel base
track	m	tread of rover
chassisData		additional data of chassis (such as cross section dimensions, etc.)
thermalMass	kg	mass of thermal management components (insulation blankets, radiators, etc.)
wheelLoad	N	load carried by each wheel
sinkage	%	% of wheel diameter that sinks in the regolith
obstacleHeight	m	max height of obstacle that rover can drive over
wheelDia	m	diameter of wheel
wheelWidth	m	width of wheel
wheelMass	kg	mass of wheel
nSteeredWheels		# of steered wheels in the rover
sprungMass	kg	mass supported by wheels and suspension
steeringMass	kg	mass of steering system
turningRad	m	turning radius of rover
fenderMaterial		material of fenders
fenderMass	kg	mass of fenders
wheelSlip	%	slip of wheels (% difference between rovers speed and wheel drive shaft speed)
DP	N	drawbar pull
slope	deg	gradeability of rover
soilR	N	motion resistance due to soil, such as compaction resistance, etc.
gradeR	N	motion resistance due to gravity when rover is on slope
speed	km/hr	max speed of rover on level terrain
driveType		type of drive system ('driven wheel', 'central')
motorType		type of motor('DCbrush', 'DCbrushless', 'AC')
slopeFraction	%	fraction of sortieDays time when rover is traversing slopes
levelPower	W	power needed for driving on level terrain
slopePower	W	power needed for driving on slope
levelEnergy	W-hr	energy consumed while driving on level terrain
slopeEnergy	W-hr	energy consumed while driving on slopes
driveMass	kg	mass of drive system
motorData		data about motor specs (torque, power, etc.)

Psource		kind of power source ('solar', 'fuelcell', 'battery')
PsourceType		type of power source ('Si' or 'Li-Ion', etc.)
powerMass	kg	mass of power system
PowerSize	L/m^2	volume of batteries, or area of solar panels
P all	W	
E all	W-hr	
overallLength	m	total length of rover
overallWidth	m	total width of rover
overallHeight	m	total height of rover
suspensionMass	kg	mass of suspension system
payload	kg	total payload carried by rover
PRdata		data structure of all specs of planetary rover

## A.2 Subsystems

The model consists of 10 subsystems, as well as a payload sub-system. Each of these sub-systems is modeled in a separate module, which is called by the master program. The following section details the design process and assumptions made in each sub-system.

### A.2.1 Chassis Module

Table 48. Inputs and outputs of chassis module

Inputs [units]	Description
nWheels	# of wheels in rover
frameLoadMass [kg]	total mass to be supported by chassis frame
material	material to be used for chassis frame
gplanet [m/s <sup>2</sup> ]	g of planet on which rover is used
Outputs [units]	Description
chassisFrameMass [kg]	mass of ladder frame chassis
wheelbase [m]	rover wheel base
track [m]	rover track/tread
chassisData.h [m]	height of chassis frame square cross-section
chassisData.t [m]	thickness of chassis frame square cross-section
chassisData.material	material as specified in the input

The chassis is modeled as a simple ladder frame, with a square cross-section, and a tubular chassis. The wheelbase and track are determined based on empirical data from existing vehicles, using the equations shown below.

$$wheelBase = c\_base * wheelDia$$

$$track = c\_track * wheelBase$$

Equation 41

Using data from existing vehicles,  $c_{base}$  and  $c_{track}$  were estimated to be 4.2 and 1, respectively.

The thickness and height of the chassis square cross-section are determined by using a simple model of a beam in bending. The model assumes that each side-rail of the frame supports exactly half of the loaded weight of the rover. It is further assumed that the load is evenly distributed and that the side rail is supported by two reaction forces due to the wheels attached to it. The deflection of the beam is fixed based on requirements for race-car chassis. Given the known distributed load and length of beam, the values for the thickness and height of the cross-section are calculated. Note that this loading arrangement is used even if the number of wheels is modified. In that case, the estimate will be a conservative upper bound since, in reality, there will be two or more reaction forces on the beam for six or more wheels.

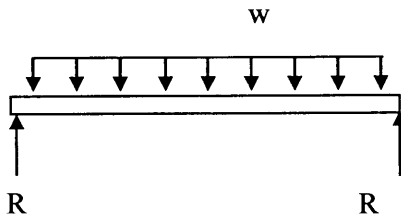


Figure 84. Load modeling of chassis side rail

### A.2.2. Thermal Module

The thermal subsystem was designed based on the Warm Electronics Box (WEB) concept used on the Mars Exploration Rovers (MERs). All sensitive electronics and components required to be maintained within a tight temperature tolerance are placed inside the WEB. The rest of the components are assumed to be able to operate and survive within the range of temperatures present on the lunar surface (120 K to 400 K). Based on the similar design of the MERs [1], the WEB is assumed to have a volume of  $0.17 \text{ m}^3$ , and is assumed to be surrounded by walls consisting of a composite structure of silica aerogel between two thin aluminum sheets with an assumed thermal conductivity of  $0.01 \text{ W/m/K}$ .

For a design using solar arrays and fuel cells, active heating is required to survive the lunar night. The system was sized using radioisotope heater units (RHUs) that each produce 1W of heat and have a mass of 0.04 kg [2]. These units are assumed to be used with variable conductance heat pipes in order to transfer the heat to the WEB as needed during lunar nights. During the lunar day, the thermal system is required to radiate heat from the electronics in the WEB.

### A.2.3 Wheels Dimensioning Module

Table 49. Inputs and outputs of wheel dimensioning module

Inputs [units]	Description
obstacleHeight [m]	max height of obstacle that rover can cross
wheelLoad [N]	load supported by one wheel
sinkage [%]	fraction of wheel diameter that is allowed to sink
planet	planetary object on which rover is used (Moon or Mars)
Outputs [units]	Description
wheelDia [m]	diameter of wheel
wheelWidth [m]	width of wheel
wheelMass [kg]	mass of wheel

This module is used to size the wheels for the rover. The diameter and width of the wheels are sized for a specified sinkage and soil bearing pressure. Typically, the sinkage is computed once the wheel dimensions are known (i.e. for a wheel of given diameter and width, its sinkage is computed based on the load it supports). However, since there are more unknowns than equations available, an assumption has to be made. The sinkage was therefore fixed as a percentage of the wheel diameter. In the current model, it is assumed to be 4%, which is a typical value quoted in literature. This means that a wheel with a diameter of 50 cm is allowed to sink up to 2 cm into a soft surface. In Figure 85, the sinkage of the wheel  $z_w$  is shown along with the chord length  $l'$  of the wheel and contact patch width  $b$  that is in contact with the soil due to sinkage. It is assumed that the width of the contact patch is the same as the width of the wheel (hence  $b_w$  and  $b$  in the schematic are the same).

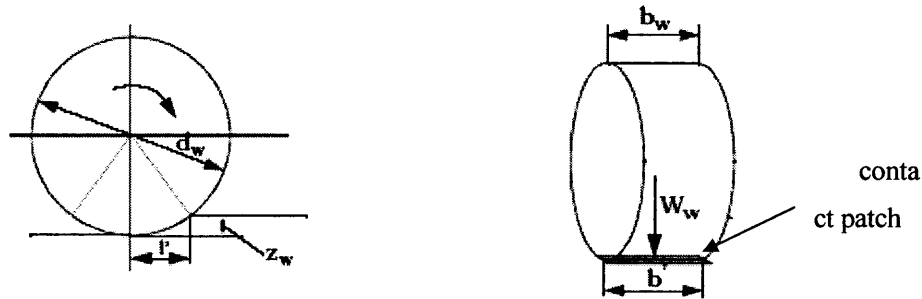


Figure 85. Schematics of wheel sinkage in soft terrain

The following three equations were used for sizing the wheels:

$$p = \left[ \frac{k_c}{b} + k_\phi \right] z^n$$

$$z = \left( \frac{3W}{(3-n)(k_c + bk_\phi)\sqrt{D}} \right)^{\frac{2}{2n+1}}$$

$$z = \alpha D$$

**Equation 42**

Where:

- p: soil pressure, [N/m<sup>2</sup>]
- k<sub>c</sub>: cohesive modulus of deformation, [N/m<sup>n+1</sup>]
- k<sub>φ</sub>: frictional modulus of deformation, [N/m<sup>n+2</sup>]
- n: sinkage coefficient, [-]
- z: sinkage [m]
- W: wheel load [N]
- D: wheel diameter [m]
- b: wheel width [m]

Equation 43 corresponds to equations 2.46 and 2.96 in [4]. The values of the soil constants for the Moon and Mars are obtained from [3] and [5].

Using Equation 43, the known quantities are: *p* (set to soil bearing pressure), the constant  $\alpha$  (the ‘sinkage’ variable in the model, and NOT the sinkage in meters, but the fraction of the wheel diameter that sinks) set to 4%, and *W* (the wheel load). The unknowns are then *z*, *D* and *b* (i.e. sinkage in meters, wheel diameter and width). After simplification and solving for *D*, the following relationship is obtained:

$$D^{n+1} + D^n \frac{3Wk_\phi}{(3-n)\alpha^{0.5}k_cp} - \frac{3W}{(3-n)k_c\alpha^{n+0.5}} = 0$$

**Equation 43**

If *n* is assumed to be equal to 1 or 0, then the above equation becomes a polynomial of *D*. The model finds the roots of this polynomial to predict the wheel diameter required. However, *n* is restricted for the case of *n* = 0 or 1, due to the fact that the model breaks down as *n* increases. For Moon and Mars, *n* is set to 1.

Once the diameter is determined, the obstacle height is used to set the final value. The diameter must be at least twice the height of obstacle required to be traversed. Consequently, if the value from Equation 39 is lower than the maximum obstacle height requirement, then it is increased. The width of the wheel is then determined from Equation 43.

The wheel mass is obtained from an empirical model based on data of light race car wheels, as shown in Equation 44.

$$wheelMass = 186(wheelRadius)^{2.81}(wheelWidth)^{0.4} 0.7$$

**Equation 44**



A factor of 0.7 is applied to account for the fact that wheels used for planetary rovers will not be solid wheels as those used in race cars. Even with this factor the mass estimates are slightly high when compared with data of the Mars roving vehicles.

## A.2.4 Steering Module

Table 50. Inputs and outputs of steering module

Inputs [units]	Description
nSteeredWheels	# of wheels that are steerable
sprungMass	sprung mass of rover
wheelbase [m]	length of wheel base
track [m]	track of rover
Outputs [units]	Description
mass	steering system total mass
turningRadius [m]	turning radius of rover

The steering module assumes Ackerman steering for the rover. It models the mass of a steering motor required for each set of wheels that are steerable, along with some additional mass for links etc. It is assumed that the planetary rovers will have steer-by-wire systems (with no steering columns, rack and pinion assemblies etc.).

The motor power is estimated as:

$$motorPower = [960 / (1600 * 0.8)] * sprungMass \quad \text{Equation 45}$$

The motor power is then used to obtain the mass of the motor from an empirical model based on masses of currently available motors and motor types. DC brushless motors are assumed to be used in this case, as is typical for this application.

The turning radius is based on the initial assumption that only one axle is steerable. To account for both front and back steering, which is typically used on rovers, a factor is then added to reduce the value of the turning radius. The maximum wheel turn angle is assumed to be  $50^\circ$ , which was the requirement for MER. For Ackerman steering the following equations hold: [6]

$$\begin{aligned} \cot \alpha &= \frac{track}{wheelBase} + \cot \beta \\ \sin \alpha &= \frac{wheelBase}{R_{turn}} \end{aligned} \quad \text{Equation 46}$$

Where:

$R_{turn}$ : turning radius [m]  
 $\beta$  : wheel turn angle [deg]

Since the wheelbase, the track, and the maximum wheel turn angles are known, the maximum turn radius is computed as follows in the model:

$$R_{turn} = 0.8 * \frac{wheelBase}{\sin\left(\cot^{-1}\left(\frac{track}{wheelBase} + \cot \beta\right)\right)} \quad \text{Equation 47}$$

## A.2.5 Vehicle-Terrain Interaction Module

Table 51. Inputs and outputs of vehicle-terrain interaction module

Inputs [units]	Description
wheelDia [m]	diameter of wheel
wheelWidth [m]	width of wheel
wheelLoad [N]	load supported by one wheel
wheelSlip [%]	wheel slip
sinkage [%]	fraction of wheel diameter that is allowed to sink
planet	planet on which rover is used (Moon or Mars)
Outputs [units]	Description
DP [N]	drawbar pull per wheel
slope [deg]	slope that the rover can climb
Rc [N]	compaction resistance per wheel
Rb [N]	bulldozing resistance per wheel
H [N]	soil thrust (tractive effort) per wheel
z [m]	wheel sinkage

This module computes the motion resistances experienced by the rover. The wheels are assumed to be rigid (no pneumatic tires). Three kinds of resistances are computed which significantly affect motion of a rigid wheel on soft terrain: compaction resistance, bulldozing resistance, and rolling resistance.

*Compaction resistance* is due to the compaction work done by the wheels per unit length in pressing the ground to a depth of its sinkage. Loss of soil thrust in unprepared terrains is primarily due to the compaction resistance. It is given by: [4]

$$R_c = \frac{z^{n+1}}{n+1} (k_c + bk_\phi) \quad \text{Equation 48}$$

where  $R_c$  is compaction resistance [N], and the other variables were defined in Section 0.

*Bulldozing resistance* is developed when a substantial soil mass is displaced by a wheel. This type of resistance is common when a wheel compresses the surface layers of the soil and pushes the soil fore and aft of the tire. It is worse for wheels that are thick [7], [8].

The bulldozing resistance is given as follows [8]:

$$K_{pc} = \left( N_c - \frac{2}{3} \tan \phi \right) (\cos \phi)^2$$

$$K_{py} = \left( 3 \frac{N_\gamma}{\tan \phi} + 1 \right) (\cos \phi)^2$$

$$R_b = b \left( 0.67 cz K_{pc} + 0.5 z^2 \gamma_s K_{py} \right)$$

**Equation 49**

Where:

$R_b$ : bulldozing resistance [N]  
 $b$ : wheel width [m]  
 $\phi$ : soil internal friction angle [deg]  
 $c$ : cohesion [N/m<sup>2</sup>]  
 $z$ : sinkage [m]  
 $\gamma_s$ : specific soil weight [N/m<sup>3</sup>]

*Rolling resistance* captures the combined effect of various resistances to motion, such as scrubbing at the wheel-soil interface, deflection of tread elements, etc. It is given by:

$$R_r = \mu_r W$$

**Equation 50**

Where:

$R_r$ : rolling resistance [N]  
 $\mu_r$ : coefficient of rolling resistance  
 $W$ : load per wheel [N]

The rolling resistance coefficient is assumed to be 0.1 based, which corresponds to the works case scenario for medium hard soil, according to [4]. Estimates for rovers varied from 0.03 to 1 in literature, so the worst case scenario was taken.

The *soil thrust* (or traction) is given as:

$$H = \left( Ac + W \tan \phi \right) \left( 1 - \frac{K}{sL} \left( 1 - e^{-\frac{sL}{K}} \right) \right)$$

**Equation 51**

Where:

$A$ : area of contact patch [m<sup>2</sup>]  
 $K$ : coefficient of soil slip [m]  
 $s$ : wheel slip [%]  
 $L$ : wheel chord length [m]

The wheel chord ( $l'$  in Figure 85) is computed by:

$$L = \sqrt{(D - z)z}$$

**Equation 52**

Where:

$D$ : wheel diameter [m]  
 $z$ : sinkage [m]

The contact patch (see Figure 85) area  $A$  is  $bL$ , with the assumption that the width of the contact path is equal to wheel width. The wheel slip,  $s$ , is defined to be the percent difference between speed of wheel and speed of the rover, as shown in the equation below. A slip of 35% is assumed in the model.

$$s = \left(1 - \frac{V}{r\omega}\right)100 \quad \text{Equation 53}$$

Where:

$V$ : linear speed of wheel center [m/s]

$r$ : effective rolling radius [m]

$\omega$ : angular speed of wheel [rad/s]

The *drawbar pull*,  $DP$ , is defined as the force available at the draw bar. It is the difference between the soil thrust developed by the rover and the total resisting force on the rover. It represents the ability of a rover to pull or push additional machinery/implements etc. The  $DP$  per wheel is found by subtracting the sum of all resistances acting on the wheel from the soil thrust of the wheel [4]:

$$DP = H - \sum R \quad \text{Equation 54}$$

$$DP = H - R_c - R_b - R_r$$

The *gradeability* of a rover can be approximated by the ratio between the drawbar pull and wheel load as shown in Equation 55. This formulation can be used as a first order approximation.

$$slope = \tan^{-1}\left(\frac{DP}{W}\right) \quad \text{Equation 55}$$

The *gravitational resistance*,  $R_{grade}$ , is the resistance encountered by the rover when climbing a slope of angle  $\theta$ . It is given by:

$$R_{grade} = W(\mu_r \cos \theta + \sin \theta) \quad \text{Equation 56}$$

Note that this  $R_{grade}$  includes the rolling resistance as well. The normal forces on the wheels change when the rover is on a slope; therefore the rolling resistance component is different and is given by the  $W\mu_r \cos \theta$  term. The term  $W\sin \theta$  is purely due to the force of gravity.

## A.2.6 Drive System Module

Table 52. Inputs and outputs of drive system module

Inputs [units]	Description
driveType	type of drive system, 'drivenWheel', or 'central'
motorType	'AC', 'DCbrush', or 'DCbrushless'
soilR [N]	load supported by one wheel
R <sub>r</sub> [N]	wheel slip
grade [N]	fraction of wheel diameter that is allowed to sink
wheelDia [m]	diameter of wheel
wheelSlip [%]	
wheelbase [m]	
track [m]	
nWheels	# of wheels in rover
speed [km/hr]	speed of rover
mobilityDuration [hr]	amount of time rover is moving
slopeFraction	fraction of total moving time during which rover traverses slopes
gplanet [m/s <sup>2</sup> ]	gravitational acceleration of planet
Inputs [units]	Description
levelPower [W]	power required for level motion
slopePower [W]	power required for motion on slope
levelEnergy [W-hr]	energy expended during level motion
slopeEnergy [W-hr]	energy expended during motion on slopes
driveSysMass [kg]	total mass of drive system including motor, controller, drive shaft etc.
motorData.torque [Nm]	torque of drive motor
motorData.power [W]	power of drive motor
motorData.mass [kg]	mass of drive motor

This module models two kinds of drive systems: 'drivenWheel' and 'central'. In the first type, each wheel is driven individually by its own motor, as was the case in the Apollo LRV. In the second type it is assumed that one central motor drives the rover, and the drive system includes a drive shaft.

An empirical model for determining mass of motor (based on its power and type: AC, DCbrush, or DCbrushless) and its controller is used to obtain mass estimates.

For the *driven wheel drive system*, the required torque per wheel for moving the rover on a level surface is determined by:

$$T_{level} = R_{soil} D/2 \quad \text{Equation 57}$$

and for moving on a slope by:

$$T_{slope} = (R_{soil} + R_{grade} - R_r) D/2 \quad \text{Equation 58}$$

where  $R_r$  is subtracted since  $R_{grade}$  includes the rolling resistance on a slope.

Motor sizing is done separately for the two types of drive systems. For the ‘drivenWheel’ case, the efficiency  $\eta$  is estimated to be 98%, and harmonic drives with 80:1 ratio (similar to the ones used on the LRV) are considered. The motor power is then estimated as:

$$P_{motor} = \frac{v R_{soil}}{(1-s)\eta} \quad \text{Equation 59}$$

where  $v$  [m/s] is the top speed of the rover on level surface. The motor power is sized for full speed drive on flat surface and it is just assumed that the speed on a slope will be lower.

The torque required from the motor is sized for the worst case scenario (since the motor must be able to supply the maximum torque needed for traverse) and is given by:

$$T_{motor} = \frac{\max(T_{level}, T_{slope})}{i_g \eta} c \quad \text{Equation 60}$$

where  $i_g$  is the speed reduction ratio of the harmonic drive.

The total drive system mass for the rover is the sum of the motor mass, the harmonic drive mass and the motor controller mass, multiplied with number of wheels in the rover (since each wheel has separate motor, harmonic drive and controller).

For the *central drive system*, an efficiency of 95% and a gear ratio of 30:1 are assumed. The power required for the motor is obtained by:

$$P_{motor} = N_{wheels} \frac{v R_{soil}}{(1-s)\eta} \quad \text{Equation 61}$$

where  $N_{wheels}$  is the number of wheels in the rover. Note that  $R_{soil}$  is the total resistance experienced by a single wheels. The torque is sized as:

$$T_{motor} = N_{wheels} \frac{\max(T_{level}, T_{slope})}{i_g \eta} \quad \text{Equation 62}$$

The mass of the gearbox is obtained by an empirical model given in [9]. The drive shaft is a circular cross-section hollow shaft assumed to be made of carbon-fiber reinforced polymer. The thickness is assumed to be 3 mm and the length to be 90% the length of the wheel base. The diameter of the shaft is determined based on the torque it needs to transmit (which is the torque delivered to wheels and is given by  $i_g T_{motor}$ ) and a safety factor of 4 for the shear strength. The axle shafts are also sized similarly with the assumption that that their length is equal to the rover track and need to withstand the wheel torque. The total mass of the drive system is the mass of the motor, the motor controller, the drive shaft and the axle shafts.

The total power required for level motion at top speed is given by:

$$P_{level} = P_{motor}F,$$

where :

$$F = N_{wheels} \text{ (for drivenWheel)}$$

$$F = 1 \text{ (for central)}$$

**Equation 63**

The total power required for traversing a slope is obtained by assuming that top speed is half of level speed:

$$P_{slope} = N_{wheels} \frac{v(R_{soil} + R_{grade} - R_r)}{2}$$

**Equation 64**

The slope and power energy requirement is then computed as follows:

$$E_{slope} = P_{slope}t_{slope}$$

$$E_{level} = P_{level}(t_{mobility} - t_{slope})$$

**Equation 65**

In this equation,  $t_{slope}$  is the total time [hrs] spent in traversing slopes and will be adjusted using the planetary terrain model.  $t_{mobility}$  is the total time the rover is moving and is computed by dividing rover range with speed. The latter can also be adjusted using SEXTANT, once solar charging “breaks” are established, as explained in Chapter 4.

## A.2.7 Power System Module

**Table 53. Inputs and outputs of power system module**

<b>Inputs [units]</b>	<b>Description</b>
contP [W]	continuous power needed during operation of rover
levelP [W]	power needed for level driving
slopeP [W]	power needed for traversing slope
actP [W]	array input, power needed for exploration activities
contE [W-hr]	continuous energy needed duration operation of rover
levelE [W-hr]	energy needed for level driving
slopeE [W-hr]	energy needed for traversing slope
actE [W-hr]	array input, energy needed for exploration activities
TotalETime [hr]	Total time required for energy calculation
planet	
Source [-]	‘batteries’, ‘FuelCells’, ‘solar’ etc.
Type [-]	type of source e.g. ‘Li-Ion’, ‘AgZn’ or ‘InP’, ‘Si’ etc.
powercase [-]	1 or 2.
gplanet [m/s <sup>2</sup> ]	gravitational acceleration of planet
<b>Outputs [units]</b>	<b>Description</b>
PowerMass [kg]	array, [primarysourceMass, secondarySourceMass]
PowerSize [ ]	[m <sup>2</sup> or L etc.], array
P all [W]	array, [PrimarySourcePower, SecondarySourcePower]
E all [W-hr]	array, [PrimarySourceEnergy, SecondarySourceEnergy]

This module computes the mass of the power system given all the energy and power requirements of the rover. In addition to power required for driving, other subsystems such as payload require extra power.

There can be a single power source, or it can be of two different kinds (such as solar and batteries). The total energy is first computed as the sum of contE, levelE, slopeE, and actE. The average power,  $P_{avg}$ , is obtained by dividing total energy with TotalETime. If only a single source is specified, then the power is calculated as the maximum power load required to provide continuous power along with powering the drive of the rover or a high power activity. If two power sources are used, then computation is done in one of two ways depending on the 'powerCase' variable. If 'powerCase' equal to 1, the first source provides average power, and second source provides  $P_{peak}-P_{avg}$  and  $E_{total}-E_{avg}$ .  $P_{peak}$  is the max power among contP, levelP, slopeP and actP. If 'powerCase' is equal to 2, then the first source powers the communication and navigation systems and the mobility system power and energy, while the second source provides extra power for slope mobility and payload activities.

The power module enables the user to choose from a range of different types of solar arrays, batteries and solar cells, thus allowing for the evaluation of the effect of technology choice on the mass of the system.

### **A.2.8 Suspension Module**

The suspension system is modeled as a simple percentage of the rover mass. The sprung mass of the rover is obtained and the suspension is assumed to be 12% of that mass [4].

### **A.2.9 Payload Module**

The payload system includes the information about all the possible instrumentation a rover could carry for an exploration mission on the Moon or Mars. Each component can then be selected to be included in a rover design as required. Parameters for the tools were taken from literature on the design of payloads for future robotic explorer missions to Mars [14].

### **A.2.10 Communications**

A full link budget analysis is performed in the communications subsystem module in order to evaluate the power and mass of the communication system. The module allows the user to pick from a range of different communication frequencies (UHF, Ka-Band, X-band) and from different types of relays (rover-to-rover, direct to Earth, via a low- or high- altitude orbiter).



### A.2.11 Navigation Subsystem

The avionics subsystem was not seen as having any driving requirements on the system. While no in-depth analysis was performed on these subsystems, values were borrowed from previous similar designs to provide overall mass and power values for the subsystems.

### A.3 Benchmarking

In order to verify the fidelity of a modeling tool, two detailed benchmarking activities were conducted. Since there is a lack of lunar rovers, the results of the model were compared with the Mars Exploration Rover (MER) and the Mars Science Laboratory (MSL).

In the first case, the MER was modeled with 6 wheels, mission duration of 83 sols, speed of 0.08 km/hr, 15.5 kg of science payload, and a solar power system.

Table 54 shows the rover system mass breakdown using the results from the mass modeling tool and the available MER data. MER mass is overestimated by 13%. The largest source of the discrepancy is within the mobility systems, this is because the chassis was modeled for larger ExoMars or MSL-type rovers. The assumed constants used in the terramechanics equations above could therefore be tuned for larger and smaller rovers, if additional data was available.

**Table 54: Benchmarking with MER**

<b>Mass Model [kg]</b>		<b>MER [kg]</b>	
Payload	15.5	Payload	15.5
Comm & Nav	34.0	Comm & Nav	30.0
Chassis	72.0	Mobility	95.5- 113.5*
Fender	5.7		
Wheels	33.8		
Suspension	12.5		
Drive	0.5		
Steering	5.5		
Power	24.0	Power & Thermal	18- 44.0*
Thermal	6.0		
<b>Total Mass</b>	<b>209.5</b>	<b>Total Mass</b>	<b>185.0</b>

For the MSL case, a model with 6 wheels, mission duration of 687 sols, speed of 0.09 km/hr, 100 kg of science payload, and RTG for power system was used. Table 55 shows a rover system mass breakdown table of the result from the mass modeling tool and the MSL. MSL mass is underestimated by 8%. The mass of subsystems for which data exists shows similar values.

**Table 55: Benchmarking with MSL**

<b>Mass Model [kg]</b>		<b>MSL [kg]</b>	
Payload	150.0	Payload	150.0
Comm & Nav	85.0	Comm & Nav	80.0
Chassis	310.3	Mobility	589
Fender	12.1		
Wheels	95.0		
Suspension	73.6		
Drive	1.0		
Steering	19.3		
Power	70.5	Power & Thermal	80
Thermal	10.0		
<b>Total Mass</b>	<b>826.8</b>	<b>Total Mass</b>	<b>899</b>

The tool was also benchmarked against proposed designs in the literature and was found to fall within 15% of them, most of the discrepancies were expected to have come from the lack of data available from published designs. The accuracy of these results is acceptable for the purposes of the tool, and will give a good order of magnitude mass estimate of the rovers within each architectural option.

## A.4 Works Cited

- [1] R. Scammel, "Mars Exploration Rover Technical Data," [Online]. Available: <http://hobbiton.thisside.net/rovermanual/>. [Accessed 1 June 2011].
- [2] NASA, "Discovery AO - Radioisotope Heater Unit (RHU) Information Summary," 2004.
- [3] J. Wong, Theory of ground vehicles, Wiley-Interscience, 2008.
- [4] W. Larson and L. Pranke, Human Spaceflight: Mission Analysis and Design, McGraw-Hill Companies Inc., 1999.
- [5] P. Eckart, The Lunar Base Handbook, McGraw-Hill Primis Custom Publishing, 1999.
- [6] J. Fitch, Motor Truck Engineering Handbook, SAE International, 1994.
- [7] D. Apostolopoulos, Analytical Configuration of Wheeled Robotic Locomotion, 2001.
- [8] M. Bekker, Introduction to Terrain-Vehicle Systems, University of Michigan Press, 1969.
- [9] H. e. a. Naunheimer, Automotive Transmissions: Fundamentals, Selection, Design and Application, Springer, 2010.
- [10] M. Duke, "NASA Mars Exploration Program: Mars 2007 Smart Lander Mission Science Definition Report," 2011. [Online]. Available: <http://www.nature.com/nature/journal/v409/n6819/full/409467a0.html>. [Accessed June 2011].
- [11] P. Berkelman, "Design of a Day/Night Lunar Rover," 1995.
- [12] Spectrolab, "28.3% Ultra Triple Junction (UTJ) Solar Cells," April 2008. [Online]. Available: <http://www.spectrolab.com>. [Accessed 1 June 2011].
- [13] Yardney, "Characteristics of Yardney's Li-Ion Battery," 2007. [Online]. Available: <http://www.yardney.com/lithion/index.html> . [Accessed 1 June 2011].
- [14] N. Luo, "H<sub>2</sub>O<sub>2</sub>-Based Fuel Cells for Space Power Systems," in 3rd International Energy Conversion Engineering Conference, San Francisco, CA., 2005.



# Appendix B

## LOW-THRUST TRAJECTORIES FOR MARS SAMPLE RETURN

### B.1 Summary of Low-Thrust Trajectories and SEP Orbiter Sizing

This appendix presents the baseline trajectories that were used to size SEP orbiters for Mars Sample Return. To first order, the same trajectories can be used for different orbiter dry masses as long as the total thrust is kept constant. The following basic equations on low-thrust demonstrate this correlation:

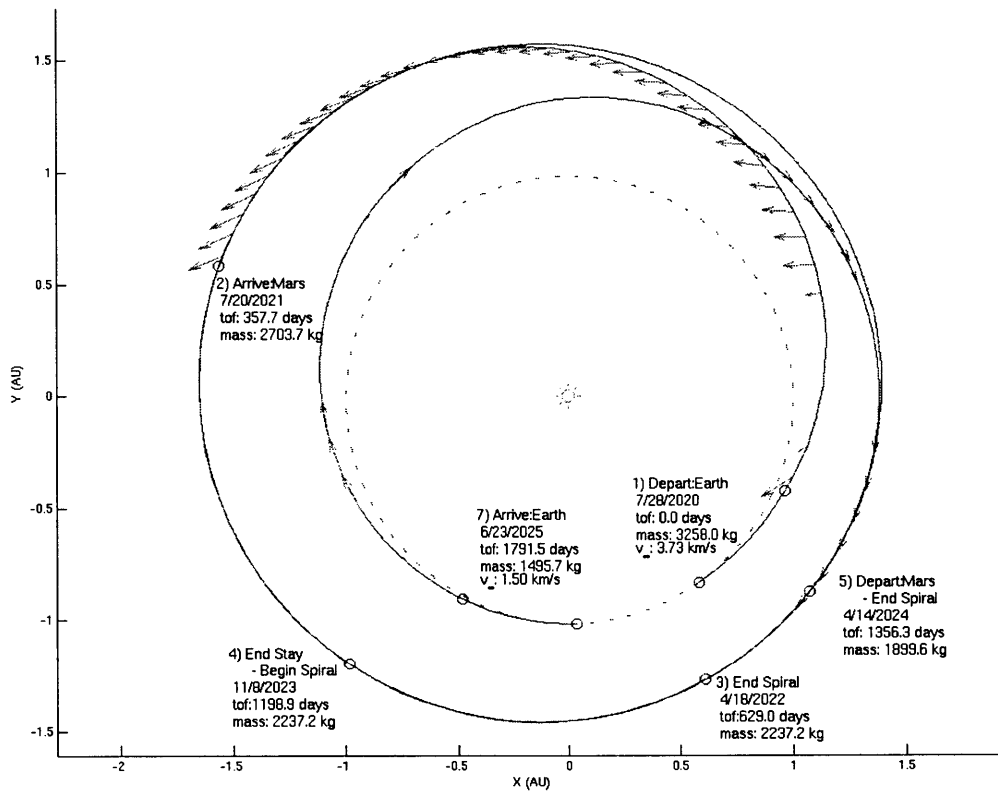
$$\begin{aligned}\dot{m} &= \frac{T}{g \cdot Isp} = \frac{T}{V_e} \\ m \cdot a &= T = \dot{m} \cdot V_e = \dot{m} \cdot g \cdot Isp \\ K &= \frac{1}{2} m V_e^2 \\ P_{jet} &= \frac{dK}{dt} = \frac{1}{2} \cdot \dot{m} \cdot V_e^2 = \frac{1}{2} \cdot \frac{T \cdot V_e^2}{V_e} = \frac{1}{2} \cdot T \cdot V_e = \frac{1}{2} \cdot T \cdot g \cdot Isp \\ P_{jet} &= \eta \cdot P_o \\ \eta \cdot P_o &= \frac{1}{2} \cdot T \cdot g \cdot Isp \\ T &= \frac{2 \cdot \eta \cdot P_o}{g \cdot Isp}\end{aligned}$$

Consequently, the wet mass of SEP orbiters were modeled by picking the trajectory with the right launch date, Mars stay duration and Earth return velocity. Then, using the estimated dry mass (or Earth return mass) of the orbiter (which uses the same parametric model as the orbiters with chemical

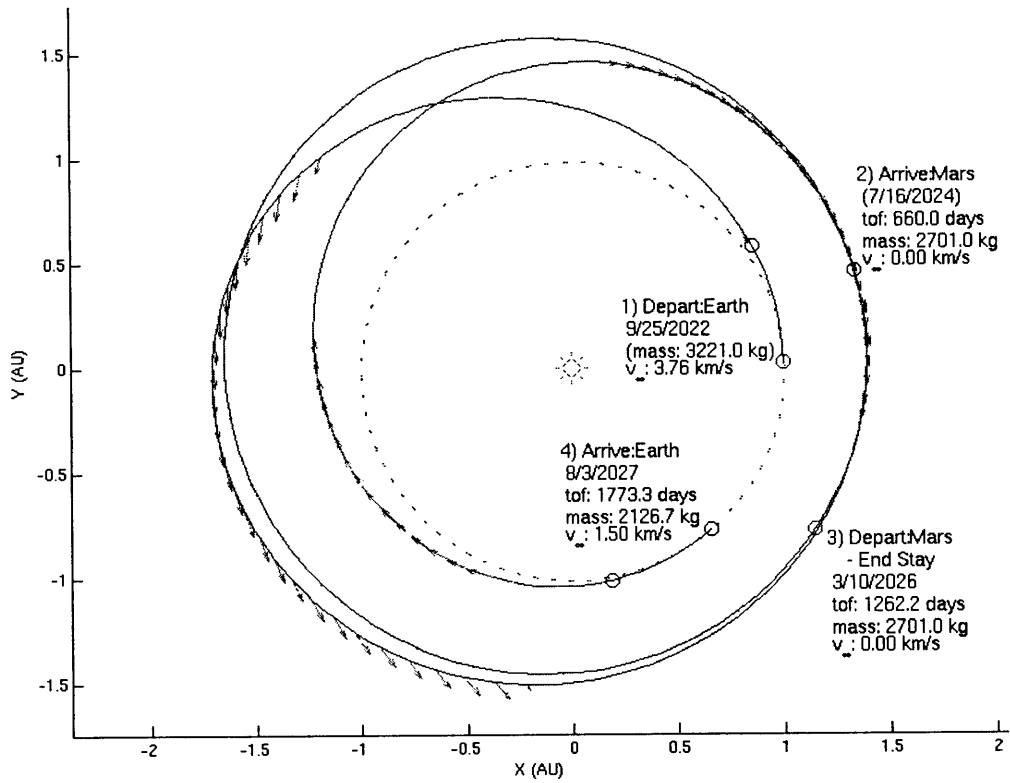
propulsion) and the dry mass of the baseline from the trajectory, the wet mass was calculated by keeping the mass ratios, the power ratio, and thus the thrust, constant. The masses obtained were compared to designs from other studies that had been modeled using more detailed analysis and were found to fall within 20% of these designs.

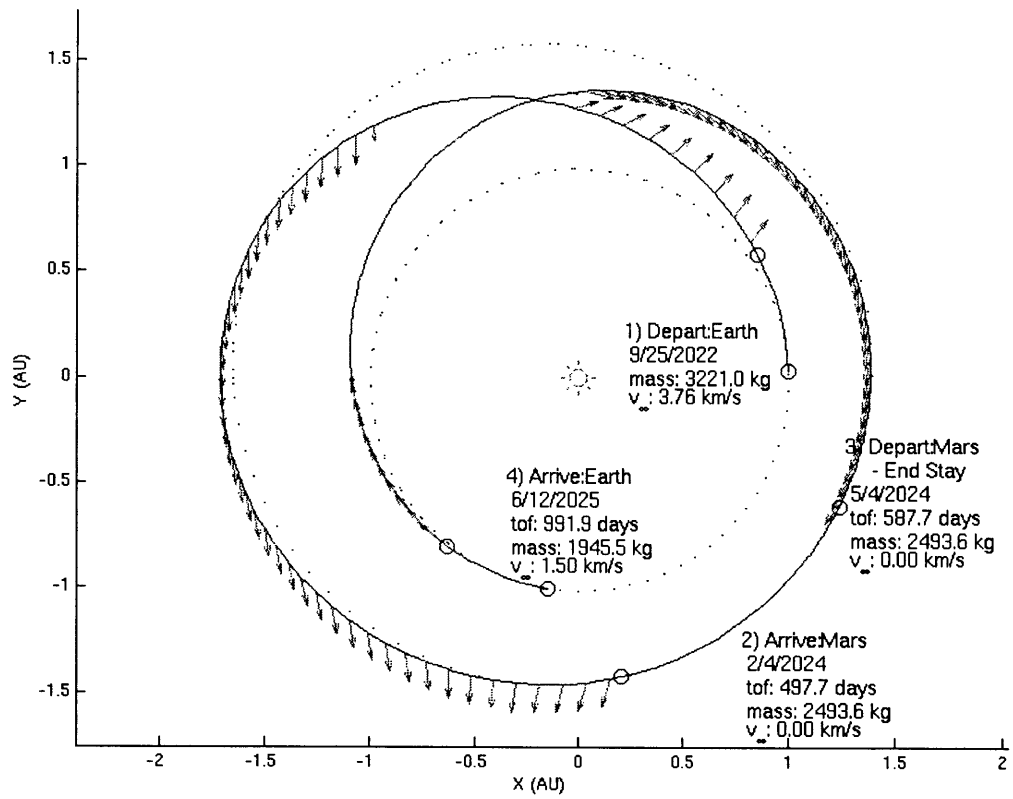
These trajectories were created by Damon Landau and Theresa Kowalkowski based on requirement inputs from the author using a JPL developed tool, MALTO.

## B.2 2020 Trajectories

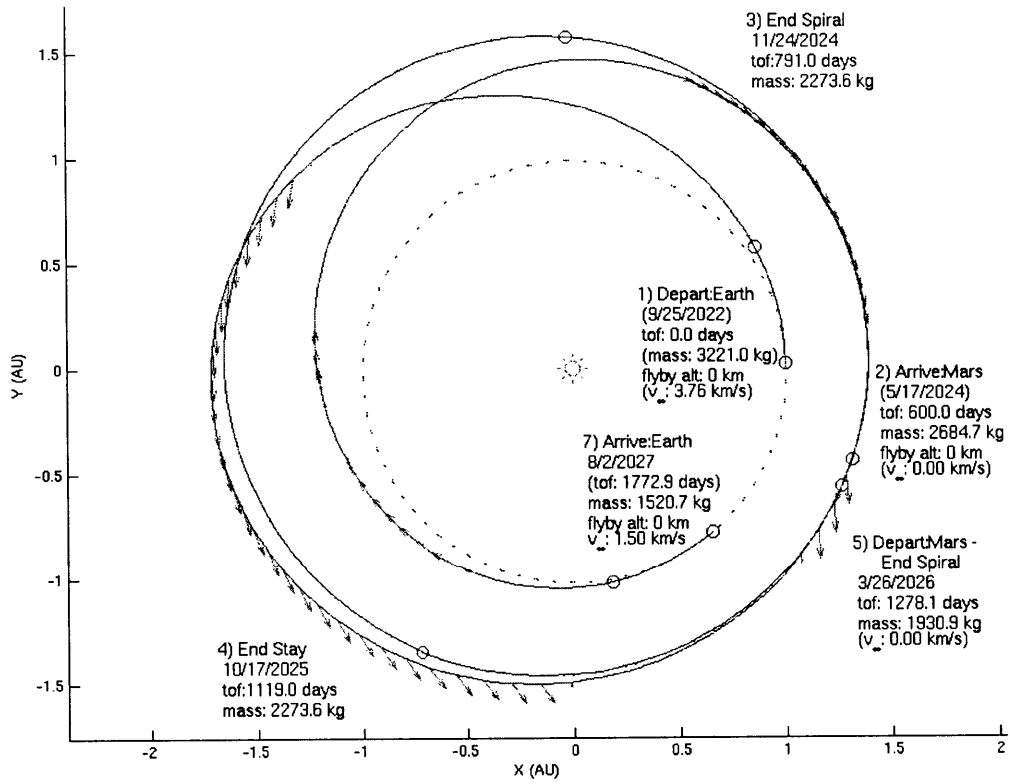


### B.3 2022 Trajectories





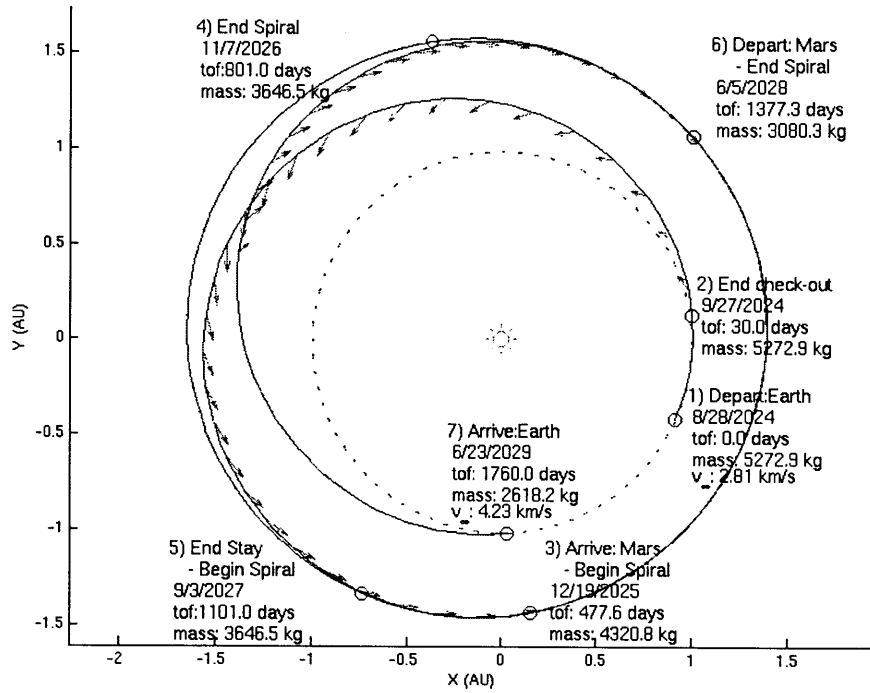




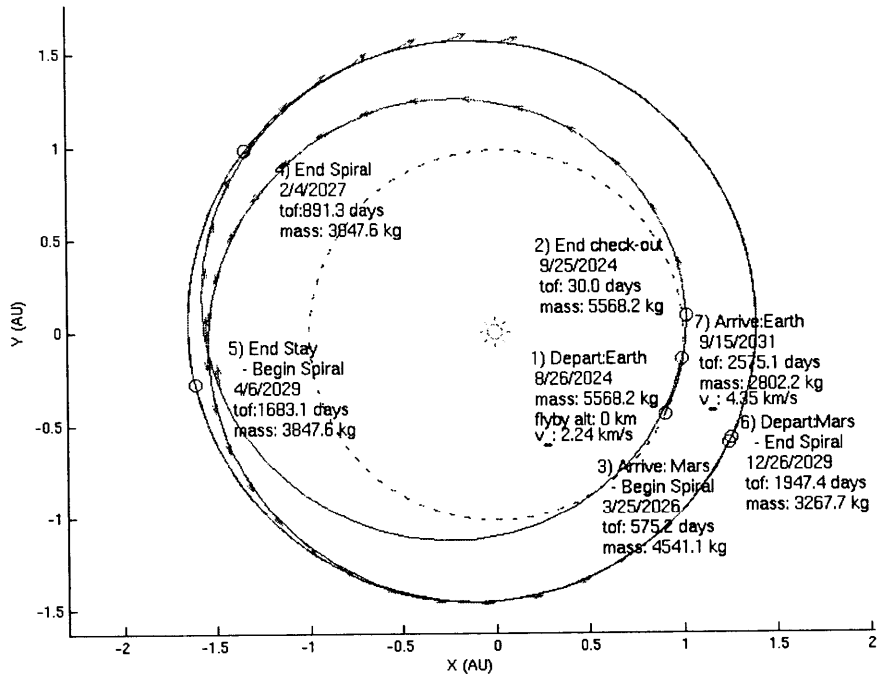
## B.4 2024 Trajectories

### B.4.1 Earth Return

#### B.4.1.1 Short Mars Stay

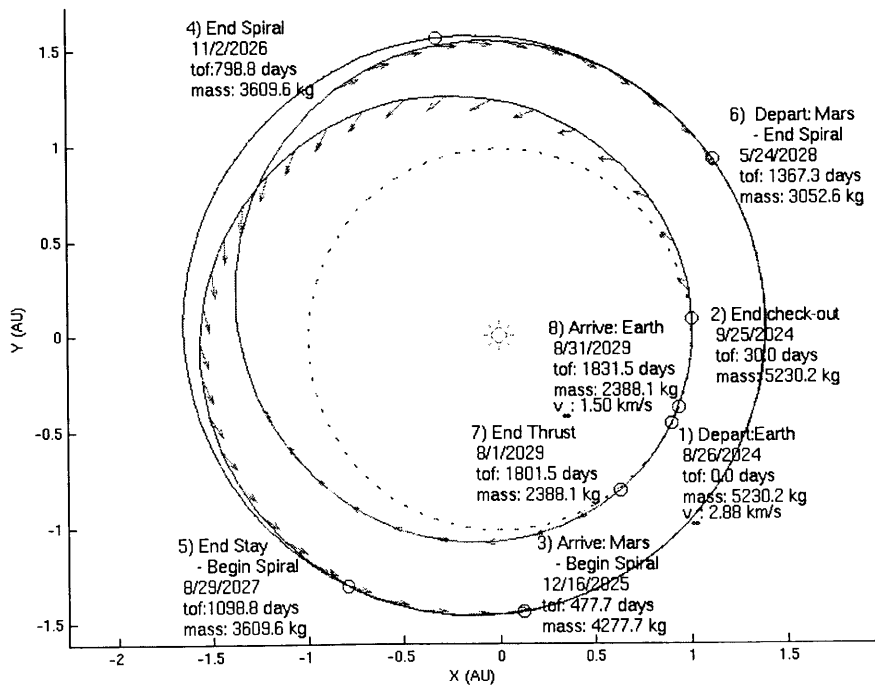


### B.4.1.2 Long Mars Stay

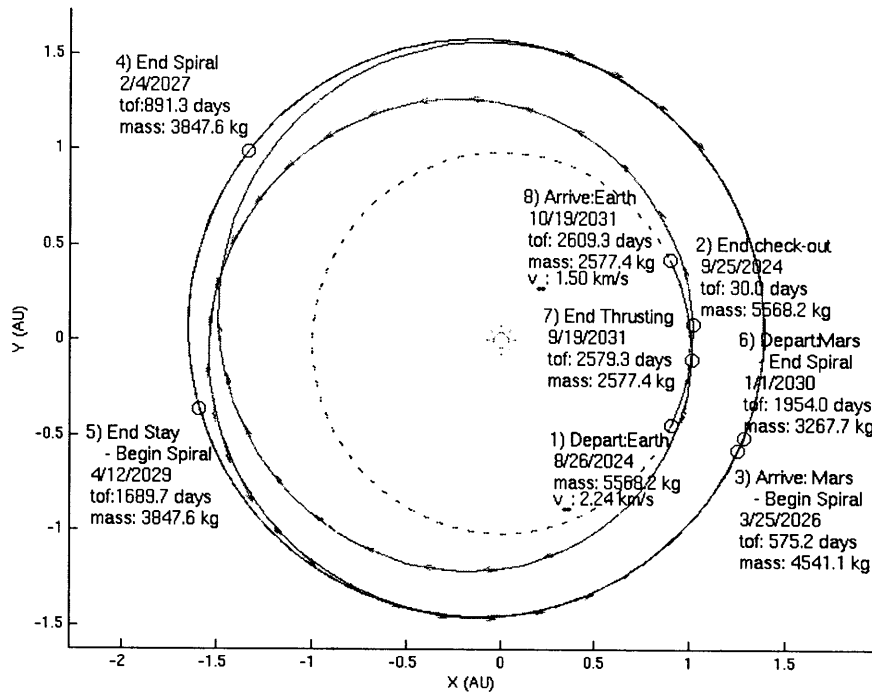


### B.4.2 Lunar Return

#### B.4.2.1 Short Mars Stay



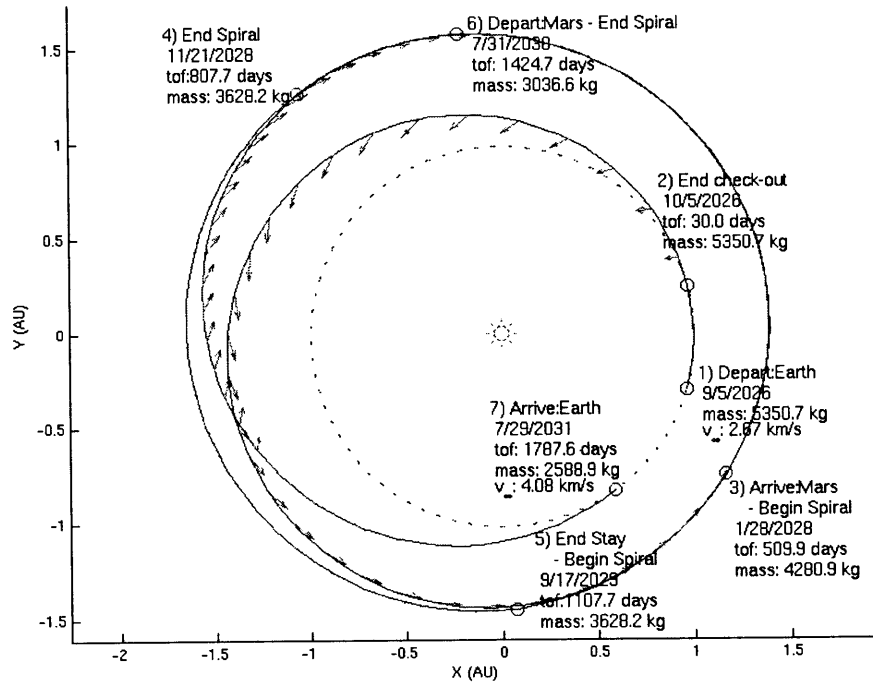
### B.4.2.2 Long Mars Stay



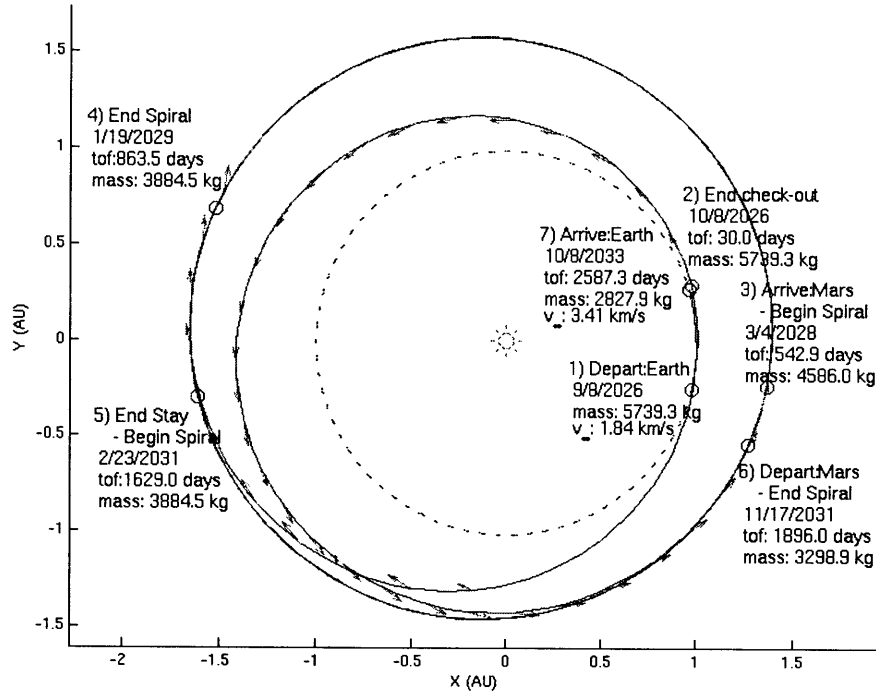
## B.5 2026 Trajectories

### B.5.1 Earth Return

#### B.5.1.1 Short Mars Stay

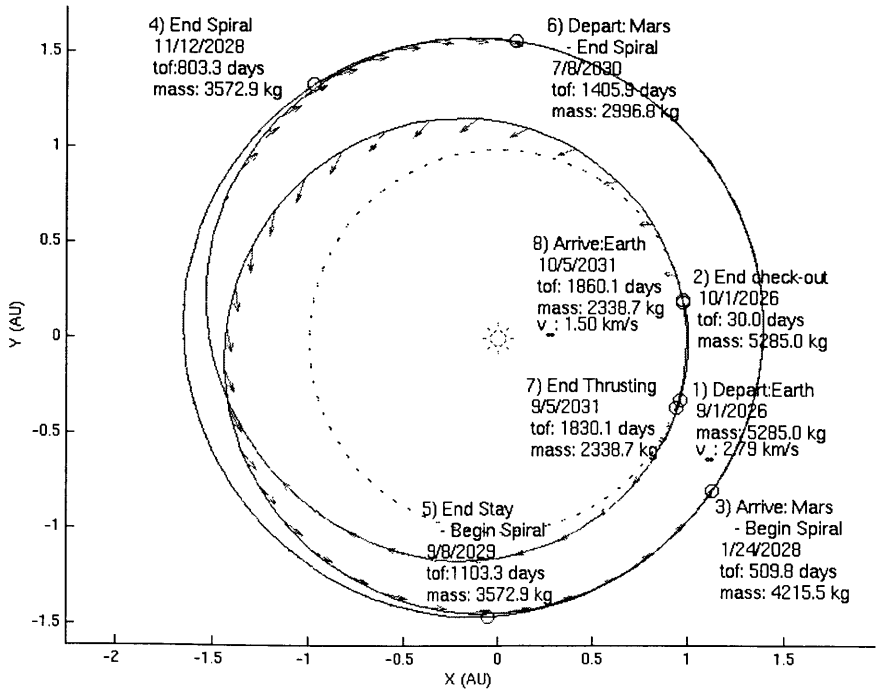


### B.5.1.2 Long Mars Stay

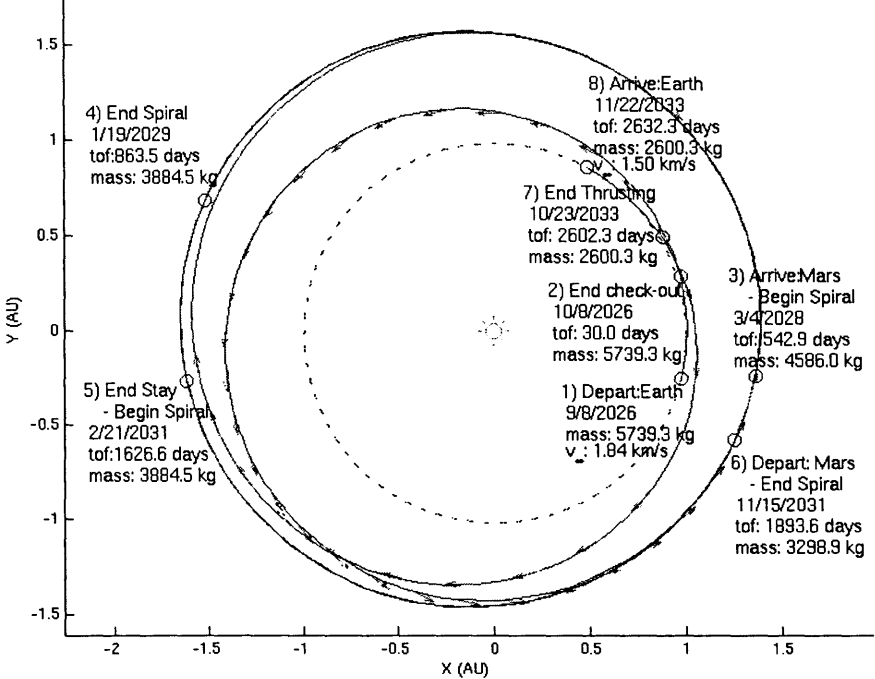


### B.5.2 Lunar Return

#### B.5.2.1 Short Mars Stay



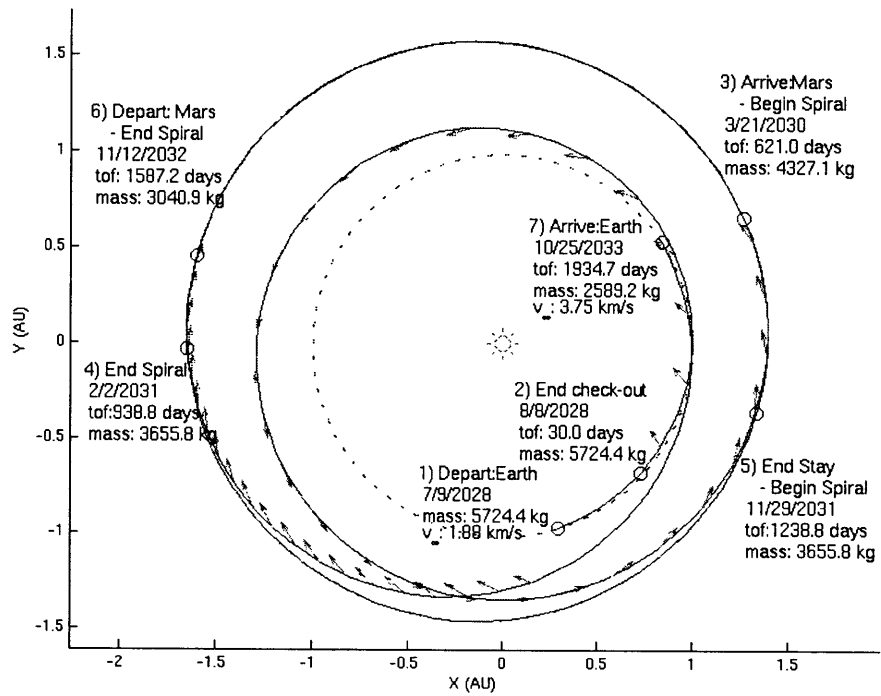
**B.5.2.2 Long Mars Stay**



## B.6 2028 Trajectories

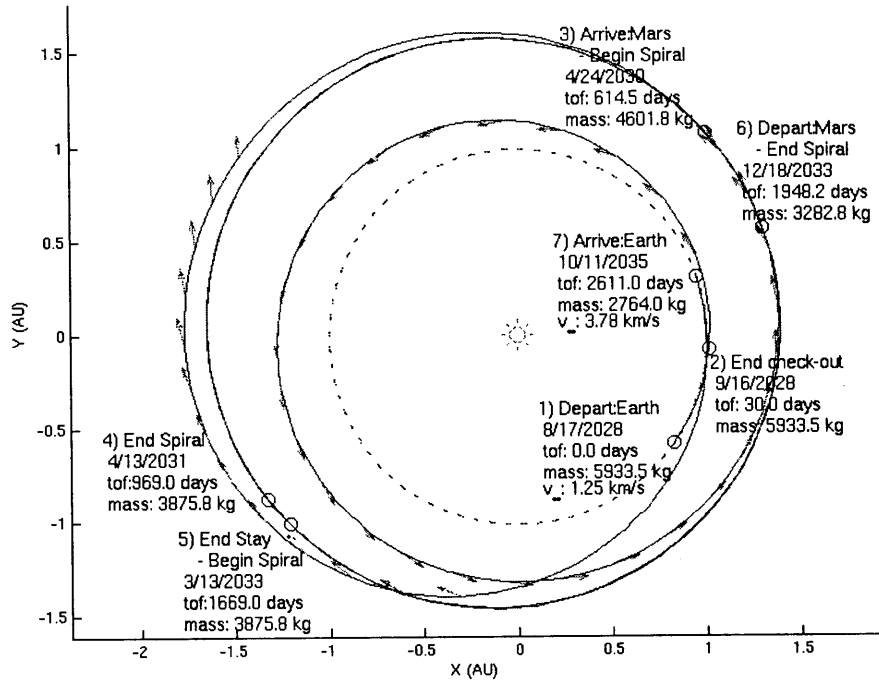
### B.6.1 Earth Return

#### B.6.1.1 Short Mars Stay



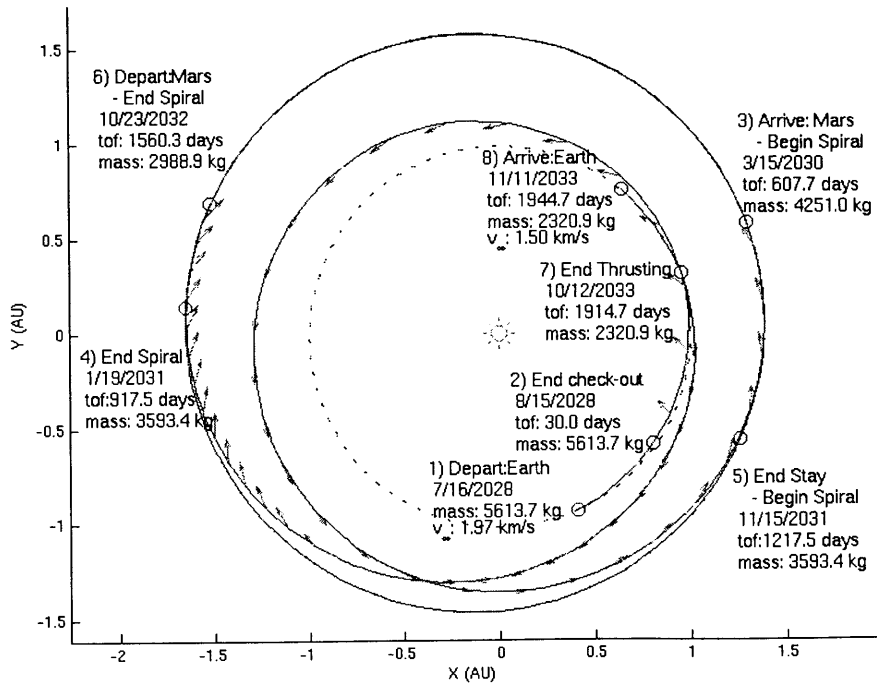


### B.6.1.2 Long Mars Stay

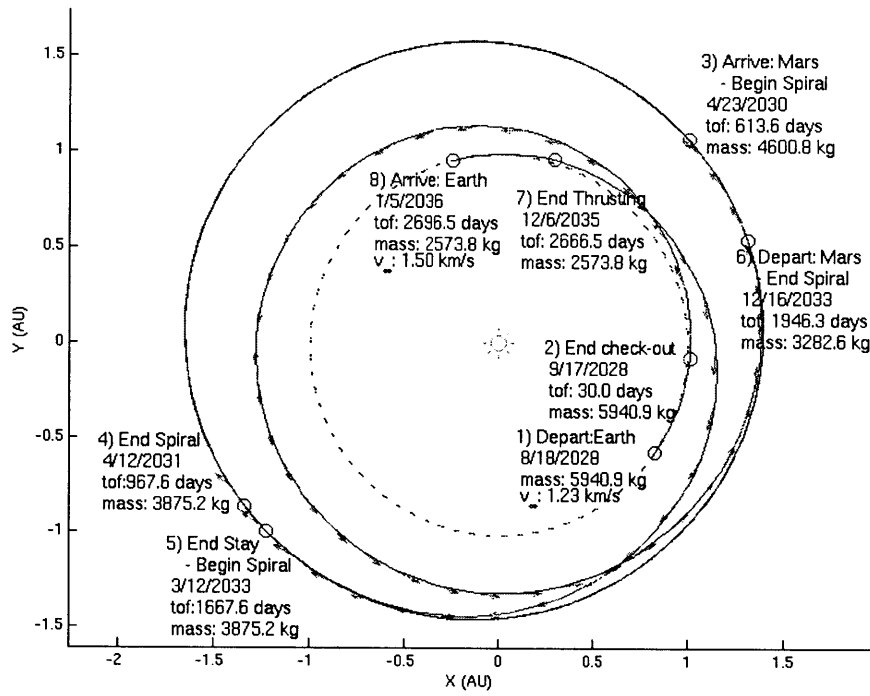


### B.6.2 Lunar Return

#### B.6.2.1 Short Mars Stay



### B.6.2.2 Long Mars Stay



# Appendix C

## SOFTWARE AND SUPPORTING DOCUMENTS

The software developed for this thesis, along with supporting documentation such as project reports, user guides and input files for case studies are publically available at: <http://bit.ly/FarahAlibayThesis>. Any questions or requests can be sent to [farah@alum.mit.edu](mailto:farah@alum.mit.edu).